



HAL
open science

Photolabile N-hétérocycliques carbènes (NHCs) pour la polymérisation médianée par lumière (photoROMP)

Thi Kim Hoang Trinh

► **To cite this version:**

Thi Kim Hoang Trinh. Photolabile N-hétérocycliques carbènes (NHCs) pour la polymérisation médianée par lumière (photoROMP). Polymers. Université de Haute Alsace - Mulhouse, 2019. English. NNT : 2019MULH3242 . tel-03704199

HAL Id: tel-03704199

<https://theses.hal.science/tel-03704199>

Submitted on 24 Jun 2022

HAL is a multi-disciplinary open access archive for the deposit and dissemination of scientific research documents, whether they are published or not. The documents may come from teaching and research institutions in France or abroad, or from public or private research centers.

L'archive ouverte pluridisciplinaire **HAL**, est destinée au dépôt et à la diffusion de documents scientifiques de niveau recherche, publiés ou non, émanant des établissements d'enseignement et de recherche français ou étrangers, des laboratoires publics ou privés.

This thesis submitted in partial fulfillment of the requirements of the degree of

Doctor of Philosophy

from

University of Haute Alsace

L'Ecole Doctorale Physique et Chimie-Physique (ED 182)

by

PhD student: **Thi Kim Hoang TRINH**

**Photolabile N-heterocyclic Carbenes (NHCs)
for Photomediated Ring-Opening Metathesis
Polymerization (photoROMP)**

Supervisor: **Dr. Abraham CHEMTOB**

17th September, 2019

Committee members:

Dr. Davy-Louis VERSACE, University Paris XII	Rapporteur
Prof. Jean-Luc SIX, University of Lorraine	Rapporteur
Dr. Karine ANSELME, IS2M-CNRS	Examinatrice
Dr. Delphine CHAN-SENG, ICS-CNRS	Examinatrice
Dr. Julien PINAUD, University of Montpellier	Invité

This thesis submitted in partial fulfillment of the requirements of the degree of

Doctor of Philosophy

from

University of Haute Alsace

L'Ecole Doctorale Physique et Chimie-Physique (ED 182)

by

PhD student: **Thi Kim Hoang TRINH**

**Photolabile N-heterocyclic Carbenes (NHCs)
for Photomediated Ring-Opening Metathesis
Polymerization (photoROMP)**

Supervisor: **Dr. Abraham CHEMTOB**

17th September, 2019

Committee members:

Dr. Davy-Louis VERSACE, University Paris XII	Rapporteur
Prof. Jean-Luc SIX, University of Lorraine	Rapporteur
Dr. Karine ANSELME, IS2M-CNRS	Examinatrice
Dr. Delphine CHAN-SENG, ICS-CNRS	Examinatrice
Dr. Julien PINAUD, University of Montpellier	Invité

GENERAL INTRODUCTION

In the field of polymer chemistry, an increasing number of studies have involved the use of N-heterocyclic carbenes (NHCs) either as organocatalyst or ancillary ligand.¹⁻³ Despite their high utility, there are practical issues when handling highly reactive free carbenes including premature degradation or dimerization reactions due to their high Brønsted basicity and nucleophilic character.^{4,5} To overcome these challenges, a series of thermally triggerable latent NHC precursors have been developed where NHC reactivity can be tamed by the presence of different protecting groups such as CO₂ or appropriate metal ions.⁶ In this case, the free NHC species can be released on demand by application of heat, enabling a temporal control of polymerization and the use of a storable and ready-to-use formulation containing both the latent catalyst and the monomer(s).

Recently, radiation has emerged as a versatile stimulus offering an even more accurate activation of polymerization than heat.⁷ A distinctive advantage of photolabile generator is to make possible a spatially-controlled polymerization, opening avenue for the development of patterned materials. Surprisingly, there is hardly any research activity in the field of NHC photogenerator. Herein, the main goal of my thesis is the development, for the first time, an air-stable photolabile NHC and its exploitation as photoligand in photoactivated ring-opening metathesis polymerization (ROMP). This PhD thesis is part of the ANR collaborative project “Photolabile N-heterocyclic carbenes for delayed ring-opening polymerizations” (PHOTO DROP) in which a multidisciplinary approach is undergone to harness the potential of new NHC photogenerators in a range of photochemically initiated polymerizations such as ROMP but also ring-opening anionic polymerization (ROAP) in solution and in dispersed media. The project partners are **ICGM, Université de Montpellier** (Dr. Julien Pinaud, Dr. Patrick Lacroix-Desmazes, Dr. Emeline Placet and Dr. Shashikala Indudhara) and at **LCPO, Université de Bordeaux** (Dr. Valérie Héroguez and Dr. Loïc Pichavant).

Returning to my PhD subject, the key idea is that upon exposure to radiation a photolabile NHC precursor can generate a free NHC, which subsequently reacts with an inactive Ru precatalyst to drive the in situ formation of an active metathesis NHC-coordinated ruthenium-arene complex. The use of this methodology is desirable because it

gives access to a truly photolabile ROMP initiator easy to prepare and exhibiting a high catalytic activity. ROMP has been targeted as the main application field for our new photolabile NHC because ROMP polymers have an excellent record of mechanical properties and chemical resistance, and there is currently no UV-curable ROMP polymer coatings.⁸ Polymers obtained by ROMP have been widely used as an alternative to metals in commercial and industrial materials (**Figure 0.1**). With respect to the NHC photogenerator, a complete photochemical study was carried out to elucidate the photochemical process associated with the free NHC liberation. On the other hand, the use of photolabile NHC has been also broadened to assess their utility as organocatalyst in other polymerization reactions.

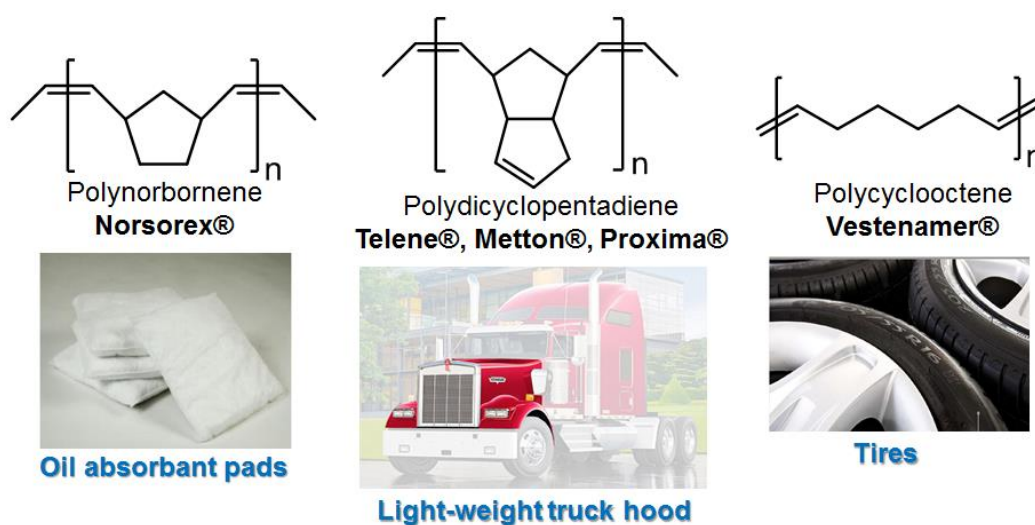


Figure 0.1. Chemical structures of common ROMP polymers and their industrial applications.

This thesis dissertation includes 4 chapters. The main concepts and challenges are described schematically in **Figure 0.2**:

- A literature review in *chapter I* gives an advanced update on emerging trends in latent NHC progenitors. In particular, the various synthetic pathways to produce in situ NHC and their application in the polymerization are discussed. On the other hand, the different techniques and strategies for photochemically activated ROMP (photoROMP) are commented in details. A critical approach has been adopted to highlight advantages and drawbacks of each study.

- *Chapter II* describes the synthesis and characterization of a two-component air-stable NHC photogenerating system based on a mixture of 2-isopropylthioxanthone (ITX) and 1,3-bis(mesityl)imidazoli(ni)um tetraphenylborate ($\text{NHCH}^+\text{BPh}_4^-$). The photoinduced liberation of NHC at 365 nm is evidenced by reaction with a mesityl radical to form a NHC-

radical adduct detectable by electron paramagnetic resonance (EPR) spectroscopy. The NHC yield can be determined by ^1H NMR through the formation of a soluble and stable NHC-carbodiimide adduct. Three different photoNHC-mediated polymerizations are described: synthesis of polyurethane and polyester by organocatalyzed step-growth polymerization and ring-opening copolymerization, respectively, and generation of polynorbornene by ring-opening metathesis polymerization using a NHC-coordinated Ru catalyst formed in situ.

- *Chapter III* presents the investigation on the photochemical mechanism that drives the formation of NHC at 365 nm from the mixture of $\text{IMesH}^+\text{BPh}_4^-/\text{ITX}$. The reaction intermediates and final photo-products are identified via a combination of laser flash photolysis, ^1H , ^{13}C and ^{11}B NMR spectroscopy, EPR, acid/base titration and gas chromatography-mass spectrometry (GC-MS).

- In *chapter IV*, photoactivated ROMP of norbornene (NB), 5-ethyliden-2-norbornene (ENB) and dicyclopentadiene (DCPD) at different wavelengths (365 and 405 nm) were carried out using $\text{IMesH}^+\text{BPh}_4^-/\text{ITX}$ as NHC photogenerator and a commercially available dimeric Ru complex as metathesis inactive catalyst. The main aim is to demonstrate the utility of this tandem approach for the photoinduced preparation of cross-linked ROMP films

- An *Appendix* contains additional figures, experimental procedures, emission spectra of lamps as well as the set-up for photoROMP reactions.

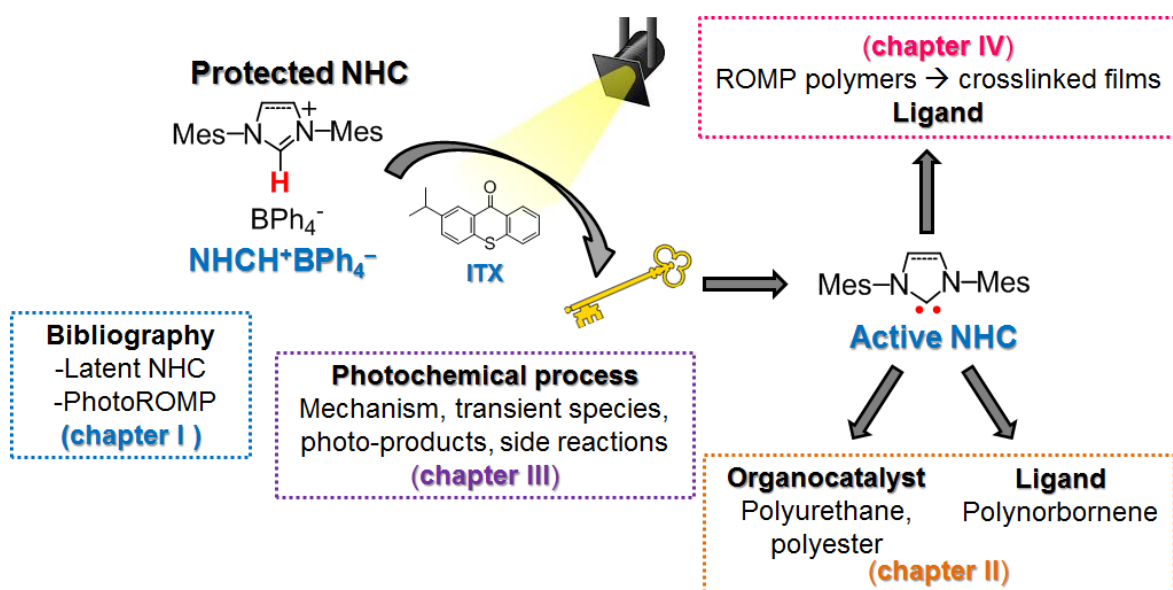


Figure 0.2. Summary of the scope of studies presented in this thesis.

References

- 1 M. Fèvre, J. Pinaud, Y. Gnanou, J. Vignolle and D. Taton, N-Heterocyclic carbenes (NHCs) as organocatalysts and structural components in metal-free polymer synthesis, *Chem. Soc. Rev.*, 2013, **42**, 2142–2172.
- 2 S. Díez-González, N. Marion and S. P. Nolan, N-Heterocyclic Carbenes in Late Transition Metal Catalysis, *Chem. Rev.*, 2009, **109**, 3612–3676.
- 3 S. Naumann and A. P. Dove, N-Heterocyclic carbenes as organocatalysts for polymerizations: trends and frontiers, *Polym. Chem.*, 2015, **6**, 3185–3200.
- 4 A. Poater, F. Ragone, S. Giudice, C. Costabile, R. Dorta, S. P. Nolan and L. Cavallo, Thermodynamics of N-Heterocyclic Carbene Dimerization: The Balance of Sterics and Electronics, *Organometallics*, 2008, **27**, 2679–2681.
- 5 M. N. Hopkinson, C. Richter, M. Schedler and F. Glorius, An overview of N-heterocyclic carbenes, *Nature*, 2014, **510**, 485–496.
- 6 S. Naumann and M. R. Buchmeiser, Liberation of N-heterocyclic carbenes (NHCs) from thermally labile progenitors: protected NHCs as versatile tools in organo- and polymerization catalysis, *Catal. Sci. Technol.*, 2014, **4**, 2466–2479.
- 7 N. Corrigan, J. Yeow, P. Judzewitsch, J. Xu and C. Boyer, Seeing the Light: Advancing Materials Chemistry through Photopolymerization, *Angew. Chem. Int. Ed.*, 2019, **58**, 5170–5189.
- 8 A. Leitgeb, J. Wappel and C. Slugovc, The ROMP toolbox upgraded, *Polymer*, 2010, **51**, 2927–2946.

ACKNOWLEDGEMENTS

Today, I submitted my PhD thesis for an external examination. This thesis was conducted at **Institution of Materials Science in Mulhouse (IS2M)** from 01.2017 to 09.2019. It was financed by French National Research Agency (ANR program: DS0304 2016, contract number: ANR-16-CE07-0016). To accomplish this thesis, it was a long and wonderful journey and would not have been successful without the inspiration and support of many great individuals.

First and foremost, I would like to express my sincere gratitude to my advisor Dr. Abraham Chemtob who has been major supportive of my PhD study. Under his academic guidance, this dissertation became a reality. He spent endless hours proofreading my research papers and giving me excellent suggestions, which always resulted in improved versions of my dissertation.

Besides my advisor, it is a pleasure to thank Dr. Julien Pinaud and Dr. Patrick Lacroix-Desmazes (**ICGM, Université de Montpellier**) and Dr. Valérie Héroguez (**LCPO, Université de Bordeaux**), who are project partners, for sharing their expertise and experiences, as well as their insight into addressing problems throughout this project.

I am forever thankful to all my colleagues in **IS2M** for their friendship and supports, and for creating a convivial working environment. Furthermore, my sincere thanks also goes to Dr. Jean-Pierre Malval, Dr. Séverinne Rigolet, Mr. Gautier Schrodj, Mr. Aissam Airoudj and Mr. Stephan Knopf (**IS2M, Université de Haute-Alsace**), Dr. Didier le Nouen and Dr. Cécile Joyeux (**LIMA, Université de Haute-Alsace**), Dr. Rémi Métivier and Mr. Arnaud Brosseau (**PPSM, ENS Cachan, Université Paris-Saclay**), Dr. Emeline Placet and Ms. Corine Reibel (**ICGM, Université de Montpellier**) and Dr. Loïc Pichavant (**LCPO, Université de Bordeaux**) for their extensive help with experiment and commitment towards many concepts presented in this thesis.

Also, I thank my friends, who shared with me special moments, gave me the necessary distractions from my research and made my stay in France memorable.

Last but not least, I would like to express my warmest gratitude to my family: my mom, uncles, aunts and cousins, for their continuous and unparalleled love, help and support throughout my life.

List of Schemes

Title.....	Page
Scheme 1.1. General approaches to NHCs.....	5
Scheme 1.2. Principle thermal liberation of NHCs from their corresponding precursors.	7
Scheme 1.3. Schematic preparation of [NHC(H)][HCO ₃] using NHC.CO ₂ adducts and azolium halides and reversible release of corresponding NHCs therefrom.....	9
Scheme 1.4. Thermal-triggering liberation of NHC-supported metal ions.	11
Scheme 1.5. Ultrasound activation of Ag(I)-NHC-polymer complex and subsequent transesterification catalyzed by NHC formed in situ.	12
Scheme 1.6. Schematic depiction of the external force induced geometry change of NHC-CDI amidinate followed by liberating the free NHC.....	13
Scheme 1.7. Schematic generation of free carbene based on NHC-carboxylic acids.....	14
Scheme 1.8. General mechanism of generation of NHCs involving photoinduced decarboxylation accompanied by proton transfer.	14
Scheme 1.9. Schematic representation of monomer-activated ROP of lactam and lactone mediated by NHC.CO ₂ precursors.....	16
Scheme 1.10. Schematic representation of chain-end activated ROP of lactone mediated by NHC.CO ₂ precursors.....	17
Scheme 1.11. Formation of polyester based on Lewis acid/base activation of thermally labile NHC-metal adducts.....	18
Scheme 1.12. Thermal activation mechanism of NHC.CO ₂ precursors in ROP of PO.	18
Scheme 1.13. Schematic initiation step of a latent one-component epoxide/ anhydride mixture in the presence of protected NHCs.....	19
Scheme 1.14. Proposed mechanism for thermal liberation of NHCs from their inactive precursors applied in PU syntheses.....	21
Scheme 1.15. General synthetic process of aliphatic polycarbonates employing 7a .CO ₂ as precatalyst.	21
Scheme 1.16. General mechanism of metal-mediated ROMP.....	21
Scheme 1.17. Highly active NHC-ruthenium complex obtained via reaction of ruthenium dimer and NHC.CO ₂ adducts.....	22
Scheme 1.18. General mechanism for the formation of active ROMP catalyst by photo driven ligand dissociation.	24

Scheme 1.19. Photogeneration of an active catalyst by irradiation of solution containing a photoacid generator (PAG) and a ruthenium complex.	29
Scheme 1.20. Photogeneration of an active catalyst by irradiation of solution containing a PAG and a ruthenium complex.	30
Scheme 1.21. In situ formation of Noels' catalyst by sensitized photogeneration of NHC IMes	30
Scheme 2.1. Photolysis mechanism for the photogeneration of IMes (or SIMes) from the bicomponent photogenerating system ITX/ IMesH⁺BPh₄⁻ (or ITX/ SIMesH⁺BPh₄⁻).	51
Scheme 2.2. Reaction pathway to generate NHC-radical adduct after irradiation of ITX/ IMesH⁺BPh₄⁻ in presence of TPO.	61
Scheme 2.3. Formation of zwitterionic IMes -CDI adduct by reaction between CDI and NHC IMes	63
Scheme 2.4. Photochemical mechanism for the generation of NHC IMes and SIMes combining electron-transfer and proton transfer.	66
Scheme 2.5. Photoreduction of ITX by IMes (or SIMes) generates NHC radical cations.	66
Scheme 2.6. Synthesis of polyurethane catalyzed by photogenerated NHC.	70
Scheme 2.7. ROCOP of PA and CHO using photogenerated NHC IMes and SIMes as catalyst.	72
Scheme 2.8. Strategy for in situ formation of RuCl ₂ (<i>p</i> -cymene)NHC from the inactive precatalyst [RuCl ₂ (<i>p</i> -cymene)] ₂ dimer and photogenerated NHC IMes and SIMes . The active NHC-coordinated Ru complexes referred to as Noels' catalysts can be used as active for the ROMP of NB.	75
Scheme 3.1. Photochemical reactivity of arylborates.	84
Scheme 3.2. Photochemical pathway based on electron and proton transfer reactions resulting in the generation of NHC.	86
Scheme 3.3. Colour changes during an acid/ base titration utilizing phenol red as the titrant.	97
Scheme 3.4. Possible side-reactions involving ITX ketyl radical produced after protonation of ITX radical anion.	100
Scheme 3.5. Schematic formation of diphenylboric acid.	104
Scheme 3.6. The mechanistic pathway involved in the formation of IMes during the photolysis of a mixture ITX/ IMesH⁺BPh₄⁻	105

Scheme 4.1. Irradiation of a mixture of a NHC photogenerator (IMesH⁺BPh₄⁻ , 1) and a dimeric Ru(II) complex, inactive catalyst (Ru-1), results in a active olefin metathesis photocatalyst (Ru-1-IMes).....	113
Scheme 4.2. Proposed photoactivation mechanism of Noels' catalyst	124
Scheme 4.3. Schematic preparation of a cross-linked film through ROMP of NB and DCPD	126
Scheme A.II.1. Proposed mechanism of urethane formation for reaction of PEG ₄₀₀ and IPDI catalyzed by in situ generated IMes (or SIMes).	145
Scheme A.II.2. Possible mechanism for ring-opening copolymerization of CHO and PA. .	147
Schéma R.II.1. Mécanisme de photolyse pour la photogénération de 1 (ou 2) à partir du système bicomposant ITX / 1H⁺BPh₄⁻	158
Schéma R.III.1. Réactivité photochimique des espèces arylborate. La voie 1 est basée sur la photolyse directe alors que la voie 2 est un transfert d'électron photoinduit (TEP) avec un sensibilisateur accepteur d'électron (EA)..	163
Schéma R.III.2. Mécanisme photochimique pour la production de NHC	165
Schéma R.IV.1. L'irradiation d'un mélange d'un photogénérateur NHC (1) et d'un catalyseur inactif (Ru-1) conduit à un catalyseur de métathèse actif (Ru-1-IMes).	170

List of Figures

Title.....	Page
Figure 0.1. Chemical structures of common ROMP polymers and their industrial applications.	ii
Figure 0.2. Summary of the scope of studies presented in this thesis.....	iii
Figure 1.1. General structure of: (a) conventional carbenes and (b) Arduengo carbenes.	2
Figure 1.2. General ground-state electronic features of singlet and triplet carbenes. Arrows: electrons	3
Figure 1.3. Stabilization of NHCs via electronic push-pull effect.	4
Figure 1.4. Chemical structures and nomenclatures of some classes of NHCs found so far in literature.	5
Figure 1.5. Chemical structures of common betaine adducts.	8
Figure 1.6. Chemical structures of thermal latent NHCs protected by organic compounds halogenated and alcohols.	10
Figure 1.7. General air stable NHC-metal precursors.....	11
Figure 1.8. A range of novel photogenerator NHCs based on decarboxylation.	14
Figure 1.9. 4 strategies to develop photochemically activated ROMP.....	24
Figure 1.10. Structure of well-defined tungsten catalysts developed by Van der Schaaf <i>et al.</i>	25
Figure 1.11. Ruthenium and osmium based photocatalysts prepared by Mühlebach <i>et al.</i>	26
Figure 1.12. Ruthenium photocatalysts with NHC ligands.	28
Figure 1.13. Monomers employed for PROMP by Bushmeiser <i>et al.</i>	28
Figure 1.14. S chelated latent ruthenium benzylidene catalysts used in photoROMP (Ru14 and Ru16). Ru15 is the first isomerizable chelated ruthenium catalyst, the Ru15-cis form being much more latent than Ru15-trans	31
Figure 1.15. N-Chelated latent ruthenium benzylidene catalysts used in photoROMP. Only Ru17 and Ru19 proceed via a presumed photoisomerization mechanism.....	34
Figure 1.16. A. [2+2] cyclo-addition of an electron rich olefin mediated by single electron transfer to an unactivated olefin. B. Putative mechanism of photoinduced electron transfer ROMP of NB as envisaged by Boydston <i>et al.</i>	36

Figure 1.17. Pyrylium salt (P1) and thiopyrylium salt (P2) used as photo-oxidant in metal-free PET ROMP.	37
Figure 1.18. A range of vinyl ether initiators used by Boydston <i>et al.</i>	37
Figure 2.1. IMes and SIMes are among the most frequently employed NHCs.	49
Figure 2.2. UV-vis absorption spectra of NaBPh ₄ (black), IMesH⁺Cl⁻ (blue) and IMesH⁺BPh₄⁻ (red) in acetonitrile (4×10^{-4} M).	59
Figure 2.3. ¹³ C- NMR spectra in DMSO- <i>d</i> ₆ of the IMes -CS ₂ adduct.	60
Figure 2.4. EPR spectrum of: (a) a solution of ITX/ IMesH⁺BPh₄⁻ /TPO (1/3/6 equiv., [ITX] = 5×10^{-3} M) in THF after different irradiation times and (b) EPR spectrum obtained after 30 s irradiation of a solution of IMes /TPO in THF (5/1 equiv., [TPO] = 3×10^{-3} M). The experimental and simulated spectra are both consistent with the formation of the mesitoyl-NHC adduct radical IMes[•]-M	62
Figure 2.5. ¹ H NMR spectra in THF- <i>d</i> ₈ of: (a) IMes (0.21 M), (b) CDI (0.21 M), (c) IMes /CDI, (1/1 equiv., [IMes] = 0.1 M), and (d) IMesH⁺BPh₄⁻ /ITX/CDI (3/1/3 equiv., [ITX] = 0.01 M). In sample d, IMesH⁺BPh₄⁻ /ITX was irradiated 5 min then CDI was immediately added.	64
Figure 2.6. UV spectra of ITX, SIMesH⁺BPh₄⁻ and IMesH⁺BPh₄⁻ in acetonitrile ([ITX] = 10^{-4} M, [IMesH⁺BPh₄⁻] = [SIMesH⁺BPh₄⁻] = 3×10^{-4} M).	64
Figure 2.7. Photobleaching kinetics of ITX (2×10^{-4} M in acetonitrile) monitored at 365 nm in the presence of different quenchers: azolium salts (a) and tetraphenylborate salts (b) (Quencher concentration is 6×10^{-4} M).	65
Figure 2.8. Temporal evolution of absorbance at 365 nm of ITX solution in acetonitrile (2×10^{-4} M) in the absence of quencher and presence of IMes and SIMes (6×10^{-4} M).	67
Figure 2.9. (a) Effect of ITX concentration on NHC IMes yield produced by irradiation of ITX/ IMesH⁺BPh₄⁻ ([IMesH⁺BPh₄⁻] = 0.03 M) and (b) Effect of irradiation time on NHC IMes yield following the photolysis of ITX/ IMesH⁺BPh₄⁻ mixture.	68
Figure 2.10. NCO conversion during polyaddition reaction between PEG ₄₀₀ and IDPI.	71
Figure 2.11. FT-IR spectra of aliquots taken at different times during the bulk polyaddition between PEG ₄₀₀ and IPDI (PEG ₄₀₀ /IPDI (342/342 equiv.)).	72
Figure 2.12. ¹ H NMR spectra of in CDCl ₃ of aliquots taken at different times during the ROCOP of CHO/PA (500/100 equiv.)).	74
Figure 3.1. Transition absorption spectra of (a) [ITX] = 10^{-4} M, (b) ITX/NaBPh ₄ = 6×10^{-3} M and (c) ITX/ IMesH⁺BPh₄⁻ = 6×10^{-3} M.	93

Figure 3.2. Decays of $^3\text{ITX}^*$ at 600 nm in the presence and absence of: (a) $\text{IMesH}^+\text{Cl}^-$, (b) NaBPh_4 , (c) NaBPh_4 (under O_2) and (d) $\text{IMesH}^+\text{BPh}_4^-$	93
Figure 3.3. EPR spectra of radical adduct from a solution: (a) $\text{ITX} - \text{NaBPh}_4 - \text{PBN}$ and (b) $\text{ITX} - \text{IMesH}^+\text{BPh}_4^- - \text{PBN}$ after 60 s of irradiation.	95
Figure 3.4. EPR spectra of Ph-PBN radical from a solution $\text{ITX} - \text{IMesH}^+\text{BPh}_4^- - \text{PBN}$ in acetonitrile after exposure under LED 365 nm at given time.	95
Figure 3.5. ^1H NMR spectra change of ITX (0.07 M) and $\text{IMesH}^+\text{BPh}_4^-$ (0.21 M) in $\text{ACN}-d_3$: (a) prior to exposure, (b) after 5 min irradiation and (c) after addition of CS_2	96
Figure 3.6. (a) Change of UV-Vis spectra of an acetonitrile solution of $\text{IMesH}^+\text{BPh}_4^-$ (3.0×10^{-4} M) and ITX (1×10^{-4} M) irradiated during 2 min (LED, 365 nm, 65 mW cm^{-2}) upon gradual addition of PR (2×10^{-4} M) and (b) Titration plot showing the absorbance at 580 nm for the same photoNHC/sensitizer solution irradiated 1, 2 or 5 min as a function of PR (titrant) volume.	98
Figure 3.7. GC chromatogram of photoproducts obtained from the photolysis media of $\text{ITX} - \text{IMesH}^+\text{BPh}_4^-$ after 5 min of irradiation.	100
Figure 3.8. ^{11}B -NMR spectra of a mixture of ITX (0.03 M) and $\text{IMesH}^+\text{BPh}_4^-$ (0.03 M) in $\text{THF}-d_8$: (a) prior irradiation, (b) after 10 min UV exposure, and (c) after adding CS_2 into medium.	102
Figure 3.9. ^{11}B -NMR spectra in $\text{THF}-d_8$: (a) $\text{IMesH}^+\text{BPh}_4^- - \text{IMes}$, (b) $\text{IMesH}^+\text{BPh}_4^- - \text{IMes} - \text{BPh}_3$	103
Figure 3.10. ^{11}B NMR spectra in non-dried $\text{THF}-d_8$: (a) Hydrolyzed BPh_3 , (b) Addition of IMes into hydrolyzed BPh_3	104
Figure 4.1. ^1H NMR spectrum of the reaction medium after reaction of $[(p\text{-cymene})\text{RuCl}_2]_2$ (Ru-1 , 1 equiv.) with IMes (2.02 equiv.) in $\text{THF}-d_8$ ($[\text{Ru-1}] = 0.05 \text{ M}$).	119
Figure 4.2. Conversion-time curve for the ROMP of NB in solution in CH_2Cl_2 : light off (grey area), light on (white area). NB/ Ru-1 / ITX = 510/1/5/0.5 equiv. Irradiation conditions: LED@365 nm, $65 \text{ mW}\cdot\text{cm}^{-2}$	124
Figure 4.3. Photopolymerization kinetic of NB, DCPD and NB/DCPD (50/50 mol%) using photocatalyst system Ru-1 / ITX in CH_2Cl_2 (Monomer/ Ru-1 / ITX = 510/ 1/ 5/ 2.5 equiv.). Conversions of NB, NB/DCPD (50/ 50 mol%) and DCPD were 100 %, 94 % and 70, respectively.	125

Figure 4.4. Photographs of: (a) General set up for the preparation of cross-linked films and (b) Images of polymeric films (i) NB-100, (ii) NB-75, (iii) NB-50, (iv) NB25 and (v) DCPD-100.....	126
Figure 4.5. Characterizations of different polymeric specimens: (a) Polymer yield determined by gravimetry method and (b) Gel content determined by extracting with CH ₂ Cl ₂	127
Figure 4.6. FTIR- ATR spectra of polymer films obtained by photoROMP at 365 nm: (a) NB-100, (b) NB-75, (c) NB-50, (d) NB-25 and (e) DCPD-100: (A) Expanded spectra in a range of 675 – 1700 cm ⁻¹ and (B) Expanded spectra in a range of 2960 – 3100 cm ⁻¹	128
Figure 4.7. ¹³ C NMR CPMAS spectra of polymeric films: (a) NB-100, (b) NB-75, (c) NB-50, (d) NB-25 and (e) DCPD-100.....	130
Figure 4.8. (A) Glass transition temperature as measured by DSC of different polymer films in nitrogen with (a) NB-100, (b) NB-75, (c) NB-50, (d) NB-25 and (e) DCPD-100 and (B) TGA thermograms of different polymer films obtained as heating under nitrogen environment	131
Figure 4.9. SEM images of the fracture surface of homo and copolymer specimens with 5000× magnification.	133
Figure A.II.1. Formation of IMesH⁺BPh₄⁻ as NaBPh ₄ put in contact with IMesH ⁺ Cl ⁻ in ethanol.....	141
Figure A.II.2. (a) A set-up for photopolymerization with LED at 365 nm light stripe (SMD3528-60LED/Meter, Lightingwill, 6.5 mW·cm ⁻²) and (b) Emission spectra of the Lightingwill LED.....	141
Figure A.II.3. Changes of a mixture containing NB/ Ru-1 / IMesH⁺BPh₄⁻ / ITX in CD ₂ Cl ₂ as irradiated with LED at 365 nm light tripe (6.5 mW·cm ⁻²).....	141
Figure A.II.4. A LED at 365 nm (LC-L1V3, Hamamatsu, 65 mW·cm ⁻²): (a) an image of the set-up and (b) its emission spectra.....	142
Figure A.II.5. Color changes of an as-irradiated IMesH⁺BPh₄⁻ / ITX in THF- <i>d</i> ₈ at different given times	142
Figure A.II.6. Color changes of an as-irradiated IMesH⁺BPh₄⁻ / ITX (3/ 1 equiv.) in THF- <i>d</i> ₈ at different given times and after an addition of CDI (irradiation conditions: LED at 365 nm (LC-L1V3, Hamamatsu, 65 mW·cm ⁻²)).	142
Figure A.II.7. A set-up for photo-bleaching experiment.....	143
Figure A.II.8. Thermal analysis of tetraphenylborate imidazolium IMesH⁺BPh₄⁻ : (a) DSC thermogram, (b) TGA thermogram.....	143

Figure A.II.9. Enthalpy calculation of reactions of IMes with phosphonyl (P^\bullet) and mesitoyl (M^\bullet) radicals by using uB3LYP/6-31G* level of theory.....	143
Figure A.II.10. EPR spectrum obtained at different given irradiation times of a solution of IMes /TPO in THF (5/1 equiv., [TPO] = 3×10^{-3} M).....	144
Figure A.II.11. 1H NMR spectra in THF- d_8 of: (a) IMesH⁺BPh₄⁻ (0.03 M), (b) IMes/IMesH⁺BPh₄⁻ (1/3 equiv., [IMes] = 0.01 M), (c) The later mixture, then addition of 3 equiv. of CDI.	144
Figure A.II.12. SEC traces in THF of precipitated polyurethane samples prepared by step-growth polymerization of PEG ₄₀₀ /IPDI (342/342 equiv.).	145
Figure A.II.13. 1H NMR spectrum of refined (precipitated) polyester in CDCl ₃ obtained by the ROCOP of CHO/PA (500/100 equiv.) at 110°C for 60 min using an as-irradiated IMesH⁺BPh₄⁻ /ITX solution (1/1 equiv.) (photogenerated IMes) as an initiator.....	146
Figure A.II.14. Positive MALDI-ToF MS spectrum of isolated poly(PA- <i>alt</i> -CHO) obtained by the ROCOP of CHO/PA (500/100 equiv.) at 110°C for 60 min using an as-irradiated IMesH⁺BPh₄⁻ /ITX solution (1/1 equiv.) (photogenerated IMes) as an initiator (entry a in Table 2.3)..	146
Figure A.II.15. SEC traces in THF of refined polyesters gained from entry a and b (Table 2.3) prepared by the ROCOP of CHO/PA (500/100 equiv.) at 110°C for 60 min using different initiators: as-irradiated IMesH⁺BPh₄⁻ /ITX solution (1/1 equiv., brown trace) and as-irradiated SIMesH⁺BPh₄⁻ /ITX solution (1/1 equiv., blue trace).	147
Figure A.II.16. SEC traces of precipitated polynorbornene prepared by the ROMP of NB (510 equiv.) irradiated for 60 s with LED 365 nm (6.5 mW cm^{-1}) using different catalysts: (a) IMesH⁺BPh₄⁻ /ITX/[RuCl ₂ (<i>p</i> -cymene)] ₂ solution (5/2.5/1 equiv.) and (b) SIMesH⁺BPh₄⁻ /ITX/[RuCl ₂ (<i>p</i> -cymene)] ₂ solution (5/2.5/1 equiv.). Three detectors were used: 1/. LS: light scattering detector, 2/. UV, and 3/. dRI: refractive index detector.	148
Figure A.III.1. Color changes of an as-irradiated IMesH⁺BPh₄⁻ /ITX (3/ 3 equiv.) in ACN- d_3 at different given time and formation of IMes-CS₂ adduct after CS ₂ added.	148
Figure A.III.2. Color changes of an as-irradiated IMesH⁺BPh₄⁻ /ITX (3/ 1 equiv.) in ACN before and after addition of phenol red.....	149
Figure A.III.3. EPR spectra of Ph-PBN radical from a solution ITX – IMesH⁺BPh₄⁻ – PBN in acetonitrile after exposing under LED 365 nm for 60 s (concentration: [ITX] = 5×10^{-3} M, [IMesH⁺BPh₄⁻] = 1.5×10^{-2} M and [PBN] = 3×10^{-3} M, respectively).	149

Figure A.III.4. ^1H NMR spectra in THF- d_8 of: (a) $\text{IMesH}^+\text{BPh}_4^-$, (b) IMes , (c) the mixture of $\text{IMesH}^+\text{BPh}_4^-$ and IMes (9/1 equiv.) and (d) irradiated ITX – $\text{IMesH}^+\text{BPh}_4^-$ (1/1 equiv.).....	150
Figure A.III.5. Amount of IMes existing in acetonitrile against exposure time determined by an acid/base titration with phenol red.	150
Figure A.III.6. ^{11}B -NMR spectra of photolysis of $[\text{ITX}] = 0.03 \text{ M}$ - $[\text{BPh}_3] = 0.03 \text{ M}$ in THF- d_8 :(a) prior to exposure, (b) after exposure for 10 min (LED 365 nm, $65 \text{ mW}\cdot\text{cm}^{-2}$).....	151
Figure A.IV.1. A Hg-Xe lamp at 254 nm (LC-9588/01A, Hamamatsu, $75 \text{ mW}\cdot\text{cm}^{-2}$): (a) an image and (b) its emission spectra with (red color) and without a filter at 365 nm (blue color).	152
Figure A.IV.2. A LED at 405 nm (M405L2, ThorLabs, $100 \text{ mW}\cdot\text{cm}^{-2}$): (a) an image and (b) its emission spectra.	152
Figure A.IV.3. (a) A set-up for photopolymerization with LED at 405 nm (SMD2835-60LED/Meter, Banggood, $4.7 \text{ mW}\cdot\text{cm}^{-2}$) and (b) Emission spectra of the Banggood LED....	153
Figure A.IV.4. (a) An image of Specac® sealed flow cell for IR spectroscopy and (b) Insight component parts of the Specac® sealed flow cell (the cell windows are CaF_2 pellets, Teflon space has a thickness of 0.1 mm).....	153
Figure A.IV.5. A set-up of top UV curing LED at 365 nm (Tao Yuan, $5.5 \text{ mW}\cdot\text{cm}^{-2}$).....	154
Figure A.IV.6. Changes in FT-IR profiles during photopolymerization in solution CH_2Cl_2 using the catalytic system $\text{Ru-1}/\text{IMesH}^+\text{BPh}_4^-/\text{ITX}$ of various monomers: (a) NB and (b) DCPD.....	154
Figure A.IV.7. ^1H NMR of $1/\text{Ru-1}/\text{ITX}$ in THF- d_8 : (a) Prior to exposure to light and (b) After 30 min of irradiation (Conditions: $1/\text{Ru-1}/\text{ITX} = 5/1/2.5$ equiv., $[\text{Ru-1}] = 0.002 \text{ M}$, Xe-Hg lamp@ 254 nm with intensity of $20 \text{ mW}\cdot\text{cm}^{-2}$).....	155

List of Tables

Title.....	Page
Table 1.1. Photoinduced ROMP employing photoisomerizable complexes Ru-14-cis^a	32
Table 1.2. Photoinduced ROMP employing N-chelating complexes Ru18^a and Ru19^b	35
Table 1.3. Photoinduced ROMP of NB using a photocatalyst P1^a	38
Table 2.1. Effect of the photooxidant's nature on the release of photogenerated NHC IMes	69
Table 2.2. Results of step-growth polymerization of PEG ₄₀₀ /IPDI (342/342 equiv.).	70
Table 2.3. Results of ROCOP of CHO/PA (500/100 equiv.).	73
Table 2.4. Results for the photoROMP of NB conducted at ambient conditions.	76
Table 3.1. Triplet energy simulation of ITX and IMesH⁺BPh₄⁻ estimated.....	94
Table 4.1. Effect of excitation wavelength on the release of free NHC IMes in THF- <i>d</i> ₈ ([1] = 0.03 M, [ITX] = 0.03 M) after 5 min of irradiation.	118
Table 4.2. Photolateness results of Ru dimer/ITX/monomer mixture in CD ₂ Cl ₂ ([Monomer] = 1 M). All the samples were stored in the dark (Ru dimer/ITX/monomer = 1/2.5/510 equiv.).	120
Table 4.3. Photopolymerization results of NB using Ru dimer/ 1 /ITX photoinitiating system in CD ₂ Cl ₂ ([NB] = 1 M, 510 equiv.). Irradiation conditions: 365 nm, 6.5 mW cm ⁻² , 1 min.. ..	121
Table 4.4. Photopolymerization results of ENB using Ru dimer/ IMesH⁺BPh₄⁻ /ITX photoinitiating system in CD ₂ Cl ₂ ([ENB] = 1 M, 510 equiv.). Irradiation conditions: 365 nm, 6.5 mW·cm ⁻² , 10 min.....	122
Table 4.5. Thermo-mechanical results of curing NB/ DCPD films using Ru-1/1 /ITX photoinitiating system in CH ₂ Cl ₂ . Irradiation conditions: 365 nm, 5.5 mW cm ⁻²	132
Table A.III.1. Identification of photoproducts by GC-MS after the photolysis course of ITX/ IMesH⁺BPh₄⁻	151

List of Abbreviations

Chemical compounds

ACN	: acetonitrile
BPh ₃	: triphenylborane
BPh ₄ ⁻	: tetraphenylborate anion
CD ₂ Cl ₂	: deuterium dichloromethane
CDCl ₃	: deuterium chloroform
CDI	: 1,3-di- <i>p</i> -tolylcarbodiimide
CH ₂ Cl ₂	: dichloromethane
CHO	: cyclohexene oxide
COD	: cyclooctadiene
COE	: cyclooctene
CQ	: camphorquinone
CS ₂	: carbon disulphide
DCPD	: dicyclopentadiene
DMSO	: dimethyl sulfoxide
DTDL	: dibutyltin dilaurate
EAB	: 4,4'-bis(diethylamino)benzophenone
ENB	: 5-ethylidene-2-norbornene
IDPI	: isophorone diisocyanate
IMes	: 1,3-bis(2,4,6-trimethylphenyl)imidazol-2-ylidene
IMesH⁺BPh₄⁻	: 1,3-bis(2,4,6-trimethylphenyl)imidazolium tetraphenylborate
IMesH ⁺ Cl ⁻	: 1,3-bis(2,4,6-trimethylphenyl)imidazolium chloride
ITX	: isopropylthioxanthone
NaBPh ₄	: sodium tetraphenylborate
NB	: norbornene

NHC	: N-heterocyclic carbene
PA	: phthalic anhydride
PBN	: N-tert-Butyl- α -phenylnitrone
pDCPD	: polydicyclopentadiene
PEG ₄₀₀	: polyethylene glycol 400 g·mol ⁻¹
pENB	: poly(5-ethylidene-2-norbornene)
Ph ₂ BOH	: diphenylboric acid
PMND	: phenylmercury neodecanoate
pNB	: polynorbornene
PR	: phenol red
Ru-1	: dichloro(<i>p</i> -cymene)ruthenium(II) dimer
Ru-2	: diiodo(<i>p</i> -cymene)ruthenium(II) dimer
Ru-3	: dichlorodi- μ -chlorobis[(1,2,3,6,7,8- η -2,7-dimethyl-2,6-octadiene-1,8-diyl)]diruthenium(IV)
SIMes	: 1,3-bis(mesityl)imidazolidin-2-ylidene
SIMesH⁺BPh₄⁻	: 1,3-bis(mesityl)imidazolium tetraphenylborate
THF	: tetrahydrofuran
TPO	: diphenyl(2,4,6-trimethylbenzoyl)phosphine oxide
TX	: thioxanthone

Characterization techniques

AFM	: atomic force microscopy
CPMAS ¹³ C NMR	: cross-polarization magic angle spinning nuclear magnetic resonance
DSC	: differential scanning calorimetry
EPR	: electron paramagnetic resonance
FT-IR	: fourier-transform infrared spectroscopy
GC-MS	: gas chromatography–mass spectrometry
LFP	: laser flash photolysis

Maldi-ToF	: matrix-assisted laser desorption/ionization
SEC	: size-exclusion chromatography
SEM	: emission scanning electron microscopy
TGA	: thermogravimetric analysis
UV	: ultraviolet
<u>Others</u>	
ΔG_{et}	: the energy change for photoinduced electron transfer process
BET	: back electron transfer
D	: polydispersity
E_{T}	: triplet energy
k_{q}	: quenching rate constant
LED	: light-emitting diode
M_{n}	: number average molecular weight
M_{w}	: weight average molecular weight
PET	: photoinduced electron transfer
PhotoROMP	: photochemically activated ring-opening metathesis polymerization
ROMP	: ring-opening metathesis polymerization
$T_{10\%}$: temperature at which 10 % weight loss
T_{g}	: glass transition temperature
T_{max}	: temperature at which maximum weight loss
wt%	: weight percent
δ	: chemical shift
ε	: extinction coefficient

TABLE OF CONTENTS

CONTENT	Page
GENERAL INTRODUCTION	i
ACKNOWLEDGEMENTS	v
List of Schemes.....	vi
List of Figures.....	ix
List of Tables	xv
List of Abbreviations	xvi
TABLE OF CONTENTS	xix
CHAPTER I. STATE OF THE ART	1
A LIBERATION OF N-HETEROCYCLIC CARBENES FROM LATENT PROGENITORS AND THEIR USE IN POLYMER SYNTHESIS	2
1.1 Essential features of N-Heterocyclic carbenes	2
1.1.1. Electronic structures of N-Heterocyclic carbenes.....	3
1.1.2. Stabilization of N-Heterocyclic carbenes	3
1.1.3. Synthesis of N-Heterocyclic carbenes	4
1.1.4. Principal applications of N-Heterocyclic carbenes.....	6
1.2 Liberation of NHCs from their latent progenitors	6
1.2.1. By thermal-trigger.....	7
1.2.2. By mechanochemistry.....	12
1.2.3. By photochemistry	13
1.3 Latent NHC progenitors for polymerization reactions	15
1.3.1. Ring-opening polymerization	15
1.3.2. Step-growth polymerization.....	19
1.3.3. Ring-opening metathesis polymerization	21
1.4 Conclusions.....	22
B RECENT DEVELOPMENTS IN PHOTOCHEMICALLY ACTIVATED RING-OPENING METATHESIS POLYMERIZATION	23
1.5 Catalyst activation through ligand photodissociation	24
1.6 Catalyst activation through in situ photogeneration of ligands	29

1.7	Catalyst activation through conformational change of chelated ligand.....	30
1.8	Metal-free photoROMP via photoinduced electron transfer	35
1.9	Conclusions.....	38
C	REFERENCES	39
CHAPTER II. MIXTURE OF AZOLIUM TETRAPHENYLBORATE WITH ISOPROPYLTHIOXANTHONE: A NEW CLASS OF N-HETEROCYCLIC CARBENE (NHC) PHOTOGENERATOR FOR POLYURETHANE, POLYESTER AND ROMP POLYMERS SYNTHESIS.....		
2.1	INTRODUCTION	49
2.2	EXPERIMENTALS.....	52
2.2.1	Materials	52
2.2.2	Synthesis	52
2.2.3	Characterization methods.....	54
2.3	RESULTS AND DISCUSSION	58
2.3.1	Synthesis and characterization of photogenerated NHC	58
2.3.2	Identification and quantification of photogenerated NHC.....	59
2.3.3	Insight into photochemical mechanism: coupled electron/proton transfer	63
2.3.4	Optimization of NHC yield.....	67
2.3.5	Use of NHC photogenerator in polymerization	69
2.4	CONCLUSIONS.....	76
2.5	REFERENCES	77
CHAPTER III. PHOTOREDUCTION OF TRIPLET THIOXANTHONE DERIVATIVES BY AZOLIUM TETRAPHENYLBORATE: A WAY TO PHOTOGENERATE N-HETEROCYCLIC CARBENES.....		
3.1	INTRODUCTION	84
3.2	EXPERIMENTALS.....	87
3.2.1	Materials	87
3.2.2	Synthesis of $\text{IMesH}^+\text{BPh}_4^-$	87
3.2.3	Characterization methods.....	87
3.3	RESULTS AND DISCUSSION	90
3.3.1	Assignment of transient species.....	90
3.3.2	Assignment of photoproducts	95
3.4	CONCLUSIONS.....	105
3.5	REFERENCES	105

CHAPTER IV. COMBINING A LIGAND PHOTOGENERATOR AND A RUTHENIUM PRECATALYST: A PHOTOINDUCED APPROACH TO CROSS-LINKED ROMP POLYMER FILMS110

4.1 INTRODUCTION111

4.2 EXPERIMENTALS.....113

4.2.1 Materials113

4.2.2 Experimental protocols114

4.2.3 Characterization methods.....116

4.3 RESULTS AND DISCUSSION117

4.3.1 Study and optimization of the tandem photocatalytic system117

4.3.2 Preparation of cross-linked ROMP polymer films125

4.4 CONCLUSIONS.....133

4.5 REFERENCES134

CONCLUSIONS139

APPENDIX.....141

SUMMARY IN FRENCH OF CHAPTER II, III AND IV156

Chapitre II. Mélange d'azolium tétraphénylborate avec l'isopropylthioxanthone: une nouvelle classe de photogénérateur de NHC pour la synthèse de polyuréthane, polyester et polymère de ROMP157

Chapitre III. Photoréduction d'un dérivé du thioxanthone par un sel d'azolium tétraphénylborate: Un moyen de photogénérer des N-carbènes hétérocycliques163

Chapitre IV. La combinaison d'un photogénérateur de ligand et d'un pré-catalyseur de ruthénium: une approche photoinduite pour la synthèse de film polymère réticulé par ROMP168

List of Publications173

CHAPTER I. STATE OF THE ART

The text in this chapter is reproduced in part with permission from:

E. Cao, L. Pichavant, T. K. H. Trinh, A. Chemtob, D. Quémener, J. Pinaud, V. Héroguez, “Emerging trends in ring opening metathesis polymerization”, *Macromolecular Engineering: From Precise Synthesis to Macroscopic Materials and Applications*, 2019 (Book chapter, accepted).

©Wiley-VCH 2016
69451 Weinheim, Germany

A LIBERATION OF N-HETEROCYCLIC CARBENES FROM LATENT PROGENITORS AND THEIR USE IN POLYMER SYNTHESIS

Over the last three decades, N-Heterocyclics Carbenes (NHCs) have become essential tools for chemists, either employed as ligands for organometallic complexes, thus providing better catalytic activity and stability, or as organocatalysts where they allowed expanding the scope of chemical reactions by providing unexpected chemical mechanisms. Nevertheless, their strong reactivity associated with their relative stability has humped back their use at industrial level and to some extent at academic level. Consequently, several strategies have been developed to generate them in situ and to facilitate their handling. While most of them relied on the thermal liberation of NHCs in the reaction media from a variety of progenitors, no report was made, at the start of this PhD thesis, which described the liberation of NHCs by a photochemical pathway.

In the frame of the PHOTON DROP project, one of the objectives of this PhD thesis was the determination of the photochemical mechanisms underlying the generation of NHCs under UV irradiation from various progenitors. The photogenerated NHCs could then be employed for the catalysis of different polymerization reactions thus bringing temporal control and potentially spatial control. Consequently, after a brief description of the main features of NHCs, this bibliographic chapter will provide a comprehensive overview of the different strategies that have been employed to generate NHCs in a reaction media through the trigger of an external stimulus. Furthermore, the success in polymer chemistry of previous latent systems is also discussed and has been a source of inspiration to expand the scope and potential applications of our well-designed photolabile NHCs.

1.1 Essential features of N-Heterocyclic carbenes

Carbenes are defined as neutral compounds featuring a divalent carbon atom and a six-electron valence shell (**Figure 1.1**).¹ The best-known and simplest carbene sought to date is methylene, :CH_2 . Despite pioneered as early as 1835,² attempts to isolate carbenes remained fruitless, due to their elusive nature such as high reactivities and short life-times, until the ground-breaking works of Bertrand *et. al.*³ and Arduengo *et al.*⁴

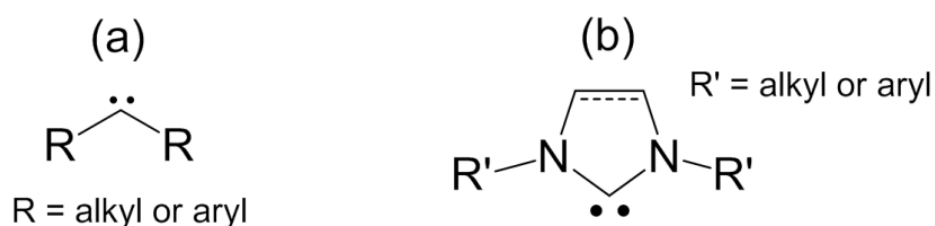


Figure 1.1. General structure of: (a) conventional carbenes and (b) Arduengo carbenes.

1.1.1. Electronic structures of N-Heterocyclic carbenes

According to Heinemann *et al.*⁵ and Carter *et al.*,⁶ the usual reactivity of free and uncoordinated carbenes depends primarily on the electronic configuration of their non-bonding electrons.^{1,7} Within this criterion falls two classes of carbenes, conventionally termed as singlet and triplet carbenes. In the singlet ground state, the two unpaired electrons only occupy a sp^2 hybridized orbital of the sp^2 hybridized carbon center (HOMO) (**Figure 1.2**). Whereas, in the case of triplet carbene, each of the non-bonding electrons occupy either a sp^2 or a p_π orbital, bearing a parallel or an antiparallel spin orientation (SOMO).^{1,7,8} Consequently, these ground-state electronic configurations drive towards carbene's reactivity. While the singlet carbenes possess an ambiphilic behavior, their triplet cousins are regarded as diradicals.^{1,9} However, it is known that singlet carbenes are much more stable than the triplet species.¹⁰

N-heterocyclic carbenes are a specific form of the singlet carbenes; therefore, they bear both a filled sp^2 orbital and an empty p_π orbital.¹¹

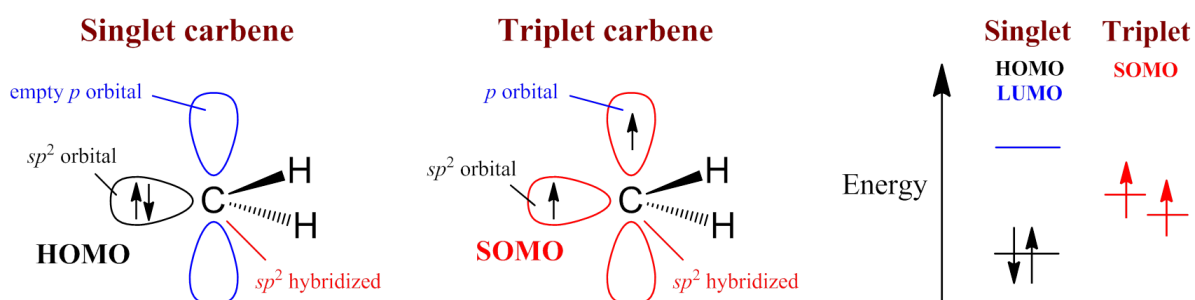


Figure 1.2. General ground-state electronic features of singlet and triplet carbenes. Arrows: electrons.

1.1.2. Stabilization of N-Heterocyclic carbenes

The pioneering work of Arduengo⁴ describing the first synthesis and isolation of a bare NHC has paved the way for an enormous amount of studies on NHCs properties and reactivities. In particular, it provided strategies to avoid unexpected reactions during NHC synthesis such as NHCs dimerization. Shedding light into their structural features, NHCs are stable and isolable due to the electronic and steric effects of *N*-substituents. According to Bertrand *et al.*,³ most stable NHCs, standing out in singlet state, are stabilized by a combination of σ -electron withdrawing and π -electron donating properties of adjacent nitrogen atoms (**Figure 1.3**). Both these inductive and mesomeric effects induce respectively a decrease in energy of the sp^2 orbital, and a raise in energy of the unoccupied p_π orbital. This leads to an increase of the energy band-gap between the singlet and triplet forms which governs the excellent properties of NHCs such as high stability, nucleophilicity and σ -

donating ability. On the other hand, the architecture of *N*-substituents also has an impact on the NHC stabilization.¹ Introducing bulky R groups is a key factor to achieve stable monomeric NHCs owing to increased steric shielding.^{7,12}

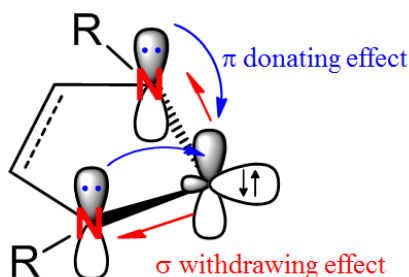


Figure 1.3. Stabilization of NHCs via electronic push-pull effect. Arrows: electrons.

Consequently, the first isolation of a NHC was made possible through the incorporation of a bulky adamantane on α -amino substituents of the carbene center. Since this outstanding achievement, it brought an explosion of investigations on properties and applications of divergent NHCs.¹³ Among the different structural motifs (**Figure 1.4**), the five-membered rings, imidazolinyliene (**1**) and imidazolylidene (**2**), have been widely used, for instance in organometallic chemistry and in the field of organocatalysis. When serving as ligands, the NHCs are able to enhance stability and reactivity of transition metal complexes for two reasons. Firstly, the great σ -donor ability of C^2 carbon brings strong binding to the metal centers. Secondly, simple modulation of *N*-substituent architectures eases to turn and optimize the reactivity and hindrance of the carbene center.^{14,15} Thanks to their high nucleophilicity and Brønsted basicity, NHCs have also proven to be powerful tools to mediate organic transformations^{16,17} and polymerizations,^{18,19} potentially reducing cost and toxicity in comparison to organometallic catalysts.

1.1.3. Synthesis of N-Heterocyclic carbenes

Because of their strong nucleophilicity and basicity, NHCs are highly sensitive to moisture and to substrates, which limits their use as bare compounds.^{13,20,21} Thus, several strategies to generate NHC in solution have been reported so far. The most common method is the deprotonation in aprotic solvent of the corresponding azolium salt precursors upon contact with a suitable strong base (**Scheme 1.1a**).^{11,13,22} A wide range of bases with high pK_a ($pK_a \geq 14$), such as $KOt\text{-Bu}$,²³ potassium hydride²⁴ and 1,8-diazabicyclo[5.4.0]undec-7-ene (DBU)^{25,26} have been used to accelerate the proton transfer at C^2 position.

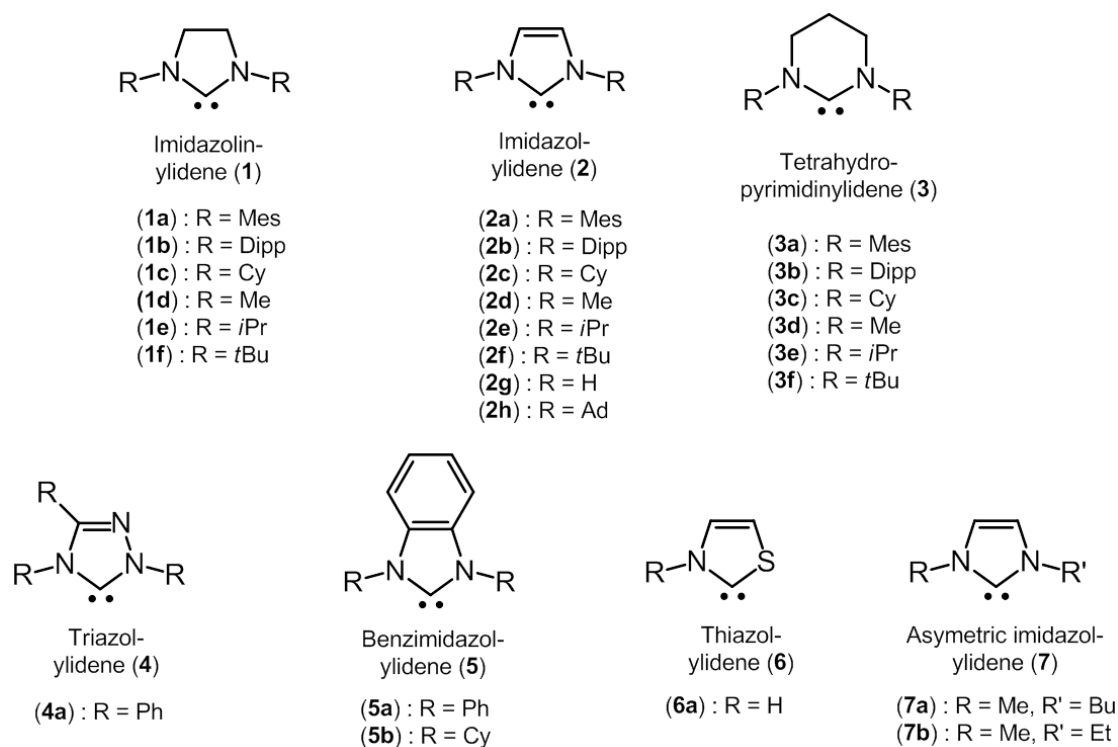
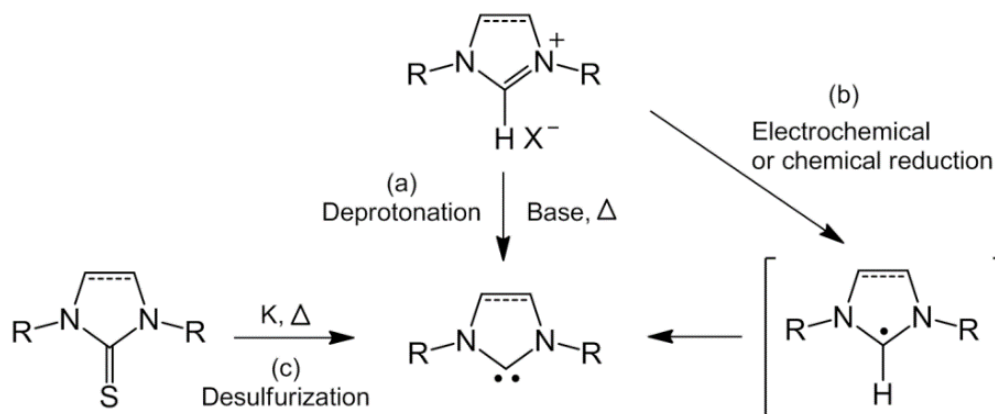


Figure 1.4. Chemical structures and nomenclatures of main classes of NHCs.²⁷

Another option to produce free carbenes is the electrochemically or chemically driven reduction of azolium salts (**Scheme 1.1b**).^{20,28} In both of these synthetic methods, NHCs are revealed via the cleavage of a hydrogen radical from a transiently formed radical $[\text{NHC-H}]^\bullet$. Generally, the latter is generated by activating the azolium salt either electronically or in the presence of an excess of potassium. Other alternative NHC precursors are thione compounds, undergoing thermal-induced desulfurization in molten potassium (**Scheme 1.1c**).²⁹ Here, the insoluble potassium sulfide can be filtered off and thereby allows obtaining the free NHC in high yield. In all synthetic routes, the NHC precursors, which are commercially available or easy to prepare, are very stable. Thus, they can be stored for long periods prior to use.



Scheme 1.1. General approaches to produce NHCs.^{13,20,28,29}

Finally, when NHCs have to be employed in the presence of substrates that are sensitive to strong bases, NHCs can be also generated in the reaction media from air-stable stimuli-responsive progenitors. Their synthesis and use, in particular for polymerization reactions, have been the subject of an intense research over the past 10 years and will be the subject of part 1.2 and 1.3 of this bibliographic report.

1.1.4. Principal applications of N-Heterocyclic carbenes

As ancillary ligands, NHCs have been found to be stronger σ -donating and less π -accepting as compared to their neighbor analogues such as phosphine. These two features allow for both an improved stability and catalyst efficiency of NHC-metal analogues, making them nowadays at the forefront of organometallic chemistry.^{15,30} To date, the most prestigious utility of NHCs ligands is perhaps in the well-defined Grubbs' family catalysts, where the labile phosphine ligands were substituted by the persistent NHCs **1a** or **2a**. Displaying air-stability and outstanding efficiency, these catalysts have become crucial synthetic tools for metathesis reactions.^{1,13,31,32} More recently, Pd complexes with mono coordination of **2a** or **2c** have shown remarkable catalytic activity in various C–C and C–N cross-coupling reactions.^{31,33} On the other hand, NHCs have also contributed to surface functionalization of nanoparticles with respect to stabilization and control of morphologies.^{34–37}

Besides being employed as ancillary ligands, NHCs have emerged as powerful organocatalysts in a variety of Umpolung and coupling reactions because of their strong nucleophilic character.^{16,22} In particular, they are well suited to drive the polymerization of a number of common monomers, including lactones,³⁸ epoxides,³⁹ siloxanes,⁴⁰ cyclic anhydrides,⁴¹ N-carboxyanhydrides⁴² (via ring-opening polymerization (ROP)), (meth)acrylic monomers⁴³ (via group transfer polymerization (GTP)), and isocyanates and polyols⁴⁴ (via step-growth polymerization). By simply washing or using trapping agents, the NHCs are easily separated from resultant polymers, thus leading to reduce costs and toxicity for use in the polymer industry.

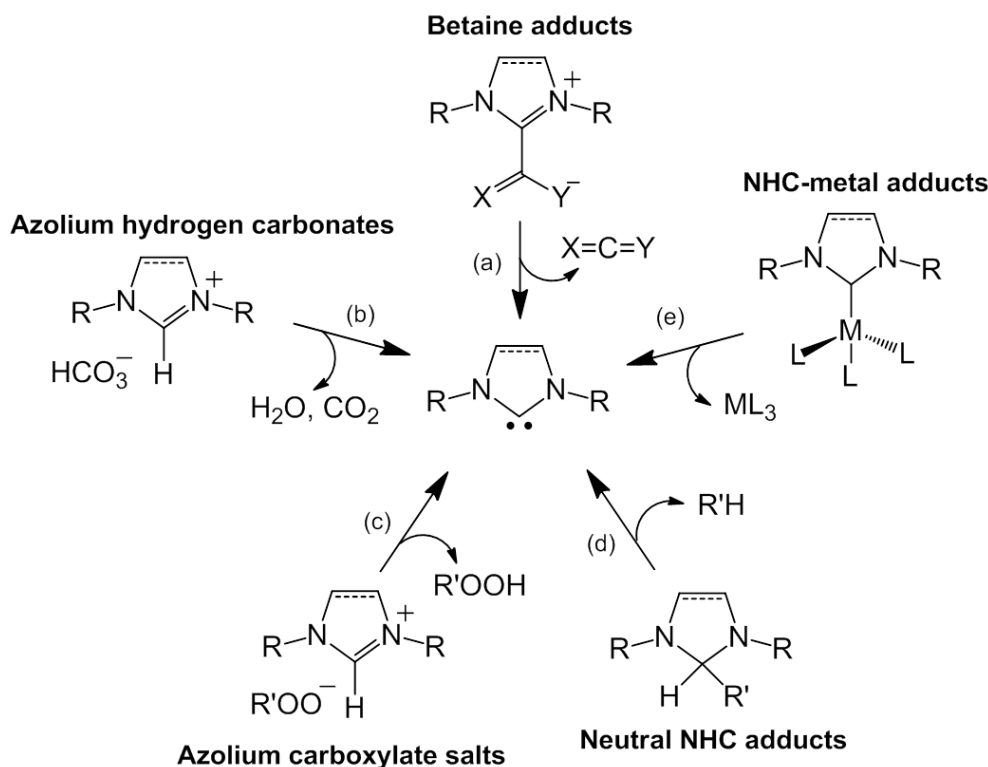
1.2. Liberation of NHCs from stimuli-responsive latent progenitors

Despite being known as one of the most popular methods to produce NHCs in situ, use of strong bases to deprotonate azolium cations retains some problems when regarding organic or macromolecular reactions. The key issues have been identified as (a) the need of harsh experimental conditions (anhydrous aprotic solvent, inert atmosphere), (b) the presence of bases/ protonated bases residues, which can be either reactive to some sensitive substrates

or competitive to generated NHCs, and (c) the difficulties in final product purification. To overcome these drawbacks, many chemists have turned their scope of research towards the development of latent NHC progenitors that can generate the free NHCs upon application of a stimulus (temperature, ultra-sound, light). Among them, thermo-latent NHC progenitors (**Scheme 1.2**) that can regenerate the free NHCs by heating have been certainly the most studied.

1.2.1. By thermal-trigger

One of the main advantages of utilizing thermo-latent NHC progenitors is the temporal control brought to the polymerization reaction. By simply alternating temperature, the reaction can successively undergo on/off state “on demand”. Furthermore, when using these compounds it does not only avoid drawbacks resulting from incomplete mixing, but also allows reactions to be performed in a one-pot process. According to the “blocking groups” used, protected NHCs can be divided into 5 typical categories: (a) betaine adducts, (b) azolium hydrogen carbonate, (c) azolium carboxylate salts, (d) neutral NHC adducts and (e) NHC-metal adducts (**Scheme 1.2**).⁴⁵ Eventually, the thermolysis of these adducts leads to the formation of by-products that can strongly affect the activation and growth of polymer chains (in a positive or negative manner depending on the by-product).



Scheme 1.2. Principle thermal liberation of NHCs from their corresponding precursors.

a. Betaine adducts

Protecting free NHCs by heteroallene species of general formula $X=C=Y$ to afford corresponding betaine adducts is a common strategy to produce thermo-latent NHC progenitors shown in **Figure 1.5**. With a weak electrophilic carbene atom, heteroallene are indeed subject to the nucleophilic attack of the carbene of NHCs.⁴⁶ It has been proven that the stability of such complexes is significantly dependent on the heteroallene nature with, for example, the degradation temperature of crystal adducts derived from **2h** increasing in the order: **2h.CO₂** (110 °C) < **2h.COS** (140 °C) < **2h.CS₂** (210 °C).⁴⁷ **2h.CO₂** and **2h.COS** can readily dissociate upon heating in the solid state, while the highly stable **2h.CS₂** adduct degrades entirely without affording its parent NHC **2h** after onset of thermolysis.

Like typical NHC betaine adducts mentioned above, the lability of NHCs-isothiocyanate zwitterionic compounds (**Figure 1.5d**) decreases with the electron-donating properties of moieties (R' = aryl or alkyl) present onto the isothiocyanates.^{45,48} On the other side, when protected by the same heteroallene molecule like CO₂, the adduct degradation is decisively influenced by both solvent polarity and steric hindrance of *N*-substituents of the azolium part.^{49–51} Besides, large and bulky substituents on N atoms flanking the C² carbon lead to an increase of steric pressure on C_{carbene}–CO₂ bond compared to less bulky substituents. That results in reduce conjugation and subsequently in a rise of temperature dissociation of carbon dioxide. For example, **2f.CO₂** begins to lose its CO₂ moiety at 71 °C, **2e.CO₂** at around 140 °C, whereas **2d.CO₂** is stable up to 162 °C.⁵²

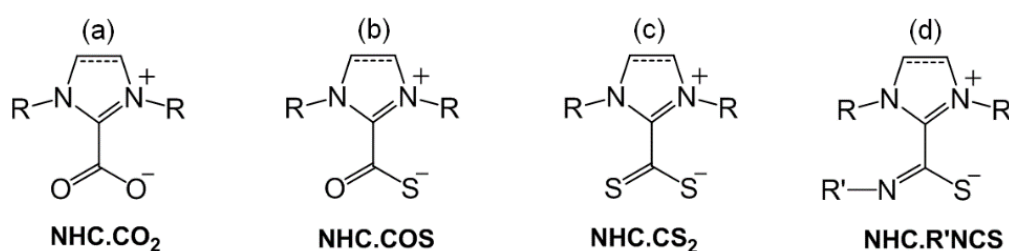
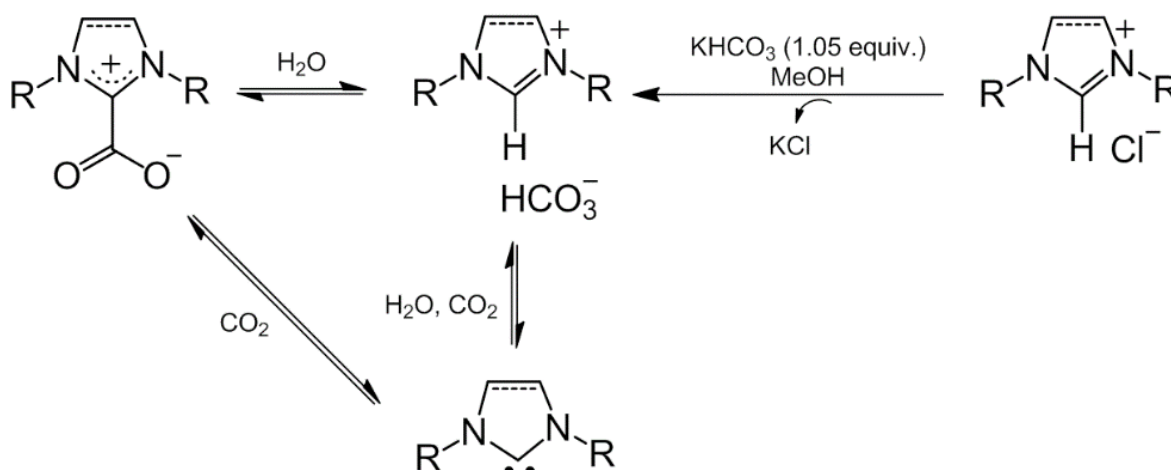


Figure 1.5. Chemical structures of common betaine adducts.

Thanks to the innocuity and abundance of carbon dioxide, NHC-CO₂ complexes are the most employed compounds to generate NHCs in a reaction media, either to be used in the formation of organometallic complexes, or as organic catalysts. Nevertheless, they are prone to hydration upon storage under air for a long time, resulting in the formation of azolium hydrogen carbonate salts. As discussed below, the latter are also able to generate NHC upon thermolysis, although much higher temperatures are required than compared to their NHC-CO₂ counterparts.

b. Azolium hydrogen carbonates

Azolium hydrogen carbonates, denoted as $[\text{NHC}(\text{H})][\text{HCO}_3]$, are special azolium salts enabling access to free NHCs upon heating that have been reported recently.^{43,53} Two facile routes are described to prepare $[\text{NHC}(\text{H})][\text{HCO}_3]$ salts (**Scheme 1.3**). The first one is *via* hydrolysis of $\text{NHC}\cdot\text{CO}_2$ adducts; whereas the other relates to an anion metathesis process between azolium halides and KHCO_3 , thus avoiding the necessity of NHCs generation prior to be masked by CO_2 .



Scheme 1.3. Schematic preparation of $[\text{NHC}(\text{H})][\text{HCO}_3]$ using $\text{NHC}\cdot\text{CO}_2$ adducts and azolium halides and reversible release of corresponding NHCs therefrom.

These adducts are very robust and can be stored under ambient conditions without special precautions. Based on TGA experiments and DFT calculations, Taton *et al.*^{43,53,54} have demonstrated that the temperature activation of these NHC-precursors (generally higher than $100\text{ }^\circ\text{C}$) causes a formal loss of H_2O and CO_2 . Similarly to $\text{NHC}\cdot\text{CO}_2$ adducts, the temperature degradation can be altered by varying *N*-substituents of azolium cations. Eventually, a challenge coming from the use of these NHC salts is the elimination of H_2O during thermolysis, otherwise causing the hydrolysis of free NHC or the termination of several reactions. To avoid such side reactions, $[\text{NHC}(\text{H})][\text{HCO}_3]$ have often been employed in combination with molecular sieves to trap the released water and eventually drive the release of the NHCs.

c. Azolium carboxylate salts

Alternatively, azolium carboxylate salts, referred to $([\text{NHC}(\text{H})][\text{R}'\text{OO}])\text{s}$, have been widely used as a reservoir of NHCs in many fields of chemistry.⁵⁵⁻⁵⁷ According to Taton *et al.*⁵⁶⁻⁵⁸ and Sander *et al.*,⁵⁹ the carboxylate counter-anions with a slightly basic character such as acetate and *bis*-carboxylate anions are able to deprotonate azolium cation as activated by

simple heating. It drives to the spontaneous formation of NHCs and carboxylate acids on demand. Besides, recent studies ruled out the influence of solvent and suggested that the deprotonation is favored in a non-polar or weakly polar environment.^{60,61} For the preparation of $[\text{NHC}(\text{H})][\text{R}'\text{OO}]$, the carboxylate anion is easily incorporated into the ionic liquid motifs after an anion metathesis process⁵⁶ or a simple anion-exchange reaction from the corresponding azolium halide salts.⁵⁷

d. Neutral adducts

Due to inherent electron-donating properties, the nucleophilic center of NHCs can insert into a labile $\text{R}'\text{-H}$ bond of organic species such as chloroform, pentafluorobenzene and alcohols, allowing obtaining neutral adducts (**Figure 1.6**).^{45,62} Such compounds are capable of providing a facile entry to the preparation of NHC-metal complexes because it avoids the need of working under air-free conditions. However, some downsides when using these adducts have also been found. As a matter of fact, full latency of these adducts was only obtained in rare cases with weak Brønsted-basic NHCs or high- $\text{p}K_{\text{a}}$ alcohols, where the NHC/alcohol interaction stands in the direction of adduct formation. Most of them were less stable in solution, gradually releasing free NHC and protecting species even at low temperatures. For example, **1a.MeOH** adduct dissociates entirely after 10 min at 25 °C, while **4a.MeOH** requires higher temperature to fully release NHCs **4a** (80 °C, 16h).⁶³ Another disadvantage is the production of alcohol during thermolysis of NHC-alcohol adducts which can be restrictive for using with low-oxophilic metal or in anionic polymerization.

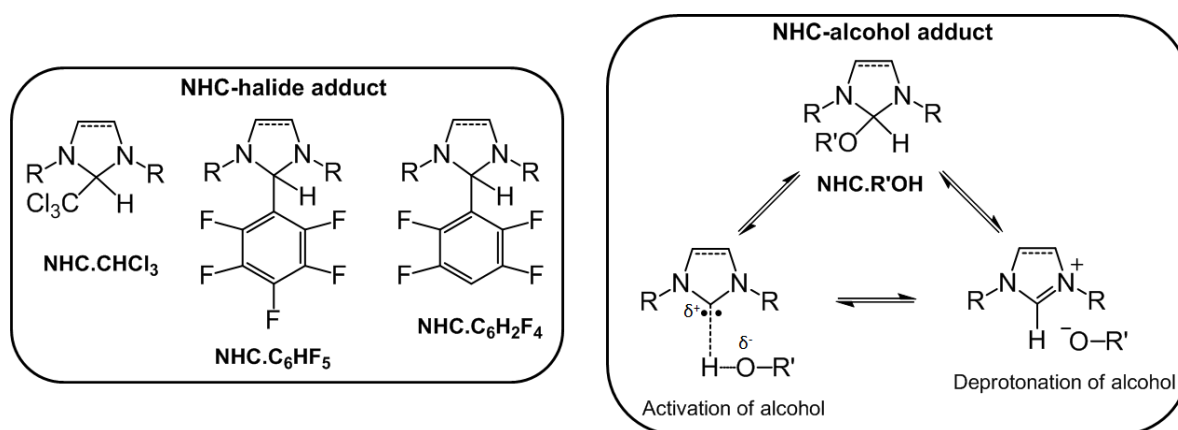


Figure 1.6. Chemical structures of thermal latent NHCs protected by organic compounds halogenated and alcohols.^{45,62}

e. NHC-metal adducts

In recent studies, halogenated metal complexes have been used to mask NHCs resulting in the formation of NHC-metal adducts (**Figure 1.7**), which are highly air- and moisture-stable and inactive for catalysis at room temperature.^{45,64}

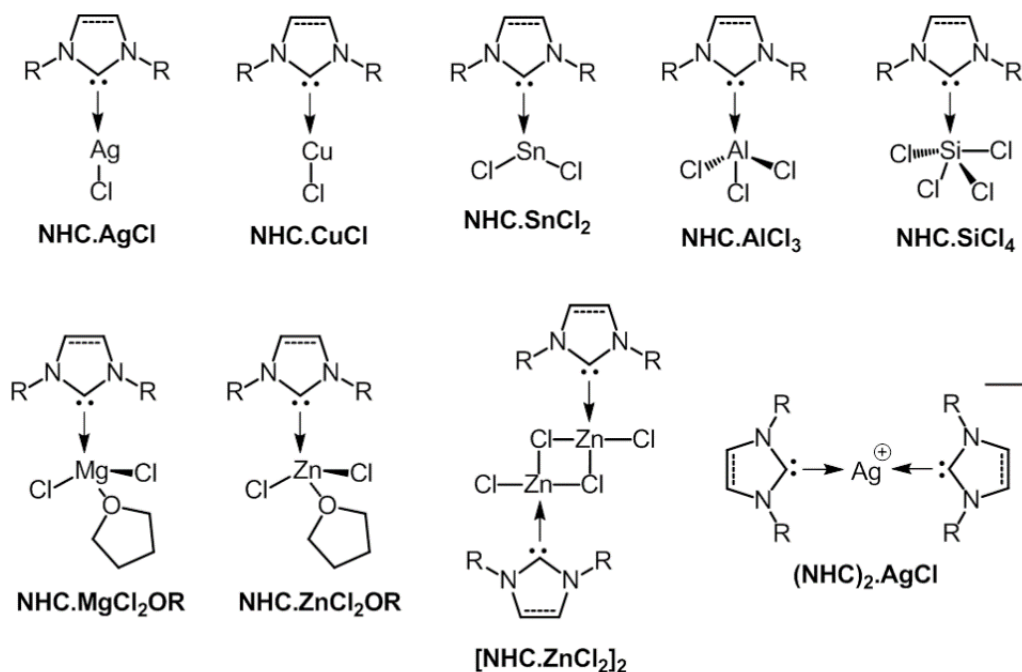
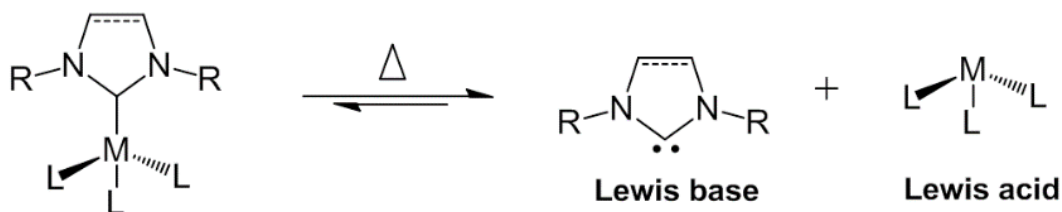


Figure 1.7. General air stable NHC-metal precursors.^{45,64}

Despite the drawback of introducing metal residues in the reaction media, which can be detrimental for biomedical and microelectronic applications, there are two attractive features driving the development of such NHC-metal species. First, there is a variety of inexpensive and non-toxic halogenated metal compounds that can serve as alternative protecting sources of NHCs. Second, at elevated temperatures, such complexes with low binding energy, can equally dissociate into free NHCs (Lewis bases) and metal ions (Lewis acids), providing respectively a nucleophilic and an electrophilic activation of the substrate which results in enhanced catalytic activities. In addition, proper recombination of these Lewis acids/bases at low temperatures provides an effective control of catalytic activity (**Scheme 1.4**).

NHC-metal adduct



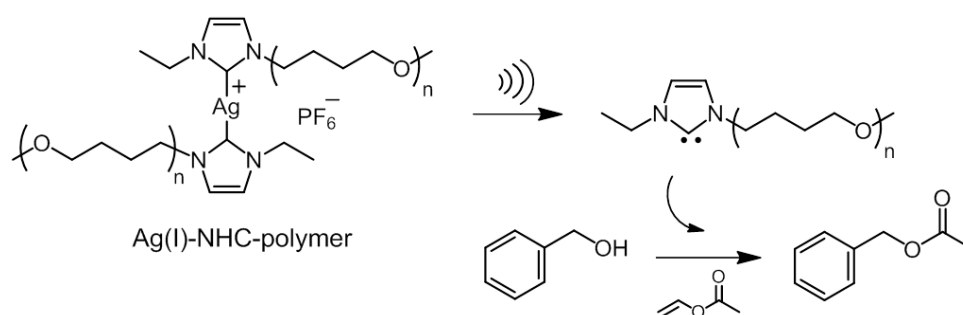
Scheme 1.4. Thermal-triggering liberation of NHC-supported metal ions.⁴⁵

These coinage NHC-metal complexes are very facile to synthesize outside a glovebox via one-step reaction between metal precursors and two major latent NHC progenitors, azolium salts and $\text{NHC}\cdot\text{CO}_2$.^{31,45} Among the various NHC-metal compounds, NHC-Ag

complexes have attracted much interest in a variety of applications such as transmetalation agents in organometallic chemistry, luminescent materials and homogeneous catalysis.^{15,35,45}

1.2.2. By mechanochemistry

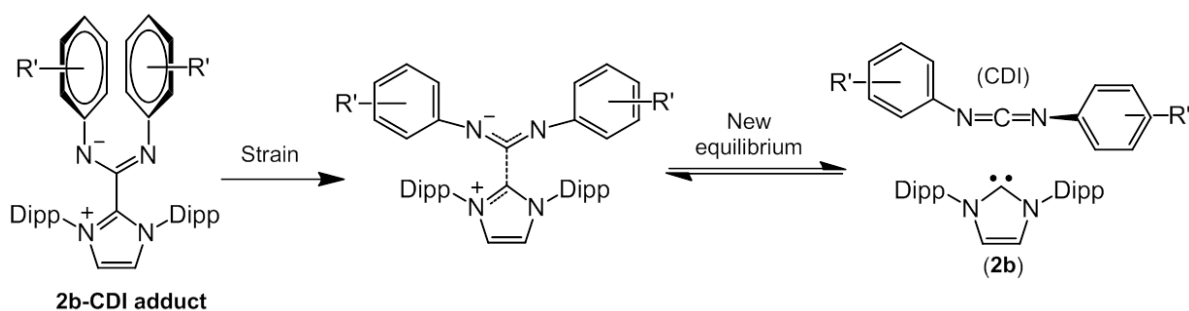
The “mechanochemistry” is recognized as a green method that can activate transformation of covalent bonds based on the use of mechanical energy such as compression, shear, vibration or friction.⁶⁵ Recently, Sijbesma *et al.*^{66–68} used ultrasound to apply mechanical forces to an Ag(I)-NHC-polymer compound inside a reaction media. The high fluid strain caused by the rapid collapse of cavitation bubbles allowed breaking of the dative NHC-Ag bond thus liberating the free NHC to catalyze transesterification reactions (**Scheme 1.5**). In a subsequent contribution, the authors demonstrated that an increase of the molecular weight of the polymer chain attached to the NHC moiety allowed for the increase of the free NHC in the reaction media for the same time of sonication. It has also been shown that the use of sonication can cause the generation of radicals, leading to deactivation of active NHC species. However, this phenomenon can be suppressed by the use of methane as saturation gas.



Scheme 1.5. Ultrasound activation of Ag(I)-NHC-polymer complex and subsequent transesterification catalyzed by NHC formed in situ.

Bench-stable amidinate adducts resulting from the reaction between NHCs and carbodiimides (CDIs) exist in the bound form under ambient conditions.⁶⁹ Unlike betaine adducts, the amidinates-NHC adducts are thermally very stable and thus unable to serve as NHC precursors. However, Larsen *et al.* reported that the NHC-CDI adducts are capable of in situ generation of the free carbenes upon activation by an external force.⁷⁰ Shedding light on the mechanism, the reorganization of CDI moiety can cause the disruption of the central **2b**-CDI C-C bond and then reversibly release the desired NHC **2b** (**Scheme 1.6**). In their work, the geometry change of amidinate can be achieved by incorporating CDI portion at specific

point along the polymer backbone able to channel elongational force distribution. The presence of **2b** was confirmed by trapping with a second CDI.

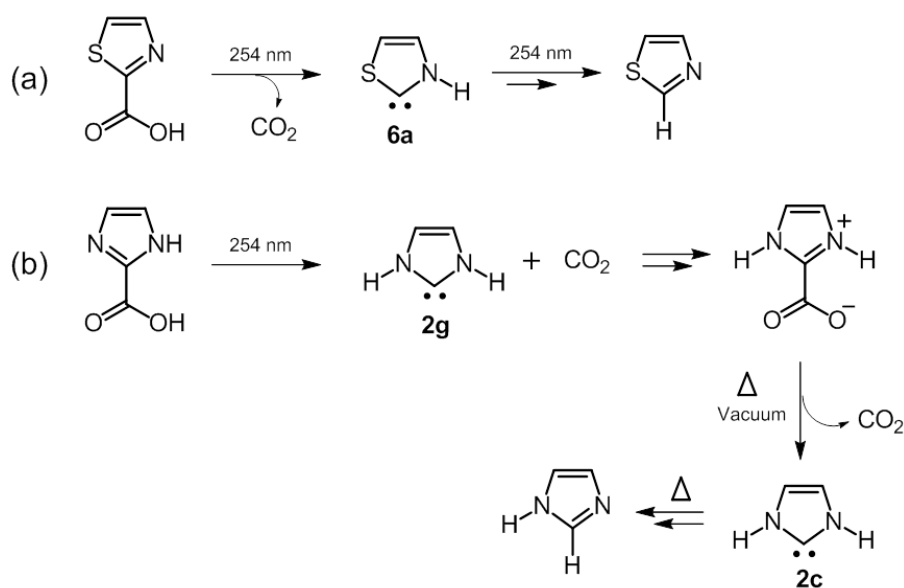


Scheme 1.6. Schematic depiction of the external force induced geometry change of NHC-CDI amidinate followed by liberating the free NHC.

1.2.3. By photochemistry

Though not practical from a synthetic chemist point of view, Endres *et al.*^{71,72} have pioneered photolabile NHCs by revealing the formation of 2,3-dihydrothiazol-2-ylidene (**6a**) and 2,3-dihydroimidazol-2-ylidene (**2g**) upon photolysis of their corresponding carboxylic acids under 254 nm UV-light and at a temperature of 10 K (**Scheme 1.7**). Unexpectedly, these primary NHC products (**6a** and **2g**) reacted instantly with carbon dioxide giving air-stable crystals, **NHC.CO₂**. Furthermore, both **6a** and **2g** were sought to easily isomerize upon warm-up or exposure to light, making their trapping unsuccessful, even when handled under vacuum.

A series of photolabile NHCs containing protonated NHCs and carboxylated-fragment chromophores such as ketoprofenate (Keto⁻), xanthate (Xanth⁻) and phenylglyoxylate (PA⁻) (**Figure 1.8**) has been recently designed by Placet *et al.*⁷³ Subjecting these photogenerator NHCs at 254 nm and 365 nm enables to photorelease the desired NHCs via photoinduced electron transfer (PET) followed by decarboxylation and proton transfer (**Scheme 1.8**). Herein, the carboxylated-functional chromophores behave as both electron donor and acceptor. Moreover, the irreversible decarboxylation avoids the back electron transfer (BET) and therefore increase the yield of generated NHCs. One main drawback of such motifs is the need to work under vacuum conditions in order to remove generated CO₂ and then avoid the formation of insoluble NHC.CO₂ adducts.



Scheme 1.7. Schematic generation of free carbene based on NHC-carboxylic acids.

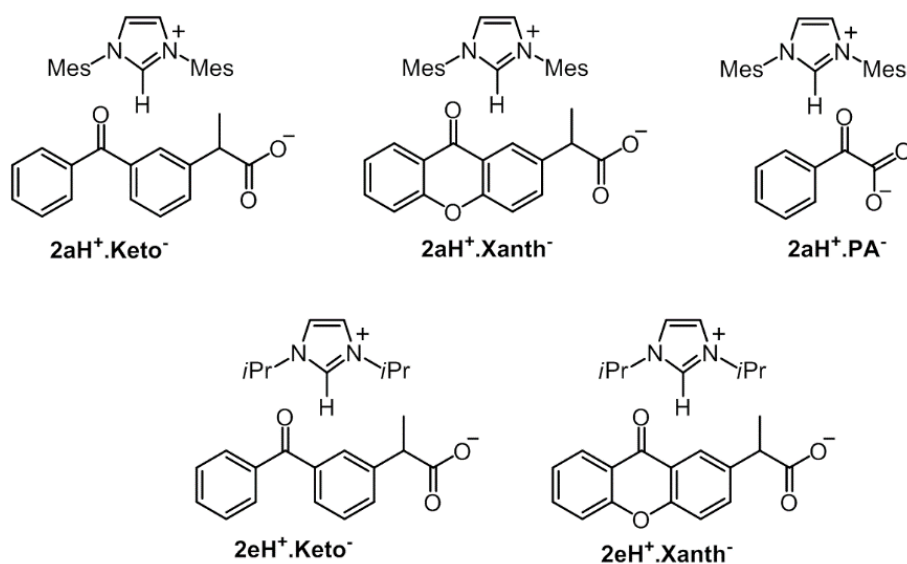
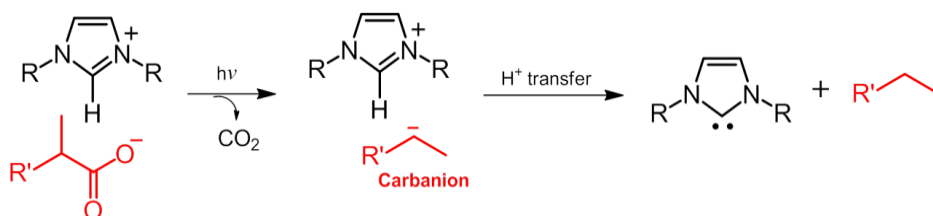


Figure 1.8. A range of novel photogenerator NHCs based on decarboxylation.



Scheme 1.8. General mechanism of generation of NHCs involving photoinduced decarboxylation accompanied by proton transfer.

1.3. Latent NHC progenitors for polymerization reactions

NHCs have been figured as exceptionally versatile tools for the preparation of macromolecular architectures.^{22,74,75} In recent years, the use of latent NHC progenitors has significantly increased, mainly due to its ability in switching on NHCs' catalysis in situ when required. Thereby, the following discussion emphasizes on valuable achievements and problematic findings when these latent systems are employed in polymer syntheses. It provides also a desirable source of inspiration for perspective applications of our NHCs photogenerators.

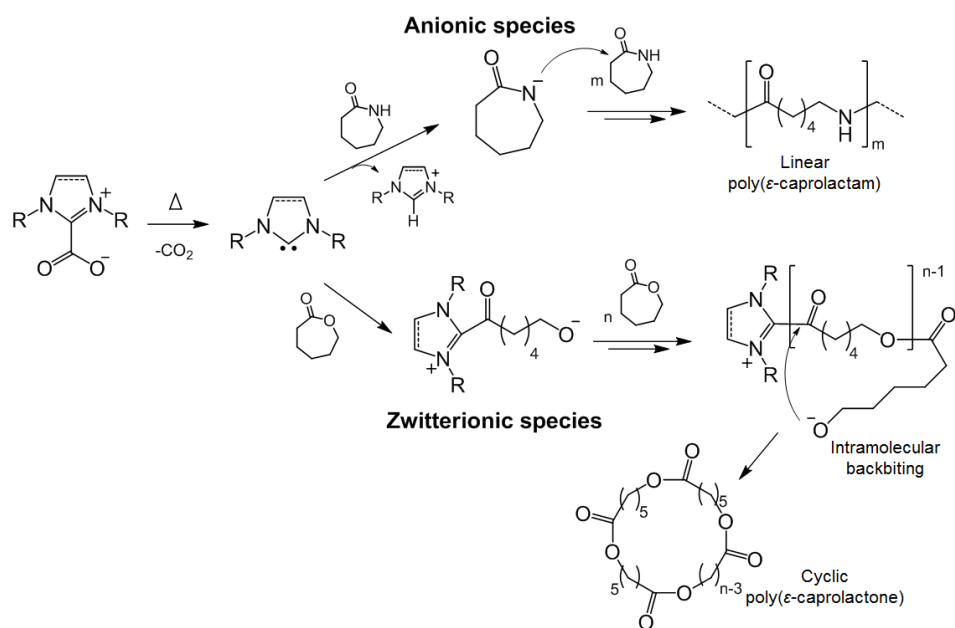
1.3.1. Ring-opening polymerization

a. ROP of cyclic esters and cyclic amides

Among the prolific research studies that have been conducted on organic catalysis for ring-opening polymerization (ROP) of cyclic esters, employing NHCs as organocatalysts has proven to be a powerful strategy to obtain polyesters with various architectures. To facilitate NHC handling and polyester synthesis, some of this work has focused on the development of latent NHC catalysts. Hedrick *et al.*⁶² presented a range of NHC-chloroform and NHC-pentafluorobenzene adducts which can eliminate saturated NHC by thermolysis. These adducts are effective to induce ROP of *L*-lactide in the presence of benzyl alcohol as co-initiator at temperature as low as 65 °C, thus generating narrowly dispersed polylactides in high yield.

With the aim at liberating NHC at lower temperatures, a new series of thermo-latent NHCs in the form of alcohol adducts of **1a** was then prepared by the same group.⁷⁶ While being air-stable solids at ambient conditions, these compounds rapidly decompose at 25 °C in solution to release **1a** as well as different alcohols in a reversible manner. Accordingly, when employed for the ROP of lactide, they generated effective single-component catalysts/initiators, resulting in a complete consumption of the monomer within minutes. In following studies, Hedrick *et al.*⁶³ used **4a.MeOH** adduct to provide a facile entry to ROP of lactide and β -butyrolactone “on demand” by controlling the temperature. However, due to the remarkable stability of the **4a.MeOH** species, the polymerization process required long periods of time to obtain quantitative monomer consumption at 90 °C. This certainly reveals the difficulty to achieve latent catalysts exhibiting pronounced latency at ambient conditions and high activity when triggered.

To improve this situation, a wide range of NHC.CO₂ adducts acting as thermally latent precatalysts were applied in bulk polymerization of lactide,⁷⁷ lactones (ϵ -caprolactone and β -butyrolactone)^{64,77} and lactams (ϵ -caprolactam and laurylactam).⁷⁸ As desired, when mixed with initiators and monomers, some of the NHC.CO₂ species (**1f**.CO₂, **2f**.CO₂, **3c**.CO₂ and **3e**.CO₂) acted as truly latent catalysts at low temperature, while by simple heating, polymerization occurred swiftly and in a controlled manner. According to Hedrick *et al.*, the in situ generated NHCs behave as nucleophilic agents, thus driving the ROP in two different mechanisms: (i) a monomer activated mechanism (zwitterionic or anionic) when alcohol initiators are absent from the reaction media (**Scheme 1.9**) and (ii) chain-end activated mechanism in the presence of protic species (alcohol) (only for lactones and lactide) (**Scheme 1.10**).^{63,64,77,78} Success in ROP of these monomers highly depends on the ring size and *N*-substituents of the initiating NHC. For example, in the synthesis of polyamides, when using six-membered NHCs behaving as stronger Brønsted bases than their five-membered ring counter-parts, high yield (85%) production of polycaprolactam was accessible within relative short reaction times of 45 min at 180 °C. In contrast, only 62% yield were achieved in the same conditions upon employing their five-membered counterparts.^{78,79}

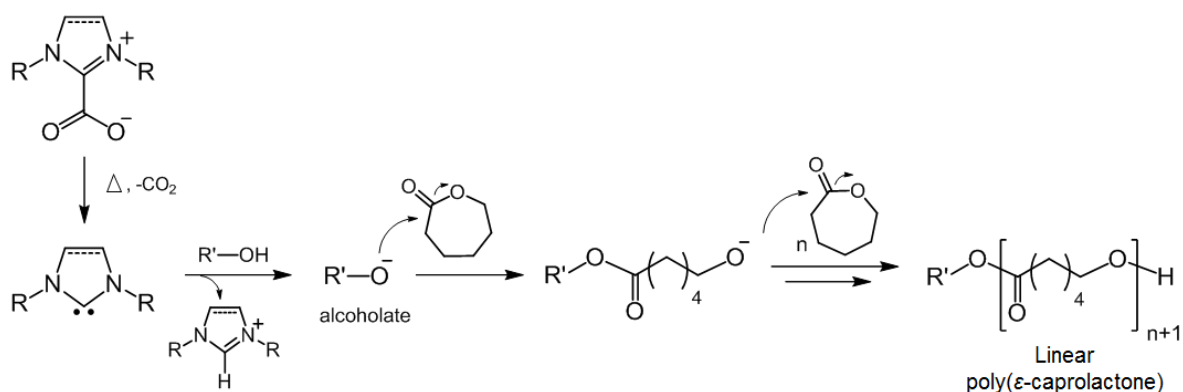


Scheme 1.9. Schematic representation of monomer-activated ROP of lactam and lactone mediated by NHC.CO₂ precursors.

On the other hand, Kuckling *et al.* focused on using, for the first time, the NHC.CO₂ progenitors for the ROP of trimethylene carbonate (TMC) in bulk and in different solvents.⁸⁰ As a result of the solvation effect, active NHCs are readily available in TMC/solvent mixture

even at ambient conditions. Thus, the ROP can proceed at relative low temperature. When **2a.CO₂** is employed, the best control over molecular weight and polydispersity of the resulting polymer was achieved in less polar solvent CH₂Cl₂ at 60 °C.

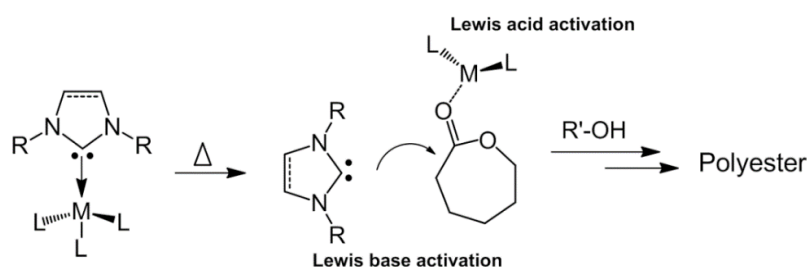
Highly moisture-stable [NHC(H)][HCO₃] salts, which are hydrolyzed products of NHC.CO₂ adducts, have also been utilized as precatalysts for the ROP of *D,L*-Lactide and ϵ -caprolactone in THF.⁴³ Molecular sieves were systematically introduced in the reaction media to drive the NHC release by removing generated H₂O (byproduct) and to avoid deactivation of the NHC as well as quenching of propagating species. These [NHC(H)][HCO₃] adducts displayed good efficacy but much lower catalytic activity than the NHC.CO₂ moieties bearing the same parent NHCs.^{43,45} Upon using [**5b(H)**][HCO₃] at 25 °C, after only 5 min, the best polymerization of *D,L*-Lactide was obtained with a high turnover frequency, TOF = 1555 h⁻¹, and a conversion of 96 %. The high catalytic activity observed at 25 °C can be attributed to solvation effect in the generation of NHC.



Scheme 1.10. Schematic representation of chain-end activated ROP of lactone mediated by NHC.CO₂ precursors.

Naumann *et al.* also got interested in the ROP of lactone using thermolatent NHCs progenitors. In their study, a homologous series of different NHC-metal complexes was designed, using water-free metal salts such as SnCl₂, ZnCl₂ and MgCl₂ as blocking groups.^{45,64} Quite surprisingly, polymerizations of ϵ -caprolactone in the presence of such type of adducts were found to be much faster than those obtained when using NHC.CO₂. This difference in behavior clearly resulted from the release of metal salts (Lewis acids) from NHC-metal complexes upon heating. As such, a Lewis-acid activation was possible, related to the coordination of metal ions towards the carbonyl moiety (reducing electron density of C–O bond), thus enhancing the nucleophilic ring opening action of the free NHC (**Scheme 1.11**). On the other hand, under identical conditions, the efficiency of the precatalysts was found to depend mainly on the binding energy of metal ions and NHC. Because of weaker

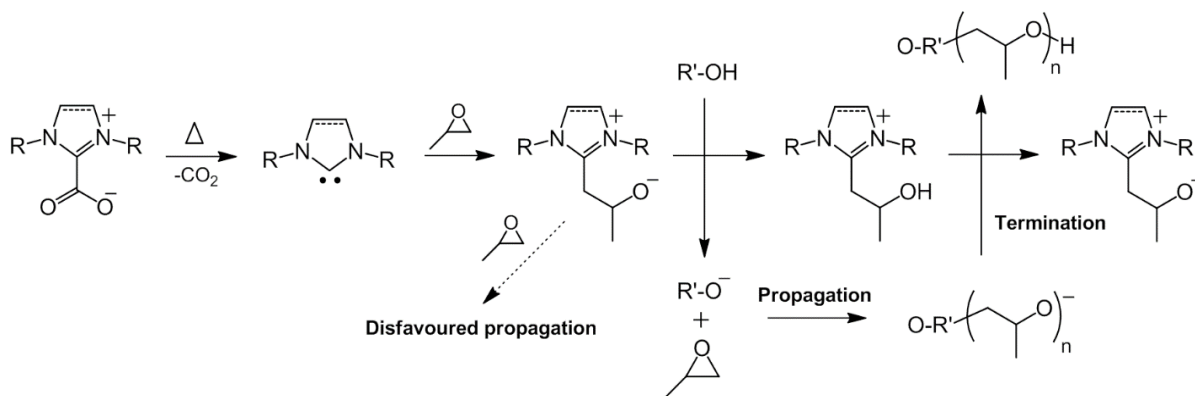
coordination of NHCs to MgCl_2 compared to ZnCl_2 , MgCl_2 -bearing NHC homologues allowed to gradually polymerize ϵ -caprolactone at room temperature (12%, 5 h), whereas perfect latency was observed in the presence of NHC- ZnCl_2 compounds (0%, 20 h). Upon heating at 130°C , the latter reaction delivered quantitative poly(ϵ -caprolactone) after only 5 minutes. Therefore, the ZnCl_2 -bearing homologues, containing non-toxic ion Zn^{II} , are regarded as one of the best thermo-latent NHCs for the ROP of ϵ -caprolactone.^{64,81}



Scheme 1.11. Formation of polyester based on Lewis acid/base activation of thermally labile NHC-metal adducts.

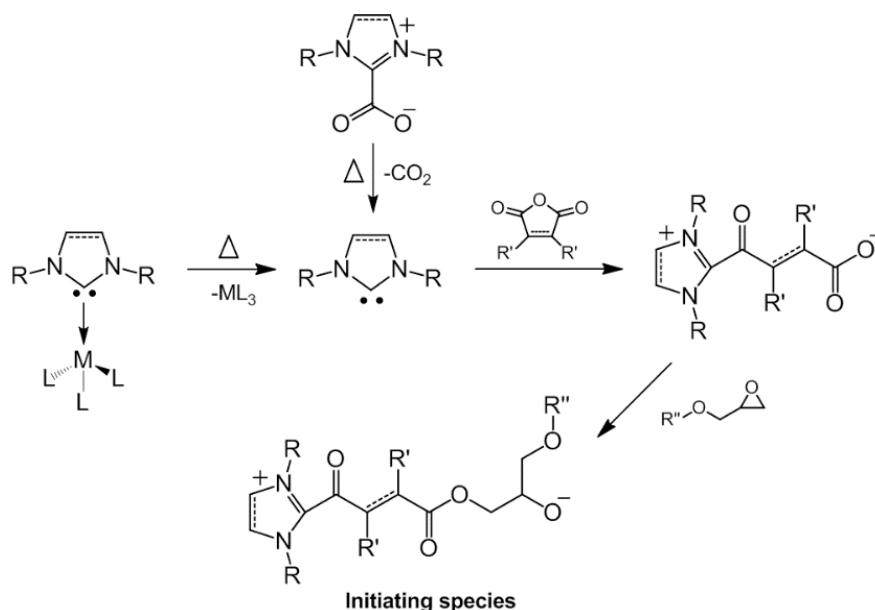
b. ROP of epoxides

Preliminary results obtained by Taton *et al.*^{39,82} indicate that NHCs are very promising catalysts for the ROP of epoxides (ethylene oxide and propylene oxide (PO)). As usual, the application of NHCs in their free forms being problematic due to the need of strictly water-free conditions, Limbach *et al.*⁸³ used $\text{NHC}\cdot\text{CO}_2$ as thermo-latent precatalysts for the ROP of PO at 120°C , in the presence of diethylene glycol as initiator. The precatalyst **2e** $\cdot\text{CO}_2$ bearing the least bulky *N*-substituents was sought to be the most active species. With a catalyst loading of 5 % mol (relative to PO), this species provided the highest conversion of 73.7 %. However, only PO oligomers resulted. With regards to DFT calculations, ROP of epoxides is supposed to prefer a free anionic mechanism, causing an inherently slow process and side reactions (transfer to monomer) (**Scheme 1.12**).



Scheme 1.12. Thermal activation mechanism of $\text{NHC}\cdot\text{CO}_2$ precursors in ROP of PO.

Recently, Naumann *et al.*^{41,84} described the thermo-latent curing of epoxide and anhydride using CO₂- or metal-protected NHC species as sources of base/catalyst. Herein, the in situ generated NHCs were found to be well suited to activate the curing of anhydrides and bisphenol A diglycidylether (BADGE) at relatively low temperature (120–160 °C), the reaction reaching completion within a few minutes. When shedding light into the mechanism, nucleophilic attack of NHCs on the anhydride allows ring-opening and generation of a carboxylate for subsequent alternating copolymerization (**Scheme 1.13**). Because of the low reactivity between epoxides and anhydrides at room temperature and the robustness of such NHC adducts, one-pot synthesis can be achieved without undesired premature reaction.



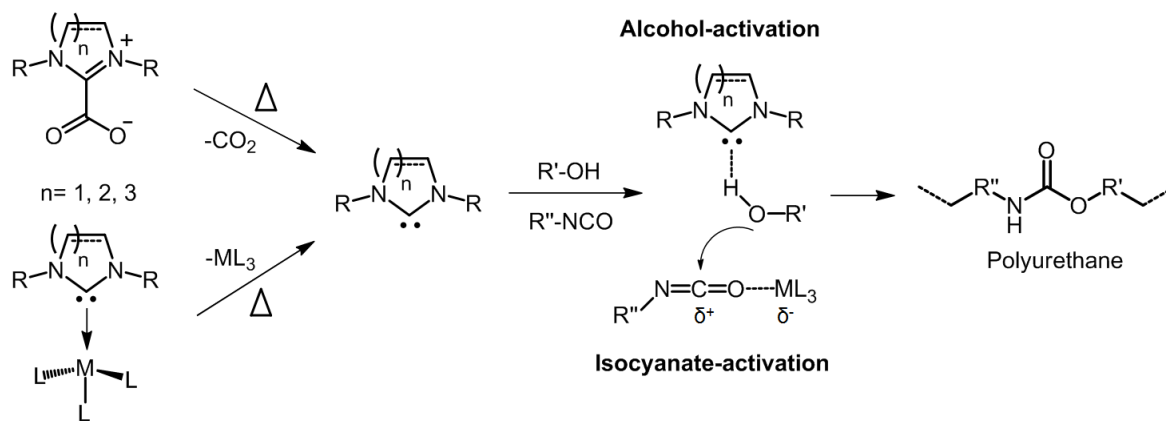
Scheme 1.13. Schematic initiation step of a latent one-component epoxide/ anhydride mixture in the presence of protected NHCs.^{41,84}

1.3.2. Step-growth polymerization

a. Polyurethanes

In 2012, Taton *et al.* reported that NHCs can trigger the formation of polyurethane by nucleophilic attack of the NHC to the alcohol followed by its addition onto the isocyanate moiety (**Scheme 1.14**).⁴⁴ In term of efficacy, NHCs have been demonstrated to be more active than conventional organic bases including tertiary amines. Regarding latent NHC catalysts, Buchmeiser *et al.*^{85,86} prepared a number of thermally labile NHC progenitors serving as delayed-action catalysts for the synthesis of polyurethanes (PUs). The catalytic activity of these latent precatalysts was probed and then compared to phenylmercury neodecanoate (PMND) and dibutyltin dilaurate (DBTDL) as references. As expected, DBTDL revealed no latency at all, while PMND and the protected NHCs showed no activity

at room temperature. More interestingly, the performances of the protected NHCs were in some cases even better than those exhibited by PMND upon thermal activation. Additionally, among the latent NHC precursors, all CO_2^- , Sn^{II} -, and Zn^{II} -protected NHCs displayed pronounced activity, while slower activity was observed using $\text{Mg}(\text{II})$, and $\text{Al}(\text{III})$ as protecting agents.^{45,85,86}

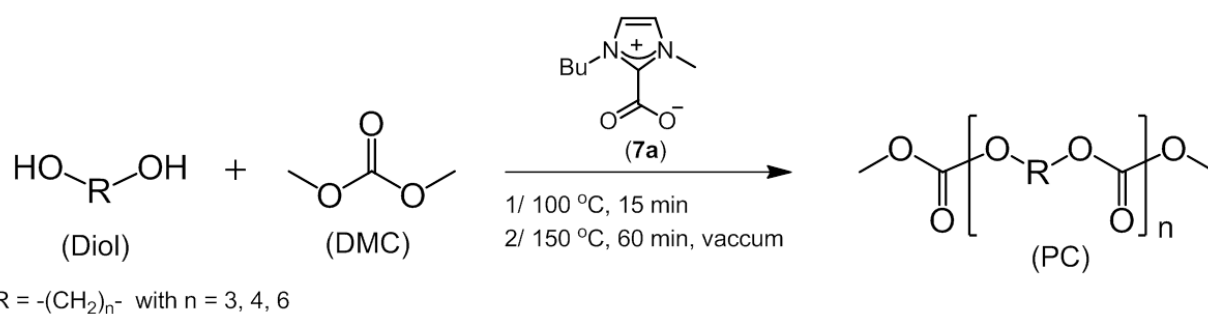


Scheme 1.14. Proposed mechanism for thermal liberation of NHCs from their inactive precursors applied in PU syntheses.^{45,85,86}

Regarding environmental aspects, $\text{NHC}\cdot\text{CO}_2$ are of great interest owing to their ability to provide favorable surrogates to metal-free PU formation. Nevertheless, metal-protected NHCs thermally liberating metal salts displaying Lewis acidity were found to enhance efficiency in the syntheses of cross-linked PUs because of a dual activation effect (alcohol/isocyanate-activation pathways).⁸⁶

b. Polycarbonates

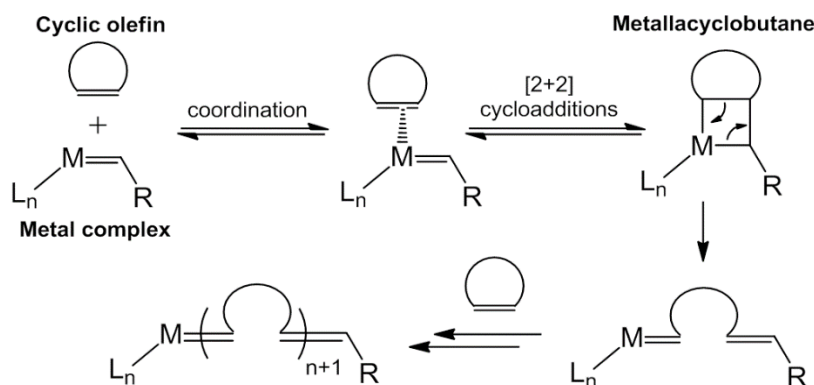
Extent application of **7a**· CO_2 precursors for the bulk synthesis of polycarbonates (PCs) has been explored by Plasseraud *et al.*⁸⁷. In their study, the polycondensation of dimethylcarbonate (DMC) and a number of diols proceeded in two subsequent steps (**Scheme 1.15**). First, the reaction mixture was heated at 100 °C for 15 min to accelerate decarboxylation of the $\text{NHC}\cdot\text{CO}_2$ adduct, thereby releasing **7a** that was immediately available to promote the transesterification of monomers. Then, the reaction temperature was increased to 150 °C while applying vacuum to remove by-product (MeOH). The PCs obtained after 1 h showed relatively low molecular weights (1700 – 6700 $\text{g}\cdot\text{mol}^{-1}$) and broad polydispersities ($D= 1.4 - 2.8$).



Scheme 1.15. General synthetic process of aliphatic polycarbonates employing **7a**.CO₂ as precatalyst.

1.3.3. Ring-opening metathesis polymerization

Ring-opening metathesis polymerization (ROMP)⁸⁸ is a chain growth polymerization where ring-strain olefins insert into active sites of metal centers affording unsaturated polymeric materials (**Scheme 1.16**).

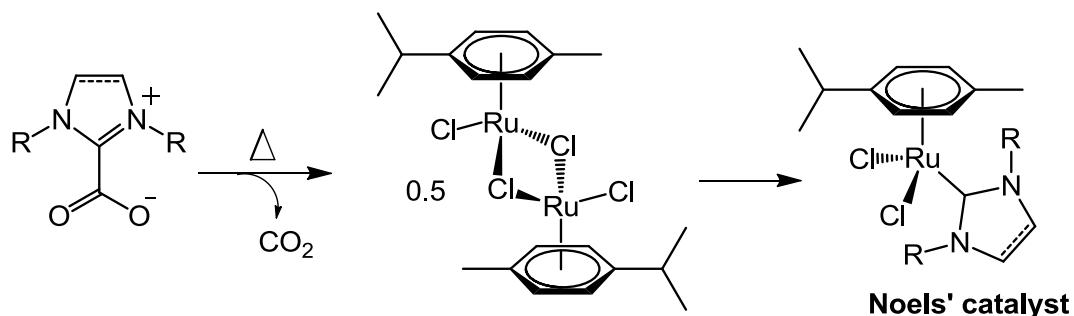


Scheme 1.16. General mechanism of metal-mediated ROMP.

Among the well-defined NHC-ruthenium complexes, Noels' catalysts with principle formula RuCl₂(NHC)(*p*-cymene) have high utility due to their great performance towards ROMP.^{89,90} Such complexes can be generated in situ via a combination of [RuCl₂(*p*-cymene)]₂, azolium salts and strong bases such as *t*-BuOK, NaH or Cs₂CO₃. It is a much simpler procedure in comparison to the multi-step exchange of ligands required to obtain Grubbs' second-generation catalysts and its derivatives.⁹¹

Accordingly, NHC.CO₂ betaines that show strong lability upon heat or dissolution can act as efficient NHC precursors for in situ preparation of ROMP catalysts without the need for additional bases.^{91,92} Delaude *et al.* have explored the synthesis of Noels' analogues using two-fold excess of NHC.CO₂ adducts (**Scheme 1.17**). The metathesis activity of these complexes was assessed in visible light induced ROMP of cyclooctene and compared to those prepared by in situ deprotonation of azolium salt counterparts such as NHCH⁺Cl⁻ and NHCH⁺BF₄⁻. In all cases, for polymerizations carried out at 60 °C, the introduction of five-

membered NHCs such as **1a**, **1b**, **2a** and **2b** significantly enhanced the catalytic behavior in comparison to **1c** and **2c**. Additionally, at this temperature, similar catalytic performances and physico-chemical parameters of polyoctenamers were observed for active species derived from azolium salts and from NHC.CO₂ adducts. However, at room temperature, superior catalytic efficiencies were only achieved in the carboxylate systems rather than in the corresponding azolium salts.⁹² Solubility limit of azolium salts at ambient temperature was invoked to consider on this lack of evolution in ROMP.



Scheme 1.17. Highly active NHC-ruthenium complex obtained via reaction of ruthenium dimer and NHC.CO₂ adducts.

1.4. Conclusions

NHCs with extreme versatility continue to be valuable tools for polymer synthesis. The developments of a variety of inert and air stable protected NHCs have overcome the challenges occurring when applying directly the free carbenes. The use of these protected forms enables an ease in handling and potentially latent polymerization systems, paving the way for the use of NHCs at industrial-scale. Among the approaches to generate NHCs in situ, less attention has been paid to photolabile NHCs, even if they can provide a precise temporal and potential spatial control of the polymerization reactions, which would be well suited for photolithography technology. Thus, it encouraged us to drive the scope of this thesis towards the further development and application of NHCs photogenerators.

B RECENT DEVELOPMENTS IN PHOTOCHEMICALLY ACTIVATED RING-OPENING METATHESIS POLYMERIZATION

Progress in olefin metathesis has been driven by a wide variety of increasingly advanced and well-defined catalysts.⁹³ However, these developments have generally met the needs of synthetic organic chemists, and are less suited to polymer applications. As a result, the use of ROMP polymers has so far been restricted to the manufacturing of specific structural and engineering materials including heavy-vehicle exterior components, sport products and day-to-day items.⁹⁴ The weak development at industrial level of ROMP polymers does not stem from limited intrinsic properties but rather from restrictive conditions imposed by the manufacturing process. “Smarter” catalysts able to release active species in situ and “on demand” are currently the main lever to ease polymerization processing.⁹⁵ Of high interest are ROMP photolabile catalysts, for which activity can be triggered under visible or ultraviolet irradiation.⁹⁶ Firstly, they enable the use of storable, ready-to-use, and cost-effective formulations without pot-life issue. This decreases risk potential of misuse and hazard due to incomplete mixing or early polymerization. Secondly, solvent-free, fast and energy-saving cross-linking procedures may be implemented for the synthesis of new UV-curable coatings and inks for example, as has already been described with radical and cationic radiation curing technology.⁹⁷ Last but not least, phototriggered catalysts allow spatially-controlled polymerizations and surface modification.

Unlike recent reviews devoted to photochemically induced olefin metathesis in general,^{98,99} our description shall be confined to photochemically activated ROMP (photoROMP). Other means for externally regulated ROMP such as heat, mechanical stimulus or ultrasound shall not be covered.¹⁰⁰ For sake of clarity, the studies are not classified according to the type of catalyst as is usually the case, but rather on the mechanism. Following this idea, four main strategies have been built in the literature, as depicted in **Figure 1.9**. The first three routes (**1-3**) rely on a photolabile transition metal complex converted into an active catalytic species through different photochemical reactions. Route **1** involves a photodissociation of one or more ligand(s) from the metal center. Route **2** uses a photosensitive exogenous species (PL) to liberate ligand(s), subsequently reacting with the precatalyst to generate an active catalyst. Route **3** relies on a *cis-to-trans* photoisomerization of ligand in chelated ruthenium alkylidene complexes. Unlike previous approaches, route **4** is metal-free and does not follow the conventional metathesis mechanism. It consists in a

photoredox-mediated ROMP using vinyl ethers as initiator and pyrilium salt as photo-oxidant.

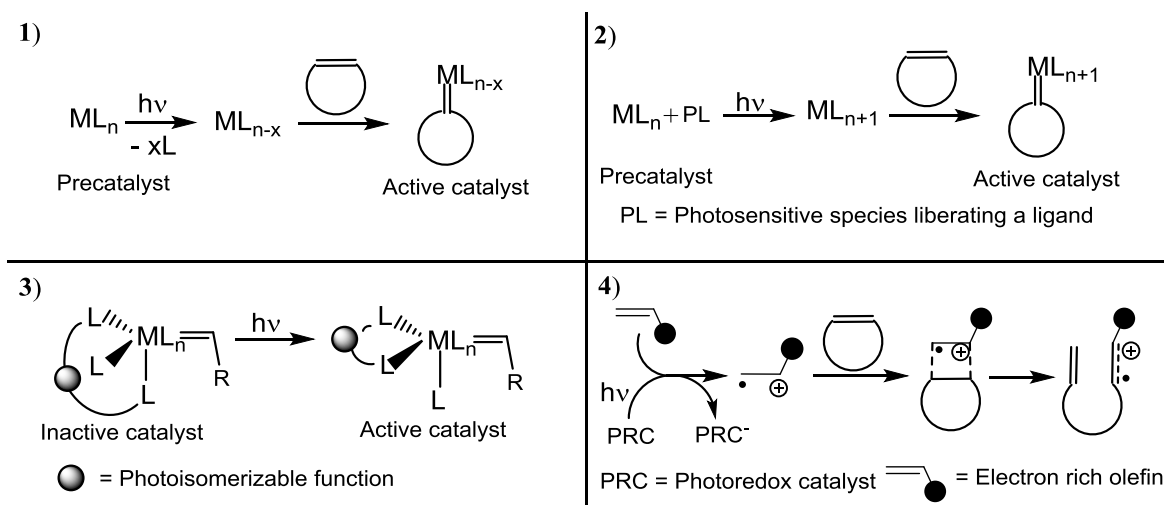
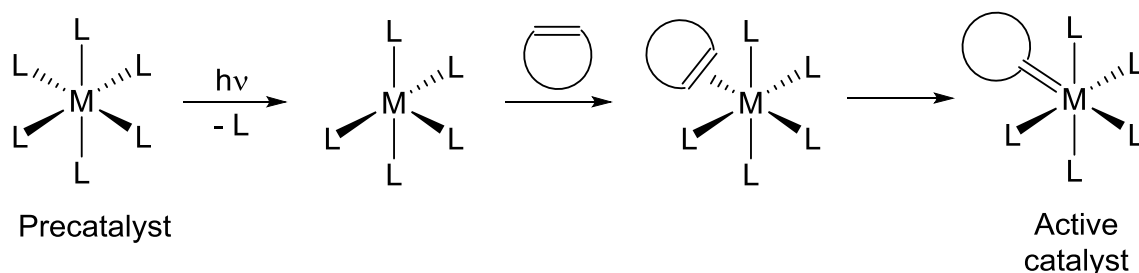


Figure 1.9. 4 strategies to develop photochemically activated ROMP.

1.5 Catalyst activation through ligand photodissociation

Light-induced dissociation of one or more ligands from the metal center to trigger ROMP dates back more than 40 years ago with the concomitant reports by K. F. Castner¹⁰¹ and A. Harfouch *et al.*¹⁰² It has been currently the most studied methodology to perform photoROMP and numerous catalysts based on Ru, W or Os were released. Following this strategy, the active ROMP catalyst is usually generated from alkylidene-free complexes (precatalyst), the propagating metal–carbene species being generated in situ after displacement of the ligand (**Scheme 1.18**). Most often, the precatalysts employed have the advantage of being commercially available and cost-effective.



Scheme 1.18. General mechanism for the formation of active ROMP catalyst by photo driven ligand dissociation.

Tungsten based precatalysts. In the first mention of photoROMP, K. F. Castner¹⁰¹ and A. Harfouch *et al.*¹⁰² demonstrated that UV-irradiation (200 W Hg lamp, 5 min) of the tungsten derivatives WCl_6 and $W(CO)_6$, in the presence of pentachlorophenol or CCl_4 respectively, led to an active ROMP catalyst. With the WCl_6 /pentachlorophenol mixture, only

moderate catalytic activity was observed in the ROMP of cyclooctadiene (COD), cyclopentene (CP) or dicyclopentadiene (DCPD). In contrast, the second system $W(CO)_6/CCl_4$ proved to be much more active, thus reaching 100 % conversion with norbornene (NB) and CP as monomers.

The high catalytic activity of this latter system then encouraged many research groups to gain deeper insight into the photochemical pathway.^{103–105} It is now well established that the primary step is CO ligand photodissociation (360 nm) and finally leads to a catalyst containing carbonyl and chlorine ligands around the tungsten center, in addition to the metal carbene unit.¹⁰⁴ However, the intermediate reaction steps as well as the precise structure of the final catalyst are still not clearly defined. Interestingly, the system is also active for the polymerization of phenylacetylene (PA),¹⁰⁵ and while investigating the presence of the metal carbene bond in this active species, Sudarajan *et al.* performed the synthesis of a PNB-*b*-PPA block copolymer. The reaction was possible due to the living nature of the polymer chains that could be coupled by end-capping with terephthalaldehyde.

Photolability in ROMP could also be accessed from well-defined tungsten catalysts **W1** and **W2** as reported by Van der Schaaf *et al.*¹⁰⁶ (**Figure 1.10**). **W2** was certainly the most attractive since it displayed full latency with DCPD at 80 °C (no polymerization is observed after 6 h) and allowed fast polymerization under UV-irradiation at room temperature (polymerization complete after 20 min with a 200 W Hg lamp). As proposed by the authors, formation of the active Schrock-type catalyst slightly differed from the general mechanism in **Scheme 1.18**. Instead, elimination of tetramethylsilane occurred upon α -H abstraction reaction from two trimethylsilylmethyl groups in a *cis* position, thus generating the active tungsten-alkylidene complexes.

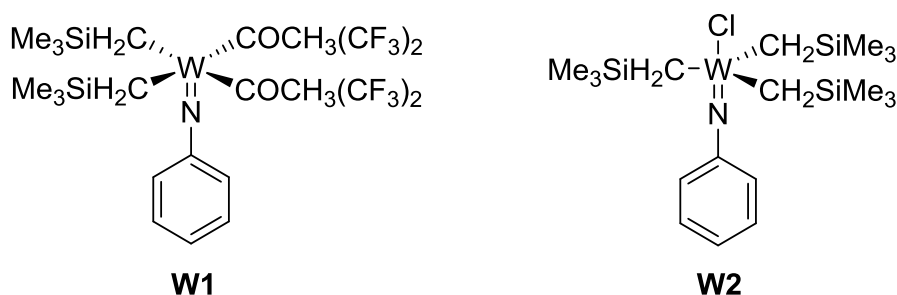


Figure 1.10. Structure of well-defined tungsten catalysts developed by Van der Schaaf *et al.*

Ruthenium based precatalysts. In the mid 1990's, the development of ruthenium-based catalysts, displaying tolerance towards moisture and functional groups, motivated Mühlebach *et al.* to investigate the behavior of η^6 -arene sandwich, half-sandwich and nitrile complexes **Ru1-3** (**Figure 1.11**) for the photopolymerization of strained cyclic olefins (NB

and oxaNB).¹⁰⁷ Due to their cationic character, the 27 complexes studied were only soluble in polar solvent and photoROMP reactions were thus mostly performed in ethanol. Although these systems displayed moderate activities after UV-irradiation at 364 nm, they provided good photolateny. In particular, no polymerization was observed when heating the sandwich complexes with the monomers for 24 h at 50 °C. However, addition of the monomer to the irradiated complex and rise of the temperature to 60 °C produced polymers with high molecular weights ($M_w > 100 \text{ kg}\cdot\text{mol}^{-1}$) and high dispersities ($\mathcal{D} > 2.0$). Sandwich and half-sandwich complexes were proposed to proceed through arene ligand dissociation to generate the active $[\text{Ru}(\text{solvent})_6]^{2+}$ complex. With nitrile complexes, gradual photodissociation of the nitrile ligands might account for the formation of the active species $\text{Ru}(\text{NC-R}')_{6-x}(\text{H}_2\text{O})$ ($\text{R}' = \text{CH}_3, \text{CH}_2\text{CH}_3$ or Ph).

In an effort to access organosoluble and active photocatalysts, Mühlebach *et al.* then introduced phosphine ligand to ruthenium and osmium arene complexes (**Ru4** and **Os1**, **Figure 1.11**).¹⁰⁸ Although no thermal latency was observed with NB, **Os1** proved to be inactive after 6 h at 80 °C with the same monomer. By contrast, the later complex displayed high activity under UV-irradiation, complete monomer consumption being achieved after 10 min at 30 °C. Displacement of the *p*-cymene ligand under UV irradiation was proposed as first step to generate the active catalyst. In addition, activity of the osmium complex **Os1** was found to increase with steric hindrance of the phosphine ligand.

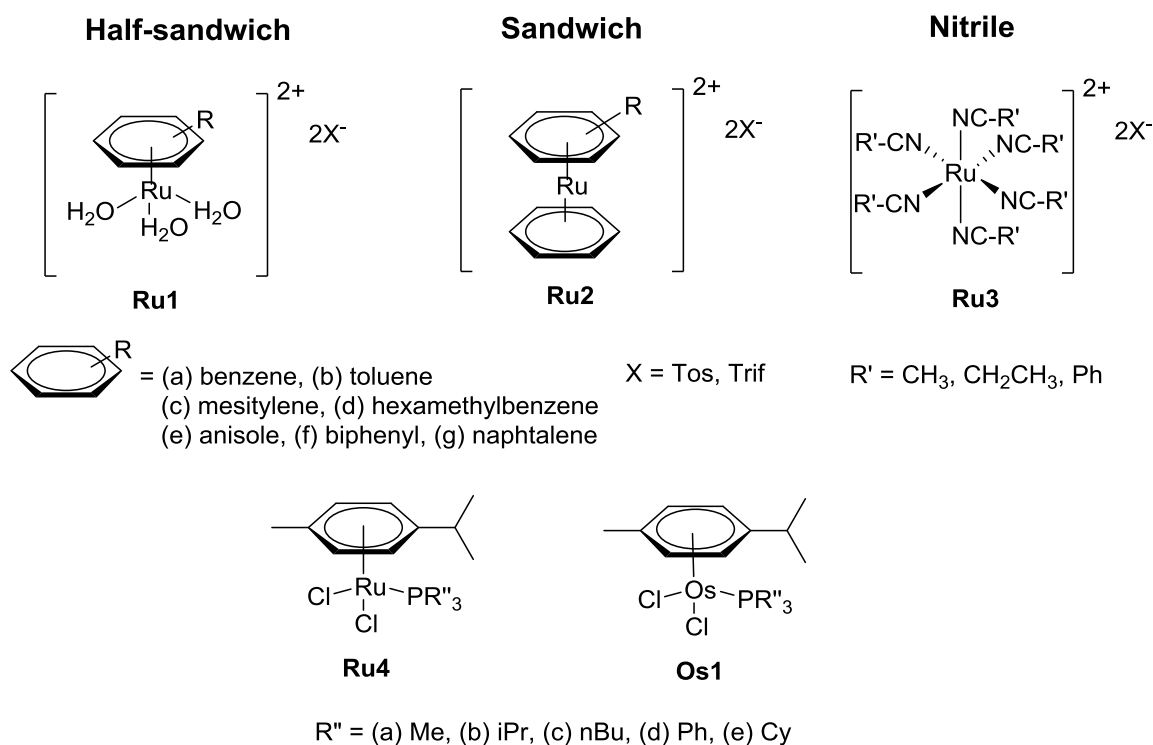


Figure 1.11. Ruthenium and osmium based photocatalysts prepared by Mühlebach *et al.*.

The story of photocatalysts proceeding through arene ligand dissociation continued with the famous Noels' complex (**Ru5**, **Figure 1.12**).¹⁰⁹ Introduction of the N-heterocyclic carbenes (NHCs) 1,3-dimesitylimidazol-2-ylidene (**IMes**) in the place of phosphine ligands resulted in a visible light sensitive catalyst able to polymerize cyclooctene (COE) in a few minutes at room temperature. Nevertheless, poor latency was observed with this catalyst, 22 % monomer conversion being reached after 2 h in the dark. In order to improve latency of such precatalysts, Buchmeiser *et al.* argued that replacement of the chlorine ligands with trifluoroacetate ligands was necessary and thus prepared complexes **Ru6a** and **Ru6b** (**Figure 1.12**).¹¹⁰ Although these catalysts were found to polymerize NB quantitatively in 2 h at room temperature, they indeed displayed good latency with norborn-5-ene-2-ylmethanol as monomer. Irradiation of a solution containing **Ru6b** and the monomer for 30 min at 172 nm resulted in the quantitative formation of an insoluble polymer. Similar results were also achieved with catalysts **Ru7** featuring phenylisocyanide instead of *p*-cymene ligand.

With the aim to improve latency, Buchmeiser *et al.* developed the cationic ruthenium photocatalysts **Ru8-10** (**Figure 1.12**) in 2008¹¹¹ and 2010.¹¹² Unlike **Ru10** that converted quantitatively DCPD at room temperature in 1 h, the other compounds displayed no activity after 24 h at 45 °C with the monomers represented in **Figure 1.13**. In general, catalysts featuring the NHC **SIMes** were more active than their **IMes** analogues for the photoROMP of the monomers at 254 nm. Moreover, no noticeable difference of activity was observed between photocatalysts featuring trifluoroacetate (**Ru8**) and trifluoromethanesulfonate anion (**Ru9**). Polymers having molar masses in the range $1.0 \times 10^5 - 4.8 \times 10^5 \text{ g}\cdot\text{mol}^{-1}$ and dispersities between 1.8 and 4.9 were usually obtained in yields of 85 – 100 %. Catalysts **Ru8a** and **Ru8b** were also found to be active at 308 nm, although lower yields were obtained in the same reaction time. It was hypothesized that these catalysts (**Ru8-10**) became active upon loss of two tert-butylisocyanide ligands under UV irradiation.

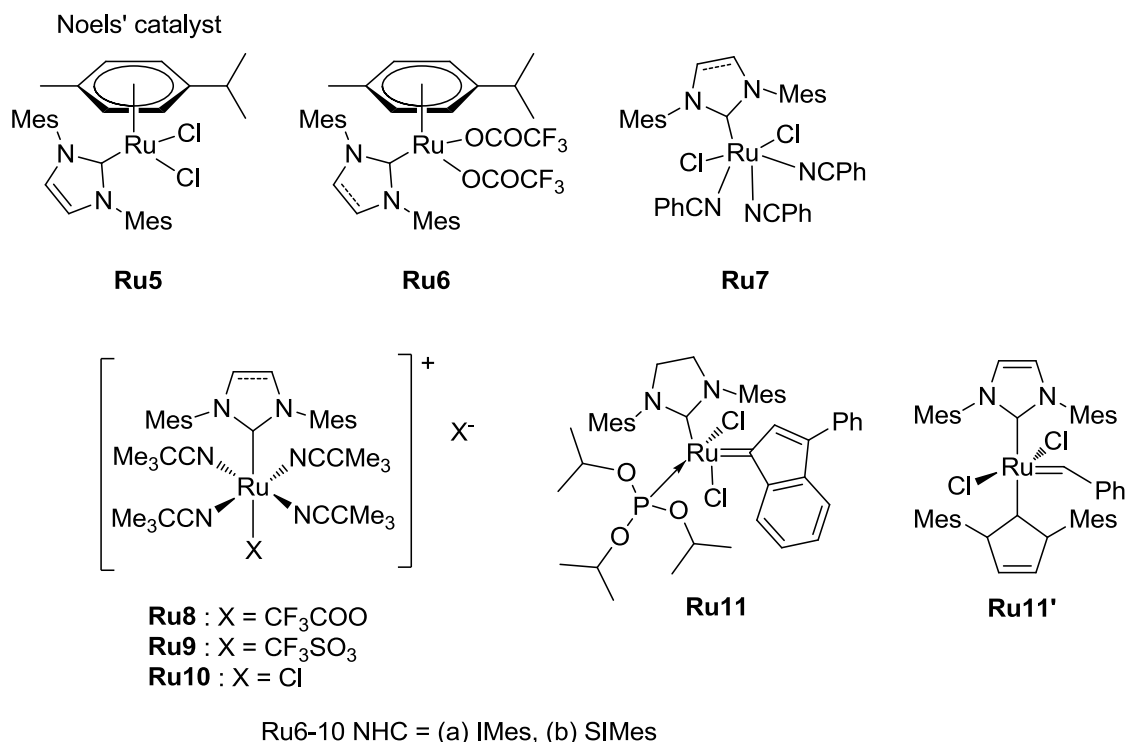


Figure 1.12. Ruthenium photocatalysts with NHC ligands.

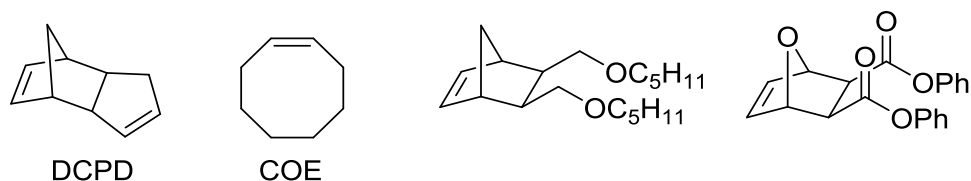


Figure 1.13. Monomers employed for photoROMP by Bushmeiser *et al.*

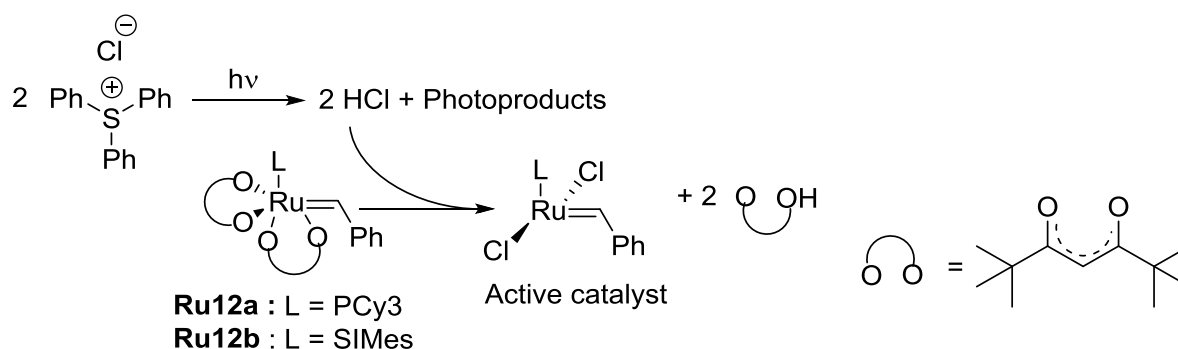
Other precatalyst base on Ru center was disclosed by Lemcoff *et al.*¹¹³ The commercially available ruthenium phosphite complex **Ru11** was found able to liberate the phosphite ligand under 350 nm irradiation, thus allowing quantitative polymerization of COE and COD at room temperature in 1 h and 2 h respectively. Polymers with molecular weights close to theoretical molar masses and with relatively low dispersities ($\mathcal{D} < 1.8$) were obtained, which suggests that a high proportion of the photocatalyst was active under UV irradiation. This is in direct contrast with previous photocatalysts that usually displayed 10-20 % active species under UV-irradiation.

A last strategy for Ru proceeding through ligand dissociation was recently demonstrated by Rovis *et al.*¹¹⁴ In their study, an inactive bis-NHC ligated ruthenium (**R11'**) was merged with 2,4,6-triphenylpyrylium tetrafluoroborate as a highly oxidizing photocatalyst. Upon exposure to visible light (450 nm), a photoredox process occurred promptly that led to the dissociation of one NHC. Subsequently, 14-electron active Ru

complex was formed in situ and thus readily initiating the ROMP of norbornene and its derivatives with high conversion (> 95 %) within 1 h.

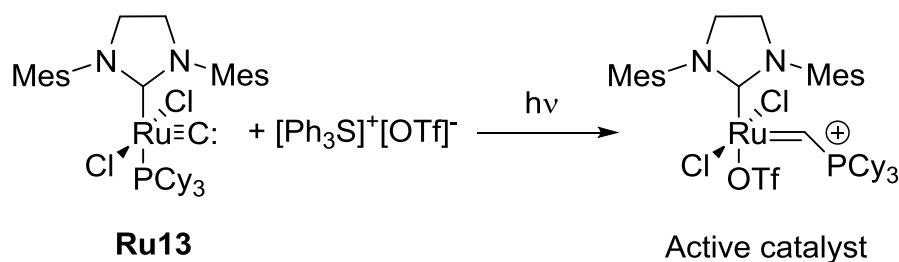
1.6 Catalyst activation through in situ photogeneration of ligands

Active ROMP catalysts can also be generated from an inactive and non-absorbing precatalyst after reaction with a ligand liberated by an exogenous photosensitive species (route 2, **Figure 1.9**). The concept was first introduced by Grubbs *et al.* in 2009 by using the photoacid generator (PAG) triphenylsulfonium chloride and the precatalyst **Ru12** (**Scheme 1.19**).¹¹⁴ Upon irradiation at sub-300 nm, HCl was released which allowed protonation and subsequent displacement of the acac ligands of **Ru12a** or **Ru12b**. Subsequent formation of the active 14 electron complex was proposed that featured the chloride anion as ligand. The system was found to be inactive in the absence of radiation or without the PAG. Also noteworthy is that the replacement of the chlorine anion in the PAG by a non-nucleophilic nonaflate anion resulted in a complete loss of activity, thus demonstrating the critical role of Cl⁻ in the formation of the active catalyst. The tandem system **Ru12**/PAG provided excellent conversion in the photoROMP of COE, DCPD and NB derivatives at room temperature, although incomplete catalyst activation was observed.



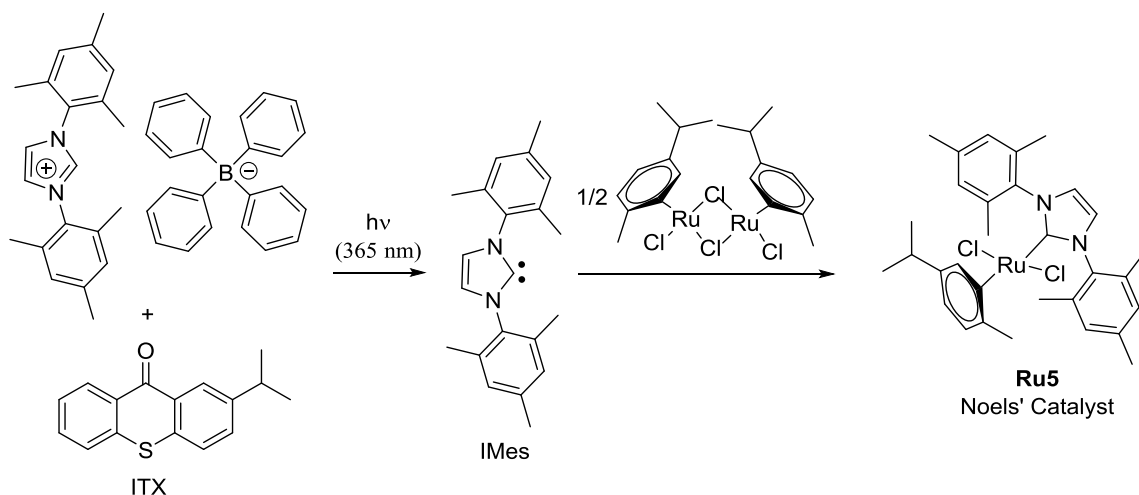
Scheme 1.19. Photogeneration of an active catalyst by irradiation of solution containing a photoacid generator (PAG) and a ruthenium complex.

A PAG based on triphenylsulfonium was also employed by Piers *et al.* to activate the ruthenium carbide complex **Ru13** (**Scheme 1.20**).¹¹⁵ Triflate anion was employed in place of the chloride anion. The approach proved effective since under 254 nm irradiation, ROMP of NB, DCPD, COE or COD could be achieved in 5 minutes. Nevertheless, incomplete catalyst activation was observed as attested by the presence of peaks attributed to **Ru13** in the ¹H NMR spectrum of the reaction medium. Latency of the system was confirmed at room temperature, since without UV irradiation no polymerization was observed. Eventually, presence of the PAG was found to be not necessary for ROMP to proceed, even though lower activity was observed.



Scheme 1.20. Photogeneration of an active catalyst by irradiation of solution containing a PAG and a ruthenium complex.

Using a N-heterocyclic carbene (NHC) photogenerator based on tetraphenylborate dimesitylimidazolium salt with respect of generating in situ the Noels' catalyst **Ru5** from the commercially available ruthenium dimer $[\text{RuCl}_2(p\text{-cymene})]_2$ (**Scheme 1.21**) for the ROMP is reported in this PhD thesis. Motivated by the promising results, the latter use of this catalytic system was broadened to polymerize NB in an aqueous miniemulsion. Finally, resulting PNB particles with diameters in range of 100 nm were obtained.^{116,117}



Scheme 1.21. In situ formation of Noels' catalyst by sensitized photogeneration of NHC **IMes**.

1.7 Catalyst activation through conformational change of chelated ligand

Switching metathesis catalyst's conformation upon exposure to UV irradiation is the third strategy to control reactivity. The concept of photoinduced *cis-to-trans* isomerization has been an area of interest for decades, as illustrated by the plethora of azobenzene-containing materials.¹¹⁸ *Cis-trans* photoisomerization induces both molecular movement and geometric change, which account for the activity regulation of many biomolecules. Currently, this photochemical reaction has been extensively exploited to devise smart molecular machines able to change form or to move.¹¹⁸ By contrast, there are much less examples of

photoreactive compounds in which a photoinduced conformational transition drives the change from latent to active form.¹¹⁹ For this purpose, photoswitchable N and S chelated ruthenium complexes have been studied for less than 10 years.

Chelation by sulfur atom. In 2009, the group of Lemcoff demonstrated that a *cis*-to-*trans* photoisomerization of ligand in sulfur chelated NHC ruthenium benzylidene complexes was a way to switch from a latent form (*cis*-dichloro) stable in air to an active ROMP catalyst (*trans*-dichloro).¹²⁰ The first structure **Ru14-cis** (Figure 1.14), *cis*-(Cl)₂(SiMes)Ru=CHPhS-Ph, is nothing more than a sulfur chelated form of the well-known Hoveyda–Grubbs type complex. **Ru14-cis** has two primary features that make it a suitable ROMP photocatalyst:

- *Chelation by sulfur resulting in a latent cis isomer.* At the time of research for this precatalyst, chelation of Ru metallic by N or O through alkylidene moiety was already a well-established approach to decrease metathesis activity.^{121,122} Because the S-Ru bond is generally stronger than O-Ru, Lemcoff *et al.* postulated that it was possible to completely suppress activity, which is the first step forward to a photolabile ROMP catalyst. Accordingly, **Ru14-cis** was inert in presence of *exo* substituted NB, COD or COE at ambient temperature.¹²⁰ However, reaction occurred spontaneously with more strained cyclic olefins such as NB or DCPD (Table 1.1).

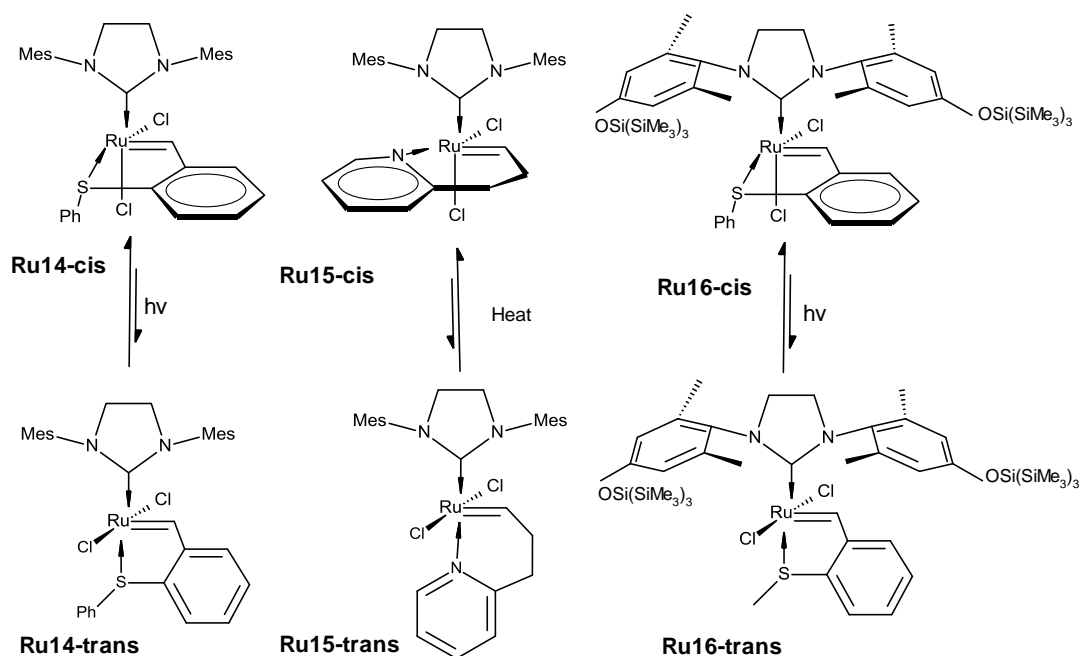
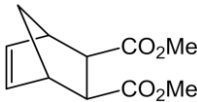
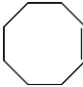
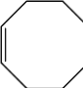

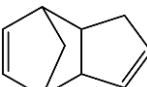


Figure 1.14. S chelated latent ruthenium benzylidene catalysts used in photoROMP (**Ru14** and **Ru16**). **Ru15** is the first isomerizable chelated ruthenium catalyst, the **Ru15-cis** form being much more latent than **Ru15-trans**.

- *Photoisomerisation into an active trans isomer.* The first complex that exhibited *cis-trans*-dichloro isomerization was developed in 2004 by Grubbs and Schrodi using a pyridine alkylidene chelated ruthenium catalyst (**Ru15**, **Figure 1.14**).¹²³ However, the reaction was induced by heat and resulted only in a reactivity jump; **Ru15-cis** was not originally latent. Inspired by this work, Lemcoff *et al.* first examined in 2008 the sulfur-chelated complex **Ru14-cis** as a thermolabile catalyst for ROMP.¹²⁴ Polymerization of *exo* substituted norbornene was successfully triggered upon heating at 100 °C. Only a year later, they developed the idea of using the same precatalyst in photopolymerization starting from the assumption that many isomerizable groups can be interconverted not only thermally but also photochemically.¹¹⁸ To their great delight, **Ru14-cis** precatalyst was partially (30 %) converted into **Ru14-trans** in dichloromethane solution at 365 nm, driving the ROMP at room temperature of three conventional cyclic olefins: *exo*-dimethyl-5-norbornene-2,3-dicarboxylate, COE and COD (40 – 90 % after 24 h, **Table 1.1** (entry **1 – 3**)).¹²⁰ Visible irradiation yielded smaller conversions because of poorer photoisomerization yield.

Entry	Monomer	Latent behavior ^b	λ (nm) ^c	Irradiation time (h)	Conv. (%)	M_n (g·mol ⁻¹)/ PDI
1		Excellent	365	5	40	2.5×10^5 / 1.7
2		Excellent	365	5	96	1.1×10^5 / 1.3
3		Excellent	365	5	86	0.5×10^5 / 1.4
4		No	-	-	-	-
5		No	-	-	-	-

^aReaction conditions : CH₂Cl₂, ratio monomer/ **Ru-14-cis** 300:1.

^bThe mixture of monomer/ **Ru-14-cis** was kept at 30 °C for 3 days.

^cA medium pressure 100 W Black Ray B100AP UVP was used as an irradiation source.

In photoROMP, Lemcoff proved that replacing the phenyl substituent of the sulfur atom by β -naphthyl¹²⁰ and trifluoromethyl⁹⁸ groups resulted in a higher activity. In addition, they showed that supersilyl groups attached to the NHC (see **Ru16** in **Figure 1.14**) could improve activity^{99,125} leading to full conversion of COE and functional NB within 4 h when irradiated with a fluorescent lamp ($\lambda_{\text{max}} = 350 \text{ nm}$) inside a Rayonet photoreactor. Interestingly, irradiation at 254 nm caused the destruction of the catalyst by photocleavage of the silyl protecting group. Lemcoff *et al.* also engaged a complete structural investigation of S-chelated NHC benzylidene structures with the aim of increasing the stability of the *cis* form and enhancing the activity of the *trans* form in heat or irradiation-activated metathesis reaction. In photochemistry, unfortunately, most results concerned small-molecule transformations using photoinduced Ring-Closing Metathesis (RCM) of dienes,^{113,114} and in less extent photoROMP.^{98,99,120,125} Regardless of the metathesis reaction, they elegantly evidenced that the thermodynamically stable form was the *cis*-dichloro configuration, while the *trans*-dichloro isomer was the kinetic product.⁹⁹ The catalytic activity of the *trans* isomer may be attributed to the fact that the benzylidene ligand is in *trans* to the NHC, and therefore dissociate more easily (than its *cis* analogue) by Ru-S bond cleavage, to yield the 14 electrons catalytically active species. Therefore, a dissociative pathway takes place, but in contrast to route **1**, irradiation is not responsible for the dissociation of the chelating ligand.

Chelation by nitrogen atom. The well-known azobenzene *cis-trans* photoisomerization has been used as leverage to tune the activity of N-chelated Ru complexes. Without having a clear vision of the effect of the photoisomerization on catalyst activity, the presumed idea was that such conformational change may entail a modification of the coordination sphere of the complex, driving the shift from a latent species to an active species. In 2010, Lemcoff was the first to propose an azobenzene-based complex **Ru17** (**Figure 1.15**) with a nitro group whose strongly electron withdrawing properties might be enhanced in the *trans* isomer. Unfortunately, the complex decomposed under UV irradiation.¹²⁶

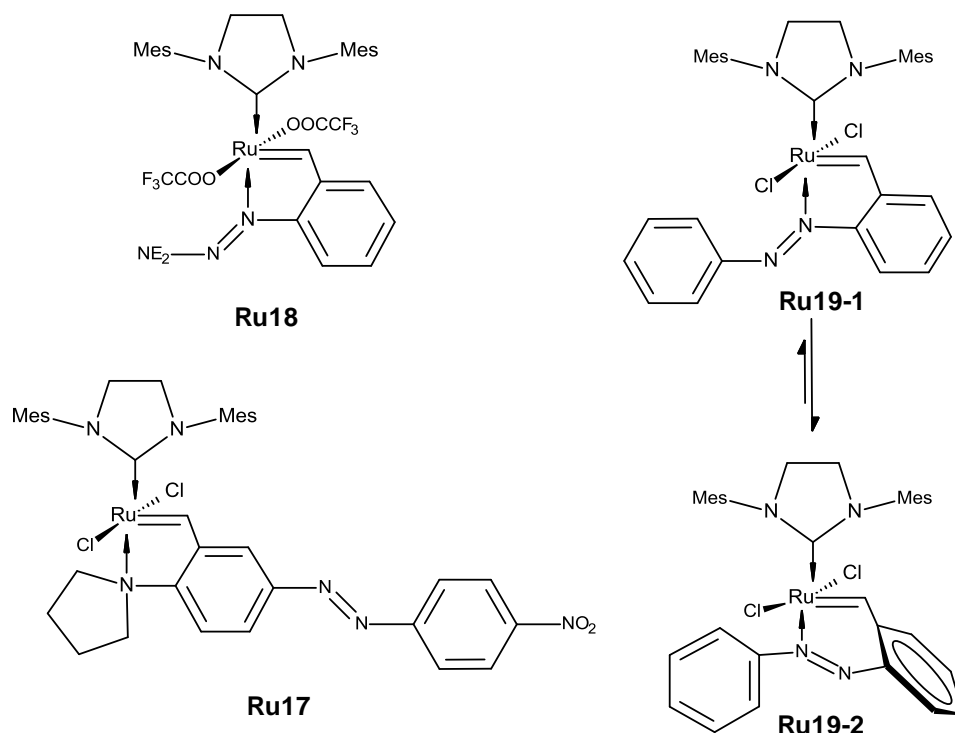
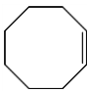
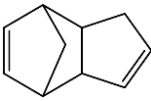
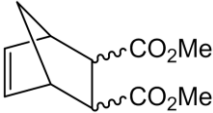


Figure 1.15. N-Chelated latent ruthenium benzylidene catalysts used in photoROMP. Only **Ru17** and **Ru19** proceed via a presumed photoisomerization mechanism.

In 2013, Buchmeiser and coworkers synthesized another N chelated complex displaying a triazene group (**Ru18**).¹²⁷ Unlike azobenzene groups, this latter is not photoisomerizable, and the activity under irradiation was attributed to a photocleavage liberating N_2 , then causing a decooordination of the chelated ligand. This complex showed significant photo-ROMP activity for both COE and DCPD (**Table 1.2, entry 1 – 2**). In 2016, Sashuk *et al.* synthesized the N-chelating complex **Ru19** existing as two isomers: a 5-membered ring (**Ru19-1**) as active kinetic product and a 6-membered ring (**Ru19-2**) as stable thermodynamic product.¹²⁸ Starting from the latent form **Ru19-2**, ROMP of diethyl norborn-5-ene-2,3-dicarboxylate was only possible by irradiation at 254 nm and not at 320 nm, the established excitation wavelength of azobenzene (**Table 1.2, entry 3**). Obviously, this result questions the photoisomerization as the main pathway leading to the formation of an active form. As a final comment, Bielawski and coworkers reported the reversible photocyclization of diethylene-functionalized NHC Ru benzylidene complex.¹²⁹ A photoisomerization governs the formation (UV) or the ring-opening (Vis) of a 6-membered cycle depending on the excitation wavelength. However, this reaction does not allow to switch from a dormant to an active substance, but only to modulate the rate of ROMP.

Table 1.2. Photoinduced ROMP employing N-chelating complexes **Ru18**^a and **Ru19**^b

Entry	Monomer	Catalyst	Latent behavior	λ (nm)	Irradiation time (h)	Conv. (%)	M_n (g·mol ⁻¹)/ PDI
1		Ru18	Excellent	254	2	60	< 2000/ -
2		Ru18	No	254	2	30	< 2000/ -
3		Ru19	Excellent	254	24	54	6.7×10^4 / 2.24

^aReaction conditions: CHCl₃, ratio monomer/ **Ru18** 200:1. The photolatency was performed at room temperature for 24 h, while a 9W Hg lamp was used as an irradiation source.

^bReaction conditions: toluene-*d*₈, ratio monomer/ **Ru19** 300:1. The photolatency was performed at room temperature for 2 weeks, while a Benda UV lamp (254 nm, 4W) was used as an irradiation source.

1.8 Metal-free photoROMP via photoinduced electron transfer

Genesis and general principle. Before the breakthrough of metal-free ROMP by Boydston and coworkers in 2015,¹³⁰ it was deeply rooted that the development of ROMP was closely linked to that of metal transition catalysts. Metal alkylidene reacts with cyclic olefin in a [2+2] cycloaddition to form a metallo cyclobutane, which is recognized as a key intermediate in the polymerization mechanism. In this context, it is not surprising that most efforts to improve photoROMP have focused on photosensitive metal complexes (routes **1** and **3**). For Boydston *et al.*, the point of departure was the observation that most olefin [2+2] cycloaddition reactions in organic chemistry proceed without the aid of metal catalyst to form a cyclobutane, which is reminiscent of the metallo cyclobutane.¹³¹ The most inspiring example was the electron transfer-induced intermolecular olefin cross-coupling established by Chiba *et al.* involving an electron rich olefin and an unactivated olefin.^{132,133} Mechanistically, the group of Chiba used a vinyl ether (electron rich olefin) which was oxidized at a carbon fiber anode in lithium perchlorate/nitromethane electrolyte solution (**Figure 1.16A**). The resulting radical cation adds intermolecularly to an unactivated olefin to form radical intermediate, which cyclizes to cyclobutane prior to back electron transfer (reduction).

Starting from the same electrochemical set-up, Boydston used an electron-rich vinyl ether as initiator and NB as monomer (unactivated olefin).¹³⁰ Remarkably, ROMP polynorbornene (pNB) was produced with a molecular weight of 11.8×10^3 g·mol⁻¹, but only

in low yield (3 %). Thus, they envisaged that a cyclobutane species might form (**Figure 1.16B**). Because the cyclic species was not obtained as final product (olefin cross-coupling), they hypothesized that reduction was likely to be out-competed by ring-opening reaction driven by the alleviation of the NB ring strain. This would maintain the radical cation species, and ensure chain propagation by iterative ring-opening of NB. They later envisaged also a reversible deactivation polymerization mechanism between a propagating radical cation species and a dormant neutral species through a reversible electron transfer reaction.¹³⁴

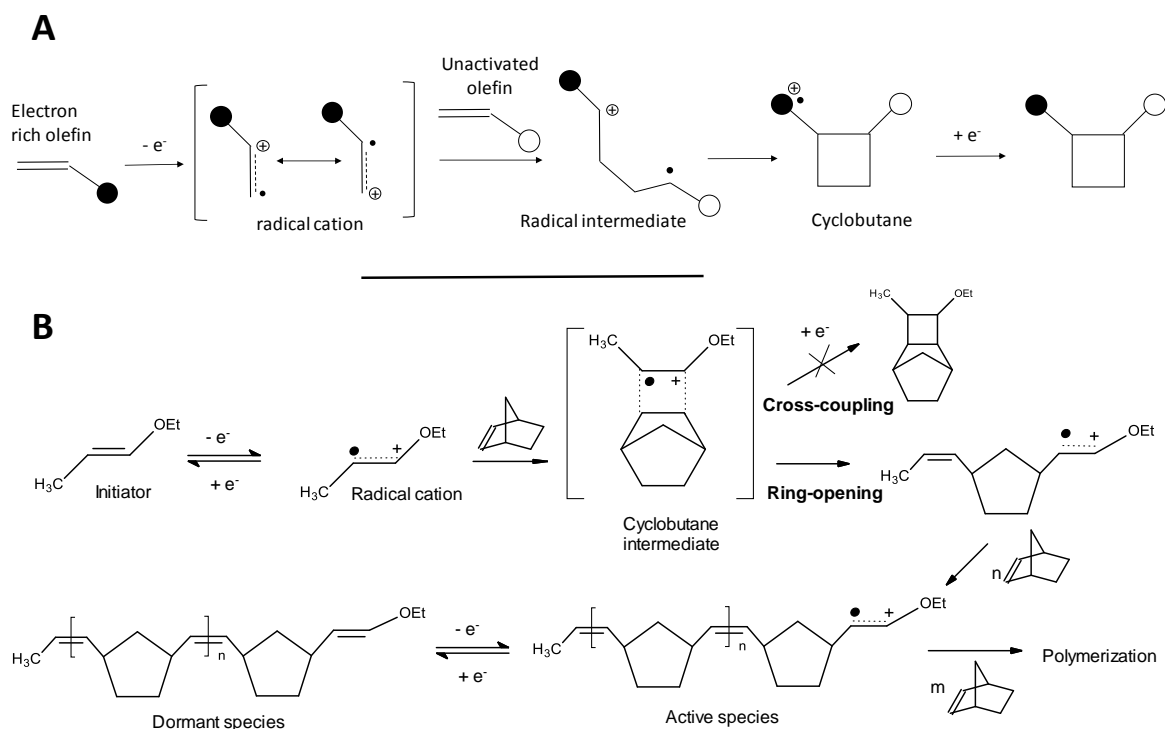


Figure 1.16. **A.** [2+2] cyclo-addition of an electron rich olefin mediated by single electron transfer to an unactivated olefin. **B.** Putative mechanism of photoinduced electron transfer ROMP of NB as envisaged by Boydston *et al.*.

Photoredox ROMP. From an electrochemical electron transfer to a photoinduced electron transfer (PET), the shift was easily made. For this, a broad list of photocatalysts such as ketones, pyrylium salts, organic dyes, metal-polypyridyl complexes was available, and redox catalysis was already in 2015 an intensively investigated field.¹³⁵ In a model experiment, Boydston used a tri(4-methoxyphenyl)pyrylium tetrafluoroborate **P1** as photocatalyst ($\lambda_{\text{excitation}} = 450 - 480 \text{ nm}$) (**Figure 1.17**) and ethyl 1-propenyl ether as initiator (NB:initiator:**P1** = 100:1:0.03 equiv.). **P1** turned out to be able to oxidize selectively the vinyl ether initiator into the reactive radical cation, to be regenerated subsequently by back electron transfer. In 1998, Steckhan and coworkers were the first to use **P1** to catalyze the reaction between 2-vinylbenzofuran and styrene.¹³⁶ Use of photocatalytic process instead of

electrochemical reactions enabled homogeneous polymerization in CH_2Cl_2 , a good solvent of pNB. This improvement afforded a relative control of the polymerization although linearity between molar mass and conversion was not obtained. Conversion was approx. 90 % after 30 min irradiation ($\lambda = 450 - 480 \text{ nm}$).¹³⁰ By varying initiator concentration and initiators (**Figure 1.18**), polymers ranging from 8×10^3 to $60 \times 10^3 \text{ g}\cdot\text{mol}^{-1}$ were achieved displaying a narrow dispersity ($\bar{D} = 1.3\text{-}1.7$) (**Table 1.3**). The polymers obtained were mostly atactic, and the pseudo-living character was further exploited to synthesize block copolymers.¹³⁷ NB polymerization was followed by chain extension using *exo*-dihydroDCPD. Light exposure not exceeding 1 h was necessary to minimize the fraction of dead chains by irreversible end chain coupling. Subsequently, they optimized protocols to enable copolymerization of NB with DCPD¹³⁸ or with functionalized NBs.¹³⁹ Use of divinyl ether initiators enabled to produce ditopic pNB macroinitiator via bidirectional chain growth.¹⁴⁰ Thiopyrilium **P2** performed better than pyrilium **P1** (**Figure 1.17**), but the authors were not able to correlate the photophysical properties of the photocatalyst (oxidation potential) with final conversions.¹⁴¹

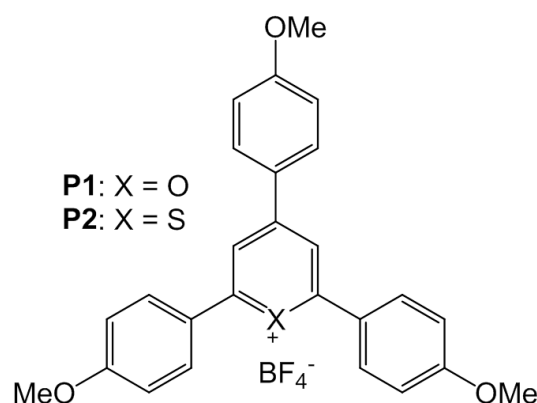


Figure 1.17. Pylrium salt (**P1**) and thiopyrilium salt (**P2**) used as photo-oxidant in metal-free PET ROMP.

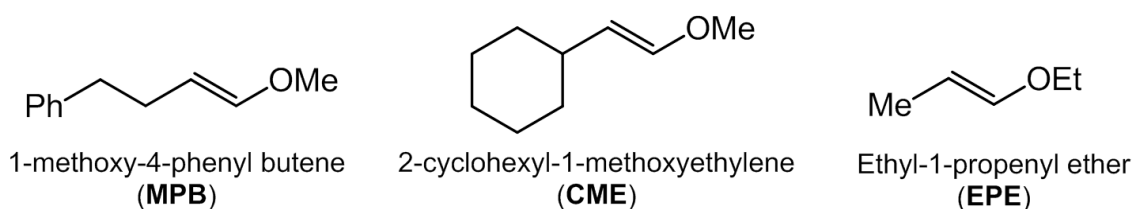


Figure 1.18. A range of vinyl ether initiators used by Boydston *et al.*¹³⁰

Table 1.3. Photoinduced ROMP of NB using a photocatalyst **P1**^a

Entry	Initiator	Molar ratio NB : initiator : P1	[NB] ₀ (M) ^b	Time (min)	Conv.(%)	M _n (g·mol ⁻¹)/ PDI
1	MPB	97 : 1 : 0.03	1.9	30	88	15.1 × 10 ³ / 1.7
2	CME	97 : 1 : 0.03	1.9	30	92	14.9 × 10 ³ / 1.6
3	EPE	106 : 1 : 0.03	2.0	30	87	15.8 × 10 ³ / 1.6
4	EPE	104 : 1 : 0.1	1.9	150	80	13.5 × 10 ³ / 1.4
5	EPE	104 : 1 : 0.25	1.9	120	90	19.2 × 10 ³ / 1.6
6	EPE	48 : 1 : 0.03	1.8	60	95	8.1 × 10 ³ / 1.4
7	EPE	57 : 1 : 0.03	1.2	120	93	11.5 × 10 ³ / 1.4
8	EPE	491 : 1 : 0.03	5.3	120	51	22.2 × 10 ³ / 1.5
9	EPE	494 : 1 : 0.03	1.8	60	72	43.9 × 10 ³ / 1.5
10	EPE	1000 : 1 : 0.03	1.9	120	61	60.2 × 10 ³ / 1.6
11 ^c	EPE	103 : 1 : 0.03	1.9	2580	53	7.2 × 10 ³ / 1.3

^aReaction conditions: CH₂Cl₂, reaction mixture was irradiated by a 2W Miracle blue LED indoor gardening bulb.

^bInitial concentration of NB.

^cReaction mixture was exposed under the light from fume hood.

For the moment, metal-free photoROMP has been exclusively explored by the group of Boydston, a situation that is expected to evolve in the future. We envision that the advantage of this process is not only related to its photochemical control and use of visible light, but to the absence of metal. The advantages of organocatalyzed ROMP are well recognized in chemistry.¹⁴²

1.9 Conclusions

Over the past 40 years, photoROMP has gain-increased attention, leading to a variety of precatalysts and/or photochemical ROMP approaches (see the 4 routes presented in **Figure 1.9**). Nevertheless, very few photoROMP systems can boast full thermal stability and high activity at room temperature. Additionally, most catalysts proved effective only in solution and with a limited range of monomers, if not with a specific monomer. It is striking how little attention has been paid to innovative applications made possible by spatiotemporal control of the photopolymerization such as thermoset preparation¹¹¹ or photolithography.¹⁴³ With the advent of LED and the recent developments of stereolithography, it is unquestionable that photoROMP will be the subject of numerous research efforts in a near future.

C REFERENCES

- 1 S. Díez-González, *N-Heterocyclic Carbenes: From Laboratory Curiosities to Efficient Synthetic Tools*, Royal Society of Chemistry, 2016.
- 2 D. Jean-Baptiste and P. Eugène, Mémoire sur l'esprit-de-bois et les divers composés éthers qui en proviennent, *Ann. Chim. Phys.*, 1835, **58**, 5–74.
- 3 Alain. Igau, Hansjorg. Grutzmacher, Antoine. Baceiredo and Guy. Bertrand, Analogous .alpha.,.alpha.'-bis-carbenoid, triply bonded species: synthesis of a stable .lambda.3-phosphino carbene-.lambda.5-phosphaacetylene, *J. Am. Chem. Soc.*, 1988, **110**, 6463–6466.
- 4 A. J. Arduengo, R. L. Harlow and M. Kline, A stable crystalline carbene, *J. Am. Chem. Soc.*, 1991, **113**, 361–363.
- 5 C. Heinemann and W. Thiel, Ab initio study on the stability of diaminocarbenes, *Chem. Phys. Lett.*, 1994, **217**, 11–16.
- 6 E. A. Carter and W. A. Goddard, Relation between singlet-triplet gaps and bond energies, *J. Phys. Chem.*, 1986, **90**, 998–1001.
- 7 M. N. Hopkinson, C. Richter, M. Schedler and F. Glorius, An overview of N-heterocyclic carbenes, *Nature*, 2014, **510**, 485–496.
- 8 D. J. Nelson and S. P. Nolan, Quantifying and understanding the electronic properties of N-heterocyclic carbenes, *Chem. Soc. Rev.*, 2013, **42**, 6723–6753.
- 9 M. Feroci, I. Chiarotto and A. Inesi, Advances in the Knowledge of N-Heterocyclic Carbenes Properties. The Backing of the Electrochemical Investigation, *Catalysts*, 2016, **6**, 178.
- 10 T. Itoh, Y. Nakata, K. Hirai and H. Tomioka, Triplet Diphenylcarbenes Protected by Trifluoromethyl and Bromine Groups. A Triplet Carbene Surviving a Day in Solution at Room Temperature, *J. Am. Chem. Soc.*, 2006, **128**, 957–967.
- 11 D. J. Nelson and S. P. Nolan, in *N-Heterocyclic Carbenes*, John Wiley & Sons, Ltd, 2014, pp. 1–24.
- 12 A. Poater, F. Ragone, S. Giudice, C. Costabile, R. Dorta, S. P. Nolan and L. Cavallo, Thermodynamics of N-Heterocyclic Carbene Dimerization: The Balance of Sterics and Electronics, *Organometallics*, 2008, **27**, 2679–2681.
- 13 P. de Frémont, N. Marion and S. P. Nolan, Carbenes: Synthesis, properties, and organometallic chemistry, *Coord. Chem. Rev.*, 2009, **253**, 862–892.
- 14 S. Díez-González, N. Marion and S. P. Nolan, N-Heterocyclic Carbenes in Late Transition Metal Catalysis, *Chem. Rev.*, 2009, **109**, 3612–3676.
- 15 E. Peris, Smart N-Heterocyclic Carbene Ligands in Catalysis, *Chem. Rev.*, 2018, **118**, 9988–10031.
- 16 N. Wang, J. Xu and J. K. Lee, The importance of N-heterocyclic carbene basicity in organocatalysis, *Org. Biomol. Chem.*, 2018, **16**, 8230–8244.
- 17 G. A. Grasa, R. Singh, N. M. Scott, E. D. Stevens and S. P. Nolan, Reactivity of a N-heterocyclic carbene, 1,3-di-(1-adamantyl) imidazol-2-ylidene, with a pseudo-acid: structural characterization of Claisen condensation adduct, *Chem. Commun.*, 2004, **0**, 2890–2891.
- 18 A. T. Biju, *N-Heterocyclic Carbenes in Organocatalysis*, John Wiley & Sons, 2019.

-
- 19 E. F. Connor, G. W. Nyce, M. Myers, A. Möck and J. L. Hedrick, First Example of N-Heterocyclic Carbenes as Catalysts for Living Polymerization: Organocatalytic Ring-Opening Polymerization of Cyclic Esters, *J. Am. Chem. Soc.*, 2002, **124**, 914–915.
 - 20 M. Feroci, I. Chiarotto, F. D’Anna, F. Gala, R. Noto, L. Ornano, G. Zollo and A. Inesi, N-Heterocyclic Carbenes and Parent Cations: Acidity, Nucleophilicity, Stability, and Hydrogen Bonding-Electrochemical Study and Ab Initio Calculations, *ChemElectroChem*, 2016, **3**, 1133–1141.
 - 21 S. Gehrke and O. Hollóczki, Are There Carbenes in N-Heterocyclic Carbene Organocatalysis?, *Angew. Chem. Int. Ed.*, 2017, **56**, 16395–16398.
 - 22 M. Fèvre, J. Pinaud, Y. Gnanou, J. Vignolle and D. Taton, N-Heterocyclic carbenes (NHCs) as organocatalysts and structural components in metal-free polymer synthesis, *Chem. Soc. Rev.*, 2013, **42**, 2142–2172.
 - 23 L. Jafarpour, E. D. Stevens and S. P. Nolan, A sterically demanding nucleophilic carbene: 1,3-bis(2,6-diisopropylphenyl)imidazol-2-ylidene). Thermochemistry and catalytic application in olefin metathesis, *J. Organomet. Chem.*, 2000, **606**, 49–54.
 - 24 A. J. Arduengo, J. R. Goerlich and W. J. Marshall, A stable diaminocarbene, *J. Am. Chem. Soc.*, 1995, **117**, 11027–11028.
 - 25 H. Sun, X. Fang, Y. R. Chi and G. Li, Theoretical Study of N-Heterocyclic Carbenes-Catalyzed Cascade Annulation of Benzodienones and Enals, *Chirality*, 2013, **25**, 521–528.
 - 26 P. Verma, P. A. Patni and R. B. Sunoj, Mechanistic Insights on N-Heterocyclic Carbene-Catalyzed Annulations: The Role of Base-Assisted Proton Transfers, *J. Org. Chem.*, 2011, **76**, 5606–5613.
 - 27 T. Dröge and F. Glorius, The Measure of All Rings—N-Heterocyclic Carbenes, *Angew. Chem. Int. Ed.*, 2010, **49**, 6940–6952.
 - 28 B. Gorodetsky, T. Ramnial, N. R. Branda and J. A. C. Clyburne, Electrochemical reduction of an imidazolium cation: a convenient preparation of imidazol-2-ylidenes and their observation in an ionic liquid, *Chem. Commun.*, 2004, 1972.
 - 29 N. Kuhn and T. Kratz, Synthesis of Imidazol-2-ylidenes by Reduction of Imidazole-2(3H)-thiones, *Synthesis*, 1993, **1993**, 561–562.
 - 30 B. Hogan and M. Albrecht, in *Reference Module in Chemistry, Molecular Sciences and Chemical Engineering*, Elsevier, 2016.
 - 31 R. Zhong, A. C. Lindhorst, F. J. Groche and F. E. Kühn, Immobilization of N-Heterocyclic Carbene Compounds: A Synthetic Perspective, *Chem. Rev.*, 2017, **117**, 1970–2058.
 - 32 C. W. Bielawski and R. H. Grubbs, Highly Efficient Ring-Opening Metathesis Polymerization (ROMP) Using New Ruthenium Catalysts Containing N-Heterocyclic Carbene Ligands, *Angew. Chem. Int. Ed.*, 2000, **39**, 2903–2906.
 - 33 A. C. Hillier, G. A. Grasa, M. S. Viciu, H. M. Lee, C. Yang and S. P. Nolan, Catalytic cross-coupling reactions mediated by palladium/nucleophilic carbene systems, *J. Organomet. Chem.*, 2002, **653**, 69–82.
 - 34 A. V. Zhukhovitskiy, M. J. MacLeod and J. A. Johnson, Carbene Ligands in Surface Chemistry: From Stabilization of Discrete Elemental Allotropes to Modification of Nanoscale and Bulk Substrates, *Chem. Rev.*, 2015, **115**, 11503–11532.

-
- 35 S. Roland, X. Ling and M.-P. Pileni, N-Heterocyclic Carbene Ligands for Au Nanocrystal Stabilization and Three-Dimensional Self-Assembly, *Langmuir*, 2016, **32**, 7683–7696.
- 36 L. Mercs and M. Albrecht, Beyond catalysis: N-heterocyclic carbene complexes as components for medicinal, luminescent, and functional materials applications, *Chem. Soc. Rev.*, 2010, **39**, 1903–1912.
- 37 C. Richter, K. Schaepe, F. Glorius and B. J. Ravoo, Tailor-made N-heterocyclic carbenes for nanoparticle stabilization, *Chem. Commun.*, 2014, **50**, 3204–3207.
- 38 N. E. Kamber, W. Jeong, S. Gonzalez, J. L. Hedrick and R. M. Waymouth, N-Heterocyclic Carbenes for the Organocatalytic Ring-Opening Polymerization of ϵ -Caprolactone, *Macromolecules*, 2009, **42**, 1634–1639.
- 39 J. Raynaud, C. Absalon, Y. Gnanou and D. Taton, N-Heterocyclic Carbene-Organocatalyzed Ring-Opening Polymerization of Ethylene Oxide in the Presence of Alcohols or Trimethylsilyl Nucleophiles as Chain Moderators for the Synthesis of α,ω -Heterodifunctionalized Poly(ethylene oxide)s, *Macromolecules*, 2010, **43**, 2814–2823.
- 40 M. Rodriguez, S. Marrot, T. Kato, S. Stérin, E. Fleury and A. Baceiredo, Catalytic activity of N-heterocyclic carbenes in ring opening polymerization of cyclic siloxanes, *J. Organomet. Chem.*, 2007, **692**, 705–708.
- 41 H. J. Altmann, S. Naumann and M. R. Buchmeiser, Protected N-heterocyclic carbenes as latent organocatalysts for the low-temperature curing of anhydride-hardened epoxy resins, *Eur. Polym. J.*, 2017, **95**, 766–774.
- 42 Y. Zhang, R. Liu, H. Jin, W. Song, R. Augustine and I. Kim, Straightforward access to linear and cyclic polypeptides, *Commun. Chem.*, 2018, **1**, 40.
- 43 M. Fèvre, J. Vignolle and D. Taton, Azolium hydrogen carbonates and azolium carboxylates as organic pre-catalysts for N-heterocyclic carbene-catalysed group transfer and ring-opening polymerisations, *Polym. Chem.*, 2013, **4**, 1995.
- 44 O. Coutelier, M. El Ezzi, M. Destarac, F. Bonnette, T. Kato, A. Baceiredo, G. Sivasankarapillai, Y. Gnanou and D. Taton, N-Heterocyclic carbene-catalysed synthesis of polyurethanes, *Polym. Chem.*, 2012, **3**, 605.
- 45 S. Naumann and M. R. Buchmeiser, Liberation of N-heterocyclic carbenes (NHCs) from thermally labile progenitors: protected NHCs as versatile tools in organo- and polymerization catalysis, *Catal Sci Technol*, 2014, **4**, 2466–2479.
- 46 L. Delaude, Betaine Adducts of N-Heterocyclic Carbenes: Synthesis, Properties, and Reactivity, *Eur. J. Inorg. Chem.*, 2009, **2009**, 1681–1699.
- 47 M. Hans, J. Wouters, A. Demonceau and L. Delaude, Synthesis and Organocatalytic Applications of Imidazol(in)ium-2-thiocarboxylates, *Eur. J. Org. Chem.*, 2011, **2011**, 7083–7091.
- 48 B. C. Norris, D. G. Sheppard, G. Henkelman and C. W. Bielawski, Kinetic and Thermodynamic Evaluation of the Reversible N-Heterocyclic Carbene–Isothiocyanate Coupling Reaction: Applications in Latent Catalysis, *J. Org. Chem.*, 2011, **76**, 301–304.
- 49 D. M. Denning, M. D. Thum and D. E. Falvey, Photochemical Reduction of CO₂ Using 1,3-Dimethylimidazolyliidene, *Org. Lett.*, 2015, **17**, 4152–4155.
- 50 D. M. Denning and D. E. Falvey, Solvent-Dependent Decarboxylation of 1,3-Dimethylimidazolium-2-Carboxylate, *J. Org. Chem.*, 2014, **79**, 4293–4299.
-

-
- 51 D. M. Denning and D. E. Falvey, Substituent and Solvent Effects on the Stability of *N*-Heterocyclic Carbene Complexes with CO₂, *J. Org. Chem.*, 2017, **82**, 1552–1557.
- 52 B. R. Van Ausdall, J. L. Glass, K. M. Wiggins, A. M. Aarif and J. Louie, A Systematic Investigation of Factors Influencing the Decarboxylation of Imidazolium Carboxylates, *J. Org. Chem.*, 2009, **74**, 7935–7942.
- 53 M. Fèvre, J. Pinaud, A. Leteneur, Y. Gnanou, J. Vignolle, D. Taton, K. Miqueu and J.-M. Sotiropoulos, Imidazol(in)ium Hydrogen Carbonates as a Genuine Source of *N*-Heterocyclic Carbenes (NHCs): Applications to the Facile Preparation of NHC Metal Complexes and to NHC-Organocatalyzed Molecular and Macromolecular Syntheses, *J. Am. Chem. Soc.*, 2012, **134**, 6776–6784.
- 54 M. Fèvre, P. Coupillaud, K. Miqueu, J.-M. Sotiropoulos, J. Vignolle and D. Taton, Imidazolium Hydrogen Carbonates versus Imidazolium Carboxylates as Organic Precatalysts for *N*-Heterocyclic Carbene Catalyzed Reactions, *J. Org. Chem.*, 2012, **77**, 10135–10144.
- 55 I. Chiarotto, L. Mattiello, F. Pandolfi, D. Rocco and M. Feroci, NHC in Imidazolium Acetate Ionic Liquids: Actual or Potential Presence?, *Front. Chem.*, 2018, **6**, article 355.
- 56 R. Lambert, P. Coupillaud, A.-L. Wirotius, J. Vignolle and D. Taton, Imidazolium-Based Poly(Ionic Liquid)s Featuring Acetate Counter Anions: Thermally Latent and Recyclable Precursors of Polymer-Supported *N*-Heterocyclic Carbenes for Organocatalysis, *Macromol. Rapid Commun.*, 2016, **37**, 1143–1149.
- 57 S. Garmendia, R. Lambert, A.-L. Wirotius, J. Vignolle, A. P. Dove, R. K. O'Reilly and D. Taton, Facile synthesis of reversibly crosslinked poly(ionic liquid)-type gels: Recyclable supports for organocatalysis by *N*-heterocyclic carbenes, *Eur. Polym. J.*, 2018, **107**, 82–88.
- 58 R. Lambert, A.-L. Wirotius and D. Taton, Intramolecular Quaternization as Folding Strategy for the Synthesis of Catalytically Active Imidazolium-Based Single Chain Nanoparticles, *ACS Macro Lett.*, 2017, **6**, 489–494.
- 59 B. P. Kar and W. Sander, Reversible Carbene Formation in the Ionic Liquid 1-Ethyl-3-Methylimidazolium Acetate by Vaporization and Condensation, *ChemPhysChem*, 2015, **16**, 3603–3606.
- 60 F. Yan, N. R. Dhumal and H. J. Kim, CO₂ capture in ionic liquid 1-alkyl-3-methylimidazolium acetate: a concerted mechanism without carbene, *Phys. Chem. Chem. Phys.*, 2017, **19**, 1361–1368.
- 61 J. X. Mao, J. A. Steckel, F. Yan, N. Dhumal, H. Kim and K. Damodaran, Understanding the mechanism of CO₂ capture by 1,3 di-substituted imidazolium acetate based ionic liquids, *Phys. Chem. Chem. Phys.*, 2016, **18**, 1911–1917.
- 62 G. W. Nyce, S. Csihony, R. M. Waymouth and J. L. Hedrick, A General and Versatile Approach to Thermally Generated *N*-Heterocyclic Carbenes, *Chem.: Eur. J.*, 2004, **10**, 4073–4079.
- 63 O. Coulembier, B. G. G. Lohmeijer, A. P. Dove, R. C. Pratt, L. Mespouille, D. A. Culkin, S. J. Benight, P. Dubois, R. M. Waymouth and J. L. Hedrick, Alcohol Adducts of *N*-Heterocyclic Carbenes: Latent Catalysts for the Thermally-Controlled Living Polymerization of Cyclic Esters, *Macromolecules*, 2006, **39**, 5617–5628.
- 64 N. Stefan, S. Friedrich Georg, F. Wolfgang and B. Michael Richard, Protected *N*-heterocyclic carbenes as latent pre-catalysts for the polymerization of ϵ -caprolactone, *Polym. Chem.*, 2013, **4**, 1995–2003.

-
- 65 T. K. Achar, A. Bose and P. Mal, Mechanochemical synthesis of small organic molecules, *Beilstein J. Org. Chem.*, 2017, **13**, 1907–1931.
- 66 R. Groote, R. T. M. Jakobs and R. P. Sijbesma, Performance of Mechanochemically Activated Catalysts Is Enhanced by Suppression of the Thermal Effects of Ultrasound, *ACS Macro Lett.*, 2012, **1**, 1012–1015.
- 67 R. Groote, L. van Haandel and R. P. Sijbesma, The effect of molecular weight and catalyst concentration on catalytic activity in mechanochemically activated transesterification using silver(I)-N-heterocyclic carbene latent catalysts, *J. Polym. Sci. Part A: Polym. Chem.*, 2012, **50**, 4929–4935.
- 68 A. Piermattei, S. Karthikeyan and R. P. Sijbesma, Activating catalysts with mechanical force, *Nat. Chem.*, 2009, **1**, 133–137.
- 69 A. V. Zhukhovitskiy, J. Geng and J. A. Johnson, Cycloelimination of Imidazolidin-2-ylidene N-Heterocyclic Carbenes: Mechanism and Insights into the Synthesis of Stable “NHC-CDI” Amidinates, *Chem.: Eur. J.*, 2015, **21**, 5685–5688.
- 70 M. B. Larsen, Mechanochemical activation of latent N-heterocyclic carbene catalysts, *PhD Thesis Eindhoven Univ. Tech.*, 2015.
- 71 G. Maier, J. Endres and H. P. Reisenauer, 2,3-Dihydrothiazol-2-ylidene, *Angew. Chem. Int. Ed.*, 1997, **36**, 1709–1712.
- 72 G. Maier and J. Endres, 2,3-Dihydroimidazol-2-ylidene, *Eur. J. Org. Chem.*, 1998, **1998**, 1517–1520.
- 73 P. Emeline, Catalyseurs organiques photolatents pour la polymérisation par ouverture de cycle différée, *PhD Thesis University of Montpellier*, 2018.
- 74 S. Naumann and A. P. Dove, N-Heterocyclic carbenes as organocatalysts for polymerizations: trends and frontiers, *Polym. Chem.*, 2015, **6**, 3185–3200.
- 75 S. Naumann and A. P. Dove, N-Heterocyclic carbenes for metal-free polymerization catalysis: an update, *Polym. Int.*, 2016, **65**, 16–27.
- 76 S. Csihony, D. A. Culkin, A. C. Sentman, A. P. Dove, R. M. Waymouth and J. L. Hedrick, Single-Component Catalyst/Initiators for the Organocatalytic Ring-Opening Polymerization of Lactide, *J. Am. Chem. Soc.*, 2005, **127**, 9079–9084.
- 77 E. Brulé, V. Guéineau, P. Vermaut, F. Prima, J. Balogh, L. Maron, A. M. Z. Slawin, S. P. Nolan and C. M. Thomas, Polymerization of cyclic esters using N-heterocyclic carbene carboxylate catalysts, *Polym. Chem.*, 2013, **4**, 2414–2423.
- 78 S. Naumann, F. G. Schmidt, M. Speiser, M. Böhl, S. Epple, C. Bonten and M. R. Buchmeiser, Anionic Ring-Opening Homo- and Copolymerization of Lactams by Latent, Protected N-Heterocyclic Carbenes for the Preparation of PA 12 and PA 6/12, *Macromolecules*, 2013, **46**, 8426–8433.
- 79 S. Naumann, S. Epple, C. Bonten and M. R. Buchmeiser, Polymerization of ϵ -Caprolactam by Latent Precatalysts Based on Protected N-Heterocyclic Carbenes, *ACS Macro Lett.*, 2013, **2**, 609–612.
- 80 A. K. Reitz, Q. Sun, R. Wilhelm and D. Kuckling, The use of stable carbene-CO₂ adducts for the polymerization of trimethylene carbonate, *J. Polym. Sci. Part A: Polym. Chem.*, 2017, **55**, 820–829.
- 81 S. Naumann and M. R. Buchmeiser, Latent and Delayed Action Polymerization Systems, *Macromol. Rapid Commun.*, 2014, **35**, 682–701.
- 82 J. Raynaud, C. Absalon, Y. Gnanou and D. Taton, N-Heterocyclic Carbene-Induced Zwitterionic Ring-Opening Polymerization of Ethylene Oxide and Direct Synthesis of α,ω -Difunctionalized Poly(ethylene

-
- oxide)s and Poly(ethylene oxide)-b-poly(ϵ -caprolactone) Block Copolymers, *J. Am. Chem. Soc.*, 2009, **131**, 3201–3209.
- 83 R. Lindner, M. L. Lejkowski, S. Lavy, P. Deglmann, K. T. Wiss, S. Zorbakhsh, L. Meyer and M. Limbach, Ring-Opening Polymerization and Copolymerization of Propylene Oxide Catalyzed by N-Heterocyclic Carbenes, *ChemCatChem*, 2014, **6**, 618–625.
- 84 S. Naumann, M. Speiser, R. Schowner, E. Giebel and M. R. Buchmeiser, Air Stable and Latent Single-Component Curing of Epoxy/Anhydride Resins Catalyzed by Thermally Liberated N-Heterocyclic Carbenes, *Macromolecules*, 2014, **47**, 4548–4556.
- 85 B. Bantu, G. M. Pawar, U. Decker, K. Wurst, A. M. Schmidt and M. R. Buchmeiser, CO₂ and Sn^{II} Adducts of N-Heterocyclic Carbenes as Delayed-Action Catalysts for Polyurethane Synthesis, *Chem.: Eur. J.*, 2009, **15**, 3103–3109.
- 86 B. Bhasker, P. Gajanan Manohar, W. Klaus, D. Ulrich, S. Alex Michael and B. Michael Richard, CO₂, Magnesium, Aluminum, and Zinc Adducts of N-Heterocyclic Carbenes as (Latent) Catalysts for Polyurethane Synthesis, *Eur. J. Inorg. Chem.*, 2009, **2009**, 1970–1976.
- 87 P. U. Naik, K. Refes, F. Sadaka, C.-H. Brachais, G. Boni, J.-P. Couvercelle, M. Picquet and L. Plasseraud, Organo-catalyzed synthesis of aliphatic polycarbonates in solvent-free conditions, *Polym. Chem.*, 2012, **3**, 1475–1480.
- 88 O. M. Ogba, N. C. Warner, D. J. O’Leary and R. H. Grubbs, Recent advances in ruthenium-based olefin metathesis, *Chem. Soc. Rev.*, 2018, **47**, 4510–4544.
- 89 L. Delaude, A. Demonceau and A. F. Noels, Synthesis and Application of New N-Heterocyclic Carbene Ruthenium Complexes in Catalysis: A Case Study, *Curr. Org. Chem.*, 2006, **10**, 203–215.
- 90 A. Demonceau, A. W. Stumpf, E. Saive and A. F. Noels, Novel Ruthenium-Based Catalyst Systems for the Ring-Opening Metathesis Polymerization of Low-Strain Cyclic Olefins, *Macromolecules*, 1997, **30**, 3127–3136.
- 91 L. Delaude and A. Demonceau, Retracing the evolution of monometallic ruthenium–arene catalysts for C–C bond formation, *Dalton Trans.*, 2012, **41**, 9257–9268.
- 92 A. Tudose, A. Demonceau and L. Delaude, Imidazol(in)ium-2-carboxylates as N-heterocyclic carbene precursors in ruthenium–arene catalysts for olefin metathesis and cyclopropanation, *J. Organomet. Chem.*, 2006, **691**, 5356–5365.
- 93 R. H. Grubbs, Ed., *Handbook of metathesis. Vol. 1: Catalyst development and mechanism*, Wiley-VCH, Weinheim, 2. ed., 2015.
- 94 C. Slugovc, in *Olefin metathesis: theory and practice*, Grela, Karol, Hoboken, New Jersey, Wiley., 2014, pp. 329–33.
- 95 S. Naumann and M. R. Buchmeiser, Latent and Delayed Action Polymerization Systems, *Macromol Rapid Commun*, 2014, **35**, 682–701.
- 96 Y. Vidavsky and N. G. Lemcoff, Light-induced olefin metathesis, *Beilstein J Org Chem*, 2010, **6**, 1106–1119.
- 97 P. Glöckner, T. Jung, S. Struck and K. Studer, Eds., *Radiation curing: coatings and printing inks ; technical basics, applications and trouble shooting*, Vincentz Network, Hannover, 2008.

-
- 98 O. Eivgi and N. Lemcoff, Turning the Light On: Recent Developments in Photoinduced Olefin Metathesis, *Synthesis*, 2018, **50**, 49–63.
- 99 O. Reany and N. Gabriel Lemcoff, Light guided chemoselective olefin metathesis reactions, *Pure Appl. Chem.*, 2017, **89**, 829–840.
- 100 K. A. Ogawa, A. E. Goetz and A. J. Boydston, Developments in Externally Regulated Ring-Opening Metathesis Polymerization, *Synlett*, 2016, **27**, 203–214.
- 101 United States, US4060468A, 1977.
- 102 C. Tanielian, R. Kieffer and A. Harfouch, Reactions photoinduites et photoactives des olefines en presence de metaux carbonyles du 6° groupe dans CCl₄, *Tetrahedron Lett.*, 1977, **52**, 4589–4592.
- 103 P. Krausz, F. Garnier and J.-E. Dubois, Reaction de metathese des olefines induite photochimiquement en presence d'un complexe de metal de transition: III. Caracterisation generale de la transformation, *J Organomet Chem*, 1978, **146**, 125–134.
- 104 P. G. M. Schilder, D. J. Stufkens, A. Oskam and J. C. Mol, Metathesis of 2-pentene with the W(CO)₆/CCl₄/hv- system. Role and physical properties of the photogenerated precipitate, *J. Organomet. Chem.*, 1992, **426**, 351–359.
- 105 G. Bhukta, R. Manivannan and G. Sundararajan, Studies on the nature of active species in W(CO)₆/CCl₄/hw system as applied to metathesis polymerisation reactions, *J. Organomet. Chem.*, 2000, **601**, 16–21.
- 106 P. A. van der Schaaf, A. Hafner and A. Mühlebach, Photoinduced Ring-Opening Metathesis Polymerization(PROMP) with Photochemically Generated Schrock-Type Catalysts, *Angew. Chem. Int. Ed.*, 1996, **35**, 1845–1847.
- 107 T. Karlen, A. Ludi, A. Mühlebach, P. Bernhard and C. Pharis, Photoinduced ring opening metathesis polymerization (PROMP) of strained bicyclic olefins with ruthenium complexes of the type [(η⁶-arene₁)Ru(η⁶-arene₂)₂]² and [Ru(Nc-R)₆]², *J. Polym. Sci. Part A: Polym. Chem.*, 1995, **33**, 1665–1674.
- 108 A. Hafner, A. Mühlebach and P. A. van der Schaaf, One-Component Catalysts for Thermal and Photoinduced Ring Opening Metathesis Polymerization, *Angew. Chem. Int. Ed.*, 1997, **36**, 2121–2124.
- 109 L. Delaude, A. Demonceau and A. F. Noels, Visible light induced ring-opening metathesis polymerisation of cyclooctene, *Chem. Commun.*, 2001, 986–987.
- 110 Y. Zhang, D. Wang, P. Lönnecke, T. Scherzer and M. R. Buchmeiser, Novel Initiators for Thermally and UV-Trigged ROMP, *Macromol. Symp.*, 2006, **236**, 30–37.
- 111 D. Wang, K. Wurst, W. Knolle, U. Decker, L. Prager, S. Naumov and M. R. Buchmeiser, Cationic RuII Complexes with N-Heterocyclic Carbene Ligands for UV-Induced Ring-Opening Metathesis Polymerization, *Angew. Chem. Int. Ed.*, 2008, **47**, 3267–3270.
- 112 D. Wang, K. Wurst and M. R. Buchmeiser, Cationic versus Neutral RuII-N-Heterocyclic Carbene Complexes as Latent Precatalysts for the UV-Induced Ring-Opening Metathesis Polymerization, *Chem.: Eur. J.*, 2010, **16**, 12928–12934.
- 113 O. Eivgi, S. Guidone, A. Frenklah, S. Kozuch, I. Goldberg and N. G. Lemcoff, Photoactivation of Ruthenium Phosphite Complexes for Olefin Metathesis, *ACS Catal.*, 2018, **8**, 6413–6418.
- 114 B. K. Keitz and R. H. Grubbs, A Tandem Approach to Photoactivated Olefin Metathesis: Combining a Photoacid Generator with an Acid Activated Catalyst, *J. Am. Chem. Soc.*, 2009, **131**, 2038–2039.

-
- 115 A. Y. Khalimon, E. M. Leitaó and W. E. Piers, Photogeneration of a Phosphonium Alkylidene Olefin Metathesis Catalyst, *Organometallics*, 2012, **31**, 5634–5637.
- 116 L. Pichavant, P. Lacroix-Desmazes, A. Chemtob, J. Pinaud and V. Héroguez, Photolabile ring-opening metathesis polymerization in miniemulsion: a powerful approach to produce polynorbornene latexes, *Polym. Chem.*, 2018, **9**, 5491–5498.
- 117 J. Pinaud, E. Placet, P. Lacroix-Desmazes, T. K. H. Trinh, J. P. Malval, A. Chemtob, L. Pichavant and V. Héroguez, Photogeneration of N-Heterocyclic Carbenes: Application in Photoinduced Ring-Opening Metathesis Polymerization, *JoVE J. Vis. Exp.*, 2018, e58539.
- 118 E. Merino and M. Ribagorda, Control over molecular motion using the *cis* – *trans* photoisomerization of the azo group, *Beilstein J. Org. Chem.*, 2012, **8**, 1071–1090.
- 119 R. S. Stoll, M. V. Peters, A. Kuhn, S. Heiles, R. Goddard, M. Bühl, C. M. Thiele and S. Hecht, Photoswitchable Catalysts: Correlating Structure and Conformational Dynamics with Reactivity by a Combined Experimental and Computational Approach, *J. Am. Chem. Soc.*, 2009, **131**, 357–367.
- 120 A. Ben-Asuly, A. Aharoni, C. E. Diesendruck, Y. Vidavsky, I. Goldberg, B. F. Straub and N. G. Lemcoff, Photoactivation of Ruthenium Olefin Metathesis Initiators, *Organometallics*, 2009, **28**, 4652–4655.
- 121 J. A. Mata, M. Poyatos and E. Peris, Structural and catalytic properties of chelating bis- and tris-N-heterocyclic carbenes, *Coord. Chem. Rev.*, 2007, **251**, 841–859.
- 122 Y. Vidavsky, A. Anaby and N. G. Lemcoff, Chelating alkylidene ligands as pacifiers for ruthenium catalysed olefinmetathesis, *Dalton Trans*, 2012, **41**, 32–43.
- 123 T. Ung, A. Hejl, R. H. Grubbs and Y. Schrodi, Latent Ruthenium Olefin Metathesis Catalysts That Contain an N-Heterocyclic Carbene Ligand, *Organometallics*, 2004, **23**, 5399–5401.
- 124 C. E. Diesendruck, Y. Vidavsky, A. Ben-Asuly and N. G. Lemcoff, A latent s-chelated ruthenium benzylidene initiator for ring-opening metathesis polymerization, *J. Polym. Sci. Part A: Polym. Chem.*, 2009, **47**, 4209–4213.
- 125 R. L. Sutar, E. Levin, D. Butilkov, I. Goldberg, O. Reany and N. G. Lemcoff, A Light-Activated Olefin Metathesis Catalyst Equipped with a Chromatic Orthogonal Self-Destruct Function, *Angew. Chem. Int. Ed.*, 2016, **55**, 764–767.
- 126 C. E. Diesendruck, O. Iliashevsky, A. Ben-Asuly, I. Goldberg and N. G. Lemcoff, Latent and Switchable Olefin Metathesis Catalysts, *Macromol. Symp.*, 2010, **293**, 33–38.
- 127 D. Wang, J. Unold, M. Bubrin, I. Elser, W. Frey, W. Kaim, G. Xu and M. R. Buchmeiser, Ruthenium-Triazene Complexes as Latent Catalysts for UV-Induced ROMP: Ruthenium-Triazene Complexes for UV-Induced ROMP, *Eur. J. Inorg. Chem.*, 2013, **2013**, 5462–5468.
- 128 V. Sashuk and O. Danylyuk, A Thermo- and Photo-Switchable Ruthenium Initiator For Olefin Metathesis, *Chem.: Eur. J.*, 2016, **22**, 6528–6531.
- 129 A. J. Teator, H. Shao, G. Lu, P. Liu and C. W. Bielawski, A Photoswitchable Olefin Metathesis Catalyst, *Organometallics*, 2017, **36**, 490–497.
- 130 K. A. Ogawa, A. E. Goetz and A. J. Boydston, Metal-Free Ring-Opening Metathesis Polymerization, *J. Am. Chem. Soc.*, 2015, **137**, 1400–1403.
- 131 S. Poplata, A. Tröster, Y.-Q. Zou and T. Bach, Recent Advances in the Synthesis of Cyclobutanes by Olefin [2 + 2] Photocycloaddition Reactions, *Chem. Rev.*, 2016, **116**, 9748–9815.
-

-
- 132 K. Chiba, T. Miura, S. Kim, Y. Kitano and M. Tada, Electrocatalytic Intermolecular Olefin Cross-Coupling by Anodically Induced Formal [2+2] Cycloaddition between Enol Ethers and Alkenes, *J. Am. Chem. Soc.*, 2001, **123**, 11314–11315.
- 133 T. Miura, S. Kim, Y. Kitano, M. Tada and K. Chiba, Electrochemical Enol Ether/Olefin Cross-Metathesis in a Lithium Perchlorate/Nitromethane Electrolyte Solution, *Angew. Chem. Int. Ed.*, 2006, **45**, 1461–1463.
- 134 K. Ogawa, A. Goetz and A. Boydston, Developments in Externally Regulated Ring-Opening Metathesis Polymerization, *Synlett*, 2015, **27**, 203–214.
- 135 N. A. Romero and D. A. Nicewicz, Organic Photoredox Catalysis, *Chem. Rev.*, 2016, **116**, 10075–10166.
- 136 J. Botzem, U. Haberl, E. Steckhan, S. Blechert, I. Søtofte, G. W. Francis, J. Szúnyog and B. Långström, Radical Cation Cycloaddition Reactions of 2-Vinylbenzofurans and 2-Vinylfurans by Photoinduced Electron Transfer., *Acta Chem. Scand.*, 1998, **52**, 175–193.
- 137 L. M. M. Pascual, A. E. Goetz, A. M. Roehrich and A. J. Boydston, Investigation of Tacticity and Living Characteristics of Photoredox-Mediated Metal-Free Ring-Opening Metathesis Polymerization, *Macromol. Rapid Commun.*, 2017, **38**, 1600766.
- 138 A. E. Goetz and A. J. Boydston, Metal-Free Preparation of Linear and Cross-Linked Polydicyclopentadiene, *J. Am. Chem. Soc.*, 2015, **137**, 7572–7575.
- 139 A. E. Goetz, L. M. M. Pascual, D. G. Dunford, K. A. Ogawa, D. B. Knorr and A. J. Boydston, Expanded Functionality of Polymers Prepared Using Metal-Free Ring-Opening Metathesis Polymerization, *ACS Macro Lett.*, 2016, **5**, 579–582.
- 140 P. Lu, N. M. Alrashdi and A. J. Boydston, Bidirectional metal-free ROMP from difunctional organic initiators, *J. Polym. Sci. Part A: Polym. Chem.*, 2017, **55**, 2977–2982.
- 141 L. Pascual, D. Dunford, A. Goetz, K. Ogawa and A. Boydston, Comparison of Pirylium and Thiopyrylium Photooxidants in Metal-Free Ring-Opening Metathesis Polymerization, *Synlett*, 2016, **27**, 759–762.
- 142 W. N. Ottou, H. Sardon, D. Mecerreyes, J. Vignolle and D. Taton, Update and challenges in organo-mediated polymerization reactions, *Prog. Polym. Sci.*, 2016, **56**, 64–115.
- 143 R. A. Weitekamp, H. A. Atwater and R. H. Grubbs, Photolithographic Olefin Metathesis Polymerization, *J. Am. Chem. Soc.*, 2013, **135**, 16817–16820.

CHAPTER II. MIXTURE OF AZOLIUM TETRAPHENYLBORATE WITH ISOPROPYLTHIOXANTHONE: A NEW CLASS OF N-HETEROCYCLIC CARBENE (NHC) PHOTOGENERATOR FOR POLYURETHANE, POLYESTER AND ROMP POLYMERS SYNTHESIS

The text in this chapter is reproduced in part with permission from:

J. Pinaud, T. K. H. Trinh, D. Sauvanier, E. Placet, S. Songsee, P. Lacroix-Desmazes, J.-M. Becht, B. Tarablsi, J. Lalevée, L. Pichavant, V. Héroguez and A. Chemtob, In Situ Generated Ruthenium-Arene Catalyst for Photoactivated Ring-Opening Metathesis Polymerization through Photolabile N-Heterocyclic Carbene Ligand, *Chem.: Eur. J.*, 2018, **24**, 337–341.

T. K. H. Trinh, J. P. Malval, F. Morlet-Savary, J. Pinaud, P. Lacroix-Desmazes, C. Reibel, V. Héroguez and A. Chemtob, Mixture of azolium tetrphenylborate with isopropylthioxanthone: a new class of N-heterocyclic carbene (NHC) photogenerator for polyurethane, polyester and ROMP polymers synthesis, *Chem.: Eur. J.*, 2019, DOI: doi.org/10.1002/chem.201901000.

©Wiley-VCH 2016
69451 Weinheim, Germany

2.1 INTRODUCTION

In a ground-breaking work, Arduengo *et al.* presented in 1991 the first successful isolation of a stable *N*-heterocyclic carbene (NHC).¹ Since this achievement, NHCs have been at the forefront of organometallic chemistry,^{2,3} catalysis,⁴ and more recently polymerization.⁵ To date, the most frequently encountered NHCs are 1,3-bis(mesityl)imidazol-2-ylidene (**IMes**) and its saturated congener 1,3-bis(mesityl)imidazolidin-2-ylidene (**SIMes**) (**Figure 2.1**).

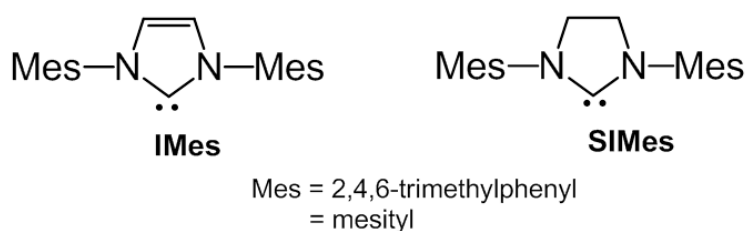


Figure 2.1. **IMes** and **SIMes** are among the most frequently employed NHCs.

Thanks to their excellent σ -donor ability, the NHC ligands have gradually replaced phosphines, that are not environmentally benign.^{6–8} After reaction with transition metals, they can form well-defined NHC-metal complexes displaying outstanding catalytic activity. The most prominent examples are the ruthenium alkylidene complexes coordinated with NHC ligand used in olefin metathesis, including the so-called Hoveyda–Grubbs second-generation catalyst and its multiple derivatives.⁹ In addition, their strong nucleophilicity and Brønsted basicity have contributed to their use as organocatalysts. In polymerization, they can replace organometallic compounds with advantages of reducing cost and toxicity. The range of NHC-mediated polymerizations^{5,10,11} already covers ring-opening polymerization (lactone,¹² lactam,¹³ epoxide¹⁴) as well as step-growth polymerization for the synthesis of polybenzoin¹⁵ or polyurethane.¹⁶

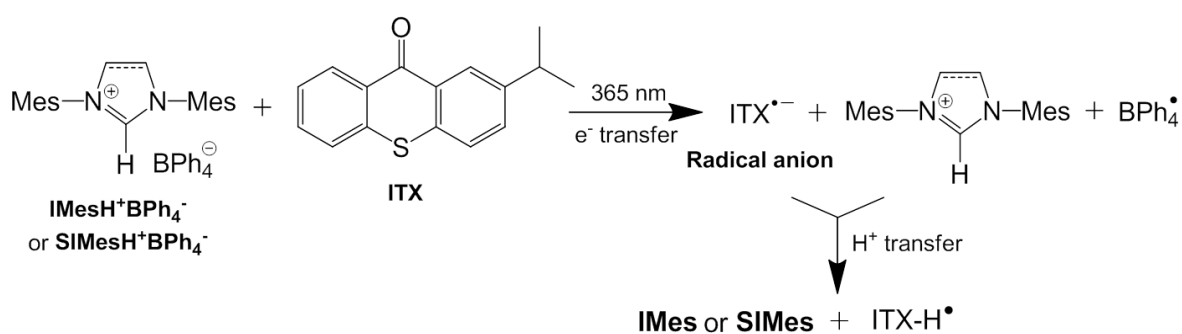
Despite the wealth of research conducted to date, the practical use of NHCs presents a number of challenges: NHCs are highly sensitive to moisture, and must be handled under dry atmosphere. Moreover, they react with acids due to their high pK_a , and are also prone to dimerize.^{17,18} Because of these constraints, NHCs are usually put in contact with substrates or monomers at the last moment. Considering the central role of NHCs in chemistry, it is essential to control and optimize their formation conditions. The issues are to facilitate storage, handling, processing, and more broadly, to promote scale-up from laboratory to production. Currently, *in situ* deprotonation of an azolium salt is by far the most commonly used methodology to access a free or ligated NHC.^{19–21} However, this methodology requires a

strong base, that limits the scope of substrates and may interfere in the polymerization process as adventitious initiator.²² In the search of smarter routes for in situ and “on demand” release of NHC, “masked” or “protected” NHCs have been investigated recently.^{22,23} Of high interest are thermally-labile NHC progenitors based on air-stable NHC-CO₂ adduct,²⁴ NHC-isothiocyanate adduct²⁵ or NHC-metal complex.²⁶ Upon heating, the adduct/complex bond may be broken and the carbene transferred. Despite promising results, such approach has important limitations related to reversible cleavage, poor solubility of many NHC adducts, incomplete latency at ambient conditions resulting in early reaction, byproducts’ formation, and additional energy expense due to heating.²²

Despite the many developments in the field of photoinitiators,^{27,28} very little attention has been given to photolabile NHC precursors. In 2015, Denning *et al.*²⁹ reported the photochemical reduction of an imidazolium-2-carboxylate (NHC-CO₂) using an excited state electron donor, N,N,N',N'-tetramethylbenzidine. The reduced formate complex might then decompose into NHC and formate ion. However, the authors only detected the corresponding imidazolium (the conjugated acid of the NHC), which was not an issue because the principal goal was actually the controlled capture and release of CO₂. The limited research effort on NHC photogenerator is in contrast with the strong interest for other photobase generators (PBGs), capable of releasing amidine or guanidine organosuperbases.³⁰ Most PBGs proceed through a photoinduced proton transfer reaction employing a salt containing the protonated superbase and an anion chromophore based on ketoprofene,³¹ thioxanthone derivatives,³² and tetraphenylborate.³³⁻³⁵

Today, there are strong motivations for developing photoNHC-mediated reactions: temporal and spatial control of reaction, use of a contactless stimulation, and NHC release at ambient condition by precise energetic and spatial dosage of radiation. Our aim is to design a novel NHC photogenerator, both stable in absence of light and capable of releasing in situ free NHC under UV exposure, preferentially UVA (320 – 400 nm) to avoid substrate or solvent excitation. For this purpose, imidazolium or imidazolium salts seem the most appropriate photolabile NHC precursors. Like many ionic liquids, they are air/moisture stable, thermally inert and chemically quite stable. The challenge is thus how to promote a photochemically induced proton transfer reaction that would convert the starting inactive azolium salt into an active NHC. The proposed solution is to produce a suitable radical anion via a photoinduced electron-transfer (PET) reaction, which can subsequently deprotonate the azolium cation (**Scheme 2.1**). To this end, we begin with a mixture of isopropylthioxanthone

(ITX) with an air-stable azolium tetraphenylborate salt, such as 1,3-bis(mesityl)imidazolium tetraphenylborate **IMesH⁺BPh₄⁻** or 1,3-bis(mesityl)imidazolium tetraphenylborate **SIMesH⁺BPh₄⁻**.³⁶ First, ITX is an inexpensive, commercially available aryl ketone, known for its ability to mediate single electron-transfer after photochemical excitation in the near UV-Vis region (350 - 420 nm); in particular, excited ITX is used as an electron acceptor sensitizer in many photoreactions.³⁷ On the other hand, the tetraphenylborate anion may act as suitable electron donating partner to make PET thermodynamically feasible.^{38,39} Therefore, the expected primary photochemical process is electron-transfer from BPh₄⁻ to triplet ITX. In second step, the resulting intermediate ITX radical anion might effectively abstract proton from **IMesH⁺** (or **SIMesH⁺**) to form NHC **IMes** (or **SIMes**).



Scheme 2.1. Photolysis mechanism for the photogeneration of **IMes** (or **SIMes**) from the bicomponent photogenerating system **ITX/IMesH⁺BPh₄⁻** (or **ITX/SIMesH⁺BPh₄⁻**).

Encouraged by preliminary results proving the release of NHC upon irradiation,³⁶ this current work describes a comprehensive study of this new class of bicomponent NHC photogenerator — **ITX/IMesH⁺BPh₄⁻** and **ITX/SIMesH⁺BPh₄⁻** — with four distinct parts. Firstly, we propose two novel analytical methods to characterize the photochemically released NHCs through their conversion in suitable adducts: carbene-radical adduct enables an identification method by using electron paramagnetic resonance (EPR) spectroscopy, while stable NHC-carbodiimide adduct facilitates the quantification of photoNHC yield using ¹H NMR. Secondly, to support the 2-step photochemical pathway based on electron/proton transfer reactions, experiments of real-time photobleaching of ITX are performed as well as calculation of the free energy change of electron-transfer with Rehm-Weller equation. Thirdly, using a mechanism-guided approach, NHC yield are optimized by investigating the effect of irradiation time, sensitizer concentration and structure. In a last part, the NHC photogenerator is harnessed to prepare a variety of polymer structures through their two fold role. As organocatalyst, polyurethane and polyester were prepared by step-growth polymerization and ring-opening copolymerization, respectively. As ligand, polynorbornene

was synthesized by ring-opening metathesis polymerization (ROMP) using a NHC-coordinated Ru catalyst.

2.2 EXPERIMENTALS

2.2.1 Materials

1,3-Bis(mesityl)imidazolium chloride ($\text{IMesH}^+\text{Cl}^-$, 98 %), sodium tetraphenylborate (NaBPh_4 , 99.5 %), diphenyl(2,4,6-trimethylbenzoyl)phosphine oxide (TPO, >98%), isophorone diisocyanate (IPDI, 99.0 %), polyethylene glycol 400 $\text{g}\cdot\text{mol}^{-1}$ (PEG_{400}), and vinyl ethyl ether (> 98.0 %) were purchased from TCI. 1,3-Bis(mesityl)imidazole-2-ylidene (**IMes**, 97 %), 1,3-bis(mesityl)imidazolidin-2-ylidene (**SIMes**, 97 %), 1,3-bis(mesityl)imidazolium chloride ($\text{SIMesH}^+\text{Cl}^-$, 98 %), acetonitrile- d_3 ($\text{ACN-}d_3$, 99.8 % D), isopropyl-9H-thioxanthen-9-one, mixture of 2- and 4-isomers (ITX, 97%), 1,3-di-*p*-tolylcarbodiimide (CDI, 96 %), 4,4'-bis(diethylamino)benzophenone (EAB, > 99 %), camphorquinone (CQ, 98 %), phthalic anhydride (PA, > 99 %), cyclohexene oxide (CHO, 98%) and dichloromethane were obtained from Sigma Aldrich. Dichloromethane- d_2 (CD_2Cl_2 , 99.5 % D), tetrahydrofuran- d_8 ($\text{THF-}d_8$, 99.5 % D), chloroform- d_1 (CDCl_3 , 99.5 % D) and dimethyl sulfoxide- d_6 ($\text{DMSO-}d_6$, 99.5 % D) were bought from Eurisotop. Dichloro(*p*-cymene)ruthenium(II) dimer ($[\text{RuCl}_2(\textit{p}\text{-cymene})]_2$, 98 %), was obtained from Strem Chemicals. Other HPLC grade solvents such as ethanol, acetonitrile and tetrahydrofuran (THF) were received from VWR. All the solvents and CHO were distilled and stored over molecular sieve (4 Å) under nitrogen atmosphere before use.

2.2.2 Synthesis

a. Synthesis of azolium tetrphenylborate salts

$\text{IMesH}^+\text{BPh}_4^-$ and $\text{SIMesH}^+\text{BPh}_4^-$ were prepared following a typical procedure below.³⁶

Two separate 250 ml RB flasks were charged with $\text{IMesH}^+\text{Cl}^-$ (4.00 g, 11.7 mmol) (or $\text{SIMesH}^+\text{Cl}^-$ (4.01 g, 11.7 mmol)) and NaBPh_4 (5.38 g, 15.7 mmol). Ethanol (120 ml) was added in each flask. Then, the $\text{IMesH}^+\text{Cl}^-$ (or $\text{SIMesH}^+\text{Cl}^-$) solution was added dropwise to NaBPh_4 solution under continuous stirring during 60 min (**Figure A.II.1**). A white precipitate formed, which was recovered by filtration, washed with ethanol and then with water, and finally dried at 60 °C during 15 h. The white solid was readily soluble in dichloromethane, tetrahydrofuran or acetonitrile, but less soluble in protic solvents such as

ethanol. It can be handled in air and was stable for more than 1 year without any particular storage precautions.

^1H NMR (300 MHz, $\text{ACN-}d_3$), **IMesH⁺BPh₄⁻**, isolated yield 93.2 % : δ_{ppm} : 2.14 (s, 12H, 4 \times *o*-ArCH₃), 2.42 (s, 6H, 2 \times *p*-ArCH₃), 6.85 – 6.89 (t, 4H, J = 6 Hz, 4 \times ArH), 6.99 – 7.04 (t, 8H, J = 7.5 Hz, 8 \times ArH), 7.2 (s, 4H, 4 \times ArH), 7.30 – 7.34 (br, 8H, 2 \times 8 \times ArH), 7.56 (s, 2H, 2 \times NCH) and 8.63 (s, 1H, NCHN). **SIMesH⁺BPh₄⁻**, isolated yield 84 % : δ_{ppm} : 2.36 (s, 6H, 4 \times *p*-ArCH₃), 2.37 (s, 12H, 2 \times *o*-ArCH₃), 4.34 (s, 4H, 2 \times NCH₂), 6.86 – 6.91 (t, 4H, J = 7.5 Hz, 4 \times ArH), 7.01 – 7.06 (t, 8H, J = 7.5 Hz, 8 \times ArH), 7.12 (s, 4H, 4 \times ArH), 7.31 – 7.36 (br, 8H, 2 \times 8 \times ArH), and 8.07 (s, 1H, NCHN).

b. Synthesis of polyurethane

A spectroscopic cell capped with a rubber septum was charged with **IMesH⁺BPh₄⁻** (9.18 mg, 0.015 mmol, 1 equiv.), ITX (3.82 mg, 0.015 mmol, 1 equiv.) and 0.5 mL of THF. A Schlenk tube containing the diol oligomer PEG₄₀₀ (2050 mg, 5.125 mmol, 342 equiv.) and diisocyanate IPDI (1139 mg, 5.125 mmol, 342 equiv.) was subjected to three freeze-thaw cycles. The cuvette containing the NHC photogenerator solution was degassed, then exposed to a 365 nm LED irradiation (65 mW·cm⁻²) for 5 min. The solution that turned dark brown color was added under inert atmosphere to the Schlenk tube. The step-growth polymerization was carried out at 60 °C for 4 h. The progress of the reaction was monitored by FT-IR by taking occasional samples. The polymer was terminated by methanol and precipitated in cyclohexane, filtered under vacuum and dried under vacuum at 60 °C until a constant weight was achieved. The resultant polymer was then analyzed by SEC.

c. Synthesis of polyester

A spectroscopic cell capped by a rubber septum was charged with **IMesH⁺BPh₄⁻** (9.18 mg, 0.015 mmol), ITX (3.82 mg, 0.015 mmol) and 0.5 mL of THF. A Schlenk tube was charged separately with PA (222.15 mg, 1.5 mmol, 100 equiv.) and CHO (725.15 mg, 7.5 mmol, 500 equiv.), then three freeze-thaw cycles were carried out. The cell was degassed, exposed to 365 nm irradiation (65 mW·cm⁻²) for 5 min, then the solution was immediately added to the Schlenk tube under inert atmosphere. The polymerization was conducted at 110 °C for 1 h and PA monomer conversion was monitored by ^1H NMR in CDCl₃. After reaction time, the crude sample was diluted in CHCl₃ and precipitated in methanol. The polymer was filtered under vacuum and dried under vacuum at 60 °C until a constant weight was achieved. The resultant polymer was then analyzed by SEC.

d. Synthesis of polynorbornene

NB (0.047 g, 5×10^{-4} mmol, 510 equiv.), **IMesH⁺BPh₄⁻** (3 mg, 4.90×10^{-3} mmol, 5 equiv.), ITX (0.63 mg, 2.48×10^{-3} mmol, 2.5 equiv.) and [RuCl₂(*p*-cymene)]₂ (0.60 mg, 9.8×10^{-4} mmol, 1 equiv.) and CD₂Cl₂ (1 M relative to NB, 0.5 ml) were placed in a 5 mL vial. The solution was mixed, transferred to a borosilicate NMR tube. The polymerization was conducted inside a LED circular photochemical reactor at room temperature. The photoreactor was constructed by winding a 365 nm LED strip (SMD3528, 60 LED/Meter, Lightingwill, length: 1000 mm) around a quartz cylinder (internal diameter: 60 mm, length: 200 mm) (see **Figure A.II.2**). The NMR tube was introduced in the axis of the quartz cylinder where it received an irradiance of $6.5 \text{ mW} \cdot \text{cm}^{-2}$. All samples were irradiated for 60s and gels obtained (see **Figure A.II.3**). Monomer conversion and *cis/trans* ratio were monitored by ¹H NMR analysis. Reactions were quenched by adding an excess amount of vinyl ethyl ether, the resultant polymer was precipitated in acetone. The collected polynorbornene was washed several times with acetone and air dried for 48 h before SEC analysis.

2.2.3 Characterization methods

a. ¹H NMR analysis of NHC-carbodiimide adduct

Four similar borosilicate NMR tubes containing **IMesH⁺BPh₄⁻** (9.18 mg, 0.015 mmol, 3 equiv.), ITX (3.82 mg, 0.015 mmol, 1 equiv.) and THF-*d*₈ (0.03 M, relative to **IMesH⁺BPh₄⁻**, 0.5 mL) were degassed with N₂. Subsequently, each tube was exposed to the UV irradiation of a 365 nm LED (LC-L1V3, Hamamatsu, $65 \text{ mW} \cdot \text{cm}^{-2}$) (**Figure A.II.4**) for a given time: 1 min, 2 min, 5 min and 10 min (when CQ was used instead of ITX, a 450 nm LED was employed: MP-LE1007, Metaphase, $55 \text{ mW} \cdot \text{cm}^{-2}$). Prior to the addition of CDI (3.35 mg, 0.015 mmol, 3 equiv.), deprotonation of **IMesH⁺BPh₄⁻** was monitored by ¹H NMR. After CDI introduction, a change of color of the reaction medium took place from yellow/brown/red, depending on **IMesH⁺BPh₄⁻**/ ITX ratio (**Figure A.II.5**), to pale/ dark orange (**Figure A.II.6**). The solution was left for 2 min, then a ¹H NMR spectrum was recorded. All yields were calculated following equation (1) below:

$$\text{Yield (\%)} = \frac{3(I_{6.26-6.28} + I_{5.76-5.78})}{3(I_{6.26-6.28} + I_{5.76-5.78}) + 4(I_{2.37})} \times 100 \quad (1)$$

where $I_{6.26-6.28}$, $I_{5.76-5.78}$ are the intensity of methine protons ($\delta_{\text{m}} = 6.26 - 6.28$ ppm, $\delta_{\text{n}} = 5.76 - 5.78$ ppm) of IMes-CDI adduct and $I_{2.37}$ is the intensity of methyl proton in *para* position ($\delta = 2.37$ ppm) of residual **IMesH⁺BPh₄⁻**.

b. Thermal analysis

Thermogravimetric analysis (TGA) and differential scanning calorimetry (DSC) experiments were performed using, respectively, a TGA/DSC3+ (Mettler Toledo) and a DSC1 (Mettler Toledo) under nitrogen atmosphere. For TGA analysis, the sample (10 mg) was heated from 30 °C to 600 °C at a heating rate of 10 °C min⁻¹. For DSC analysis, the sample (3 mg) was scanned from 0 °C to 300 °C at a heating rate of 10 °C min⁻¹.

c. Electron spin resonance (EPR) of NHC-radical adduct

IMesH⁺BPh₄⁻ (9.18 mg, 0.015 mmol, 3 equiv.), ITX (1.27 mg, 0.005 mmol, 1 equiv.), TPO (10.4 mg, 0.033 mmol, 6 equiv.) were added to 1 mL of THF. The mixture was prepared in a small vial capped with a rubber septum. The solution was degassed with N₂, then 0.2 mL were transferred into a quartz EPR tube with an internal diameter of 2.5 mm, the solution was degassed with N₂. Subsequently, the EPR tube was irradiated with a 365 nm LED (LC-L1V3, Hamamatsu, 65 mW·cm⁻²). EPR spectra were recorded before irradiation, and after 2 and 5 min irradiation. For the control experiment, an identical procedure was followed using the mixture of **IMes** (4.56 mg, 0.015 mmol, 3 equiv.) and TPO (1.04 mg, 0.003 mmol, 0.6 equiv.) in THF, cautiously prepared in a gloves box.

c. Steady-state photolysis

A stock solution containing ITX (1.27 mg, 0.005 mmol) was prepared in acetonitrile (2×10^{-4} M, 25 mL). A **IMesH⁺BPh₄⁻**/ITX solution was prepared by adding 1.10 mg of **IMesH⁺BPh₄⁻** (0.0018 mmol) into a conventional spectroscopic cell containing 3 mL of the ITX solution and a micro magnet bar. The cell was capped with a rubber septum and degassed with N₂ for 10 min before exposure to a Hg-Xe lamp (LC-9588/01A, Hamamatsu) including a filter providing a monochromatic incident irradiation (365 nm, 75 mW·cm⁻²). Continuous stirring was maintained during irradiation. Temporal change in absorbance at 365 nm was monitored by utilizing a spectrometer (USB4000 from Ocean Optics) (**Figure A.II.7**). Other solutions in the presence or the absence of other quenchers: **SIMesH⁺BPh₄⁻** (1.10 mg, 0.0018 mmol), **IMesH⁺Cl⁻** (0.61 mg, 0.0018 mmol), NaBPh₄ (0.62 mg, 0.0018 mmol), **IMes** (0.55 mg, 0.0018 mmol) and **SIMes** (0.554 mg, 0.0018 mmol) were also conducted following the aforementioned procedure.

d. Cyclic voltammetry measurement and calculation of free energy for electron-transfer

Four different solutions with a similar concentration (4×10^{-2} M) were prepared from $\text{IMesH}^+\text{Cl}^-$, NaBPh_4 , $\text{SIMesH}^+\text{BPh}_4^-$ and $\text{IMesH}^+\text{BPh}_4^-$. Cyclic voltammetry measurement was conducted as previously described.³⁶ Based on the cyclic voltammetry plots, oxidation potentials at 0.83, 0.96 and 0.94 eV (*vs.* saturated calomel electrode (SCE)) were measured, and respectively assigned to oxidation of BPh_4^- (NaBPh_4), BPh_4^- ($\text{SIMesH}^+\text{BPh}_4^-$) and BPh_4^- ($\text{IMesH}^+\text{BPh}_4^-$). No oxidation potential was detected in case of $\text{IMesH}^+\text{Cl}^-$. After a first cycle, new intense oxidation peaks at -1.52 ($\text{SIMesH}^+\text{BPh}_4^-$) and -0.84 eV *vs.* SCE ($\text{IMesH}^+\text{BPh}_4^-$) became visible. Their appearance reflects the oxidation of **SIMes** and **IMes** formed by electrochemical reduction of **SIMesH**⁺ and **IMesH**⁺. The free energy change of photoinduced electron-transfer was estimated through the Rehm-Weller equation (2):⁴⁰

$$\Delta G_{\text{et}} = E_{\text{ox}}(\text{D}) - E_{\text{red}}(\text{A}) - E_{\text{T}} + C \quad (2)$$

where ΔG_{et} is the free energy change of photoinduced electron-transfer (PET); $E_{\text{ox}}(\text{D})$, the oxidation potential of the electron donor; $E_{\text{red}}(\text{A})$, the reduction potential of the electron acceptor; E_{T} , the triplet state energy level of electron acceptor; and C , the Coulombic stabilization energy (-0.06 V in acetonitrile).⁴¹ For ITX, the measured oxidation/reduction potentials (1.5 eV/ -1.57 eV) and triplet state energy (2.64 eV) were taken from previous report.⁴² The other potentials were determined experimentally by cyclic voltammetry.

The free energy change of electron transfer (ΔG_{et}) values were determined below:

- The $\Delta G_{\text{et,NaBPh}_4}$ – electron transfer from BPh_4^- to ${}^3\text{ITX}^*$:

$$\Delta G_{\text{et,NaBPh}_4} = 0.83 + 1.57 - 2.64 + 0.06 = -0.18 \text{ eV}$$

- The $\Delta G_{\text{et,SIMesH+BPh}_4^-}$ – electron transfer from BPh_4^- to ${}^3\text{ITX}^*$:

$$\Delta G_{\text{et,SIMesH+BPh}_4^-} = 0.96 + 1.57 - 2.64 + 0.06 = -0.05 \text{ eV}$$

- The $\Delta G_{\text{et,IMesH+BPh}_4^-}$ – electron transfer from BPh_4^- to ${}^3\text{ITX}^*$:

$$\Delta G_{\text{et,IMesH+BPh}_4^-} = 0.94 + 1.57 - 2.64 + 0.06 = -0.07 \text{ eV}$$

- The $\Delta G_{\text{et,SIMes}}$ – electron transfer from **SIMes** to ${}^3\text{ITX}^*$:

$$\Delta G_{\text{et,SIMes}} = -1.52 + 1.57 - 2.64 + 0.06 = -2.53 \text{ eV}$$

- The $\Delta G_{\text{et,IMes}}$ – electron transfer from **IMes** to ${}^3\text{ITX}^*$:

$$\Delta G_{\text{et,IMes}} = -0.84 + 1.57 - 2.64 + 0.06 = -1.85 \text{ eV}$$

Additionally, the ΔG_{et} values of electron transfer from BPh_4^- of $\text{IMesH}^+\text{BPh}_4^-$ to thioxanthone (TX), 4,4'-bis(diethylamino)benzophenone (EAB) or camphorquinone (CQ), which have well-known reduction potentials (E_{red}) and triplet energies (E_{T}) in the literature, TX ($E_{\text{red}} = -1.62 \text{ eV}$, $E_{\text{T}} = 2.84 \text{ eV}$),⁴³ EAB ($E_{\text{red}} = -2.48 \text{ eV}$, $E_{\text{T}} = 3.0 \text{ eV}$)^{44,45} and CQ ($E_{\text{red}} = -1.25 \text{ eV}$, $E_{\text{T}} = 2.18 \text{ eV}$)⁴⁶ were also calculated:

- The $\Delta G_{\text{et,TX}}$ – electron transfer from BPh_4^- to $^3\text{TX}^*$:

$$\Delta G_{\text{et,TX}} = 0.94 + 1.62 - 2.84 + 0.06 = -0.22 \text{ eV}$$

- The $\Delta G_{\text{et,EAB}}$ – electron transfer from BPh_4^- to $^3\text{EAB}^*$:

$$\Delta G_{\text{et,EAB}} = 0.94 + 2.48 - 3.04 + 0.06 = 0.44 \text{ eV}$$

- The $\Delta G_{\text{et,CQ}}$ – electron transfer from BPh_4^- to $^3\text{CQ}^*$:

$$\Delta G_{\text{et,CQ}} = 0.94 + 1.25 - 2.18 + 0.06 = 0.07 \text{ eV}$$

e. NMR spectroscopy

All NMR spectra were recorded in appropriate deuterated solvents with tetramethylsilane (TMS) as the internal reference on a Varian 300 – MR. All chemical shifts are reported in parts per million (ppm) relative to the residual CD_2Cl_2 (δ 5.32 ppm), THF- d_8 (δ 1.72 ppm and 3.58 ppm), CDCl_3 (δ 7.26 ppm), DMSO- d_6 S (δ 2.50 ppm) or ACN- d_3 (δ 1.94 ppm). Peaks multiplicities in ^1H NMR spectra are abbreviated as s (single), d (double), t (triplet), m (multiplet), br (broad).

f. UV-Vis absorption

Absorption spectra were recorded on a Lambda 35 UV/vis spectrometer from PerkinElmer with a bandwidth of 1 nm and a scan speed of $400 \text{ nm}\cdot\text{min}^{-1}$. All the solutions were analyzed in a quartz cuvette of 1 cm length.

g. Size exclusion chromatography (SEC)

An Agilent 1260 Infinity series equipped with Polymer Laboratories ResiPore columns, a G1314B wavelength detector, a MDS refractive index detector and a MDS viscosimeter detector was employed to determine the molar mass values and distributions of polyurethane and polyester samples. Precise concentration solutions of polymer in THF were prepared and injected with flow rate of $1 \text{ mL}\cdot\text{min}^{-1}$. A set of EasiVial polystyrene PS-M standards was used to establish the universal calibration. High molecular weights of polynorbornene samples were determined using a SEC instrument from a Varian apparatus equipped with TOSOHAAS TSK gel columns and a refractive index detector. The mobile

phase was THF at a flow rate of 1 mL·min⁻¹; the injected volume was 100 μL. The MALS instrument was normalized using a THF solution of polystyrene standard.

h. Electron paramagnetic resonance

EPR measurements were performed in a Bruker Elexsys E500 spectrometer with X band frequency in continuous wave (around 9.8 GHz) at room temperature. Spectra were recorded with a modulation amplitude of 1 G, a modulation frequency of 100 kHz and a microwave power of ~ 2 mW. Both Bruker WIN-EPR and SimFonia software were used for spectra treatment and simulation.

i. Computational procedure

Triplet energy of **IMesH⁺BPh₄⁻** ($E_{T,BPh_4^-} = 83.97$ kcal·mol⁻¹ and $E_{T,IMesH^+} = 77.04$ kcal·mol⁻¹) and enthalpy of reactions between **IMes** and TPO were calculated by utilizing the Gaussian 03 package.^{47,48} The uB3LYP method with the 6-31G* was applied to optimize the relaxed geometries which were regularly checked.

j. MALDI-TOF analysis of poly(PA-alt-CHO)

MALDI-TOF MS spectra were recorded by a Bruker RapiFlex mass spectrometer equipped with a nitrogen laser for MALDI ($\lambda = 337$ nm). Mass spectra were accumulated in positive mode at 20 kV acceleration voltage potentials. All the polymers were dissolved in THF at a concentration of 1 mg·mL⁻¹. Sodium trifluoroacetate at a concentration of 5 mg·mL⁻¹ was utilized as the cationization agent. *Trans*-2-[3-(4-*tert*-butylphenyl)-2-methyl-2-propenylidene]malononitrile (DCTB) is the matrix dissolved in THF at a concentration of 40 mg·mL⁻¹. The mixed solution of matrix/salts/polymer (1:4:4 in vol. ratio) was hand spotted on a MALDI target until drying. Data were analyzed by using the FlexAnalysis version 3.0 (Bruker) software.

2.3 RESULTS AND DISCUSSION

2.3.1 Synthesis and characterization of photogenerated NHC

To photogenerate the well-established **IMes**, we propose the azolium tetraphenylborate salt **IMesH⁺BPh₄⁻** as a potential NHC photogenerator. For its synthesis, simple treatment in ethanol of NaBPh₄ with the commercial azolium salt **IMesH⁺Cl⁻** resulted in a quantitative anion exchange to provide the desired photolabile NHC cleanly and in excellent yield (93.2 %). Compound **IMesH⁺BPh₄⁻** appears as white crystals with a melting point at 212 °C and a decomposition threshold at 292 °C (**Figure A.II.8**). Its electronic

absorption (**Figure 2.2**) spans only the UV-C region (100-280 nm) with an intense peak at 198 nm ($\epsilon_{198} = 1.38 \times 10^5 \cdot \text{M}^{-1} \cdot \text{cm}^{-1}$) and weak peak at 254 nm ($\epsilon_{254} = 7.30 \times 10^3 \text{ M}^{-1} \cdot \text{cm}^{-1}$). A comparison with NaBPh_4 and $\text{IMesH}^+\text{Cl}^-$ salts clearly established that both the anion (BPh_4^-) and cation (IMesH^+) of **IMes** are chromophores.

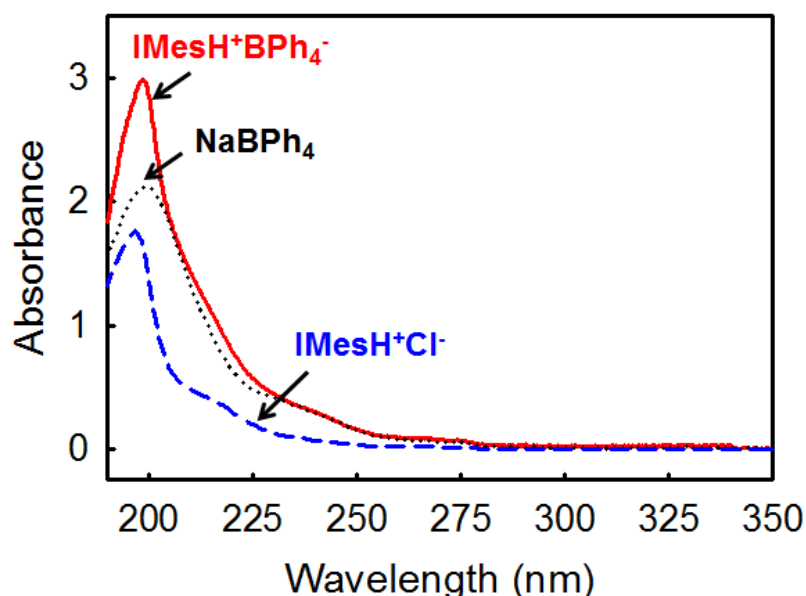


Figure 2.2. UV-vis absorption spectra of NaBPh_4 (black), $\text{IMesH}^+\text{Cl}^-$ (blue) and $\text{IMesH}^+\text{BPh}_4^-$ (red) in acetonitrile ($4 \times 10^{-4} \text{ M}$).

2.3.2 Identification and quantification of photogenerated NHC

a. EPR spectroscopy of NHC-radical adduct: Identification of NHC

$\text{IMesH}^+\text{BPh}_4^-$ (3 equiv.) was mixed with ITX (1 equiv.) under ambient conditions in $\text{THF-}d_8$. In the absence of light, the mixture is stable supporting that in its ground state, ITX cannot participate in an electron-transfer reaction. In either case, the ^1H NMR spectrum shows the disappearance of the NCHN proton after exposure during 2 min to UV radiation (365 nm , $65 \text{ mW} \cdot \text{cm}^{-2}$). In addition, reaction of the as-irradiated media with CS_2 gives the expected IMes-CS_2 complex whose structure has been identified by ^{13}C NMR (**Figure 2.3**). This characterization suggests deprotonation of the azolium salt to form the expected NHCs **IMes**. Given the high reactivity of NHCs, it is however important to develop new techniques able to characterize these species just after their formation, i.e. before secondary reactions take place.

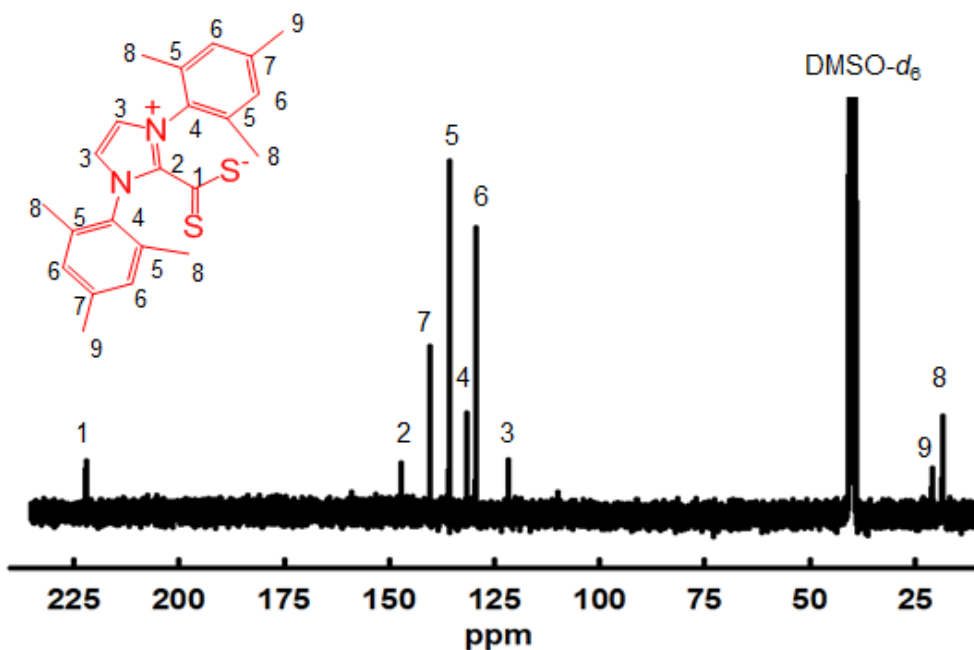
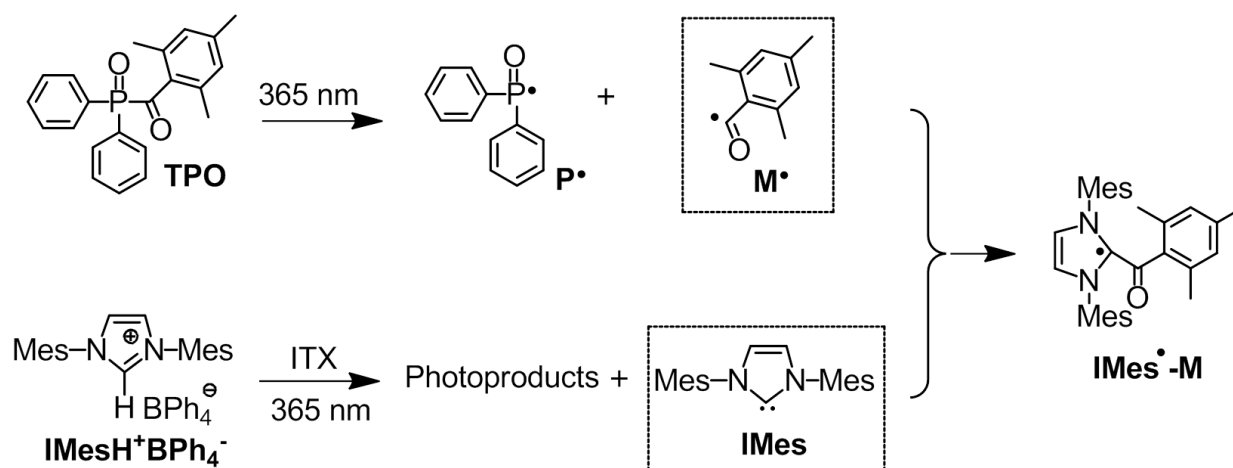


Figure 2.3. ^{13}C NMR spectra in $\text{DMSO-}d_6$ of the IMes-CS_2 adduct formed after addition of CS_2 to the as-irradiated mixture $\text{IMesH}^+\text{BPh}_4^-/\text{ITX}$.

Recently, the fast addition of a radical to NHC to afford an adduct with an unpaired electron was evidenced by Tumanskii *et al.*^{49,50} Through a judicious choice of radicals, it was possible to generate adduct radicals stable enough to be detected by EPR spectroscopy, thus providing a clean spectrum characteristic of the carbene captured. Following the same approach, we chose diphenyl(2,4,6-trimethylbenzoyl)phosphine oxide (TPO) to act as a trapper of NHCs just after their photogeneration. TPO is a commercial α -cleavable radical photoinitiator, which was not reported by Tumanskii *et al.* It proceeds through the photochemical homolysis of the C-C bond adjacent to the arylketone chromophore to yield two different phosphinoyl-type (P^\bullet) and mesityl-type (M^\bullet) radicals (**Scheme 2.2**). The main advantage is that these radicals can be photogenerated at the same wavelength (365 nm) as the NHC, allowing the NHC to be trapped as a well-defined adduct radical in a single step, and immediately after generation. The mixture $\text{IMesH}^+\text{BPh}_4^-/\text{ITX}$ (3/1 equiv.) was irradiated in THF in presence of TPO (6 equiv.), then placed after different exposure times, in the cavity of the EPR spectrometer.



Scheme 2.2. Reaction pathway to generate NHC-radical adduct after irradiation of ITX/**IMesH⁺BPh₄⁻** in presence of TPO.

As shown in **Figure 2.4a**, the EPR spectrum recorded after 2 min irradiation, is consistent with the formation of a single adduct radical, which was assigned to **IMes[•]-M**. Indeed, the spectrum clearly shows a quintuplet arising from the hyperfine coupling (hfc) of the unpaired electron with two equivalent ^{14}N atoms ($I = 1$, $a_{\text{N}} = 3.9$ G). Because of coupling with the two protons of the **IMes** moiety ($I = 1/2$, $a_{\text{H}} = 1.1$ G), each quintet line is also decomposed, but only in doublet instead of triplet, because the set of hfc transitions are probably overlapped. The formation of the phosphinoyl radical adduct **IMes[•]-P** can be ruled out because hfc with ^{31}P ($I = 1/2$) would have caused a duplication of the quintuplet. Control experiment by irradiating the preformed NHC **IMes** and TPO for 30 s reveals a similar profile (**Figure 2.4**, trace **b**), thus supporting the photoinduced liberation of **IMes** in the previous experiment and the in situ formation of a single NHC adduct radical. This latter result can be explained through DFT calculations since the addition reaction of the **M[•]** radical to **IMes** is much more exothermic ($\Delta H = -35.0$ kcal·mol⁻¹) than that of a **P[•]** radical ($\Delta H = -17.1$ kcal·mol⁻¹) as expected from the higher stability of the **IMes[•]-M** (**Figure A.II.9**). Nevertheless, the EPR spectrum shows a signal intensity declining with longer exposure time (see $t = 5$ min, **Figure 2.4**, trace **a**), in line with a slow degradation of the **IMes[•]-M** adduct radical under UV irradiation. This result was also confirmed when **IMes[•]-M** adduct was created from the preformed NHC **IMes** instead of the photoNHC (**Figure A.II.10**).

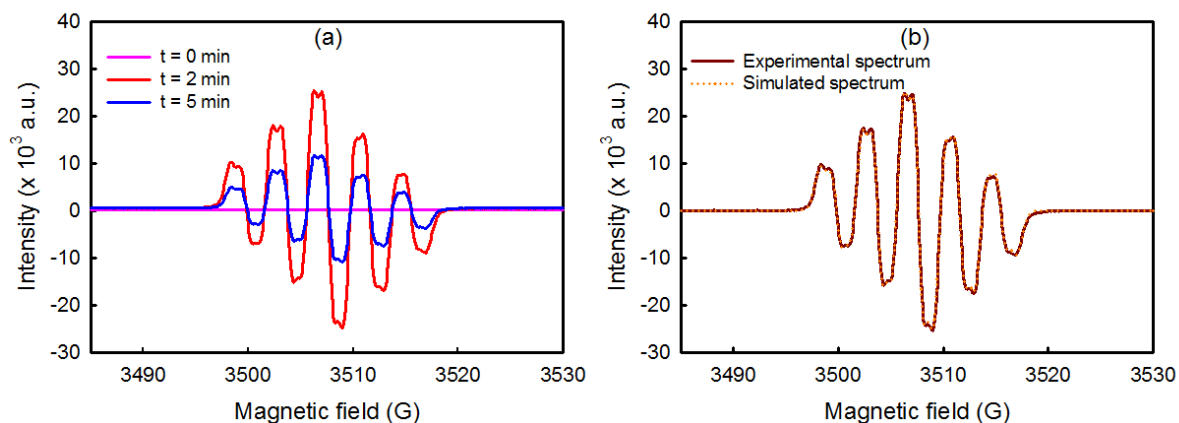
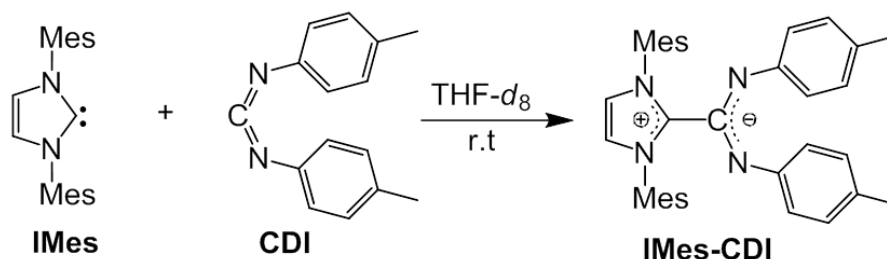


Figure 2.4. EPR spectrum of: (a) a solution of ITX/**IMesH**⁺**BPh**₄⁻/TPO (1/3/6 equiv., [ITX] = 5 × 10⁻³ M) in THF after different irradiation times and (b) EPR spectrum obtained after 30 s irradiation of a solution of **IMes**/TPO in THF (5/1 equiv., [TPO] = 3 × 10⁻³ M). The experimental and simulated spectra are both consistent with the formation of the mesitoyl-NHC adduct radical **IMes**[•]-M.

b. ¹H NMR analysis of NHC-carbodiimide adduct: Quantification of NHC

Estimation of the quantity of NHC photogenerated from the mixture of azolium salt with excited ITX can be challenging. ¹H NMR provides a deprotonation degree (from NCHN proton), but the results can be distorted when the reaction is not complete because of N-CH-N/N-C:-N hydrogen bonds forming in **IMesH**⁺-**IMes** complex (see evidences in **Figure A.II.11**). Alternatively, NHC concentration can be determined indirectly through a quantitative reaction between **IMes** and CS₂.³⁶ However, the zwitterionic **IMes**-CS₂ adduct is only partially soluble in solvents such as THF and acetonitrile, making yield calculation complex because the adduct is partitioned between solid and liquid phases. To obtain quantitatively a soluble and stable NHC adduct, we turned our attention towards the recently reported NHC-carbodiimide (CDI) adduct^{51,52} generated by addition of a CDI derivative to **IMes** (**Scheme 2.3**). Upon contact with a stoichiometric amount of 1,3-di-*p*-tolylcarbodiimide in THF, **IMes** yields a soluble carbene adduct within a few seconds, visible by the change of color from a slight yellow solution to orange. The product formed in this way was characterized by ¹H NMR when the reaction was performed in THF-*d*₈ (**Figure 2.5**). The reaction caused a complete shift of the methyl protons H_e (2.31 ppm) and H_d (2.08 ppm,) of **IMes** (spectrum **a**) and the methyl proton H_p (2.30 ppm) of CDI (spectrum **b**). In the spectrum of the mixture **IMes**/CDI (spectrum **c**), H_e' and H_d' form two overlapping peaks at 2.32 ppm, and H_p' is subjected to a upfield shift and now arises at 1.92 ppm. Additionally,

novel signals assigned to methine protons H_m (6.27 ppm) and H_n (5.77 ppm) appear in the spectrum, which established the quantitative transformation of **IMes** to the IMes-CDI adduct.



Scheme 2.3. Formation of zwitterionic IMes-CDI adduct by reaction between CDI and NHC **IMes**.

Another control experiment was performed when **IMes** (1 equiv.) was mixed with **IMesH⁺BPh₄⁻** (3 equiv.) followed by addition of CDI (1 equiv.). It cleanly gave a yield of IMes-CDI consistent with the initial amount of **IMes** (with an error of 5 %, **Figure A.II.11**), demonstrating that this reaction may also cause the disruption of the **IMesH⁺-IMes** hydrogen bonds.⁵³⁻⁵⁵ Having proved that the synthesis of NHC-CDI can be quantitative and easily monitored by ¹H NMR, 1,3-di-*p*-tolylcarbodiimide was added to the as-irradiated solutions of **IMesH⁺BPh₄⁻/ITX** and **SIMesH⁺BPh₄⁻/ITX** (3/1 equiv.). As expected, the spectrum **d** of this mixture (**Figure 2.5**) displays all the characteristic resonances of IMes-CDI adduct, enabling to determine NHC conversion. After 5 min irradiation, the yields of **IMes** and **SIMes** were respectively of 22.1 and 14.8 %. The main factor underlying this trend and the best experimental conditions to achieve high NHC yield are discussed in next sections.

2.3.3 Insight into photochemical mechanism: coupled electron/proton transfer

a. UV-Vis Absorption

Figure 2.6 shows in the same plot the UV-vis spectra of ITX, **IMesH⁺BPh₄⁻** and **SIMesH⁺BPh₄⁻** in acetonitrile. ITX has an absorption spectrum with two characteristic maxima at 257 nm (π - π^* transition) and 383 nm (n - π^* transition). The band centered at 383 nm allows excitation ($\lambda_{exc} = 365$ nm) to form triplet ITX (³ITX*), displaying a much higher reduction ability than its ground state analogue. The two azolium salts absorb only in the UVC range (100-280 nm), what is desired to avoid electronic excitation and ensure high reactivity of ITX.

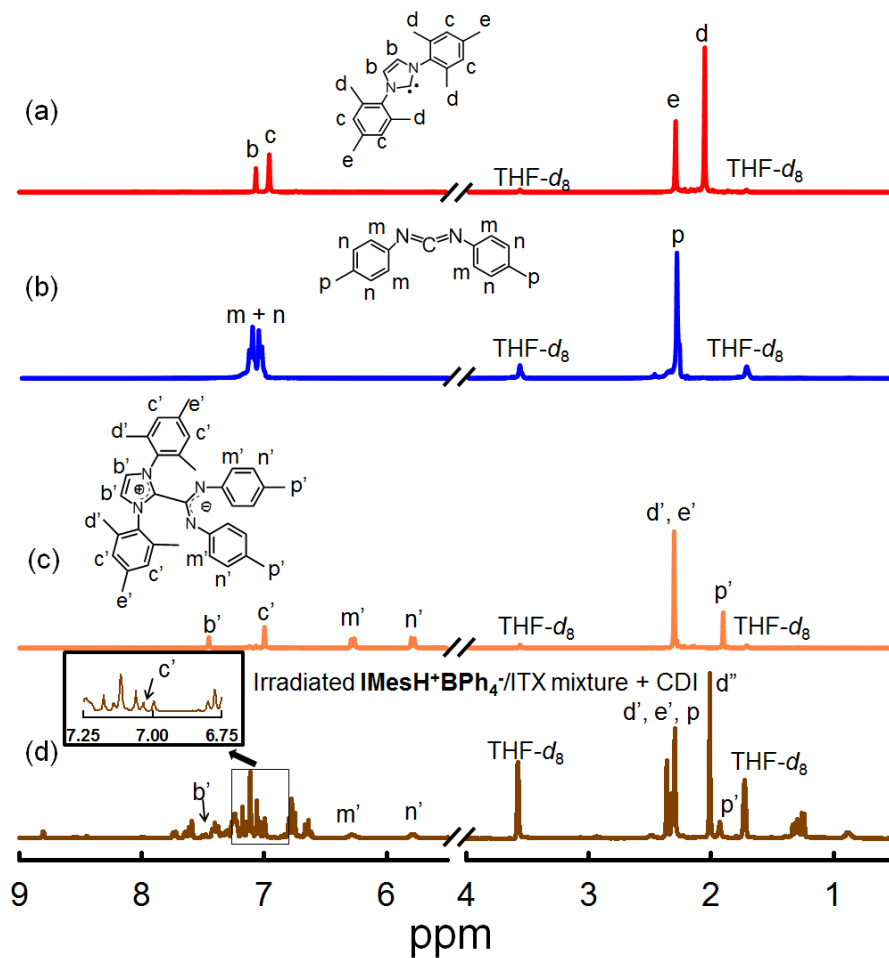


Figure 2.5. ^1H NMR spectra in $\text{THF-}d_8$ of: (a) **IMes** (0.21 M), (b) **CDI** (0.21 M), (c) **IMes/CDI**, (1/1 equiv., $[\text{IMes}] = 0.1$ M), and (d) **IMesH⁺BPh₄⁻/ITX/CDI** (3/1/3 equiv., $[\text{ITX}] = 0.01$ M). In sample **d**, **IMesH⁺BPh₄⁻/ITX** was irradiated 5 min then **CDI** was immediately added.

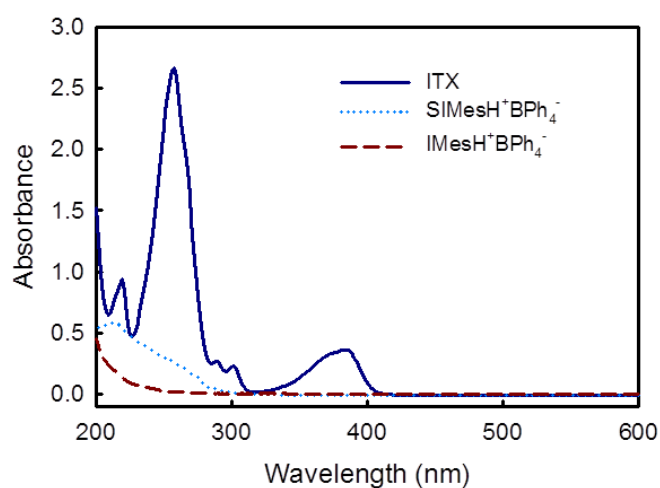


Figure 2.6. UV spectra of **ITX**, **SIMesH⁺BPh₄⁻** and **IMesH⁺BPh₄⁻** in acetonitrile ($[\text{ITX}] = 10^{-4}$ M, $[\text{IMesH⁺BPh₄⁻}] = [\text{SIMesH⁺BPh₄⁻}] = 3 \times 10^{-4}$ M).

b. Real-time photobleaching and Rehm-Weller equation

The decay of the ITX $n\text{-}\pi^*$ transition band at 365 nm was assessed throughout irradiation time with a rapid-scan spectrometer, which is able to measure absorbance change with a temporal resolution of 0.1 s. To investigate the photochemical mechanism, real-time photobleaching was performed in acetonitrile during 50 s for a range of ITX/quencher couples (**Figure 2.7**). The first series (**a**) displays azolium salts bearing anions with different electron donor properties (Cl^- and BPh_4^-), while the second (**b**) shows tetraphenylborate salts containing different cations (IMesH^+ , SIMesH^+ and Na^+). As expected, a control experiment including only ITX showed a steady absorbance value over irradiation (**Figure 2.7**, trace **a**), within the time period studied, suggesting its photostability in absence of suitable reductant.⁵⁶ This is in sharp contrast with the profile of $\text{IMesH}^+\text{BPh}_4^-/\text{ITX}$ which shows a gradual photobleaching, consistent with a modification of the structure of ITX after the electron-transfer reaction. Indeed, $\Delta G_{\text{et,IMesH}^+\text{BPh}_4^-}$, the free energy change of electron-transfer from BPh_4^- to ${}^3\text{ITX}^*$ is slightly negative (-0.07 eV, see calculation details in SI), showing that the reaction is thermodynamically feasible. Furthermore, it is the irreversible process since the back electron-transfer of the boronyl radical $\cdot\text{BPh}_4$ may be prohibited by its homolytic cleavage into BPh_3 and $\text{Ph}\cdot$ within the femto-second time scale.⁵⁷ A number of evidences are consistent with this hypothesis of sensitized reaction (**Scheme 2.4**). With $\text{IMesH}^+\text{Cl}^-$, it is explicit that ITX does not photobleach due to the lack of electron donating ability of Cl^- , as exemplified by the absence of oxidation potential during electrochemical measurements.

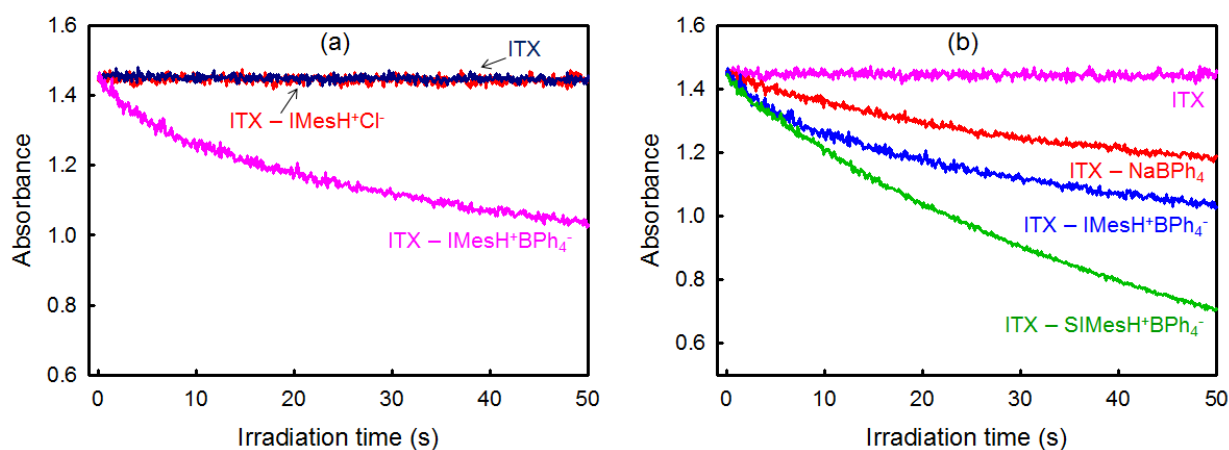
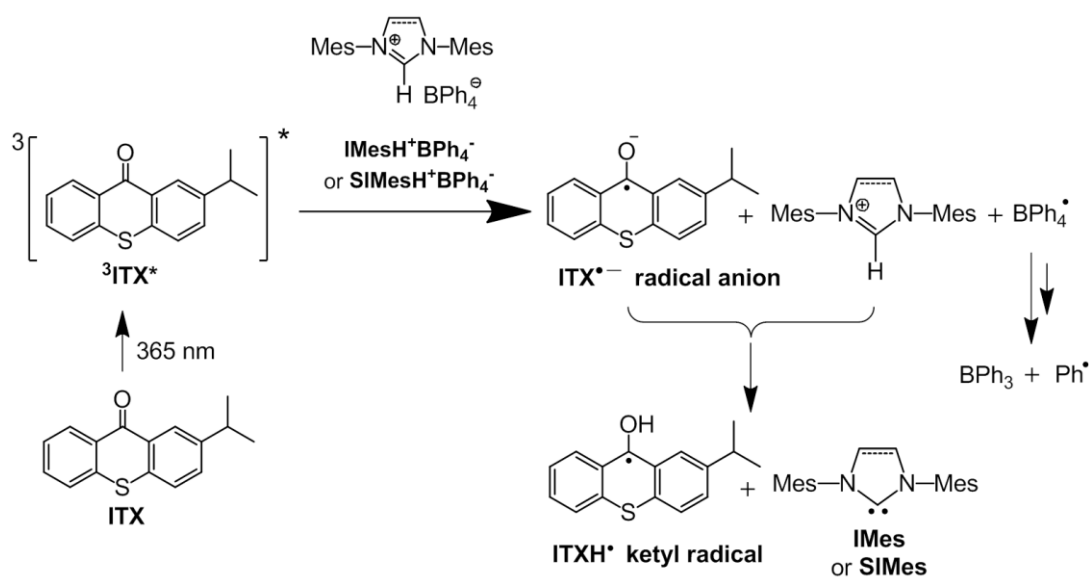


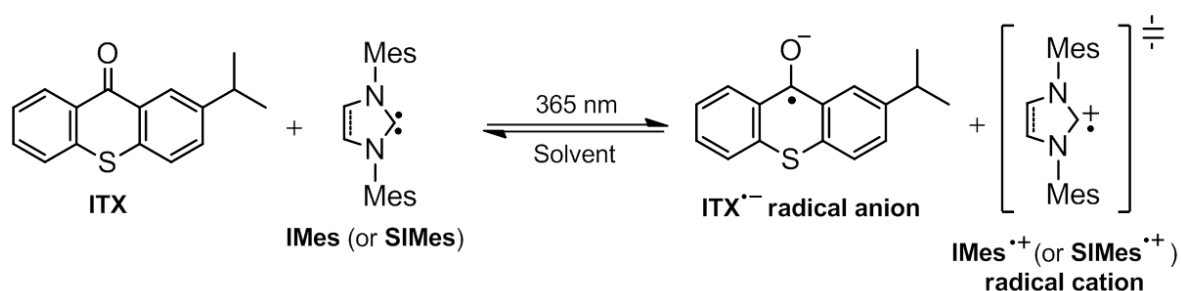
Figure 2.7. Photobleaching kinetics of ITX (2×10^{-4} M in acetonitrile) monitored at 365 nm in the presence of different quenchers: azolium salts (**a**) and tetraphenylborate salts (**b**) (Quencher concentration is 6×10^{-4} M).



Scheme 2.4. Photochemical mechanism for the generation of NHC **IMes** and **SIMes** combining electron-transfer and proton transfer.

On the other hand, useful and complementary results about the second step of proton transfer can be gained by the photobleaching of ITX in presence of various tetraphenylborate salts (**Figure 2.7**, trace **b**). Whatever the cation (**IMesH⁺**, **SIMesH⁺**, **Na⁺**), a bleaching of ITX is observed which is consistent with the irreversible electron-transfer reaction involving BPh_4^- , but the photolysis rates are clearly different. NaBPh_4 induces the lowest rate of photobleaching ($1.58 \times 10^{-7} \text{ M}\cdot\text{s}^{-1}$), compared to **IMesH⁺BPh₄⁻** ($2.40 \times 10^{-7} \text{ M}\cdot\text{s}^{-1}$) and **SIMesH⁺BPh₄⁻** ($4.04 \times 10^{-7} \text{ M}\cdot\text{s}^{-1}$) even the $\Delta G_{\text{et,NaBPh}_4}$ value is slightly more negative ($\Delta G_{\text{et,NaBPh}_4} = -0.18 \text{ eV}$). One possible explanation for the differences of ITX decomposition rate could be the slower electron-transfer rate of NaBPh_4 compared to other borate salts.³⁶

Besides, with azolium salts, proton transfer can occur leading to the formation of NHCs which are known to be excellent electron donors. Therefore, a secondary reaction involving electron-transfer from the as-formed NHC with excited ITX is likely to occur to give a carbene radical cation **IMes^{•+}** (or **IMes^{•+}**) and ITX radical anion (**Scheme 2.5**).



Scheme 2.5. Photoreduction of ITX by **IMes** (or **SIMes**) generates NHC radical cations.

Transient species $\text{IMes}^{\bullet+}$ (or $\text{SIMes}^{\bullet+}$) could undergo a dimerization to form a bicationic product or regeneration of azolium cations.⁵⁸ Supporting this hypothesis, electron-transfer between carbene IMes or SIMes and the triplet ITX is strongly exergonic ($\Delta G_{\text{et,IMes}} = -1.85$ eV and $\Delta G_{\text{et,SIMes}} = -2.53$ eV) because the oxidation potentials of IMes and SIMes are very low, -0.84 V and -1.52 V vs. SCE, respectively. Moreover, neat electron-transfer between IMes (or SIMes) and ${}^3\text{ITX}^*$ was evidenced by photobleaching rate of ITX in the presence of IMes and SIMes with significant rates, $3.6 \times 10^{-8} \text{ M}\cdot\text{s}^{-1}$ and $9.8 \times 10^{-8} \text{ M}\cdot\text{s}^{-1}$, respectively (**Figure 2.8**). Thereby, with the two azolium salts, faster decomposition rates (**Figure 2.7**, trace **b**) may be thus driven by triplet ITX electron-transfer reactions occurring not only with BPh_4^- but also with the NHC formed. In agreement with this hypothesis, the photolysis rate of $\text{SIMesH}^+\text{BPh}_4^-$ is approximately twice as large as that of $\text{IMesH}^+\text{BPh}_4^-$ which is consistent with the better electron donating properties of imidazolylidene SIMes compared to its imidazolylidene counterpart IMes .

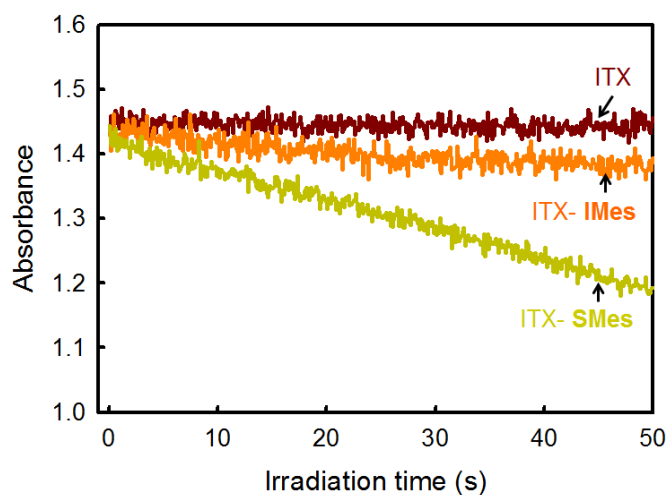


Figure 2.8. Temporal evolution of absorbance at 365 nm of ITX solution in acetonitrile (2×10^{-4} M) in the absence of quencher and presence of IMes and SIMes (6×10^{-4} M).

2.3.4 Optimization of NHC yield

a. Effect of ITX concentration

As discussed above, it is known that ${}^3\text{ITX}^*$ is not only involved in electron-transfer with BPh_4^- , but also with photogenerated IMes (or SIMes) leading to the degradation of the desired carbene under irradiation. Therefore, it is crucial to investigate the influence of ITX concentration on the yield of photogenerated NHC. For this purpose, the influence of the $\text{ITX}/\text{IMesH}^+\text{BPh}_4^-$ molar ratios (0 - 1.33) was assessed while maintaining the irradiation conditions unchanged (5 min, $65 \text{ mW}\cdot\text{cm}^{-2}$). As can be seen in **Figure 2.9a**, the increase of

the ITX/ $\text{IMesH}^+\text{BPh}_4^-$ ratio, until stoichiometry is reached, results in a nearly linear increase of **IMes** yield. A maximum amount of 70 % can be generated upon using a stoichiometric ratio. However, further increase of ratio ITX/ $\text{IMesH}^+\text{BPh}_4^-$ causes the yield to slightly decrease (56 %). Presumably, a higher concentration in ITX contributes to more side reactions between **IMes** and $^3\text{ITX}^*$.

b. Effect of irradiation time and irradiance

The effect of irradiation time on **IMes** yield is illustrated in **Figure 2.9b**. Using a sub-stoichiometric ratio in ITX (ITX/ $\text{IMesH}^+\text{BPh}_4^- = 1/3$), a gradual release of **IMes** is observed within 5 min, then the yield levels off at 30 %. Because ITX is in sub-stoichiometry, photodegradation can be minimized, but at the same time, only moderate yields can be achieved. The kinetic profile is significantly changed upon increasing the concentration of ITX to reach stoichiometry (ITX/ $\text{IMesH}^+\text{BPh}_4^- = 1/1$ equiv.). Under these conditions, more NHC can be released because of the higher $^3\text{ITX}^*$ concentration, and a maximum of 70 % is formed after 5 min. However, after longer radiation exposure, there is now a significant decrease of **IMes** yield (56 % after 10 min) due to the photochemical degradation of **IMes** by $^3\text{ITX}^*$.

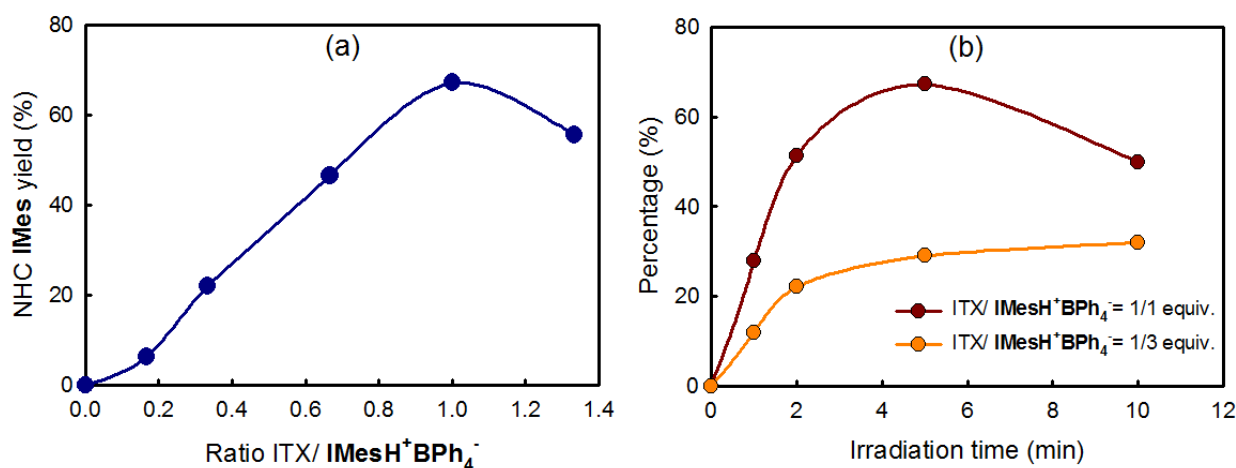


Figure 2.9. (a) Effect of ITX concentration on NHC **IMes** yield produced by irradiation of ITX/ $\text{IMesH}^+\text{BPh}_4^-$ ($[\text{IMesH}^+\text{BPh}_4^-] = 0.03$ M) and (b) Effect of irradiation time on NHC **IMes** yield following the photolysis of ITX/ $\text{IMesH}^+\text{BPh}_4^-$ mixture ($[\text{IMesH}^+\text{BPh}_4^-] = 0.03$ M). Irradiation conditions: 365 nm, 65 $\text{mW}\cdot\text{cm}^{-2}$.

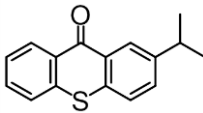
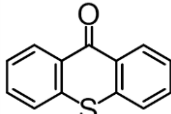
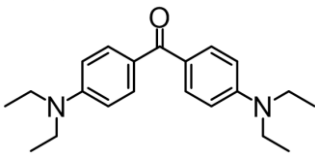
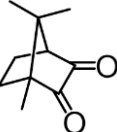
Changing irradiance has also a substantial impact on NHC yield. Keeping the ratio ITX/ $\text{IMesH}^+\text{BPh}_4^-$ of 1/3, a ten-fold decrease of light intensity, from 65 $\text{mW}\cdot\text{cm}^{-2}$ to 6.5 $\text{mW}\cdot\text{cm}^{-2}$, causes conversion of **IMes** to decrease from 22.1% to 11.3 %. Because less ITX is

excited, deprotonation of the **IMesH⁺** cation becomes slower. Consequently, less NHC is produced after a given irradiation time of 5 min.

c. Effect of photooxidant

The influence of other aryl ketone photooxidants than ITX on NHC yield was estimated using thioxanthone (TX), 4,4'-bis(diethylamino)benzophenone (EAB) and camphorquinone (CQ) (**Table 2.1**).

Table 2.1. Effect of the photooxidant's nature on the release of photogenerated NHC **IMes**. **IMesH⁺BPh₄⁻**/Photooxidant (3/1 equiv.) was irradiated in C₄D₈O ([Photooxidant] = 0.03 M). Irradiation conditions: 365 nm, 65 mW·cm⁻², 5 min irradiation).

Entry	Photooxidant	Structure	NHC IMes yield ^[a] (%)
a	ITX		22
b	TX		24
c	EAB		0
d ^[b]	CQ		0

[a] Determined by ¹H NMR spectroscopy after CDI addition.

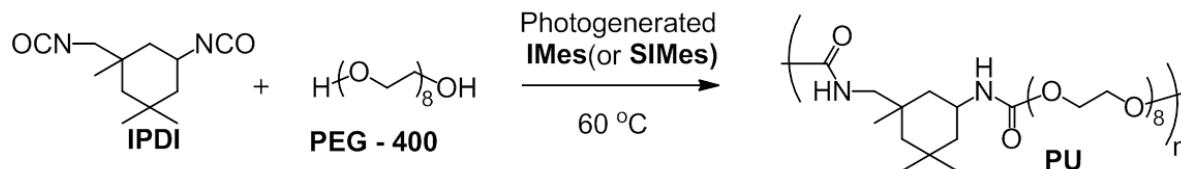
[b] Irradiation with a 450 nm LED (55 mW·cm⁻²)

As expected, the nearly similar redox properties of excited ITX (entry **a**) and TX (entry **b**) resulted in a comparable amount of **IMes** released, 22 % and 24 %, respectively. Conversely, the replacement of ITX by EAB (entry **c**) and CQ (entry **d**) prevents the formation of **IMes**. In accordance with this result, the electron-transfer between BPh₄⁻ and the excited state of these two electron donors was found to be non-thermodynamically favorable ($\Delta G_{\text{et, EAB}} = 0.44$ eV, $\Delta G_{\text{et, CQ}} = 0.07$ eV).^{44,46}

2.3.5 Use of NHC photogenerator in polymerization

a. Synthesis of polyurethane

There have been very few studies utilizing NHC organocatalyst in PU polymerizations in the literature.^{16,24} Nevertheless, NHC photogenerators were evaluated in the model linear step-growth polymerization of isophorone diisocyanate (IPDI) and poly(ethylene glycol) ($M_n = 400 \text{ g}\cdot\text{mol}^{-1}$, PEG₄₀₀) (**Scheme 2.6**).



Scheme 2.6. Synthesis of polyurethane catalyzed by photogenerated NHC.

Through a possible alcohol activation mechanism (**Scheme A.II.1**),^{16,59} a polymerization was accomplished at 60°C by mixing a stoichiometric amount of PEG₄₀₀ and IPDI followed by addition of the photogenerated NHC (0.3 mol %). **Table 2.2** summarizes yield, molecular weight and polydispersity (\bar{D}) after 4 h for each polymerization using **IMesH⁺BPh₄⁻/ITX** (entry **a**) or **SIMesH⁺BPh₄⁻/ITX** (entry **b**). For comparative purposes, the free NHC **IMes** (entry **a'**) was also included as polymerization control as well as an uncatalyzed reaction (entry **c**).

Table 2.2. Results of step-growth polymerization of PEG₄₀₀/IPDI (342/342 equiv.). Reactions were conducted for 4 h at 60 °C after the addition of the as-irradiated azolium salt/ITX solution (1/1 equiv.) or free NHC (1 equiv.).

Entry	Catalyst system	$M_n^{[a]}$ ($\text{g}\cdot\text{mol}^{-1}$)	$M_w^{[b]}$ ($\text{g}\cdot\text{mol}^{-1}$)	$\bar{D}^{[c]}$	$T_g^{[d]}$ (°C)	Yield ^[e] (%)
a	IMesH⁺BPh₄⁻/ITX	4900	7800	1.59	-17	95.7
a'	IMes	5100	7900	1.55	-14	98.3
b	SIMesH⁺BPh₄⁻/ITX	4100	6800	1.67	-18	96.2
c	No catalyst	1700	4700	2.69	-23	40.1

[a] Experimental number average molar mass M_n obtained by SEC.

[b] Experimental weight average molar mass M_w obtained by SEC.

[c] Polymer dispersity index $\bar{D} = M_w / M_n$.

[d] Glass transition temperature determined by DSC.

[e] Isolated yield.

Without catalyst, full conversion was not reached and a low molecular weight polyurethane was obtained ($M_n = 1700 \text{ g}\cdot\text{mol}^{-1}$, entry **c**). In contrast, the two photoNHCs (entry **a-b**) exhibited greater polymer yields (> 95 %), higher molecular weights (4000 - 5000 $\text{g}\cdot\text{mol}^{-1}$) and lower dispersity values \bar{D} in the range from 1.5 to 1.7 (see SEC traces in **Figure**

A.II.12). Consistently, the control experiment using the preformed NHC **IMes** (entry **a'**) resulted in polymers displaying similar M_n , D and glass transition temperature. Although the molecular weights are moderate, these results demonstrate the role of (photo)NHC in the catalysis of the polymerization. To more precisely compare catalytic activities, kinetic studies were performed for **IMes** and **IMesH⁺BPh₄⁻**/ITX during the first hour of reaction (**Figure 2.10**). The two catalysts proceeded at relatively similar rates with a significant acceleration compared to the uncatalyzed experiment. The slightly slower kinetics for photogenerated **IMes** was assigned to lower amount of NHC **IMes** present in the reaction media (as compared to the preformed-NHC **IMes**) since a maximum yield of 70 % in released NHC can be reached as demonstrated before.

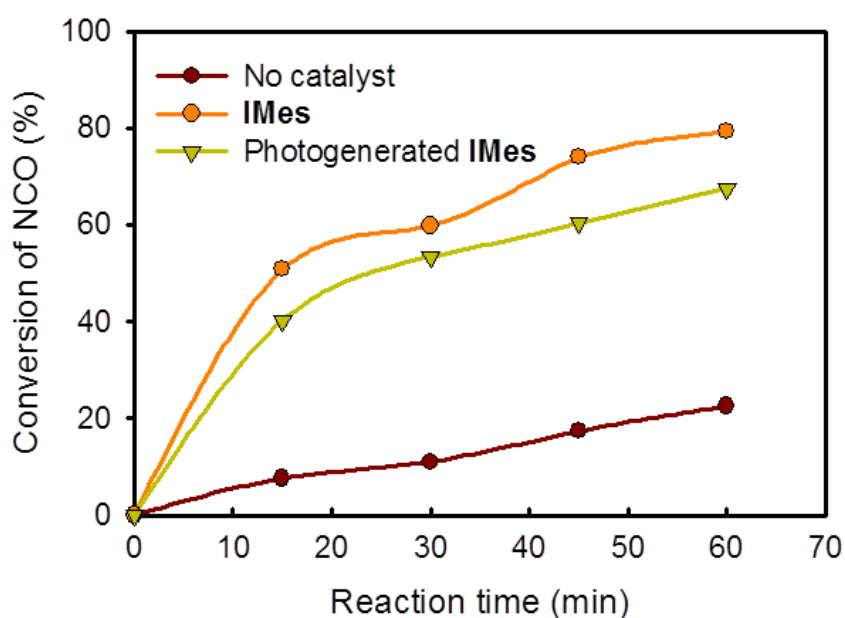


Figure 2.10. NCO conversion during polyaddition reaction between PEG₄₀₀ and IDPI. Conversion values were determined based on the NCO stretching band (ν_{NCO}) at 2255 cm^{-1} using CH₂ symmetric stretch at 2870 cm^{-1} as reference (see FTIR spectra in **Figure 2.11**). $\text{NCO conv. (\%)} = \frac{A_t - A_0}{A_0} \times 100$ where A_0 and A_t are the integrated absorbance at 2255 cm^{-1} corresponding to reaction time at 0 min and t min.

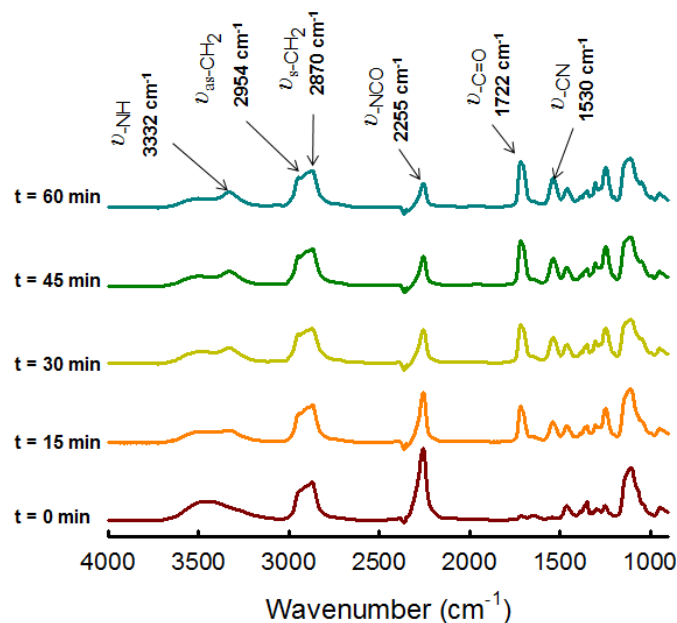
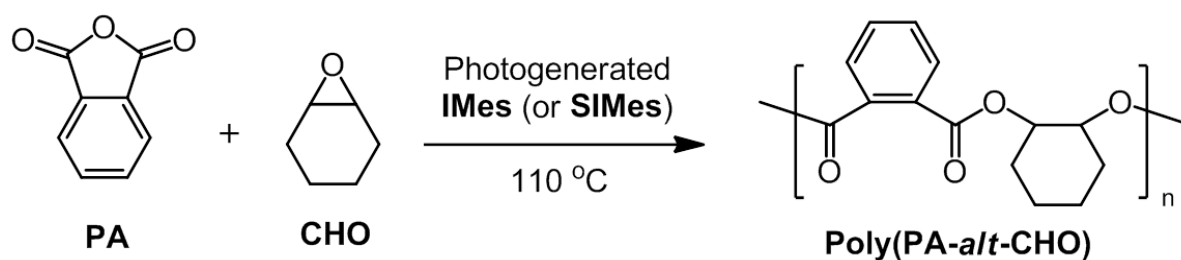


Figure 2.11. FT-IR spectra of aliquots taken at different times during the bulk polyaddition between PEG₄₀₀ and IPDI (PEG₄₀₀/IPDI (342/342 equiv.)). Polymerization was conducted at 60 °C after the addition of the as-irradiated **IMesH⁺BPh₄⁻**/ITX solution (1/1 equiv.). For each measurement, the aliquot was deposited on a CaF₂ pellet.

b. Synthesis of polyester

Encouraged by this first result, the NHC photogenerator's catalytic activity was also evaluated in ring-opening copolymerization (ROCOP) of epoxide and anhydride. This reaction offers a controlled route to polyesters, although it has been much less studied than ring-opening polymerization of cyclic esters.^{60,61} ROCOP generally requires organometallic initiators to reach efficient curing, but the use of NHC was reported very recently.^{62,63} In a model copolymerization, the as-irradiated azolium salt/ITX mixture (1/1 equiv.) was added to a mixture of cyclohexene oxide (CHO, 500 equiv.) and phthalic anhydride (PA, 100 equiv.) (**Scheme 2.7**). Polymerization was conducted at 110°C using thus CHO as both the monomer and the solvent.



Scheme 2.7. ROCOP of PA and CHO using photogenerated NHC **IMes** and **SIMes** as catalyst.

Table 2.3. Results of ROCOP of CHO/PA (500/100 equiv.). Polymerization were conducted at 110 °C for 60 min in THF after the addition of the as-irradiated azolium salt/ITX solution (1/1 equiv.) or free NHC (1 equiv.).

Entry	Catalyst system	PA conv. ^[a] (%)	Ester conv. ^[b] (%)	M_{n-SEC} ^[c] (g·mol ⁻¹)	\mathcal{D} ^[d]
a	IMesH⁺BPh₄⁻ /ITX	98	> 95	3800	1.21
a'	IMes	92	> 95	3000	1.16
b	SIMesH⁺BPh₄⁻ /ITX	84	> 95	3500	1.18
c	No catalyst	0	-	-	-
d	NaBPh ₄ /ITX	0	-	-	-

[a] Determined by ¹H NMR. PA conv.(%) = $\frac{I_{7.85-8.02}}{I_{7.85-8.02} + I_{7.31-7.62}} \times 100$ where $I_{7.85-8.02}$ is the intensity of methine protons ($\delta_a = 7.85 - 8.02$ ppm) of residual PA and $I_{7.31-7.62}$ is the intensity of methine protons ($\delta_b = 7.31 - 7.62$ ppm) of poly(PA-*alt*-CHO) (**Figure 2.12**).

[b] Percentage of ester linkages in isolated poly(PA-*alt*-CHO) calculated by ¹H NMR in CDCl₃ (**Figure A.II.13**) and MALDI-ToF (**Figure A.II.14**).

[c] Experimental number average molar mass M_n obtained by SEC.

[d] Polymer dispersity index $\mathcal{D} = M_w / M_n$ obtained by SEC.

Table 2.3 shows PA conversion, molecular weight and polydispersity (\mathcal{D}) after 1 h reaction using **IMesH⁺BPh₄⁻**/ITX (entry **a**) or **SIMesH⁺BPh₄⁻**/ITX (entry **b**) along with two control experiments (entries **c-d**). As expected, no reaction took place in the uncatalyzed control reaction (entry **c**).⁶² Conversely, almost full conversions were achieved with **IMesH⁺BPh₄⁻** (98 %) and with **SIMesH⁺BPh₄⁻** (84 %). In addition, the polyesters produced exhibited a highly alternating structure with a high fraction of ester linkages (> 95 %, see ¹H NMR spectra in **Figure A.II.13**).

By contrast, it is well-known that conventional catalytic systems such as metalloprophyrin or salen can form a significant proportions of ether linkages resulting from CHO homopolymerization.^{60,61} The alternating structure was also evidenced in the MALDI-ToF MS spectrum of polymer obtained from entry **a** (**Figure A.II.14**) which displayed an m/z increment of 246.26 g·mol⁻¹ corresponding to the exact molar mass of the [PA + CHO] repeating unit. Interestingly, no **IMes** end-capped chains were identified due to quenching of the reaction mixture in methanol. As a result, the five main populations of peaks were all assigned to α -methyl- ω -hydroxyl OH/CH₃-terminated polymers.

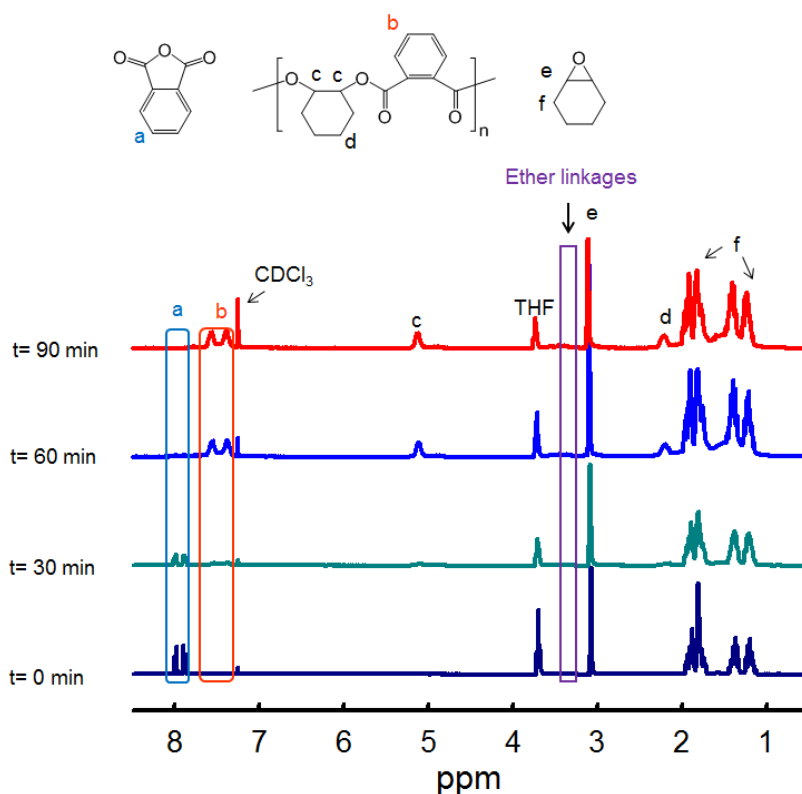


Figure 2.12. ^1H NMR spectra of in CDCl_3 of aliquots taken at different times during the ROCOP of CHO/PA (500/100 equiv.). Polymerization was conducted at $110\text{ }^\circ\text{C}$ after the addition of the as-irradiated $\text{IMesH}^+\text{BPh}_4^-$ /ITX solution (1/1 equiv.). $\text{PA conv.}(\%) = \frac{I_{7.85-8.02}}{I_{7.85-8.02} + I_{7.31-7.62}} \times 100$ where $I_{7.85-8.02}$ is the intensity of methine protons ($\delta = 7.85 - 8.02$ ppm) of residual PA and $I_{7.31-7.62}$ is the intensity of methine protons ($\delta = 7.31 - 7.62$ ppm) of poly(PA-*alt*-CHO).

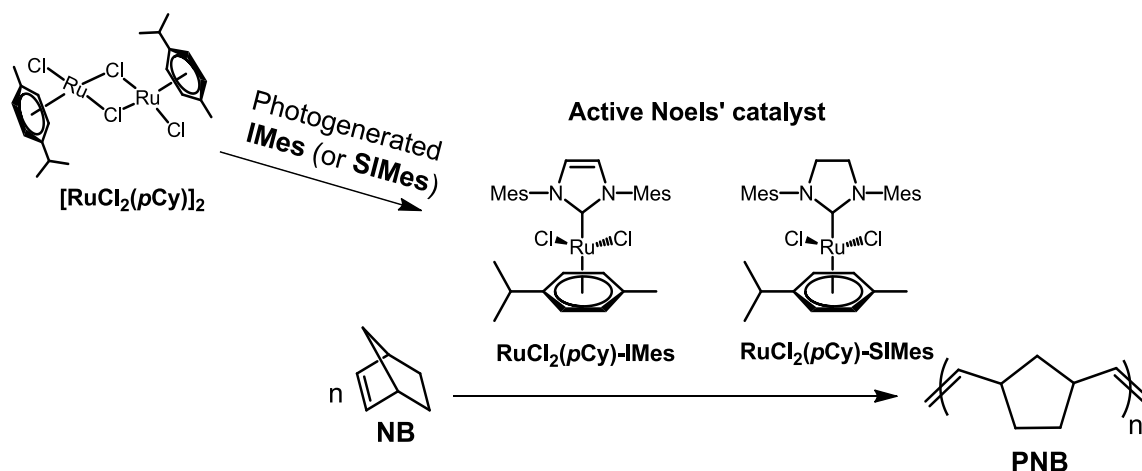
Mechanism was presumed to proceed through a nucleophilic attack of NHCs on anhydride functionality (**Scheme A.II.2**)^{62,63} Besides, copolymers resulted from entry **a** and **b** exhibited monomodal SEC traces with narrow molecular weight distributions ($D \sim 1.2$, see **Figure A.II.15**). Surprisingly, $\text{IMesH}^+\text{BPh}_4^-$ showed slightly higher conversions and M_n values than **IMes** despite incomplete deprotonation, raising doubts about the role of other photoproducts in reaction catalysis. However, the replacement of $\text{IMesH}^+\text{BPh}_4^-$ by NaBPh_4 afforded no polymer (entry **d**).

c. Synthesis of polynorbornene

In the field of catalyst precursors for olefin metathesis, NHC-coordinated ruthenium complexes with the general formula $\text{RuCl}_2(\text{arene})(\text{NHC})$ stand out by their ease of preparation. They can be produced in situ from commercial and inactive ruthenium dimers such as $[\text{RuCl}_2(p\text{-cymene})]_2$ (**Scheme 2.8**) after addition of a suitable free NHC such as **IMes** or **SIMes**, which causes the dissociation of this precatalyst.^{64,65} The resultant active

complexes, $\text{RuCl}_2(p\text{-cymene})\text{-IMes}$ or $\text{RuCl}_2(p\text{-cymene})\text{-SIMes}$, have emerged as versatile and efficient catalysts to promote the ROMP of both strained and low ring-strained cyclic olefins.^{66–68} Building on our previous study,³⁶ we show herein that it is possible to generate in situ the active $\text{RuCl}_2(p\text{-cymene})\text{NHC}$ complex bearing ligand **IMes** or **SIMes**,^{66,67,69} by irradiation of the NHC photogenerator $\text{ITX}/\text{IMesH}^+\text{BPh}_4^-$ (or $\text{ITX}/\text{SIMesH}^+\text{BPh}_4^-$) in presence of the ruthenium precatalyst $[\text{RuCl}_2(p\text{-cymene})]_2$. Using this 3-component system, it is thus possible to trigger the ROMP of cyclic olefins such as norbornene (NB) under UV exposure.

Inactive precatalyst



Scheme 2.8. Strategy for in situ formation of $\text{RuCl}_2(p\text{-cymene})\text{NHC}$ from the inactive precatalyst $[\text{RuCl}_2(p\text{-cymene})]_2$ dimer and photogenerated NHC **IMes** and **SIMes**. The active NHC-coordinated Ru complexes referred to as Noels' catalysts can be used as active for the ROMP of NB.

The catalytic activity of the three-component system $[\text{RuCl}_2(p\text{-Cy})]_2/\text{IMesH}^+\text{BPh}_4^-/\text{ITX}$ (1/5/2.5 equiv.) for the ROMP of norbornene in CD_2Cl_2 was evaluated. In contrast to previous experiments where the as-irradiated photoNHC/ITX was introduced later, NHC photogenerator was initially present in the reaction medium and polymerizations were conducted at room temperature. **Table 2.4** displays NB conversion, molecular weight and *cis* content after 1 min reaction at ambient temperature. As expected, the irradiation of a solution devoid of Ru dimer results in no reaction (entry **a**). Without photoNHC (entry **b**), a very small conversion was detected (< 2%). By contrast, much higher conversion (78 %) was achieved using the 3-component mixture $[\text{RuCl}_2(p\text{-Cy})]_2/\text{IMesH}^+\text{BPh}_4^-/\text{ITX}$ (entry **c**) suggesting the successful formation of the highly active ruthenium-arene complex bearing an NHC ligand. Replacing **IMesH}^+\text{BPh}_4^-** by **SIMesH}^+\text{BPh}_4^-** resulted in similar conversions

(76 %, entry **d**), molecular weight and \bar{D} (**Figure A.II.16**). It is well established in the literature that the unsaturation in the imidazole ring of NHC moiety is not a crucial feature altering catalytic efficiency.⁶⁸ In both cases, σ_{cis} (≈ 40 -50 %) was very similar to that found in the corresponding polymer prepared by the action of a Ru-NHC complex,^{68,70} thereby suggesting the formation of the same ROMP catalyst. As control experiments, we also conducted the polymerization of NB utilizing a combination of Ru precatalyst with free NHC **IMes**. The mixture of $[\text{RuCl}_2(p\text{-cymene})]_2$ and **IMes** was conducted in dark for 1 min showed slightly lower monomer consumption (58.9 %, entry **e**). This result supports the hypothesis that radiation facilitates the decoordination of the *p*-cymene ligand to form an active species.⁶⁶

Table 2.4. Results for the photoROMP of NB conducted at ambient conditions by 1 min irradiation (365 nm, 6.5 mW·cm⁻²) of the mixture NB/Ru dimer/photoNHC/ITX in CD₂Cl₂ (510/1/5/2.5 equiv., [NB] = 1 M).

Entry	photo-NHC	Ru dimer/ photoNHC/ITX (equiv.)	Conv. ^[a] (%)	σ_{cis} ^[b]	$M_{n\text{-th}}$ ^[c] (kg·mol ⁻¹)	$M_{n\text{-SEC}}$ ^[d] (kg·mol ⁻¹)	\bar{D} ^[e]
a	IMesH⁺BPh₄⁻	0/5/2.5	0	n.d	n.d	n.d	n.d
b	-	1/0/0	1.5	9.3	0.36	n.d.	n.d.
c	IMesH⁺BPh₄⁻	1/5/2.5	78	51.9	18.69	146.8	3.02
d	SIMesH⁺BPh₄⁻	1/5/2.5	76	42.5	18.00	138.3	3.14
e	IMes	1/2 ^[f] /0	59	59.4	14.11	319.2	3.70

[a] Determined by ¹H NMR NB conv.(%) = $\frac{I_{5.21} + I_{5.36}}{I_{5.21} + I_{5.36} + I_{5.99}} \times 100$ where $I_{5.21}$ and $I_{5.36}$ are the intensity of vinylic protons ($\delta = 5.21$ ppm and $\delta = 5.36$ ppm) of polynorbornene and $I_{5.99}$ is the intensity of vinylic proton ($\delta = 5.99$ ppm) of residual NB.

[b] *Cis* content of the polymers calculated from ¹H NMR spectrum cis (%) = $\frac{I_{5.36}}{I_{5.21} + I_{5.36}} \times 100$.

[c] Theoretical number average molar mass $M_{n\text{-th}} = \text{Conv.} \times \frac{[\text{NB}] \times M_{\text{NB}}}{2 \times [\text{Ru dimer}]}$.

[d] Experimental number average molar mass M_n obtained by SEC.

[e] Polymer dispersity index $\bar{D} = M_w / M_n$ obtained by SEC.

[f] The solution was kept in dark for 1 min, n.d. means not determined due to no polymerization or insoluble polymer.

2.4 CONCLUSIONS

In presence of ITX, imidazolium or imidazolium salts bearing tetraphenylborate anion are able to generate photochemically the corresponding free imidazolyliidene and

imidazolidinylidene species upon irradiation at 365 nm. The mechanism has been investigated by means of steady-state photolysis. It involves a first electron-transfer reaction from the easily oxidized electron donor BPh_4^- to excited ITX acting as an electron acceptor. The thioxanthone radical anion formed can then abstract a proton from the azolium cation to yield the free NHCs. The formation of the NHCs, **IMes** and **SIMes**, was proved by EPR spectroscopy in THF through the formation of a persistent NHC-mesityl radical adduct. A maximum amount of NHC of 70 % was produced in THF, based on the azolium cation precursor, as determined by ^1H NMR of a stable and soluble NHC-CDI adduct. Irradiation time should be carefully controlled to avoid overexposure resulting in secondary electron-transfer reaction between triplet ITX and the NHC formed. The easy synthesis of NHC progenitors **IMesH⁺BPh₄⁻** and **SIMesH⁺BPh₄⁻** opened the way to novel photomediated polymerization reactions where NHCs advantageously acted as organocatalysts in place of metals. Linear polyurethanes were synthesized by the step-growth polymerization of diols and diisocyanate. Additionally, the ring-opening copolymerization of anhydride with epoxy yielded polyesters with narrow polydispersity. Finally, in combination with an inactive Ru precatalyst, photolabile NHCs could also drive the formation of highly active ruthenium-NHC complexes for ring-opening polymerizations of norbornene with > 76 % conversion reached after 1 min of irradiation. It is expected that a wide variety of other NHC-mediated organic chemical reactions and polymerization reactions could benefit from this innovative NHC photogenerating system; in particular, those including thermally sensitive substrates or requiring a spatial control.

2.5 REFERENCES

- 1 A. J. Arduengo, R. L. Harlow and M. Kline, A stable crystalline carbene, *J. Am. Chem. Soc.*, 1991, **113**, 361–363.
- 2 B. Hogan and M. Albrecht, in *Reference Module in Chemistry, Molecular Sciences and Chemical Engineering*, Elsevier, 2016, pp.1– 4.
- 3 E. Peris, Smart N-Heterocyclic Carbene Ligands in Catalysis, *Chem. Rev.*, 2018, **118**, 9988–10031.
- 4 D. M. Flanigan, F. Romanov-Michailidis, N. A. White and T. Rovis, Organocatalytic Reactions Enabled by N-Heterocyclic Carbenes, *Chem. Rev.*, 2015, **115**, 9307–9387.
- 5 S. Naumann and A. P. Dove, N-Heterocyclic carbenes for metal-free polymerization catalysis: an update, *Polym. Int.*, 2016, **65**, 16–27.
- 6 N. D. Clement, L. Routaboul, A. Grotevendt, R. Jackstell and M. Beller, Development of Palladium-Carbene Catalysts for Telomerization and Dimerization of 1,3-Dienes: From Basic Research to Industrial Applications, *Chem.: Eur. J.*, 2008, **14**, 7408–7420.

-
- 7 F. E. Hahn and M. C. Jahnke, Heterocyclic Carbenes: Synthesis and Coordination Chemistry, *Angew. Chem. Int. Ed.*, 2008, **47**, 3122–3172.
 - 8 S. Díez-González, N. Marion and S. P. Nolan, N-Heterocyclic Carbenes in Late Transition Metal Catalysis, *Chem. Rev.*, 2009, **109**, 3612–3676.
 - 9 M. Scholl, S. Ding, C. W. Lee and R. H. Grubbs, Synthesis and Activity of a New Generation of Ruthenium-Based Olefin Metathesis Catalysts Coordinated with 1,3-Dimesityl-4,5-dihydroimidazol-2-ylidene Ligands, *Org. Lett.*, 1999, **1**, 953–956.
 - 10 M. Fèvre, J. Pinaud, Y. Gnanou, J. Vignolle and D. Taton, N-Heterocyclic carbenes (NHCs) as organocatalysts and structural components in metal-free polymer synthesis, *Chem. Soc. Rev.*, 2013, **42**, 2142–2172.
 - 11 S. Naumann and A. P. Dove, N-Heterocyclic carbenes as organocatalysts for polymerizations: trends and frontiers, *Polym. Chem.*, 2015, **6**, 3185–3200.
 - 12 N. E. Kamber, W. Jeong, S. Gonzalez, J. L. Hedrick and R. M. Waymouth, N-Heterocyclic Carbenes for the Organocatalytic Ring-Opening Polymerization of ϵ -Caprolactone, *Macromolecules*, 2009, **42**, 1634–1639.
 - 13 S. Naumann, S. Epple, C. Bonten and M. R. Buchmeiser, Polymerization of ϵ -Caprolactam by Latent Precatalysts Based on Protected N-Heterocyclic Carbenes, *ACS Macro Lett.*, 2013, **2**, 609–612.
 - 14 J. Raynaud, W. N. Ottou, Y. Gnanou and D. Taton, Metal-free and solvent-free access to α,ω -heterodifunctionalized poly(propylene oxide)s by N-heterocyclic carbene-induced ring opening polymerization, *Chem. Commun.*, 2010, **46**, 3203.
 - 15 J. Pinaud, K. Vijayakrishna, D. Taton and Y. Gnanou, Step-Growth Polymerization of Terephthaldehyde Catalyzed by N-Heterocyclic Carbenes, *Macromolecules*, 2009, **42**, 4932–4936.
 - 16 O. Coutelier, M. El Ezzi, M. Destarac, F. Bonnette, T. Kato, A. Baceiredo, G. Sivasankarapillai, Y. Gnanou and D. Taton, N-Heterocyclic carbene-catalysed synthesis of polyurethanes, *Polym. Chem.*, 2012, **3**, 605.
 - 17 D. C. Graham, K. J. Cavell and B. F. Yates, Dimerization mechanisms of heterocyclic carbenes, *J. Phys. Org. Chem.*, 2005, **18**, 298–309.
 - 18 A. Poater, F. Ragone, S. Giudice, C. Costabile, R. Dorta, S. P. Nolan and L. Cavallo, Thermodynamics of N-Heterocyclic Carbene Dimerization: The Balance of Sterics and Electronics, *Organometallics*, 2008, **27**, 2679–2681.
 - 19 P. de Frémont, N. Marion and S. P. Nolan, Carbenes: Synthesis, properties, and organometallic chemistry, *Coord. Chem. Rev.*, 2009, **253**, 862–892.
 - 20 H.-J. Schönherr and H.-W. Wanzlick, Chemie nucleophiler Carbene, XVIII¹⁾ 1.3.4.5-Tetraphenylimidazoliumperchlorat, *Justus Liebigs Ann. Chem.*, 1970, **731**, 176–179.
 - 21 W. A. Herrmann, M. Alison, J. Fischer, C. Köcher and G. R. J. Artus, N-Heterocyclic Carbenes: Generation under Mild Conditions and Formation of Group 8–10 Transition Metal Complexes Relevant to Catalysis, *Chem.: Eur. J.*, 1996, **2**, 772–780.
 - 22 S. Naumann and M. R. Buchmeiser, Liberation of N-heterocyclic carbenes (NHCs) from thermally labile progenitors: protected NHCs as versatile tools in organo- and polymerization catalysis, *Catal. Sci. Technol.*, 2014, **4**, 2466–2479.

-
- 23 F. Bonnette, T. Kato, M. Destarac, G. Mignani, F. P. Cossío and A. Baceiredo, Encapsulated N-Heterocyclic Carbenes in Silicones without Reactivity Modification, *Angew. Chem. Int. Ed.*, 2007, **46**, 8632–8635.
- 24 B. Bantu, G. M. Pawar, U. Decker, K. Wurst, A. M. Schmidt and M. R. Buchmeiser, CO₂ and Sn^{II} Adducts of N-Heterocyclic Carbenes as Delayed-Action Catalysts for Polyurethane Synthesis, *Chem.: Eur. J.*, 2009, **15**, 3103–3109.
- 25 B. C. Norris, D. G. Sheppard, G. Henkelman and C. W. Bielawski, Kinetic and Thermodynamic Evaluation of the Reversible N-Heterocyclic Carbene–Isothiocyanate Coupling Reaction: Applications in Latent Catalysis, *J. Org. Chem.*, 2011, **76**, 301–304.
- 26 S. Naumann, F. G. Schmidt, W. Frey and M. R. Buchmeiser, Protected N-heterocyclic carbenes as latent pre-catalysts for the polymerization of ϵ -caprolactone, *Polym. Chem.*, 2013, **4**, 4172.
- 27 N. Corrigan, J. Yeow, P. Judzewitsch, J. Xu and C. Boyer, Seeing the Light: Advancing Materials Chemistry through Photopolymerization, *Angew. Chem. Int. Ed.*, 2019, **58**, 5170–5189.
- 28 C. Fu, J. Xu and C. Boyer, Photoacid-mediated ring opening polymerization driven by visible light, *Chem. Commun.*, 2016, **52**, 7126–7129.
- 29 D. M. Denning, M. D. Thum and D. E. Falvey, Photochemical Reduction of CO₂ Using 1,3-Dimethylimidazolyidene, *Org. Lett.*, 2015, **17**, 4152–4155.
- 30 K. Suyama and M. Shirai, Photobase generators: Recent progress and application trend in polymer systems, *Prog. Polym. Sci.*, 2009, **34**, 194–209.
- 31 E. Placet, J. Pinaud, O. Gimello and P. Lacroix-Desmazes, UV-Initiated Ring Opening Polymerization of L-Lactide Using a Photobase Generator, *ACS Macro Lett.*, 2018, **7**, 688–692.
- 32 X. Dong, P. Hu, G. Zhu, Z. Li, R. Liu and X. Liu, Thioxanthone acetic acid ammonium salts: highly efficient photobase generators based on photodecarboxylation, *RSC Adv.*, 2015, **5**, 53342–53348.
- 33 X. Sun, J. P. Gao and Z. Y. Wang, Bicyclic Guanidinium Tetraphenylborate: A Photobase Generator and A Photocatalyst for Living Anionic Ring-Opening Polymerization and Cross-Linking of Polymeric Materials Containing Ester and Hydroxy Groups, *J. Am. Chem. Soc.*, 2008, **130**, 8130–8131.
- 34 S. Chatani, T. Gong, B. A. Earle, M. Podgórski and C. N. Bowman, Visible-Light Initiated Thiol-Michael Addition Photopolymerization Reactions, *ACS Macro Lett.*, 2014, **3**, 315–318.
- 35 J. Shin, H. Matsushima, C. M. Comer, C. N. Bowman and C. E. Hoyle, Thiol–Isocyanate–Ene Ternary Networks by Sequential and Simultaneous Thiol Click Reactions, *Chem. Mater.*, 2010, **22**, 2616–2625.
- 36 J. Pinaud, T. K. H. Trinh, D. Sauvanier, E. Placet, S. Songsee, P. Lacroix-Desmazes, J.-M. Becht, B. Tarablsi, J. Lalevée, L. Pichavant, V. Héroguez and A. Chemtob, In Situ Generated Ruthenium-Arene Catalyst for Photoactivated Ring-Opening Metathesis Polymerization through Photolabile N-Heterocyclic Carbene Ligand, *Chem.: Eur. J.*, 2018, **24**, 337–341.
- 37 S. Dadashi-Silab, C. Aydogan and Y. Yagci, Shining a light on an adaptable photoinitiator: advances in photopolymerizations initiated by thioxanthenes, *Polym. Chem.*, 2015, **6**, 6595–6615.
- 38 A. M. Sarker, A. Lungu, A. Mejiritski, Y. Kaneko and D. C. Neckers, Tetraorganylborate salts as convenient precursors for photogeneration of tertiary amines, *J. Chem. Soc. Perkin Trans. 2*, 1998, 2315–2322.

-
- 39 S. Chatterjee, P. D. Davis, P. Gottschalk, M. E. Kurz, B. Sauerwein, X. Yang and G. B. Schuster, Photochemistry of carbocyanine alkyltriphenylborate salts: intra-ion-pair electron transfer and the chemistry of boranyl radicals, *J. Am. Chem. Soc.*, 1990, **112**, 6329–6338.
- 40 D. Rehm and A. Weller, Kinetics of Fluorescence Quenching by Electron and H-Atom Transfer, *Isr. J. Chem.*, 1970, **8**, 259–271.
- 41 N. J. Turro, J. C. Scaiano and V. Ramamurthy, *Modern Molecular Photochemistry of Organic Molecules*, University Science Books, Sausalito, Calif, 1st edition., 2010.
- 42 J. P. Fouassier, X. Allonas, J. Lalevee and M. Visconti, Radical polymerization activity and mechanistic approach in a new three-component photoinitiating system, *J. Polym. Sci. Part A: Polym. Chem.*, 2000, **38**, 4531–4541.
- 43 H.-J. Timpe and K.-P. Kronfeld, Light-induced polymer and polymerization reactions XXXIII: direct photoinitiation of methyl methacrylate polymerization by excited states of ketones, *J. Photochem. Photobiol. Chem.*, 1989, **46**, 253–267.
- 44 Y. Toba, M. Sakamoto and T. Uesugi, Photopolymerization of an Acrylate in a PMMA Film Using the Aromatic Ketone-Sulfonium Borate Photoinitiator Systems., *J. Photopolym. Sci. Technol.*, 1999, **12**, 115–120.
- 45 X. Allonas, J. P. Fouassier, M. Kaji and Y. Murakami, Excited state processes in a four-component photosensitive system based on a bisimidazole derivative Dedicated to Professor Jean Kossanyi on the occasion of his 70th birthday., *Photochem. Photobiol. Sci.*, 2003, **2**, 224.
- 46 I. Pyszka, Z. Kucybała and J. Paczkowski, Reinvestigation of the Mechanism of the Free Radical Polymerization Photoinitiation Process by Camphorquinone-Coinitiator Systems: New Results, *Macromol. Chem. Phys.*, 2004, **205**, 2371–2375.
- 47 J. B. Foresman, Ae. Frisch and I. Gaussian, *Exploring chemistry with electronic structure methods*, Pittsburgh, PA : Gaussian, Inc, 2nd ed., 1996.
- 48 M. J. Frisch, G. W. Trucks, H. B. Schlegel, G. E. Scuseria, M. A. Robb, J. R. Cheeseman, V. G. Zakrzewski, J. A. Montgomery, J. R. E. Stratmann, J. C. Burant, S. Dapprich, J. M. Milam, A. N. D. Daniels, K. N. Kudin, M. C. Strain, O. Farkas, J. Tomasi, V. Barone, M. Cossi, R. Cammi, B. Mennucci, C. Pomelli, C. Adamo, S. Clifford, J. Ochterski, G. A. Petersson, P. Y. Ayala, Q. Cui, K. Morokuma, P. Salvador, J. J. Dannenberg, D. K. Malick, A. D. Rabuck, K. Raghavachari, J. B. Foresman, J. Cioslowski, J. V. Ortiz, A. G. Baboul, B. B. Stefanov, G. Liu, A. Liashenko, P. Piskorz, I. Komaromi, R. Gomperts, R. L. Martin, D. J. Fox, T. Keith, M. A. Al-Laham, C. Y. Peng, A. Nanayakkara, M. Challacombe, P. M. W. Gill, B. Johnson, W. Chen, M. W. Wong, J. L. Andres, C. Gonzalez, M. Head-Gordon, E. S. Replogle, J. A. Pople, *Gaussian 03, Revision B-2*, Gaussian, Inc: Pittsburgh PA, 2003.
- 49 B. Tumanskii, D. Sheberla, G. Molev and Y. Apeloig, Dual Character of Arduengo Carbene–Radical Adducts: Addition versus Coordination Product, *Angew. Chem. Int. Ed.*, 2007, **119**, 7552–7555.
- 50 D. Sheberla, B. Tumanskii, A. C. Tomasik, A. Mitra, N. J. Hill, R. West and Y. Apeloig, Different electronic structure of phosphonyl radical adducts of N-heterocyclic carbenes, silylenes and germynes: EPR spectroscopic study and DFT calculations, *Chem. Sci.*, 2010, **1**, 234.

-
- 51 A. Baishya, L. Kumar, M. Kr. Barman, T. Peddaraao and S. Nembenna, Air Stable N-Heterocyclic Carbene-Carbodiimide (“NHC-CDI”) Adducts: Zwitterionic Type Bulky Amidinates, *Chemistry Select.*, 2016, **1**, 498–503.
- 52 A. V. Zhukhovitskiy, J. Geng and J. A. Johnson, Cycloelimination of Imidazolidin-2-ylidene N-Heterocyclic Carbenes: Mechanism and Insights into the Synthesis of Stable “NHC-CDI” Amidinates, *Chem.: Eur. J.*, 2015, **21**, 5685–5688.
- 53 O. Hollóczki, Unveiling the peculiar hydrogen bonding behavior of solvated N-heterocyclic carbenes, *Phys. Chem. Chem. Phys.*, 2016, **18**, 126–140.
- 54 M. Feroci, I. Chiarotto, F. D’Anna, F. Gala, R. Noto, L. Ornano, G. Zollo and A. Inesi, N-Heterocyclic Carbenes and Parent Cations: Acidity, Nucleophilicity, Stability, and Hydrogen Bonding-Electrochemical Study and Ab Initio Calculations, *Chem. Electro. Chem.*, 2016, **3**, 1133–1141.
- 55 M. Thomas, M. Brehm, O. Hollóczki and B. Kirchner, How Can a Carbene be Active in an Ionic Liquid?, *Chem.: Eur. J.*, 2014, **20**, 1622–1629.
- 56 N. S. Allen, F. Catalina, J. Luc-Gardette, W. A. Green, P. N. Green, W. Chen and K. O. Fatinikun, Spectroscopic properties and photopolymerisation activity of 4-n-propoxythioxanthone, *Eur. Polym. J.*, 1988, **24**, 435–440.
- 57 T. Konishi, Y. Sasaki, M. Fujitsuka, Y. Toba, H. Moriyama and O. Ito, Persistent C₆₀ anion-radical formation via photoinduced electron transfer from tetraphenylborate and triphenylbutylborate, *J. Chem. Soc. Perkin Trans. 2*, 1999, **3**, 551–556.
- 58 T. Ramnial, I. McKenzie, B. Gorodetsky, E. M. W. Tsang and J. A. C. Clyburne, Reactions of N-heterocyclic carbenes (NHCs) with one-electron oxidants: possible formation of a carbene cation radical, *Chem. Commun.*, 2004, **0**, 1054–1055.
- 59 H. Sardon, A. Pascual, D. Mecerreyes, D. Taton, H. Cramail and J. L. Hedrick, Synthesis of Polyurethanes Using Organocatalysis: A Perspective, *Macromolecules*, 2015, **48**, 3153–3165.
- 60 S. Paul, Y. Zhu, C. Romain, R. Brooks, P. K. Saini and C. K. Williams, Ring-opening copolymerization (ROCOP): synthesis and properties of polyesters and polycarbonates, *Chem. Commun.*, 2015, **51**, 6459–6479.
- 61 E. Hosseini Nejad, C. G. W. van Melis, T. J. Vermeer, C. E. Koning and R. Duchateau, Alternating Ring-Opening Polymerization of Cyclohexene Oxide and Anhydrides: Effect of Catalyst, Cocatalyst, and Anhydride Structure, *Macromolecules*, 2012, **45**, 1770–1776.
- 62 S. Naumann, M. Speiser, R. Schowner, E. Giebel and M. R. Buchmeiser, Air Stable and Latent Single-Component Curing of Epoxy/Anhydride Resins Catalyzed by Thermally Liberated N-Heterocyclic Carbenes, *Macromolecules*, 2014, **47**, 4548–4556.
- 63 H. J. Altmann, S. Naumann and M. R. Buchmeiser, Protected N-heterocyclic carbenes as latent organocatalysts for the low-temperature curing of anhydride-hardened epoxy resins, *Eur. Polym. J.*, 2017, **95**, 766–774.
- 64 A. C. Hillier, W. J. Sommer, B. S. Yong, J. L. Petersen, L. Cavallo and S. P. Nolan, A Combined Experimental and Theoretical Study Examining the Binding of N-Heterocyclic Carbenes (NHC) to the Cp*RuCl (Cp* = η⁵-C₅Me₅) Moiety: Insight into Stereoelectronic Differences between Unsaturated and Saturated NHC Ligands, *Organometallics*, 2003, **22**, 4322–4326.

-
- 65 J. Huang, H.-J. Schanz, E. D. Stevens and S. P. Nolan, Stereoelectronic Effects Characterizing Nucleophilic Carbene Ligands Bound to the Cp*RuCl (Cp* = η^5 -C₅Me₅) Moiety: A Structural and Thermochemical Investigation, *Organometallics*, 1999, **18**, 2370–2375.
- 66 A. Tudose, A. Demonceau and L. Delaude, Imidazol(in)ium-2-carboxylates as N-heterocyclic carbene precursors in ruthenium–arene catalysts for olefin metathesis and cyclopropanation, *J. Organomet. Chem.*, 2006, **691**, 5356–5365.
- 67 L. Delaude, M. Szypa, A. Demonceau and A. F. Noels, New In situ Generated Ruthenium Catalysts Bearing N-Heterocyclic Carbene Ligands for the Ring-Opening Metathesis Polymerization of Cyclooctene, *Adv. Synth. Catal.*, 2002, **344**, 749.
- 68 L. Delaude, A. Demonceau and A. F. Noels, Synthesis and Application of New N-Heterocyclic Carbene Ruthenium Complexes in Catalysis: A Case Study, *Curr. Org. Chem.*, 2006, **10**, 203–215.
- 69 X. Bantreil and S. P. Nolan, Synthesis of N-heterocyclic carbene ligands and derived ruthenium olefin metathesis catalysts, *Nat. Protoc.*, 2011, **6**, 69–77.
- 70 Y. Zhang, D. Wang, P. Lönnecke, T. Scherzer and M. R. Buchmeiser, Novel Initiators for Thermally and UV-Triggered ROMP, *Macromol. Symp.*, 2006, **236**, 30–37.

CHAPTER III. PHOTOREDUCTION OF TRIPLET THIOXANTHONE DERIVATIVES BY AZOLIUM TETRAPHENYLBORATE: A WAY TO PHOTOGENERATE N-HETEROCYCLIC CARBENES

The text in this chapter is reproduced in part with permission from:

J. Pinaud, T. K. H. Trinh, D. Sauvanier, E. Placet, S. Songsee, P. Lacroix-Desmazes, J.-M. Becht, B. Tarablsi, J. Lalevée, L. Pichavant, V. Héroguez and A. Chemtob, In Situ Generated Ruthenium-Arene Catalyst for Photoactivated Ring-Opening Metathesis Polymerization through Photolabile N-Heterocyclic Carbene Ligand, *Chem.: Eur. J.*, 2018, **24**, 337–341.

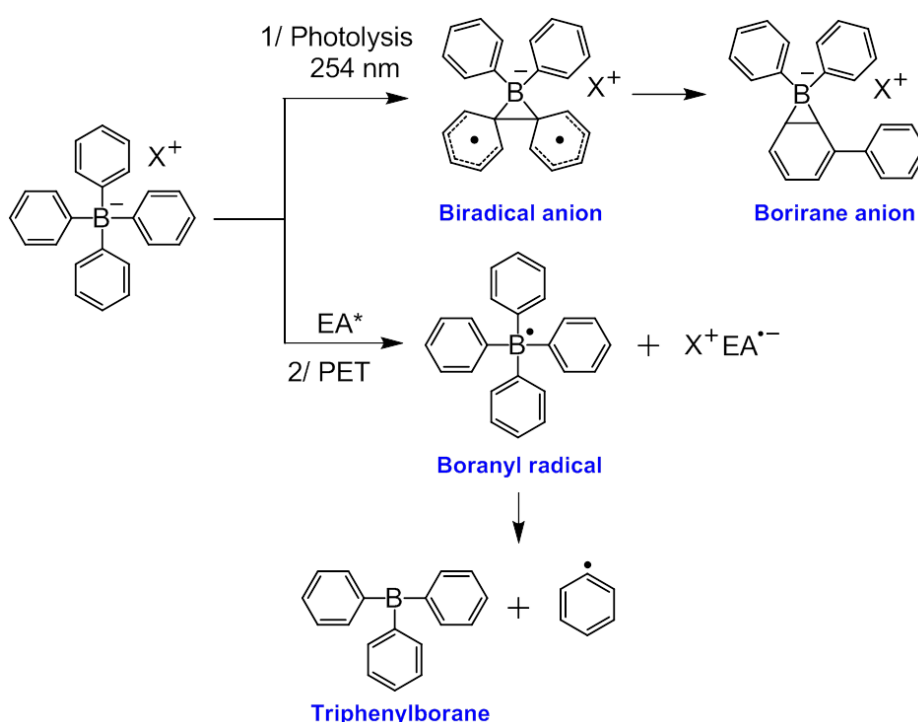
©Wiley-VCH 2016
69451 Weinheim, Germany

J. Pinaud, E. Placet, P. Lacroix-Desmazes, T. K. H. Trinh, J. P. Malval, A. Chemtob, and V. Héroguez, “Photogeneration of N-Heterocyclic Carbenes: Application in Photoinduced Ring-Opening Metathesis Polymerization”. *J. Vis. Exp.*, 2018, 141.

©MyJove Corp 2006
02140 Cambridge, USA

3.1 INTRODUCTION

Of high importance in photochemistry are arylborates, which are four-coordinate boron compounds bearing a tetrahedral geometry, a formal negative charge, and at least one aryl substituent. Although their photochemical reactivity has been studied since the late 1970s,^{1,2} progress in this field has been made at the cost of intense debates,³ and many unknowns still remain.⁴ Photoreactivity of arylborates is organized around two major types of reactions (**Scheme 3.1**): *direct photolysis* and *photoinduced electron transfer (PET)*, in this latter case, the borate anion acts as one electron reducing agent. Recently, other reactions such as photochromic isomerization or photoelimination were described for arylborate molecules with an N,C- or a C,C-chelate backbone.⁵



Scheme 3.1. Photochemical reactivity of arylborates. Route 1 is based on direct photolysis while route 2 is a photoinduced electron transfer (PET) involving an electron acceptor (EA) sensitizer. The asterisk designates an excited state.

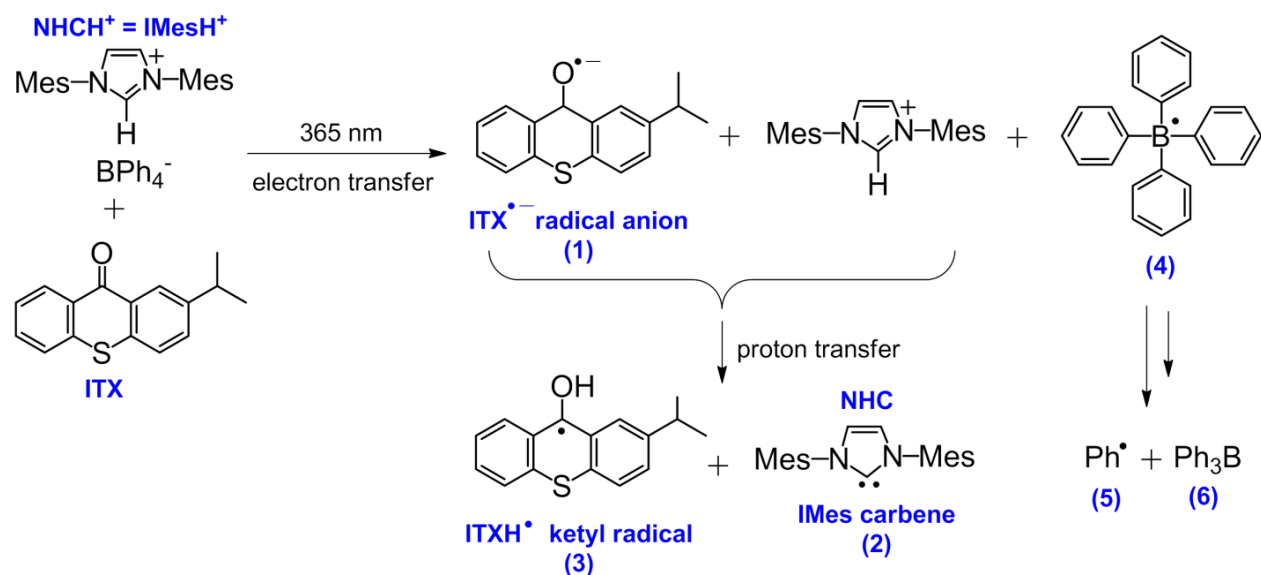
- *Photolysis* upon exposure to 254 nm irradiation was focused on tetraarylborate compounds such as NaBPh₄. The most accepted mechanism involves a di- π -borate rearrangement leading to a three-membered biradical anion, evolving towards a more stable borirane anion isomer. Most studies on direct irradiation attempted to identify photoproducts (biphenyl, 1-phenyl-cyclohexadiene mostly) and elucidate photochemical mechanism.^{1,6,7} Its utility in preparative photochemistry was

demonstrated only recently. Observing that intermediate anion species could abstract acidic protons from water and alcohol,^{7,8} Sun *et al.* proposed in 2008 a tetraphenyl borate salt containing as cation the conjugated acid of a nitrogen base (BH⁺) such as bicyclic guanidine TBD (TBDH⁺).⁶ The base was photogenerated through photoinduced proton abstraction of BH⁺ during the photolysis at 254 nm. For example, TBDH⁺BPh₄⁻ was used as photobase generator (PBG) for the organocatalyzed ring-opening polymerization of cyclic esters⁶ or thiol-epoxy polymerization.⁹ Several authors added an aryl ketone derivative to extend absorption to near UV-Vis range via a supposed triplet-triplet energy transfer.¹⁰⁻¹³

- Due to their relatively low oxidation potential,¹⁴ arylborates such as Ph₄B⁻ or triarylalkylborate salts (Ph₃BR⁻) were also used as electron donor in *inter- and intra-PET reactions* with cationic or neutral electron acceptor (EA) sensitizers such as carbocyanine,¹⁵ fullerene,¹⁶ coumarine,¹⁷ fluorone,¹⁸ benzophenone derivatives.¹⁹ A boranyl radical is formed, which in turn undergoes rapid cleavage yielding a triphenylborane (BPh₃) and an alkyl/phenyl radical (R[•]/Ph[•]). Only alkyl radicals have been applied for alkylation of the electron acceptor,²⁰ or initiation of radical polymerizations.¹⁷

Recently, we proposed another application of photoinitiated oxidation of arylborates, the photogeneration of N-heterocyclic carbene (NHC) using azolium arylborate salts (NHCH⁺BPh₄⁻) (**Scheme 3.2**).²¹ When paired with an EA sensitizer such as isopropylthioxanthone (ITX), an electron transfer from the borate (BPh₄⁻) to the excited triplet state of ITX (³ITX^{*}) may take place as described above. Unlike the previous case, the azolium cation (NHCH⁺) enables a subsequent step of proton abstraction with ITX radical anion ITX^{•-} (**1**) to take place, yielding the expected free NHC (**2**).²¹ Our recent investigations proved that it was possible to form 1,3-bis(mesityl)imidazol-2-ylidene (**IMes**) and its saturated analogue **SIMes**, the two most employed NHCs.²¹ The utility of this two-component NHC photogenerator NHCH⁺BPh₄⁻/ITX was also demonstrated in photopolymerization reactions to form polyurethane, polyester and polynorbornene.²² Indeed, although NHCs have brought profound changes in catalytic organic synthesis,²³⁻²⁵ they generally require inert atmosphere and harsh conditions for their generation. As a result, an air-stable system able to generate NHC on demand and on simple UV exposure has the potential to significantly simplify implementation of the broad spectrum of NHC-catalyzed reactions. While it is true that thermally latent NHC precursors^{26,27} also exist,

photochemically produced NHCs have net advantages including low temperature reaction, thermal stability and the possibility to finely tune NHC concentration upon adjusting the energetic dosage.



Scheme 3.2. Photochemical pathway based on electron and proton transfer reactions resulting in the generation of NHC.

Though the mechanistic hypothesis for photoreduction of thioxantone derivative by arylborates is basically acceptable, conclusive evidences in support of a coupled electron transfer/proton abstraction are required. With exception of the photogenerated NHC molecule, little is known about the transient species — $\text{ITX}^{\bullet-}$, $\text{ITX}^{\bullet-}$ (1), ITXH^\bullet (3), $\text{Ph}_4\text{B}^\bullet$ (4), Ph^\bullet (5) — which are supposed to form and the other putative products: BPh_3 (6), thioxanthone derivatives and Ph_2 . To provide conclusive evidences in support of our mechanism, it is important to clearly establish the identity of transient species and photoproducts. The structure of the organoboron compound(s) formed is particularly important given BPh_3 is likely to form ate-complexes with NHCs, with strong implications for carbene reactivity.²⁸ Indeed, trivalent boron species typically have Lewis acid characteristics, while NHCs behave as Lewis base. Motivated by this situation, this paper explores the identity of transient species and photoproducts generated by the irradiation of 1,3-bis(mesityl)imidazolium tetraphenylborate ($\text{IMesH}^+\text{BPh}_4^-$ and **Scheme 3.2**) with ITX to form the NHC **IMes**. To this purpose, a range of techniques was used: nanosecond laser spectroscopy and electron paramagnetic resonance (EPR) for the detection of the transient species, as well as gas chromatography-mass spectrometry (GC-MS) and ^{11}B NMR spectroscopy for the identification of the photoproducts.

3.2 EXPERIMENTALS

3.2.1 Materials

1,3-Bis(2,4,6-trimethylphenyl)imidazolium chloride (IMesH⁺Cl⁻, 98.0 %, TCI), sodium tetraphenylborate (NaBPh₄, 99.5 %, TCI), N-*tert*-butyl- α -phenylnitrone (PBN, 98.0 %, TCI), diphenyl(2,4,6-trimethylbenzoyl)phosphine oxide (TPO, 98 %, TCI), 2-isopropylthioxanthone (ITX, analytical standard, Aldrich), 1,3-bis(2,4,6-trimethylphenyl)imidazol-2-ylidene (IMes, 97%, Aldrich) and carbon disulfide (CS₂, anhydrous, Aldrich) were used as received unless otherwise mentioned. Acetonitrile-*d*₃ (ACN-*d*₃, 99.8 % D, Aldrich), tetrahydrofuran-*d*₈ (THF-*d*₈, 99.5 % D, Eurisotop), acetonitrile (ACN, HPLC grade, VWR) and ethanol (EtOH, HPLC grade, VWR) were dried over 4 Å molecular sieves before use.

3.3.2 Synthesis of IMesH⁺BPh₄⁻

The IMesH⁺BPh₄⁻ was synthesized as described previously.²¹ ¹H NMR (300 MHz, THF-*d*₈), IMesH⁺BPh₄⁻: δ_{ppm} : 2.03 (s, 12H, 4 \times *o*-ArCH₃), 2.37 (s, 6H, 2 \times *p*-ArCH₃), 6.62 – 6.66 (t, 4H, *J* = 6 Hz, 4 \times ArH), 6.75 – 6.80 (t, 8H, *J* = 7.5 Hz, 8 \times ArH), 7.13 (s, 4H, 4 \times ArH), 7.15 (s, 2H, 2 \times NCH) 7.22 – 7.26 (br, 8H, 2 \times 8 \times ArH), and 8.70 (s, 1H, NCHN).

3.2.3 Characterization methods

Nanosecond laser spectroscopy. All nanosecond time-resolved transient absorption spectra were performed in a 1 cm optical path length and monitored by Edinburgh Instruments LP920 laser flash photolysis spectrometer. The solutions were excited at 90° from the probe beam by a Q-switched nanosecond Nd/YAG laser ($\lambda_{\text{exc}} = 355$ nm, 8 ns pulse duration; energy reduced down to 5 mJ per pulse from Continuum (Surelite II– 10). A filter was used to remove the residual excitation light at 355nm (Schott GG385). As preliminary step, all acetonitrile solutions were purged with nitrogen for 5 min prior to measurement. The decay of the triplet-triplet state absorption of ITX (1×10^{-4} M) at 600 nm was measured and follows a first-order kinetics. The temporal change of triplet concentration [³ITX*] can be represented in equation (1):

$$[{}^3\text{ITX}^*](t) = [{}^3\text{ITX}^*](0) \times e^{-\frac{t}{\tau_0}} \quad (1)$$

where τ_0 is the lifetime of the ITX triplet without quencher.

$$Abs.(t, 600\text{ nm}) = Abs.(0, 600\text{ nm}) \times e^{-\frac{t}{\tau_0}} \quad (2)$$

Exponential fitting of the experimental decay $Abs.(t, 600\text{nm})$ provides τ_0 (cf. Equation 2). In presence of a triplet quencher (**IMesH⁺BPh₄⁻**, NaBPh₄, IMesH⁺Cl⁻), a pseudo-first-order kinetic equation can be applied to extract a triplet lifetime τ that depends on quencher concentration [Q]. Note that all the triplet lifetimes were determined by using a double exponential equation in the time range 0 - 40 μs the longer time-constant being due to the formation of the ITX radical ion at monitored wavelength. By measuring τ at different [Q], the quenching rate constants, k_q , can be obtained by the linear plot based on the Stern-Volmer equation (3).²⁹

$$\tau^{-1} = \tau_0^{-1} + k_q[Q] \quad (3)$$

Electron paramagnetic resonance (EPR). EPR measurements were performed with a Bruker Eleksys E500 spectrometer with X band frequency in continuous wave (around 9.8 GHz) at room temperature. Spectra were recorded with a modulation amplitude of 1 G, a modulation frequency of 100 kHz and a microwave power of ~ 2 mW. Both Bruker WIN-EPR and SimFonia software were used to note the spectra and carry out the simulation afterwards. In a typical experiment, an acetonitrile solution (1 mL) containing **IMesH⁺BPh₄⁻** (9.18 mg, 5 equiv.), ITX (1.27 mg, 3 equiv.) and PBN (0.54 mg, 1 equiv.) was degassed prior to transfer into an aqueous EPR cell. The cell was irradiated for different times (0 s, 30 s and 60 s) with a 365 nm LED light-guide (LC-L1V3, Hamamatsu, $65\text{ mW}\cdot\text{cm}^{-2}$) then an EPR spectrum was acquired.

¹H NMR and ¹³C NMR spectroscopy. All ¹H NMR and ¹³C NMR spectra were recorded in appropriate deuterated solvents with tetramethylsilane (TMS) as the internal reference on a Varian 300 – MR. In a typical measurement, **IMesH⁺BPh₄⁻** (9.18 mg, 0.015 mmol, 3 equiv.) and ITX (1.27 mg, 0.005 mmol, 1 equiv.) were charged into a borosilicate NMR tube. The mixture was dissolved in 0.3 mL of acetonitrile-*d*₃ (0.03 M, relative to **IMesH⁺BPh₄⁻**). Before exposure to a 365 nm LED light spot during 5 min (see details in previous section), the NMR tube was capped with a rubber septum and degassed with N₂. The as-irradiated tube was then analyzed by ¹H NMR. Excess amount of CS₂ (0.02 mL) was added subsequently into the tube. It caused a sudden color change from yellow to red followed by a gradual precipitation (**Figure A.III.1**). ¹H NMR measurement was performed to confirm the formation of the IMes-CS₂ zwitterion adduct.

¹¹B NMR spectroscopy. All ¹¹B NMR were recorded in THF-*d*₈ with BF₃.Et₂O as the internal reference on a Varian Bruker 500 MHz. All solutions were prepared under argon using a glove box technique. Prior to utilization, quartz NMR tubes were dried under vacuum overnight at 80 °C. The THF-*d*₈ solvent was dried over molecular sieves.

Gas chromatography-mass spectrometry (GC-MS). The GC instrument is a Shimadzu GC-2010 model completed with the QP-2010 mass spectrometer system. Helium is the gas vector, used at the constant linear velocity of 25 cm·s⁻¹. The sample was injected into a Supelco® BP-X5 column (0.15 mm of diameter, 25 m of length and 0.25 μm of film thickness) by using split mode with a ratio of 75:25. The temperature of the injector is maintained at 330 °C. The column temperature was heated from 70 °C to 340 °C in two subsequent steps: the first heating state to 250 °C with heating rate of 15 °C·min⁻¹ and the second to 340 °C at the rate of 4 °C·min⁻¹. Then, the sample was ionized using an Electronic ionisation source heated at 200 °C. The mass spectrum was recorded from 4 min to end of the program with scan mode from 50 m/z to 600 m/z. Mass Spectra of each peak were compared with spectra of NIST05 and NIST05s databases to identify compounds. In a typical experiment, 2 mL of acetonitrile solution including **IMesH⁺BPh₄⁻** (1.71 mg, 0.003 mmol, 3 equiv.) and ITX (0.24 mg, 0.001 mmol, 1 equiv.) were placed into a UV quartz cuvette (1 cm optical path) and closed by a rubber septum. The cuvette was degassed with N₂ during 5 min then immediately exposed to a 365 nm LED spot light (65 mW·cm⁻²) for 5 min while keeping the stirring. Finally, the irradiated solution was transfer into Agilent 2 mL glass vial with a screw top (PTFE septum) under inert condition for GC-MS analysis.

Computational procedure. Triplet energy of **IMesH⁺BPh₄⁻** molecule and ITX were calculated by utilizing the Gaussian 03 package.^{30,31} The uB3LYP method with the 6-31G* was applied to optimize the relaxed geometries which were regularly checked.

Determination of photogenerated IMes yield by phenol red spectrophotometric titration. 10 mL of acetonitrile solutions containing **IMesH⁺BPh₄⁻** (1.85 mg, 3 × 10⁻⁴ mmol, 3 equiv.) and ITX (0.25 mg, 10⁻⁴ mmol, 1 equiv.) were prepared (3 × 10⁻⁴ M relative to **IMesH⁺BPh₄⁻** and 10⁻⁴ M relative to ITX). 2 mL of solution were transferred into a spectroscopic quartz cell capped with a rubber septum. The colorless mixture was purged with nitrogen before exposing to a 365 nm LED spot light for a given irradiation time (0, 1, 2, 5 and 10 min). Subsequently, a phenol red (PR) titrating solution (2 × 10⁻⁴ M in acetonitrile) was added gradually (0.1 ml) from a 1 ml syringe into the cuvette. After each injection, an UV/vis spectrum was recorded. At the start of the spectrophotometric titration, the indicator

solution in acetonitrile was completely colorless, because the bis-protonated form, referred to as H₂PR, is the prevalent form. Before the equivalence point, the gradual addition of H₂PR solution to the irradiated solution of **IMesH⁺BPh₄⁻**/ITX caused the appearance and intensification of a pink color assigned to the bivalent anion PR²⁻ ($\lambda_{\text{max}} = 580 \text{ nm}$) formed after reaction with photogenerated **IMes** (**Figure A.III.2**). After the equivalence point was reached, i.e. when all NHC species reacted, the deep pink color disappeared gradually and the solution became pale yellow marking the conversion of PR²⁻ into the univalent anion HPR⁻ ($\lambda_{\text{max}} = 390 \text{ nm}$). The two acid-base reactions before and after equivalence points were described in the scheme below. Plotting the absorbance at 580 nm (A_{580}) as a function of the titrant volume gave two intersecting straight lines, thereby enabling the detection of the titration end-point. Performing the titration for different irradiation times revealed the progressive release of NHC and led to a maximum yield of 50 % achieved after 5 min irradiation. At the equivalence point in the acid-base titration:

$$[\text{IMes}] \times V = 2[\text{PR}] \times V_{\text{eq}} \quad (1)$$

where [IMes] is the concentration of photogenerated **IMes** released in the UV cuvette, V is initial volume of **IMesH⁺BPh₄⁻**/ITX solution, [PR] is concentration of PR and V_{eq} is total volume of PR added into the UV cuvette at the titration end-point. Therefore, the yield of **IMes** released upon irradiation of **IMesH⁺BPh₄⁻**/ITX solution was obtained from equation (2):

$$\text{Yield (\%)} = \frac{2 \times [\text{PR}] \times V_{\text{eq}}}{[\text{IMesH}^+\text{BPh}_4^-] \times V} \times 100 \quad (2)$$

where **[IMesH⁺BPh₄⁻**] is the initial concentration of **IMesH⁺BPh₄⁻**.

The validity of the method was checked by titrating a free **IMes** solution ($1 \times 10^{-4} \text{ M}$ in acetonitrile) using a similar acetonitrile PR solution as titrant ($2 \times 10^{-4} \text{ M}$). An acceptable uncertainty of the order of 10 % was obtained on the value of the initial **IMes** concentration. This difference was not only assigned to the measurement error, but also to the fact that **IMes** is not stable in air.

3.3 RESULTS AND DISCUSSION

3.3.1 Assignment of transient species

a. Nanosecond laser spectroscopy

To identify the intermediate species formed in the 2-component system ITX/**IMesH⁺BPh₄⁻** (**Scheme 3.2**), excitation transfer reactions of ITX with different quenchers were recorded by means of a nanosecond laser spectroscopy. Laser flash exposure

was performed at 355 nm in deaerated and anhydrous acetonitrile, where only the sensitizer (ITX) absorbs the light. Given the short lifetime of ITX singlet state as well as its high intersystem crossing quantum yield,^{32,33} ITX is assumed to interact mainly via its triplet state. As can be seen in **Figure 3.1**, the transient absorption spectra of ITX alone (trace **a**) shows an absorption maximum at 630 nm, fully consistent with the ITX triplet (³ITX*) in acetonitrile reported in the literature.^{29,32,34–36} Slow decrease of the transient absorption was attributed to the deactivation process of the ³ITX* with a decay of 5.7 μs at an initial ITX concentration of 10⁻⁴ M. To study the effect of the azolium cation, the reactivity of the triplet state was evaluated in presence of IMesH⁺Cl⁻ since no quenching is expected from Cl⁻ anion.³⁷ The absorption at 630 nm was weakly quenched when this imidazolium salt was added to a deoxygenated solution of ITX. A low rate constant (round to 4.7 × 10⁶ M⁻¹·s⁻¹) was determined by constructing a Stern-Volmer plot of the triplet lifetime as a function of [IMesH⁺Cl⁻], with the triplet being monitored at 600 nm (see experimental section for details). A typical decay experimental trace for the triplet decay of ITX in presence of IMesH⁺Cl⁻ is given in **Figure 3.2a**, showing clean first-order kinetics. The existence of very weak interactions is consistent with the fact that photooxidation of ³ITX* by IMesH⁺ is thermodynamically unfavorable ($\Delta G_{\text{et}} = + 0.74 \text{ eV}$)²¹ and that the triplet energy transfer between ITX ($E_{\text{T}} = 2.77 \text{ eV}$) and IMesH⁺ ($E_{\text{T}} = 3.34 \text{ eV}$) exhibits a fairly endothermic character (**Table 3.1**). It can thus be concluded that the azolium cation plays a minor role in the primary photochemical reaction.

Similarly, triplet quenching experiment was carried out with NaBPh₄ to investigate the specific role of the tetraarylborate anion given that Na⁺ cannot quench or donate proton (**Figure 3.1b**). As can be seen in **Figure 3.2b**, the decay rate was much faster, illustrating the more efficient quenching of ³ITX* by BPh₄⁻. Additionally, it can be noticed that the decay trace does not return to zero in this case; deviation to first order kinetics was attributed to the fact that the triplet absorption probably overlaps with another species. To clarify this point, **Figure 3.1** shows the temporal evolution of the transient absorption spectrum of ITX/NaBPh₄ (trace **b**). After 100 ns, it seems that the narrow 630 nm peak due to triplet absorption has disappeared and has been replaced by a new broad absorption in the region of 560 – 680 nm. Subsequent spectra show the slow decay of this broad peak. We hypothesized that this transient species could be the radical anion ITX^{•-} generated after photoreduction of ³ITX* by BPh₄⁻. To support our assignment, we rely first on the fact that the electron transfer for this reaction is slightly exothermic ($\Delta G_{\text{et}} = - 0.13 \text{ eV}$),²¹ because of the high oxidation potential

of the donor anion BPh_4^- . Second, triplet energy transfer, which is the second possible interactions process between ITX ($E_T = 2.77$ eV) and BPh_4^- ($E_T = 3.64$ eV) (**Table 3.1**), is not energetically favorable. Third, our transition absorption spectrum strongly resembles that of thioxanthone radical anion observed by Schuster *et al.*, who reported also a similar broad absorption at 650 nm.^{38,39} To the best of our knowledge, the spectrum of $\text{ITX}^{\bullet-}$ has not been previously reported. Because of the absorption overlap between $^3\text{ITX}^*$ and $\text{ITX}^{\bullet-}$ species, the quenching rate (round to $4.1 \times 10^7 \text{ M}^{-1}\cdot\text{s}^{-1}$) was obtained by analyzing the first short component of the transient absorption decay. Additionally, the triplet transient of ITX in the presence of BPh_4^- was quickly quenched if an oxygen-saturated solution is used, with a typical rate constant in order of $10^9 \text{ M}^{-1}\cdot\text{s}^{-1}$ (**Figure 3.2c**).^{40,41} This lends additional confidence to the involvement of $^3\text{ITX}^*$ and the operation of a charge transfer mechanism. However, there is no additional band in the transient spectrum that might be attributed to the boronyl radical **4** or other boron species derived from the oxidation of tetraphenyl borate anion.⁷ In borate salts, it is well established that back electron is not significant but that boronyl radical can dissociate very rapidly and irreversibly (**Scheme 3.2**). The failure to observe $\text{Ph}_4\text{B}^\bullet$ (**4**) indicates that its very short-lived character¹⁶ as it probably dissociates or rearranges during the laser pulse.

Having investigated the individual role of IMesH^+ and BPh_4^- , quenching experiment was then carried out using $\text{IMesH}^+\text{BPh}_4^-$ (**Figure 3.2d**). The similarity of quenching rate obtained by this quencher (round to $4.9 \times 10^7 \text{ M}^{-1}\cdot\text{s}^{-1}$) and NaBPh_4 (round to $4.1 \times 10^7 \text{ M}^{-1}\cdot\text{s}^{-1}$) is indicative that the photoreduction of ITX by BPh_4^- is the primary photochemical process. Additionally, a broad feature characteristic of $\text{ITX}^{\bullet-}$ was also observed in the region of 560 – 680 nm (**Figure 3.1c**). However, there is no additional absorption band in the 380 – 430 nm region that could be assigned to a thioxanthyl ketyl radical (ITXH^\bullet) derived from subsequent proton transfer step of $\text{ITX}^{\bullet-}$ with IMesH^+ .²⁹ This result can be understood on the basis of a much slower proton transfer step compared to electron transfer. The only indication for protonation of the radical anion is the shorter lifetime of $\text{ITX}^{\bullet-}$ in presence of $\text{IMesH}^+\text{BPh}_4^-$ (29.5 μs) compared to NaBPh_4 (40.1 μs). A final quenching experiment was also carried out by using **IMes**, the targeted NHC. A significant acceleration of the decay at 600 nm is observed, leading to an increased quenching rate (round to $7.2 \times 10^9 \text{ M}^{-1}\cdot\text{s}^{-1}$). Such a result is consistent with the stronger donor properties of **IMes** ($E_{\text{ox}} = -0.84$ eV) compared to BPh_4^- ($E_{\text{ox}} = 0.94$ eV).²² It also highlights a more complex mechanism where photogenerated NHC can also interact with triplet ITX and compete with BPh_4^- for charge transfer.

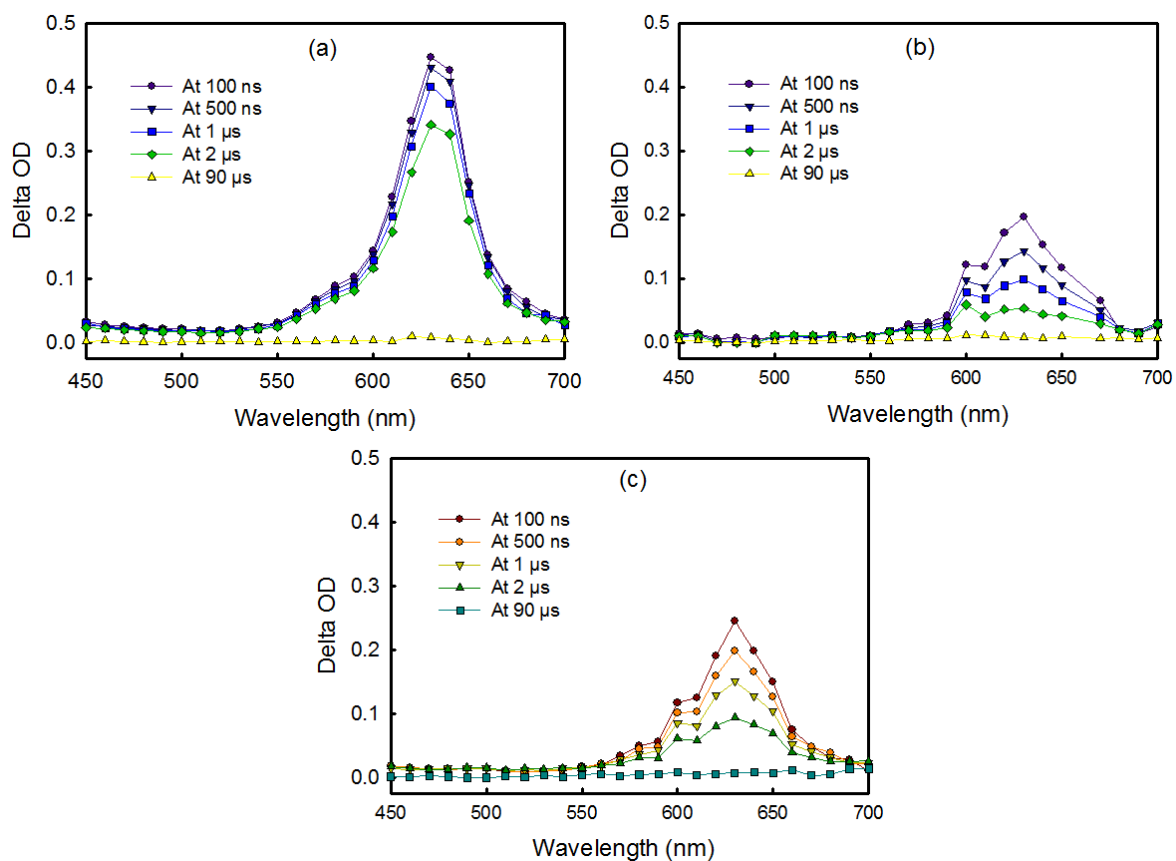


Figure 3.1. Transition absorption spectra of (a) $[ITX] = 10^{-4}$ M, (b) $ITX/NaBPh_4 = 6 \times 10^{-3}$ M and (c) $ITX/IMesH^+BPh_4^- = 6 \times 10^{-3}$ M for 100 ns – 90 μ s delay time in N_2 -saturated acetonitrile with excitation wavelength at 355 nm. (Delta OD is a change in absorbance).

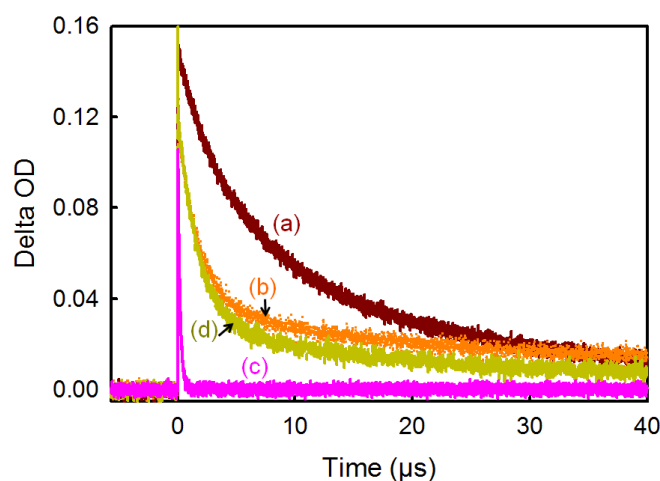
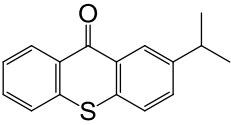
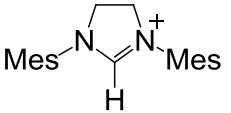
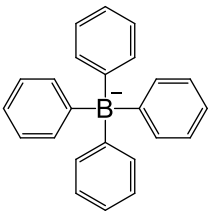


Figure 3.2. Decays of ${}^3ITX^*$ at 600 nm in the presence and absence of: (a) $IMesH^+Cl^-$, (b) $NaBPh_4$, (c) $NaBPh_4$ (under O_2) and (d) $IMesH^+BPh_4^-$ ($[ITX] = 10^{-4}$ M, $[IMesH^+Cl^-] = [NaBPh_4] = [IMesH^+BPh_4^-] = 6 \times 10^{-3}$ M, respectively, recorded in N_2 -saturated acetonitrile).

Table 3.1. Triplet energy simulation of ITX and $\text{IMesH}^+\text{BPh}_4^-$ estimated.	
Method uB3LYP/6-31G*	E_T (eV)
	2.77
	3.34
	3.64

a. EPR

As indicated in the previous section, failure to observe the boranyl radical (**4**) in the nanosecond experiment may indicate that this short-lived species dissociates very rapidly to give the phenyl radical (**5**) and triphenylborane (**6**). Spin trapping and EPR detection (with the trapping reagent α -phenyl-*N*-*tert*-butylnitrone, PBN) were employed to detect the free radical Ph^\bullet formed during in situ irradiation of ITX in presence of tetraphenyl borate anion. In **Figure 3.3**, the experimental EPR spectra from ITX/NaBPh₄/PBN (**a**) and ITX/ $\text{IMesH}^+\text{BPh}_4^-$ /PBN (**b**) are shown. Similar in both instances, the EPR spectra show a strong triple-doublet signal suggestive of a single paramagnetic species and gradually increasing with irradiation time (see **Figure 3.4**). Hyperfine coupling (hfc) constants of the spin adduct that were retrieved from simulation ($a_N = 14.7$ G and $a_H = 2.7$ G, **Figure A.III.3**) are in agreement with a PBN spin adduct of the phenyl radical. In addition, these values correspond reasonably well to previously reported values for these spin adduct in literature.^{16,19} This results strongly suggests that the transition state of oxidized BPh_4^- could dissociate into Ph^\bullet and BPh_3 .^{16,42} Moreover, it is noted that the detection of this phenyl radical is generally very challenging,¹⁶ and failures are generally reported in the literature for both electrochemically^{1,6,7} and photochemically⁴³ induced oxidation of BPh_4^- . By contrast, *n*-butyl radical was more easily detected from a similar oxidation of Ph_3BBu^- species.⁴³ As discussed later, the formation of biphenyl upon radical coupling being unlikely, the most plausible

explanation is that $\text{Ph}\cdot$ reacts rapidly with Ph_3B to produce Ph-Ph and $\text{Ph}_2\text{B}\cdot$, making the detection challenging.⁴²

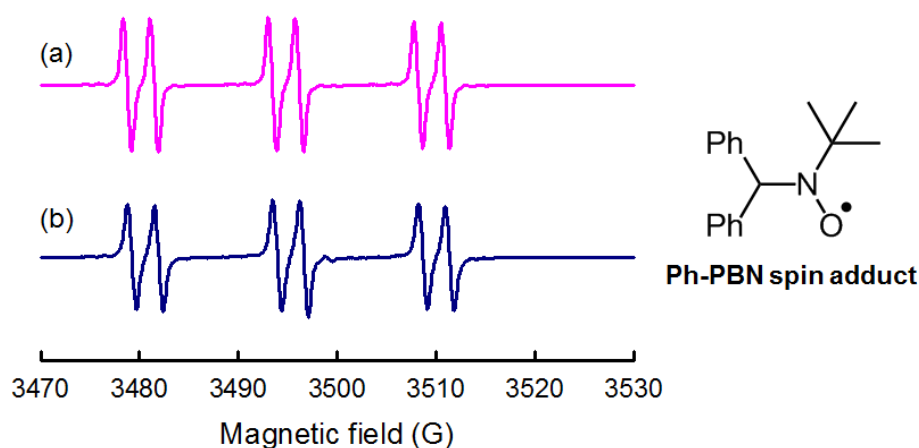


Figure 3.3. EPR spectra of radical adduct from a solution: (a) ITX – NaBPh_4 – PBN and (b) ITX – $\text{IMesH}^+\text{BPh}_4^-$ – PBN after 60 s of irradiation. $[\text{ITX}] = 5 \times 10^{-3}$ M, $[\text{IMesH}^+\text{BPh}_4^-] = 1.5 \times 10^{-2}$ M, $[\text{NaBPh}_4] = 1.5 \times 10^{-2}$ M and $[\text{PBN}] = 3 \times 10^{-3}$ M in acetonitrile.

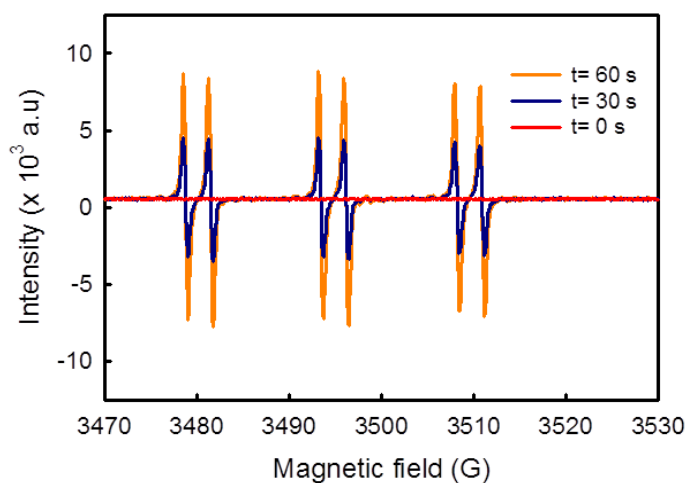


Figure 3.4. EPR spectra of Ph–PBN radical from a solution ITX – $\text{IMesH}^+\text{BPh}_4^-$ – PBN in acetonitrile after exposure under LED 365 nm at given time (concentration: $[\text{ITX}] = 5 \times 10^{-3}$ M, $[\text{IMesH}^+\text{BPh}_4^-] = 1.5 \times 10^{-2}$ M and $[\text{PBN}] = 3 \times 10^{-3}$ M, respectively).

3.3.3 Assignment of photoproducts

a. ^1H and ^{13}C NMR spectroscopy

Using ^1H NMR spectroscopy, we find that irradiation of an oxygen-free acetonitrile- d_3 solution containing ITX only (Figure 3.5a) is stable; whereas, as-irradiated solution of $\text{IMesH}^+\text{BPh}_4^-$ (1 equiv.)/ ITX (3 equiv.) at 365 nm results in a complete deprotonation at C2 position (H_a , $\delta = 8.70$ ppm) of the imidazolium cation (Figure 3.5, trace b and c).²¹ Further

evidence for the generation of **IMes** was given upon adding CS₂ to the as-irradiated medium. A red precipitate forms immediately that was straightforwardly assigned to **IMes**–CS₂ using ¹H NMR analysis (**Figure 3.5d**). With these results and the identification of **ITX**^{•-} described above, it is thus possible to formulate a tentative second step where NHC are created through proton abstraction of **IMesH**⁺ cation by **ITX**^{•-}. A method to determine NHC concentration that were described in previous paper (formation of NHC-carbodiimide adduct²²) revealed an **IMesH**⁺ conversion of 70 % after 5 min irradiation.

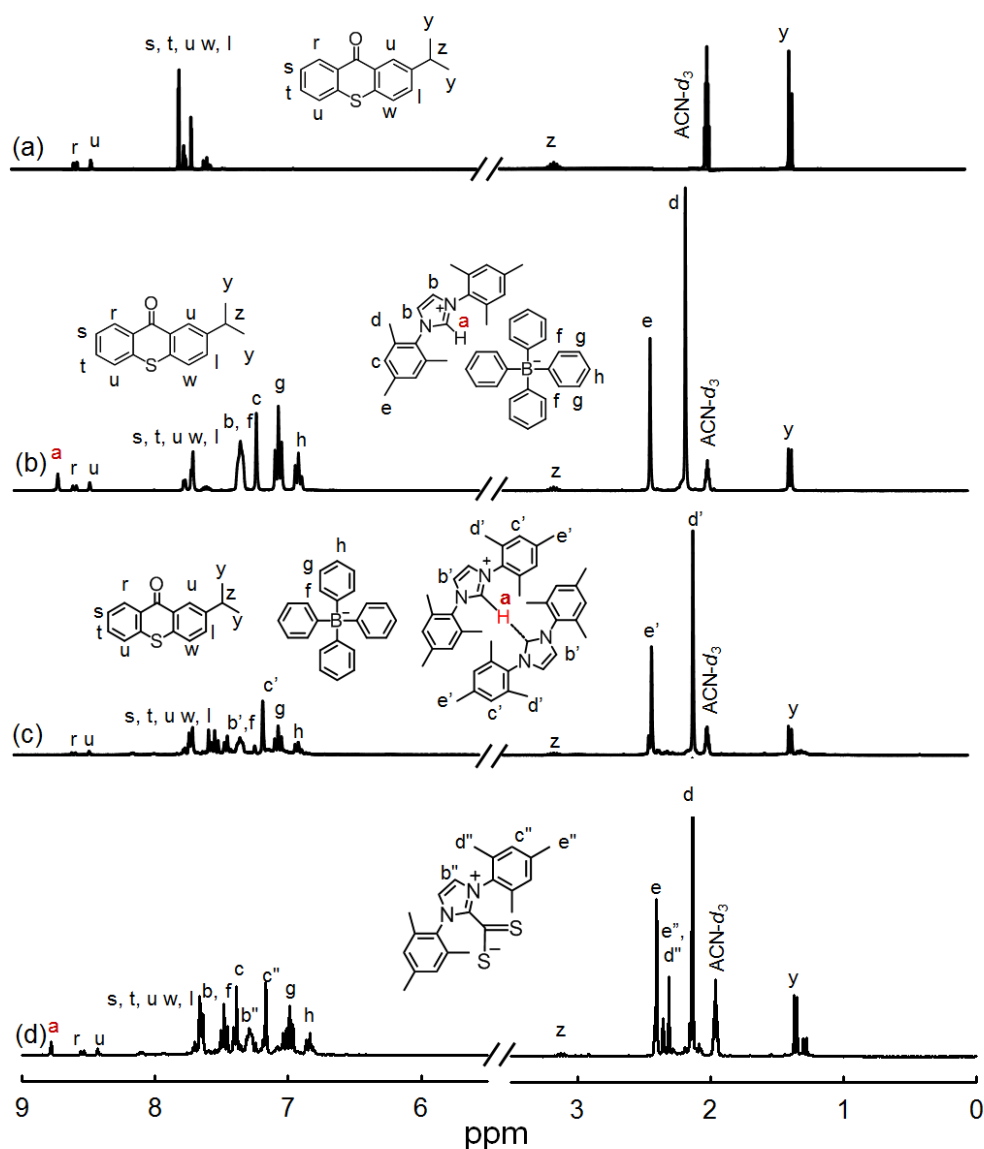
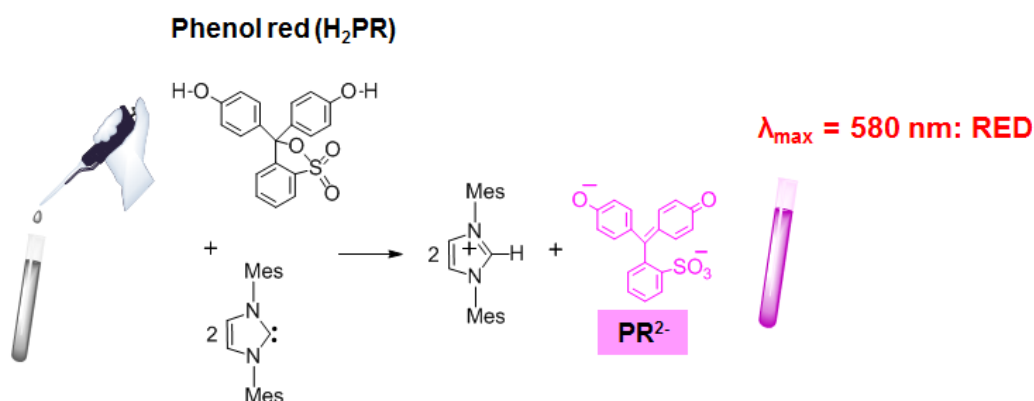


Figure 3.5. ¹H NMR spectra in ACN-*d*₃ of: (a) **ITX** after 5 min irradiation, (b) **ITX/ IMesH**⁺**BPh**₄⁻ mixture prior to exposure, (c) after 5 min irradiation of (b) and (d) after addition of CS₂ into (c). A substantial change in ¹H NMR is the emergence of protons H_{e''} ($\delta = 2.36$ ppm) and protons H_{d''} ($\delta = 2.31$ ppm), which are attributed to methylene protons of mesityl moieties from **IMes**–CS₂ adduct, and the shifting towards to the original resonance of protons H_e and H_d of unreacted **IMesH**⁺**BPh**₄⁻ (concentration: **ITX** (0.07 M) and **IMesH**⁺**BPh**₄⁻ (0.21 M)).

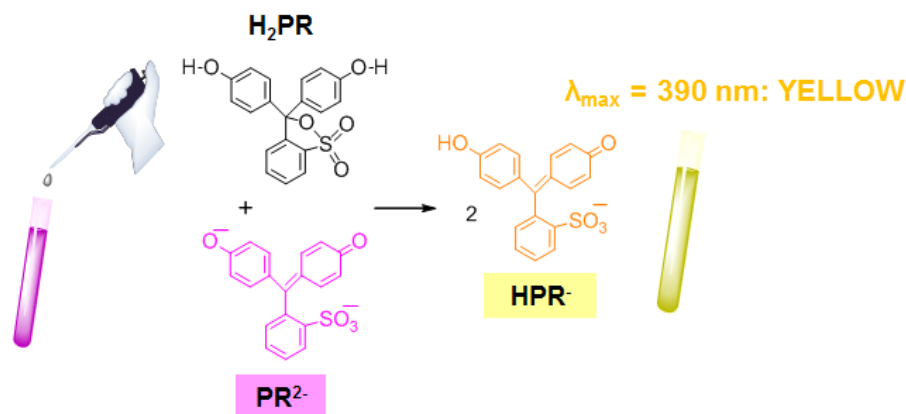
b. Acid/ base titration

In this present work, based on acid/base titration in acetonitrile using phenol red pH indicator as titrant, amount of NHC released in situ is also quantified. Basically, it is grounded on the observation in shifting absorption band at 580 nm of the basic form of phenol red derived from the deprotonation of phenol red by the carbene, to a novel band at 390 nm assigned to the acid form of phenol red, which enables us to determine the amount of carbene containing in the solution (Scheme 3.3, and Figure 3.6a).²¹

1. Before the equivalence point



2. After the equivalence point



Scheme 3.3. Colour changes during an acid/ base titration utilizing phenol red as the titrant.

Plotting the absorbance at 580 nm (A_{580}) as a function of the titrant volume (**Figure 3.6b**) gave two intersecting straight lines, thereby enabling the detection of the titration end-point. Performing the titration for different irradiation times (see insert of **Figure 3.6b**) revealed the progressive release of NHC and led to a maximum yield of 50 % achieved after 5 min irradiation. This result emphasizes that **IMes** was created and that this species coexists in the reaction medium with its conjugated acid **IMesH⁺** and may form H-bonded

bis(carbene)-proton adduct.^{44–46} Formation of this C··H–C type adduct has been already observed spectroscopically, *e.g.* UV, NMR.⁴⁶ Evidence for the formation of bis(carbene)-proton adduct is visible in the spectrum of **Figure 3.5b** with the slight shift to lower resonance of methylene protons H_e′ (δ = 2.07 ppm) and H_d′ (δ = 2.37 ppm) observed after irradiation. Similar upfield shift was evidenced when adding 1 equiv. of free **IMes** to 9 equiv. of **IMesH⁺BPh₄⁻** (**Figure A.III.4**). In this spectrum, the bridging proton H_a (δ = 8.70 ppm) of the C··H–C complex disappeared entirely due to H-bonding. This means that protonation degree cannot be used to quantitatively assess the NHC yield.

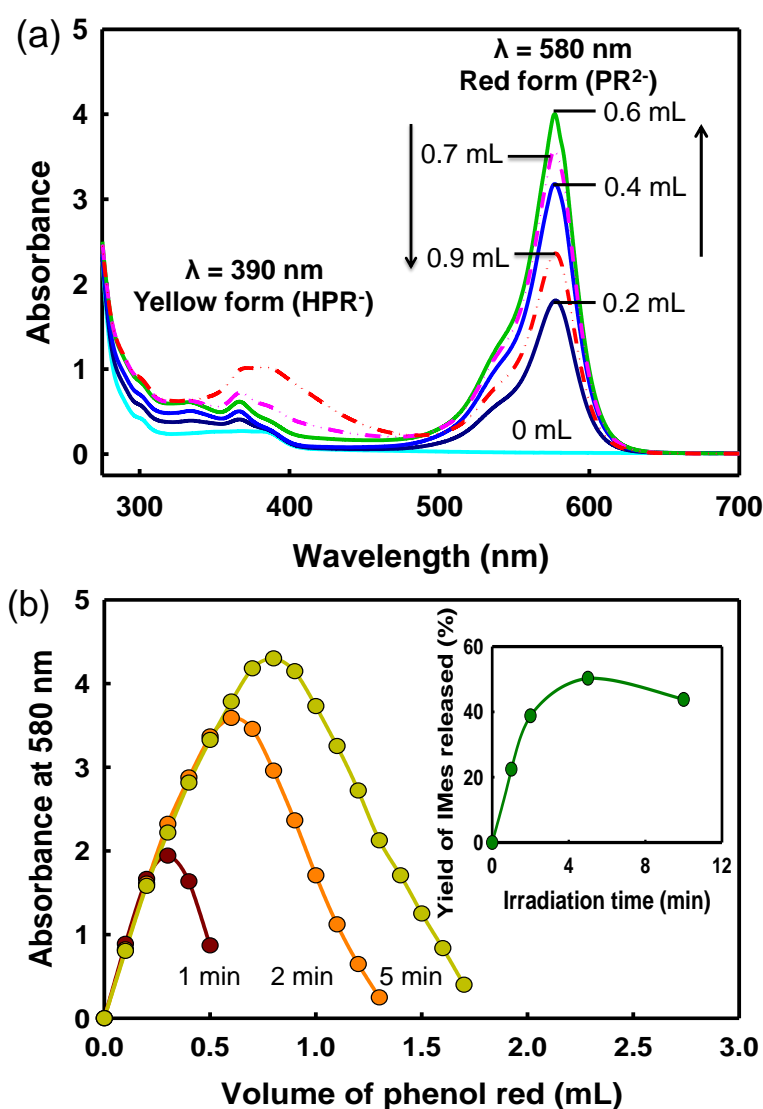


Figure 3.6. (a) Change of UV-Vis spectra of an acetonitrile solution of **IMesH⁺BPh₄⁻** (3.0×10^{-4} M) and **ITX** (1×10^{-4} M) irradiated during 2 min (LED, 365 nm, 65 mW cm^{-2}) upon gradual addition of PR (2×10^{-4} M) and (b) Titration plot showing the absorbance at 580 nm for the same

photoNHC/sensitizer solution irradiated 1, 2 or 5 min as a function of PR (titrant) volume. The insert gives the yield of photogenerated NHC deduced from the spectrophotometric titration curve.

Furthermore, through the acid/ base titration of a mixture containing **IMes**/ITX, we sought that the photooxidation of **IMes** by $^3\text{ITX}^*$ can also lead to decline the total yield of **IMes**. Both of non-irradiated and irradiated **IMes** solution gave the likable amounts of **IMes** (approximately 90%), which consolidate our perspective about the photostability of **IMes** at 365 nm (**Figure A.III.5**). However, **IMes** decomposed gradually upon exposing under UV in the presence of minor amount of ITX ($[\text{IMes}]/[\text{ITX}] = 3/1$), resulting in declining the relative amount of **IMes** recovered from 90% to 57% after 5 min exposing. Seriously, that dropped down to 37% after only 2 min exposing as amount of ITX increased ($[\text{IMes}]/[\text{ITX}] = 1/3$). Either increasing amount of ITX or prolonging irradiation afford the rising of $^3\text{ITX}^*$ amount, which postulates the photooxidation of **IMes**. In fact, occurring this undesired reaction is undesirable but the exclusion of this undesired reaction is clearly impossible owing to their chemical nature. Therefrom, it is crucial to adjust ratio between $\text{IMesH}^+\text{BPh}_4^-$ and ITX in order to sufficiently produce **IMes** and preclude prevalence of side reaction to gain a good yield of photogenerated **IMes**.

c. GC-MS

To move forward in the identification of other photoproducts, the freshly irradiated photolysis medium (N_2 -saturated acetonitrile solution of $\text{ITX/IMesH}^+\text{BPh}_4^-$) was analyzed by GC-MS. Three products were detected: biphenyl, isopropylthioxanthene and ITX (**Figure 3.7** and **Table A.III.1**). Biphenyl was obtained in good yield and its formation was also observed in other (photo)oxidation experiments of BPh_4^- anion by iron (II) complex,⁴² 1,4-dicyanonaphthalene⁷ or coumarin derivative.⁴³ Labelling studies^{7,43} revealed that two phenyl groups of the biphenyl come from the same borate, suggesting that the biphenyl was formed from carbons that were bound to boron. Having the evidence that phenyl radicals are formed in our system (EPR data), it is therefore reasonable to assume that biphenyl comes from triphenylboron. The most plausible route would be a rapid auto-oxidation of BPh_3 by Ph^\bullet followed by generation of biphenyl and $\text{Ph}_2\text{B}^\bullet$ ($\text{BPh}_3 + \text{Ph}^\bullet \rightarrow \text{Ph-Ph} + \text{Ph}_2\text{B}^\bullet$). The fate of the boron radical will be discussed in the ^{11}B NMR section. Since it does not require the addition of oxygen in the reaction medium, biphenyl is thus a primary photochemical product.

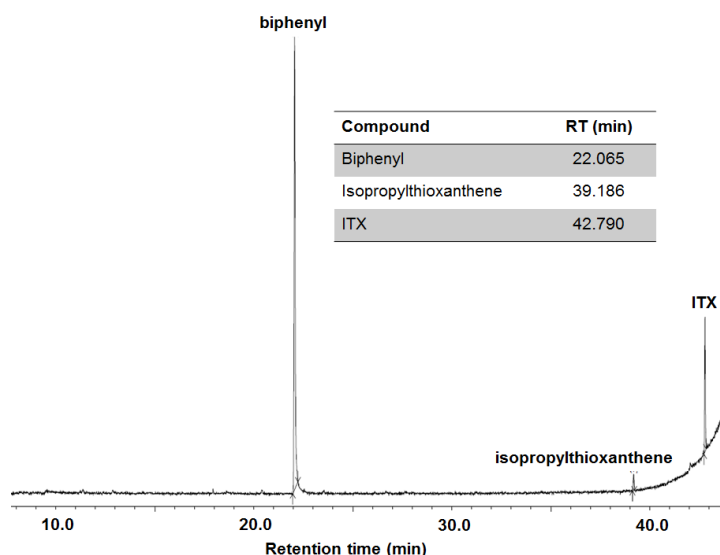
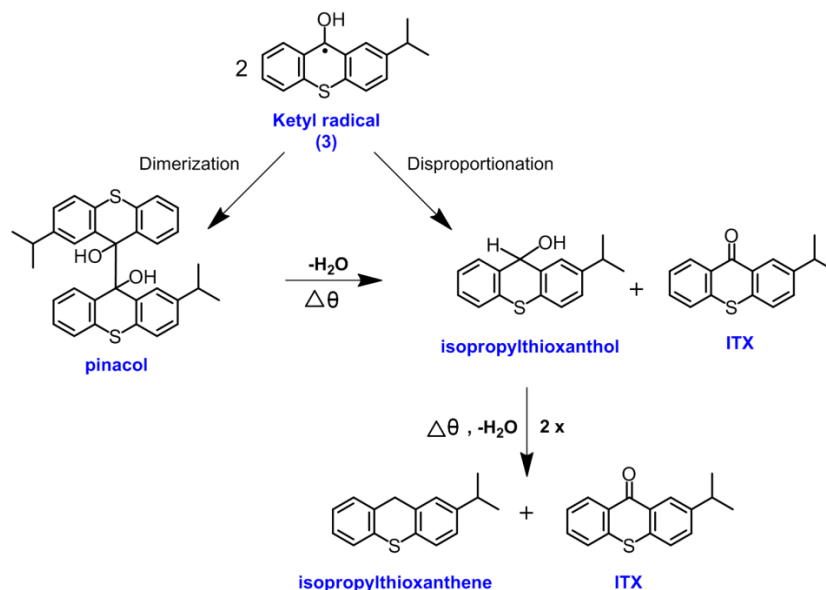


Figure 3.7. GC chromatogram of photoproducts obtained from the photolysis media of ITX – $\text{IMesH}^+\text{BPh}_4^-$ after 5 min of irradiation ($[\text{ITX}] = 5 \times 10^{-4} \text{ M}$ and $[\text{IMesH}^+\text{BPh}_4^-] = 1.5 \times 10^{-3} \text{ M}$, respectively).

In contrast, isopropylthioxanthene and ITX result from the ensuing ground-state chemistry and might derive from ITXH^\bullet (**3**), the thioxanthyl ketyl radical that is formed after the protonation process of $\text{ITX}^{\bullet-}$, and that we are not able to detect by nanosecond spectroscopy. The ketyl radical may undergo two types of reaction: first, a *disproportionation*, giving ITX and isopropylthioxanthol;^{47,48} second, a *dimerization* leading to dithioxanthyl pinacol derivative (**Scheme 3.4**).⁴⁹



Scheme 3.4. Possible side-reactions involving ITX ketyl radical produced after protonation of ITX radical anion.

However, except ITX, none of these thioxanthone reduction products were detected by GC-MS. This is apparently due to their thermal instability in the GC injection port as established by Schuster *et al.*³⁸ Isopropylthioxanthol is known to disproportionate upon heating to form ITX and isopropylthioxanthene. Additionally, pinacol can be easily oxidized under air to regenerate ITX.^{38,48} This set of reactions is consistent with the formation of a ketyl radical and the thioxanthone products detected in GC-MS. Note also that 1-phenyl-1,4-cyclohexadiene is not detected while it is a major product of the direct photolysis of BPh_4^- in presence of H donors.¹ Its absence confirms that energy transfer from ITX to BPh_4^- is not the predominant mechanism.

d. ^{11}B NMR spectroscopy

In arylboron photochemistry, the identification of boron photoproducts represents a considerable difficulty. Boron products can be involved in complex reactions where both the nature and the role of the boron species can be hard to determine; additionally, their proportion generally differ depending on whether irradiation was performed under N_2 or air. As emphasized in **Scheme 3.2**, the oxidized borate is assumed to evolve in triphenylborane.^{16,21,50,51} Nishida *et al.* continued this investigation and proposed subsequent degradation reactions.⁴² In our specific case, the photogenerated BPh_3 may also form ate complexes with NHC Lewis base.^{52,53} Despite these challenges, ^{11}B NMR spectroscopy remains the best tool to identify the boron species in our systems. In the case of photoinitiated oxidation of arylborates, the NMR identification has rarely been studied^{7,54} while it can serve to provide insights into the mechanism. Nevertheless, accurate identification of the groups attached to boron is not trivial due to the lack of detailed structural information that can be obtained from ^{11}B NMR data.

Figure 3.8 shows the ^{11}B -NMR spectrum of an argon saturated solution of $\text{ITX/IMesH}^+\text{BPh}_4^-$ (1/1 equiv.) prior (**a**) and after 10 min irradiation (**b**). As expected, **Figure 3.8a** exhibits only a narrow singlet attributed to BPh_4^- anion ($\delta = -6.3$ ppm). This chemical shift is characteristic of tetraorganoborate anions experiencing a strong deshielding. After 10 min irradiation (**Figure 3.8b**), in addition to the resonance of BPh_4^- , the ^{11}B spectrum of the photolysis solution reveals two new features: an intense resonance at 1.1 ppm, and a broad and much weaker signal at 5.9 ppm. Acting on the assumption that these species could derive from triphenylborane, a set of experiments using BPh_3 was implemented. The ^{11}B NMR spectrum of BPh_3 , shown in **Figure A.III.6**, reveals a broad singlet at 50.3 ppm that is absent in the photolysis medium. In addition, the irradiation of BPh_3 with or without

ITX (1 equiv.) did not cause any change in the spectrum. In contrast, the addition of **IMes** (1 equiv.) resulted in the formation of a white precipitate and a downfield chemical shift (-9 ppm, see **Figure 3.9**) characteristic of NHC-borane species, that was also not found in spectrum of reaction medium. Though the above experiments do not necessarily demonstrate the non-existence of BPh_3 in the photolysis solution, it is interesting to note that both free BPh_3 or BPh_3 -**IMes** adducts are not present after irradiation, and that degradation reaction with triplet excited ITX cannot be advanced as explanation. As hypothesized in the last section, it is thus more reasonable to conclude that BPh_3 may react with Ph^\bullet to form $\text{Ph}_2\text{B}^\bullet$.

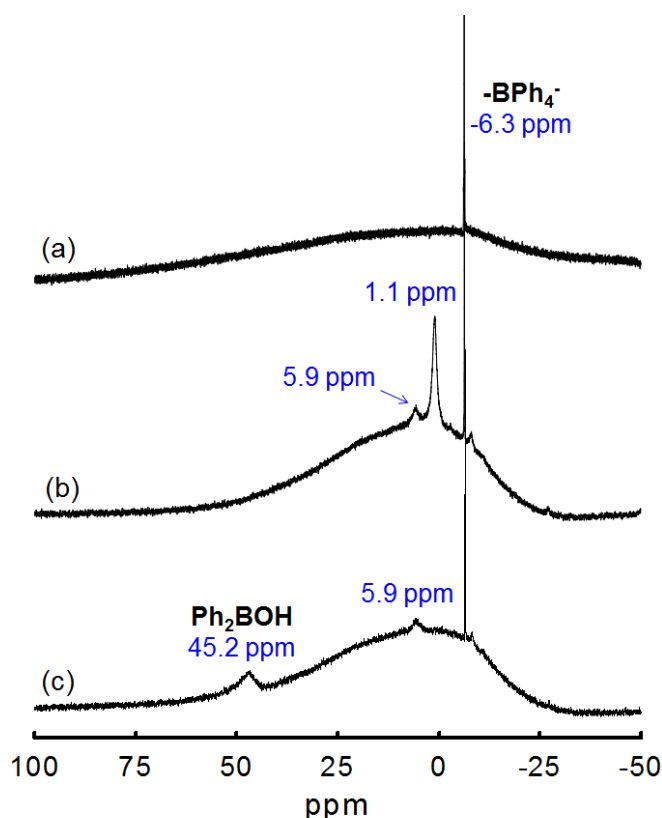


Figure 3.8. ^{11}B NMR spectra of a mixture of ITX (0.03 M) and $\text{IMesH}^+\text{BPh}_4^-$ (0.03 M) in $\text{THF-}d_8$: (a) prior irradiation, (b) after 10 min UV exposure, and (c) after adding CS_2 into medium. Irradiation conditions: LED 365 nm, $65 \text{ mW}\cdot\text{cm}^{-2}$.

To shed further light into the identity of these boron-containing species, CS_2 was added to the photolysate solution ($\text{ITX}/\text{IMesH}^+\text{BPh}_4^-$) just after irradiation (**Figure 3.8c**). This led to immediate conversion of the intermediate at 1.1 ppm to a new broad resonance at 45.2 ppm while the position of the second resonance at 5.9 ppm remained unchanged. The change of chemical shift suggests that a NHC-borane species was initially present; the addition of CS_2 causing its dissociation and the subsequent formation of the more stable

IMes-CS₂ zwitterionic adduct. By this means, a free boron species can be released whose value of ¹¹B chemical shift at 45.2 ppm can be useful for its assignment. Accordingly, observed⁵⁵ and calculated ¹¹B NMR spectra⁵⁶ are consistent with the exact chemical shift of diphenylborinic acid Ph₂BOH. Additionally, the singlet signal at 1.1 ppm could be ascribed to IMes-Ph₂BOH adduct present in the photolysis solution. However, the second weak signal at 5.9 ppm could not be assigned. Notably, this second boron-containing complex is not able to form ate-complex with **IMes** due to the absence of change in the chemical resonance when CS₂ is introduced. To provide further evidence for this assignment, Ph₂BOH was generated in situ by moderate hydrolysis of the BPh₃ in non-dried THF-*d*₈ upon exposing the solution in the NMR tube to atmosphere^{57,58} This solution revealed two broad signals centered at 45 ppm (Ph₂BOH) and 51 ppm (residual BPh₃) in the ¹¹B NMR spectrum (**Figure 3.10**). Addition of IMes into the medium caused the two signals to shift at -9 ppm (IMes-BPh₃ adduct) and 1.1 ppm (IMes-Ph₂BOH adduct), lending further confidence in our assignment.

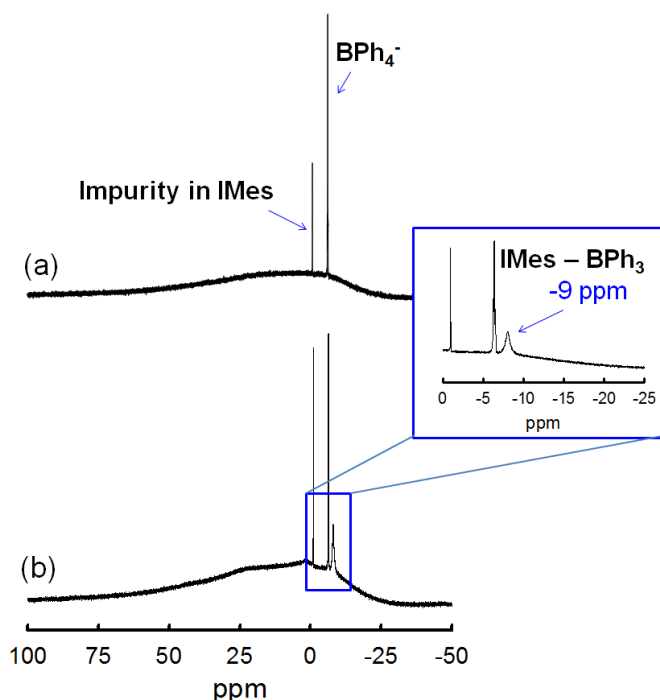


Figure 3.9. ¹¹B-NMR spectra in THF-*d*₈: (a) **IMesH⁺BPh₄⁻ – IMes**, (b) **IMesH⁺BPh₄⁻ – IMes – BPh₃** (concentrations: [IMes] = 0.01 M, [IMesH⁺BPh₄⁻] = 0.03 M, [BPh₃] = 0.01 M). A white precipitation which is IMes – BPh₃ adduct, formed immediately as BPh₃ introduced into the mixture **IMesH⁺BPh₄⁻ – IMes**.

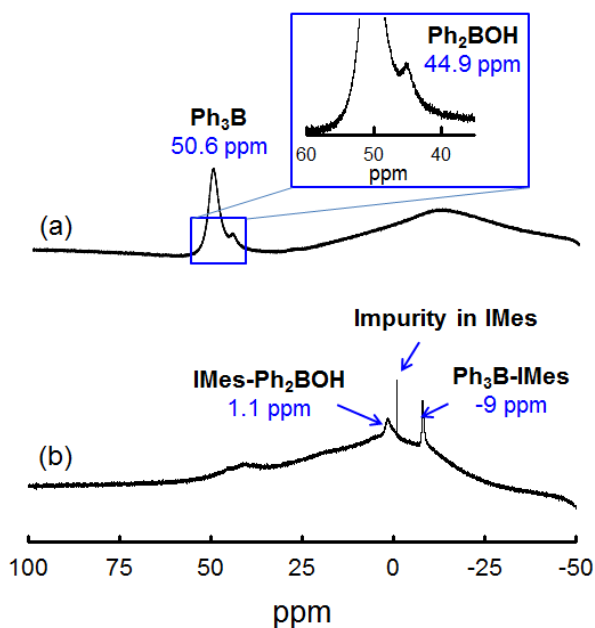
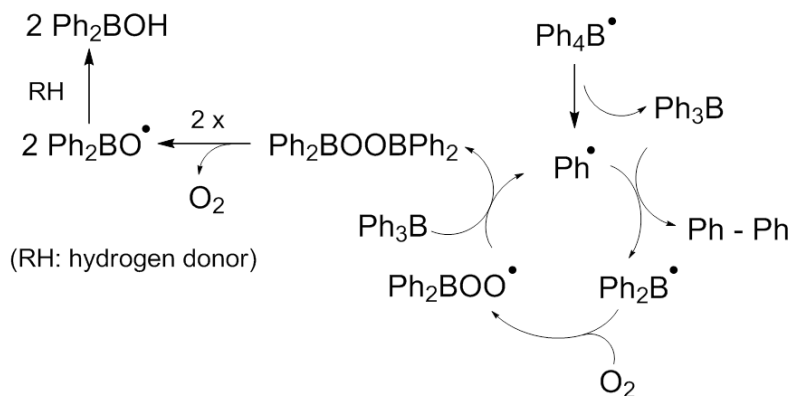


Figure 3.10. ^{11}B NMR spectra in non-dried $\text{THF-}d_8$: (a) Hydrolyzed BPh_3 , (b) Addition of **IMes** into hydrolyzed BPh_3 .

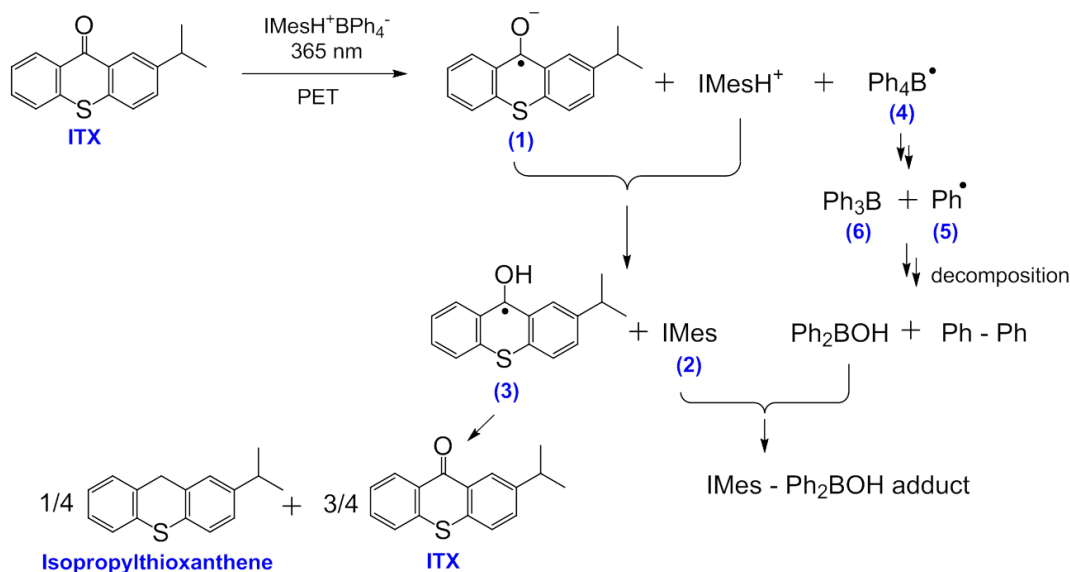
The last issue to be settled concerns the mechanism leading to the formation of Ph_2BOH . As described in **Scheme 3.5**, we postulate that the formation of Ph_2BOH may involve in an oxidation process of Ph_3B by Ph^\bullet and thus generates Ph-Ph and $\text{Ph}_2\text{B}^\bullet$. In the propagation step, attack of oxygen molecular (even if argon purged NMR tube were used) on $\text{Ph}_2\text{B}^\bullet$ species leads to rapidly produce the peroxy radical, $\text{Ph}_2\text{BOO}^\bullet$. Then, $\text{Ph}_2\text{BOO}^\bullet$ reacts further with Ph_3B to regenerate Ph^\bullet and produce $\text{Ph}_2\text{BOOBPh}_2$. The latter species can undergo the bimolecular reaction, leading to the formation of 2 equiv. of $\text{Ph}_2\text{BO}^\bullet$ and 1 equiv. of O_2 . As a termination process, $\text{Ph}_2\text{BO}^\bullet$ abstracts hydrogen from hydrogen donor such as water to give Ph_2BOH .



Scheme 3.5. Schematic formation of diphenylboric acid.

3.4 CONCLUSIONS

The photochemical mechanism underlying the release of NHC upon irradiation of $\text{IMesH}^+\text{BPh}_4^-$ with ITX has been clarified. As summarized in **Scheme 3.6**, the first step is an electron transfer ($k_q = 4.9 \times 10^7 \text{ M}\cdot\text{s}^{-1}$) between electronically excited ITX and borate anion BPh_4^- acting as electron donor to yield the ion pair $\text{IMesH}^+/\text{ITX}^{\bullet-}$ and the boranyl radical $\text{Ph}_4\text{B}^\bullet$. This latter is subjected to a rapid decomposition into Ph^\bullet and Ph_3B . A subsequent reaction of the ion pair is proton abstraction of IMesH^+ by $\text{ITX}^{\bullet-}$ to form the **IMes** (NHC) and the ketyl radical (ITXH^\bullet). Of high importance for NHC reactivity was the fate of organoboron products. Ph_3B and Ph^\bullet were proved to undergo a multi-step oxidation reaction, yielding biphenyl and diphenylborinic acid. Ph_2BOH was found to react with the photogenerated **IMes** to give an **IMes-Ph₂BOH** ate-complex. While it is difficult to avoid the formation of NHC-boron adduct, our recent investigation showed that they did not prevent the activity of its NHC photogenerator for ring-opening metathesis polymerization or synthesis of polyurethane, thus demonstrating its practical interest.



Scheme 3.6. The mechanistic pathway involved in the formation of **IMes** during the photolysis of a mixture ITX/ $\text{IMesH}^+\text{BPh}_4^-$.

3.5 REFERENCES

- 1 J. L. R. Williams, J. C. Doty, P. J. Grisdale, Roger. Searle, T. H. Regan, G. P. Happ and D. P. Maier, Boron photochemistry. I. Irradiation of sodium tetraarylborates in aqueous solution, *J. Am. Chem. Soc.*, 1967, **89**, 5153–5157.

-
- 2 A. Pelter, R. T. Pardasani and P. Pardasani, The Photochemistry of Boron Compounds, *Tetrahedron*, 2000, **56**, 7339–7369.
 - 3 J. Radtke, S. K. Møllerup, M. Bolte, H.-W. Lerner, S. Wang and M. Wagner, Aryl Insertion vs Aryl–Aryl Coupling in C,C-Chelated Organoborates: The “Missing Link” of Tetraarylborate Photochemistry, *Org. Lett.*, 2018, **20**, 3966–3970.
 - 4 W. G. Santos, J. Pina, D. H. Burrows, M. D. E. Forbes and D. R. Cardoso, New insight into the photophysics and reactivity of trigonal and tetrahedral arylboron compounds, *Photochem. Photobiol. Sci.*, 2016, **15**, 1124–1137.
 - 5 T. Baumgartner and F. Jaekle, *Main Group Strategies Towards Functional Hybrid Materials*, John Wiley & Sons, New Jersey, 2018, p.87–92.
 - 6 X. Sun, J. P. Gao and Z. Y. Wang, Bicyclic Guanidinium Tetraphenylborate: A Photobase Generator and A Photocatalyst for Living Anionic Ring-Opening Polymerization and Cross-Linking of Polymeric Materials Containing Ester and Hydroxy Groups, *J. Am. Chem. Soc.*, 2008, **130**, 8130–8131.
 - 7 J. D. Wilkey and G. B. Schuster, Irradiation of tetraphenylborate does not generate a borene anion, *J. Org. Chem.*, 1987, **52**, 2117–2122.
 - 8 J. L. R. Williams, J. C. Doty, P. J. Grisdale, T. H. Regan, G. P. Happ and D. P. Maier, Boron photochemistry. II. Irradiation of sodium tetraarylborates in alcohol solutions, *J. Am. Chem. Soc.*, 1968, **90**, 53–55.
 - 9 Y. H. Zhao, D. Vuluga, L. Lecamp and F. Burel, Photoinitiated thiol–epoxy addition for the preparation of photoinduced self-healing fatty coatings, *RSC Adv.*, 2016, **6**, 32098–32105.
 - 10 Y. Jian, Y. He, Y. Sun, H. Yang, W. Yang and J. Nie, Thiol–epoxy/thiol–acrylate hybrid materials synthesized by photopolymerization, *J. Mater. Chem. C*, 2013, **1**, 4481–4489.
 - 11 S. Chatani, T. Gong, B. A. Earle, M. Podgórski and C. N. Bowman, Visible-Light Initiated Thiol-Michael Addition Photopolymerization Reactions, *ACS Macro Lett.*, 2014, **3**, 315–318.
 - 12 J. Shin, H. Matsushima, C. M. Comer, C. N. Bowman and C. E. Hoyle, Thiol–Isocyanate–Ene Ternary Networks by Sequential and Simultaneous Thiol Click Reactions, *Chem. Mater.*, 2010, **22**, 2616–2625.
 - 13 D. Perrot, C. Croutxé-Barghorn and X. Allonas, UV-curable thio-ether-urethane network with tunable properties, *J. Polym. Sci. Part A: Polym. Chem.*, 2016, **54**, 3119–3126.
 - 14 S. Murphy and G. B. Schuster, A Kinetic Method for Determination of Redox Potentials: Oxidation of Tetraarylborates, *J. Phys. Chem.*, 1995, **99**, 511–515.
 - 15 S. Chatterjee, P. D. Davis, P. Gottschalk, M. E. Kurz, B. Sauerwein, X. Yang and G. B. Schuster, Photochemistry of carbocyanine alkyltriphenylborate salts: intra-ion-pair electron transfer and the chemistry of boranyl radicals, *J. Am. Chem. Soc.*, 1990, **112**, 6329–6338.
 - 16 T. Konishi, Y. Sasaki, M. Fujitsuka, Y. Toba, H. Moriyama and O. Ito, Persistent C₆₀ anion-radical formation via photoinduced electron transfer from tetraphenylborate and triphenylbutylborate, *J. Chem. Soc. Perkin Trans. 2*, 1999, **3**, 551–556.
 - 17 R. Popielarz, A. M. Sarker and D. C. Neckers, Applicability of Tetraphenylborate Salts as Free Radical Initiators, *Macromolecules*, 1998, **31**, 951–954.

-
- 18 A. Y. Polykarpov, S. Hassoon and D. C. Neckers, Tetramethylammonium Tetraorganylborates as Coinitiators with 5,7-Diiodo-3-butoxy-6-fluorone in Visible Light Polymerization of Acrylates, *Macromolecules*, 1996, **29**, 8274–8276.
- 19 S. Hassoon, A. Sarker, A. Y. Polykarpov, M. A. J. Rodgers and D. C. Neckers, Photoinduced Inter- and Intra-Ion-Pair Electron Transfer Reactions in N-(p-Benzoylbenzyl)-N,N,N-tri-n-butylammonium Triphenyl-n-butylborate and -Gallate Salts, *J. Phys. Chem.*, 1996, **100**, 12386–12393.
- 20 J. Y. Lan and G. B. Schuster, Photoalkylation of dicyanoarenes with alkyltriphenylborate salts, *J. Am. Chem. Soc.*, 1985, **107**, 6710–6711.
- 21 J. Pinaud, T. K. H. Trinh, D. Sauvanier, E. Placet, S. Songsee, P. Lacroix-Desmazes, J.-M. Becht, B. Tarablsi, J. Lalevée, L. Pichavant, V. Héroguez and A. Chemtob, In Situ Generated Ruthenium-Arene Catalyst for Photoactivated Ring-Opening Metathesis Polymerization through Photolabile N-Heterocyclic Carbene Ligand, *Chem.: Eur. J.*, 2018, **24**, 337–341.
- 22 T. K. H. Trinh, J. P. Malval, F. Morlet-Savary, J. Pinaud, P. Lacroix-Desmazes, C. Reibel, V. Héroguez and A. Chemtob, Mixture of azolium tetraphenylborate with isopropylthioxanthone: a new class of N-heterocyclic carbene (NHC) photogenerator for polyurethane, polyester and ROMP polymers synthesis, *Chem.: Eur. J.*, 2019, DOI: doi.org/10.1002/chem.201901000.
- 23 M. Scholl, S. Ding, C. W. Lee and R. H. Grubbs, Synthesis and Activity of a New Generation of Ruthenium-Based Olefin Metathesis Catalysts Coordinated with 1,3-Dimesityl-4,5-dihydroimidazol-2-ylidene Ligands, *Org. Lett.*, 1999, **1**, 953–956.
- 24 N. E. Kamber, W. Jeong, S. Gonzalez, J. L. Hedrick and R. M. Waymouth, N-Heterocyclic Carbenes for the Organocatalytic Ring-Opening Polymerization of ϵ -Caprolactone, *Macromolecules*, 2009, **42**, 1634–1639.
- 25 J. Raynaud, W. N. Ottou, Y. Gnanou and D. Taton, Metal-free and solvent-free access to α,ω -heterodifunctionalized poly(propylene oxide)s by N-heterocyclic carbene-induced ring opening polymerization, *Chem. Commun.*, 2010, **46**, 3203.
- 26 B. Bantu, G. M. Pawar, U. Decker, K. Wurst, A. M. Schmidt and M. R. Buchmeiser, CO₂ and Sn^{II} Adducts of N-Heterocyclic Carbenes as Delayed-Action Catalysts for Polyurethane Synthesis, *Chem.: Eur. J.*, 2009, **15**, 3103–3109.
- 27 S. Naumann, F. G. Schmidt, W. Frey and M. R. Buchmeiser, Protected N-heterocyclic carbenes as latent pre-catalysts for the polymerization of ϵ -caprolactone, *Polym. Chem.*, 2013, **4**, 4172–4181.
- 28 J. Zhang, N. Pidlynyi, M. Nieger, J. C. Namyslo and A. Schmidt, Zwitterionic borane adducts of N-heterocyclic carbenes from mesomeric betaines of uracil, *Org. Biomol. Chem.*, 2014, **12**, 2737–2744.
- 29 V. Charlot, A. Ibrahim, X. Allonas, C. Croutxé-Barghorn and C. Delaite, Photopolymerization of methyl methacrylate: effects of photochemical and photonic parameters on the chain length, *Polym. Chem.*, 2014, **5**, 6236–6243.
- 30 J. B. Foresman, Ae. Frisch and I. Gaussian, *Exploring chemistry with electronic structure methods*, Pittsburgh, PA : Gaussian, Inc, 2nd ed., 1996.
- 31 M. J. Frisch, G. W. Trucks, H. B. Schlegel, G. E. Scuseria, M. A. Robb, J. R. Cheeseman, V. G. Zakrzewski, J. A. Montgomery, J. R. E. Stratmann, J. C. Burant, S. Dapprich, J. M. Millam, A. N. D. Daniels, K. N. Kudin, M. C. Strain, O. Farkas, J. Tomasi, V. Barone, M. Cossi, R. Cammi, B. Mennucci,

-
- C. Pomelli, C. Adamo, S. Clifford, J. Ochterski, G. A. Petersson, P. Y. Ayala, Q. Cui, K. Morokuma, P. Salvador, J. J. Dannenberg, D. K. Malick, A. D. Rabuck, K. Raghavachari, J. B. Foresman, J. Cioslowski, J. V. Ortiz, A. G. Baboul, B. B. Stefanov, G. Liu, A. Liashenko, P. Piskorz, I. Komaromi, R. Gomperts, R. L. Martin, D. J. Fox, T. Keith, M. A. Al-Laham, C. Y. Peng, A. Nanayakkara, M. Challacombe, P. M. W. Gill, B. Johnson, W. Chen, M. W. Wong, J. L. Andres, C. Gonzalez, M. Head-Gordon, E. S. Replogle, J. A. Pople, *Gaussian 03, Revision B-2*, Gaussian, Inc: Pittsburgh PA, 2003.
- 32 J. Christmann, X. Allonas, C. Ley, A. Ibrahim and C. Croutxé-Barghorn, Triazine-Based Type-II Photoinitiating System for Free Radical Photopolymerization: Mechanism, Efficiency, and Modeling, *Macromol. Chem. Phys.*, 2017, **218**, 1600597–1600599.
- 33 J. Christmann, S. Shi, A. Ibrahim, C. Ley, C. Croutxé-Barghorn, M. Bessières and X. Allonas, Mechanistic Investigation of a Dual Bicyclic Photoinitiating System for Synthesis of Organic–Inorganic Hybrid Materials, *J. Phys. Chem. B*, 2017, **121**, 1972–1981.
- 34 A. Allushi, C. Kutahya, C. Aydogan, J. Kreutzer, G. Yilmaz and Y. Yagci, Conventional Type II photoinitiators as activators for photoinduced metal-free atom transfer radical polymerization, *Polym. Chem.*, 2017, **8**, 1972–1977.
- 35 X. Allonas, C. Ley, C. Bibaut, P. Jacques and J. P. Fouassier, Investigation of the triplet quantum yield of thioxanthone by time-resolved thermal lens spectroscopy: solvent and population lens effects, *Chem. Phys. Lett.*, 2000, **322**, 483–490.
- 36 E. Andrzejewska, D. Zych-Tomkowiak, M. Andrzejewski, G. L. Hug and B. Marciniak, Heteroaromatic Thiols as Co-initiators for Type II Photoinitiating Systems Based on Camphorquinone and Isopropylthioxanthone, *Macromolecules*, 2006, **39**, 3777–3785.
- 37 H. Shizuka and H. Obuchi, Anion-induced triplet quenching of aromatic ketones by nanosecond laser photolysis, *J. Phys. Chem.*, 1982, **86**, 1297–1302.
- 38 S. F. Yates and G. B. Schuster, Photoreduction of triplet thioxanthone by amines: charge transfer generates radicals that initiate polymerization of olefins, *J. Org. Chem.*, 1984, **49**, 3349–3356.
- 39 J. C. Scaiano, Intermolecular photoreductions of ketones, *J. Photochem.*, 1973, **2**, 81–118.
- 40 Amirzadeh, G. and Schnabel, W., On the photoinitiation of free radical polymerization-laser flash photolysis investigations on thioxanthone derivatives, *Makromol Chem*, 1981, **182**, 2821–2835.
- 41 M. Aydin, N. Arsu, Y. Yagci, S. Jockusch and N. J. Turro, Mechanistic Study of Photoinitiated Free Radical Polymerization Using Thioxanthone Thioacetic Acid as One-Component Type II Photoinitiator, *Macromolecules*, 2005, **38**, 4133–4138.
- 42 Y. Nishida, Y.-M. Lee, W. Nam and S. Fukuzumi, Autocatalytic Formation of an Iron(IV)–Oxo Complex via Scandium Ion-Promoted Radical Chain Autoxidation of an Iron(II) Complex with Dioxygen and Tetraphenylborate, *J. Am. Chem. Soc.*, 2014, **136**, 8042–8049.
- 43 A. M. Sarker, Y. Kaneko and D. C. Neckers, Photochemistry and photophysics of novel photoinitiators: N,N,N-tributyl-N-(4-methylene-7-methoxycoumarin) ammonium borates, *J. Photochem. Photobiol. Chem.*, 1998, **117**, 67–74.
- 44 O. Hollóczki, Unveiling the peculiar hydrogen bonding behavior of solvated N-heterocyclic carbenes, *Phys. Chem. Chem. Phys.*, 2016, **18**, 126–140.

-
- 45 M. Thomas, M. Brehm, O. Hollóczki and B. Kirchner, How Can a Carbene be Active in an Ionic Liquid?, *Chem.: Eur. J.*, 2014, **20**, 1622–1629.
- 46 A. J. I. Arduengo, S. F. Gamper, M. Tamm, J. C. Calabrese, F. Davidson and H. A. Craig, A Bis(carbene)-Proton Complex: Structure of a C-H-C Hydrogen Bond, *J. Am. Chem. Soc.*, 1995, **117**, 572–573.
- 47 S. Dadashi-Silab, C. Aydogan and Y. Yagci, Shining a light on an adaptable photoinitiator: advances in photopolymerizations initiated by thioxanthenes, *Polym. Chem.*, 2015, **6**, 6595–6615.
- 48 F. G. Kny-Jones and A. M. Ward, LXXVI.—Investigations on the bivalency of carbon. Part III. Some experiments on xanthhydrol, dixanthhydrol ether, and xanthhydrol chloride, *J. Chem. Soc.*, 1930, **0**, 535–542.
- 49 W. A. Green, *Industrial Photoinitiators: A Technical Guide*, CRC Press, Boca Raton, 1st edn., 2010, pp.69–70.
- 50 S. T. Murphy, C. Zou, J. B. Miers, R. M. Ballew, D. D. Dlott and G. B. Schuster, Tetraarylborates {[Ar]4B-}: estimation of oxidation potentials and reorganization energies from electron-transfer rates, *J. Phys. Chem.*, 1993, **97**, 13152–13157.
- 51 B. P. Sullivan, W. J. Dressick and T. J. Meyer, Photoelectrochemical cell based on the ion pair 1,1'-dimethyl-4,4'-bipyridinium bis(tetraphenylborate). Photocurrents from the direct irradiation of a donor-acceptor complex, *J. Phys. Chem.*, 1982, **86**, 1473–1478.
- 52 P. A. Chase, A. L. Gille, T. M. Gilbert and D. W. Stephan, Frustrated Lewis pairs derived from N-heterocyclic carbenes and Lewis acids, *Dalton Trans.*, 2009, **0**, 7179–7188.
- 53 P. A. Chase and D. W. Stephan, Hydrogen and Amine Activation by a Frustrated Lewis Pair of a Bulky N-Heterocyclic Carbene and B(C6F5)3, *Angew. Chem. Int. Ed.*, 2008, **47**, 7433–7437.
- 54 J. J. Eisch, J. H. Shah and M. P. Boleslawski, Skeletal rearrangements of arylborane complexes mediated by redox reactions: thermal and photochemical oxidation by metal ions, *J. Organomet. Chem.*, 1994, **464**, 11–21.
- 55 S. Arkhipenko, Approaches to Novel B-N Chemistry at the Boundary of Frustrated Lewis Pairs and Bifunctional Catalysis, *PhD Thesis Durh. Univ. Available at Durh. E-Theses Online*, 2017, **157**, DOI: 10.15128/et0012213.
- 56 H. S. Rzepa, S. Arkhipenko, E. Wan, M. T. Sabatini, V. Karaluka, A. Whiting and T. D. Sheppard, An Accessible Method for DFT Calculation of 11B NMR Shifts of Organoboron Compounds, *J. Org. Chem.*, 2018, **83**, 8020–8025.
- 57 N. Miyaura, in *Science of Synthesis: Houben-Weyl Methods of Molecular Transformations*, ed. D. E. Kaufmann and D. S. Matteson, Georg Thieme Verlag, Stuttgart, 1st edn., 2014, vol. 6, pp. 677–678.
- 58 P. Jutzi, Bor-NMR: Nuclear Magnetic Resonance Spectroscopy of Boron Compounds. Von H. Nöth und B. Wrackmeyer. Aus der Reihe NMR, Basic Principles and Progress, Grundlagen und Fortschritte. Vol. 14. Hrsg. von P. Diehl, E. Fluck, R. Kosfeld. Springer-Verlag, Berlin, Heidelberg, New York 1978. XII, 461 S., 96 Tab., geb. DM 162,—, *Nachrichten Aus Chem. Tech. Lab.*, 1978, **26**, 750–751.

CHAPTER IV. COMBINING A LIGAND PHOTOGENERATOR AND A RUTHENIUM PRECATALYST: A PHOTOINDUCED APPROACH TO CROSS-LINKED ROMP POLYMER FILMS

4.1. INTRODUCTION

As one of the most valuable tools for the generation of C=C double bonds, olefin metathesis has been exploited in many useful ways, including complex architectures,¹ pharmaceutical products,² or biodegradable copolymers.³ In all these cases, progress has been mainly driven by the development of advanced and well-defined metal alkylidene complexes, like the notorious Grubbs and Schrock catalysts.^{4,5} Ligand fine-tuning has resulted in a portfolio of catalysts featuring a broad range of reactivity, functional group tolerance and bench stability. In this respect, a major breakthrough was in 1999 the introduction of N-heterocyclic carbene (NHC) ligands in the place of the conventional phosphine compounds.^{6,7} In particular, sterically bulky and strong electron donating NHCs have proven to be highly effective, resulting in NHC-coordinated ruthenium complexes with longer life-time and superior catalytic activity.^{6,8} However, the main developments in olefin metathesis catalysis have responded more to the needs of synthetic chemistry (as the above mentioned examples show), but have been less useful for the preparation of polymer materials. Ring-opening metathesis polymerization (ROMP) of cyclic olefins is currently the main type of olefin metathesis polymerizations.^{6,9} To date, the use of ROMP polymers has been limited to the manufacturing of specific structural and engineering materials. This despite the broad spectrum of properties achievable by the major ROMP polymers, derived from norbornene (NB), cyclopentene, cyclooctene or dicyclopentadiene (DCPD). For example, polycyclooctene (Vestenamer®) and polynorbornene (pNB) (Norsorex®) elastomers are employed after vulcanization as shock absorbers and anti-grip materials. In addition, hydrogenated pNB (Zeonex®) is a high performance optical thermoplastic, while polydicyclopentadiene (pDCPD) (Metton® or Telene®) is known as a prime thermoset with mechanical properties similar to engineering thermoplastics.¹⁰ Most of these reported ROMP polymers have been utilized only as structural materials because their processing methods are restrictive. For example, pDCPD is prepared essentially by reaction injection molding, which requires separate monomer and catalyst compartments, efficient mixing and titration heads, nitrogen inerting of the mold, etc.¹¹⁻¹³

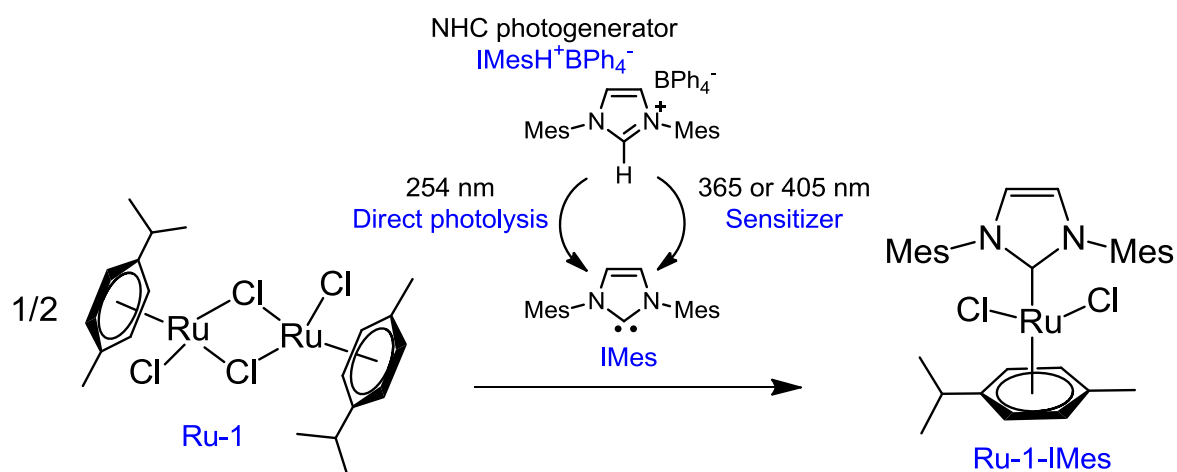
To unlock the potential of ROMP polymer materials, more efficient and “smarter” catalysts are crucial, especially to extend the shaping of ROMP polymer as film, particle or fiber, but also in general, to foster more versatile, energy-efficient and facile process conditions. To address those challenges, latent olefin metathesis catalysts complexes have emerged, i.e. catalysts able to release active species in situ and “on demand” by external

stimulation. Heat,^{14–16} mechanical force,¹⁷ and radiation^{18–20} are the most common stimuli. A separate category concerns catalysts activated after the addition of an external chemical agent.^{21–23} Among these different options, the activation brought about by visible or ultraviolet irradiation is particularly attractive.²⁴ Photolabile ROMP catalysts can be activated at ambient temperature, and make possible the use of storable and ready-to-use formulations combining together the catalyst and the monomer(s). As standard product of a photoactivated polymerization, thin films based on cross-linked ROMP polymer are also expected with prospect for the development of novel UV-curable coatings or adhesives. Finally, unlike the other triggers, the reaction can be spatially-controlled.^{23,25}

In the field of photochemically activated olefin metathesis, three main approaches have been proposed, in which the activation proceeds generally by a photochemical reaction involving the ligand of a transition metal complex (one must nevertheless note an original metal-free redox-mediated approach for ROMP using vinyl ethers as initiator and pyrilium salt as photo-oxidant¹³). The two most reported routes rely on ligand photodissociation^{26,27} and ligand *cis-to-trans* photoisomerization.^{18,20} The third route, which is the least investigated, is the focus of the present study. In the latter, the active olefin metathesis catalyst is generated from an inactive and non-absorbing precatalyst after reaction with a ligand liberated by a second photosensitive compound (ligand photogenerator). This methodology was first introduced by Grubbs *et al.* in 2009 by using a Ru-alkylidene complex ligated by acetylacetonate (*acac*) as precatalyst and a photoacid generator (PAG) based on triphenylsulfonium chloride.²¹ Upon irradiation at 254 nm, HCl was released, and the subsequent displacement of *acac* by Cl⁻ resulted in an active metathesis catalyst. A similar method was also employed by Pier *et al.* using a ruthenium carbide and Ph₃S triflate (*OTf*).²² Recently, we replaced the PAG with a NHC photogenerator and used a stable, commercially available dimeric Ru(II) complex as metathesis inactive catalyst. Our tandem system made up of the NHC progenitor 1,3-bis(mesityl)imidazolium tetraphenylborate **IMesH⁺BPh₄⁻** (**1**) and [RuCl₂(*p*-cymene)]₂ precatalyst (**Ru-1**) proved to be very efficient at ROMP of NB.^{28,29} In comparison with the examples discussed above, a safer UVA radiation (320 – 400 nm) was employed, and no ligand displacement occurred. As shown in **Scheme 4.1**, the cleavage of the Ru-chlorido bridges of **Ru-1** was rather enthalpically driven through the addition of 2 equivalents of free NHC **IMes**, that were in situ photogenerated from **1**. As a result, the presumed active catalyst (**Ru-1-IMes**) features one *p*-cymene cycle, two chlorido ligands and one **IMes** ligand. First introduced by Herman *et al.*,³⁰ this class of RuCl₂(*p*-cymene)NHC

catalyst has been extensively studied by Noels *et al.* for the ROMP of NB and cyclooctene.³¹⁻

33



Scheme 4.1. Irradiation of a mixture of a NHC photogenerator (**IMesH⁺BPh₄⁻**, **1**) and a dimeric Ru(II) complex, inactive catalyst (**Ru-1**), results in a active olefin metathesis photocatalyst (**Ru-1-IMes**). The NHC (**IMes**) can be photogenerated through two distinct routes: a *direct photolysis* or a *sensitized reaction* using an electronically excited electron acceptor.

In this contribution, the main aim is to demonstrate the utility of this tandem approach for the photoinduced preparation of cross-linked ROMP films. To this purpose, we report first our efforts to improve the photocatalytic system by addressing a number of issues: optimizing the yield of photogenerated **IMes**, ensuring a long-term photolateny, identifying the active metathesis catalyst and the initiating species (Ru-NHC complex), and finally, collecting some preliminary results on photoROMP in solution of common monomers such as NB. In a second part, a range of copolymer films was prepared by photoinduced ROMP between NB and DCPD using the photocatalytic mixture based on **1/ITX/Ru-1**. The cross-linked polymer structure was investigated by gel content measurement, FT-IR and solid-state ¹³C NMR spectroscopy. The mechanical behavior, microstructure and the thermal properties were also studied through atomic force microscopy (AFM), scanning electron microscopy (SEM), TGA and DSC.

4.2. EXPERIMENTALS

4.2.1. Materials

Dicyclopentadiene (DCPD, > 97 %, TCI), 2-norbornene (NB, > 99 %, TCI), 5-ethylidene-2-norbornene (ENB, > 98 %, TCI), vinyl ethyl ether (> 98 %, TCI), 2-isopropylthioxanthone (ITX, analytical standard, Aldrich), 1,3-bis(2,4,6-

trimethylphenyl)imidazol-2-ylidene (**IMes**, 97%, Aldrich) and 1,3-di-*p*-tolylcarbodiimide (CDI, 96 %, Aldrich) were used as received without purification. 1,3-bis(2,4,6-trimethylphenyl)imidazolium chloride (**IMesH⁺BPh₄⁻**, **1**) was prepared following a procedure published elsewhere.²⁸ Dichloro(*p*-cymene)ruthenium(II) dimer (**Ru-1**, 98 %), diiodo(*p*-cymene)ruthenium(II) dimer (**Ru-2**, 98 %) and dichlorodi- μ -chlorobis[(1,2,3,6,7,8- η -2,7-dimethyl-2,6-octadiene-1,8-diyl]diruthenium(IV) (**Ru-3**, 98 %) were bought from Strem Chemicals. Dichloromethane-*d*₂ (CD₂Cl₂, 99.5 % D, Eurisotop), tetrahydrofuran-*d*₈ (THF-*d*₈, 99.5 % D, Eurisotop) and other HPLC grade solvents such as ethanol, acetonitrile and tetrahydrofuran (THF) received from VWR were distilled and stored over molecular sieve (4 Å) under nitrogen atmosphere before using.

4.2.2. Experimental protocols

Quantification of IMes yield. Quantitative conversion of **IMes** into IMes-CDI adduct was described elsewhere.²⁹ The irradiation sources include a medium pressure Xe-Hg lamp@254 nm (75 mW·cm⁻², Hammamatsu, LC-9588/01A) (**Figure A.IV.1**) a LED@365 nm (65 mW·cm⁻², Hammamatsu LC-L1V3) and LED@405 nm (100 mW·cm⁻², Thorlabs M405L2) (**Figure A.IV.2**). The intensities of lamps were determined by using an optical power meter PM100D from Thorlabs.

*Preparation of the active metathesis catalyst (*p*-cymene)RuCl₂(IMes) (Ru-1-IMes).*

Noels' complex starting from **Ru-1** and **IMes** was synthesized based on a protocol developed by Nolan *et al.*³⁴ while Noels' complex starting from the tricomponent system **1**/ITX/**Ru-1** was prepared following procedure below.

A mixture of **Ru-1** (0.6 mg, 1 equiv.), **1** (3 mg, 5 equiv.) and ITX (0.62 mg, 2.5 equiv.) in 1 mL THF-*d*₈ was charged into a borosilicate NMR tube. Then, the tube was irradiated at 365 nm (Xe-Hg lamp, 20 mW·cm⁻²). ¹H NMR spectra were recorded at different given time (t = 0, 10, 20 and 30 min).

¹H NMR (400 MHz, THF-*d*₈): Noels' catalyst was obtained from **Ru-1** and **IMes**. δ_{ppm} : 1.08 (d, *J*=7Hz, 6H, CH(CH₃)₂), 1.75 (s, 3H, CH₃), 2.22 (s, 12H, Mes-2,6-CH₃), 2.31 (s, 6H, Mes-4-CH₃), 2.46 (m, 1H, CH(CH₃)₂), 4.55 (d, *J*=6Hz, 2H, C₆H₄), 5.00 (d, *J*=5.8Hz, 2H, C₆H₄), 6.90 (m, 4H, Mes-3,5-H), 7.05 (s, 2H, NCHCHN).

Assessment of catalyst photolability. In a typical experiment, NB (47 mg, 510 equiv.), ITX (0.63 mg, 2.5 equiv.) and ruthenium pre-catalyst **Ru-1** (0.62 mg, 1 equiv.) were

placed in borosilicate NMR tube containing 0.5 mL of CD₂Cl₂. All solutions were stored in dark. At given time, a ¹H-NMR spectrum was recorded to determine the extent of monomer conversion and *cis/trans* ratio of the polymer possibly formed.

Photoactivated ROMP in solution. To a borosilicate NMR tube was added 47 mg of NB (510 equiv.), 0.63 mg of ITX (2.5 equiv.), 3 mg of **1** (5 equiv.), 0.62 mg of **Ru-1** (1 equiv.), then 0.5 ml of CD₂Cl₂. The solutions were irradiated in a circular LED photoreactor. For this, a LED strip was wrapped around a quartz cylinder ($\phi_{int} = 60$ mm) emitting a monochromatic light centered at 365 nm (SMD3528-60LED/Meter, Lightingwill, 6.5 mW·cm⁻²) or 405 nm (SMD2835-60LED/Meter, Banggood, 4.7 mW·cm⁻²) (**Figure A.IV.3**). After 1 min irradiation, ¹H-NMR spectra were recorded; to determine monomer conversion and *cis/trans* ratio. Excess amount of vinyl ethyl ether (0.1 mL) was added to terminate the polymerization. Polymers were collected through precipitation in acetone and washed 3 times with CH₂Cl₂/acetone. SEC measurements were performed after drying under air for 48 h. For measurements of real-time kinetics by RT-FTIR (see characterization section), the same NB/ITX/**1**/**Ru-1** mixture was introduced into an IR liquid cell (Specac® Omni cell) (**Figure A.IV.4**) containing two sandwich CaF₂ windows. A 1 mm Teflon spacer in the middle of pellets was used to fix the specimen thickness. Samples were then exposed synchronously to an IR beam and an UV irradiation resource equipped with a light guide. Two types of LED were used: a LED@365 nm and LED@405 nm (see above for details).

Preparation of cross-linked ROMP polymer films. A mixture of NB and DPCD was prepared at different NB concentration ranging from 25 to 75 mol %. **Ru-1** (9 mg, 1 equiv.), ITX (9.3 mg, 2.5 equiv.) and **1** (45 mg, 5 equiv.) were first dissolved in CH₂Cl₂ (2 mL), then the monomer mixture (510 equiv.) was added and left 10 min under stirring to obtain a homogeneous solution. The catalyzed mixture was then poured into a Teflon mold covered with a borosilicate glass plate. Clamps were used to prevent air entry as well as evaporation of solvent and monomers. The weight of mold containing the reactive mixture was determined before irradiation to be used subsequently for gravimetry measurements. The mold was placed under a LED panel (365 nm, 5.5 mW·cm⁻², top UV Curing light) (**Figure A.IV.5**) for 1 h. The wet gel was removed from the mold and left overnight. Residual monomers and solvent were removed by drying under vacuum at 50 °C until a constant weight.

4.2.3. Characterization

- All ^1H NMR spectra were recorded in appropriate deuterated solvents with tetramethylsilane (TMS) as the internal reference on a Varian 300 – MR. All chemical resonances were documented in parts per million (ppm) relative to the residual THF- d_8 (δ 1.72 ppm and 3.58 ppm), and CD_2Cl_2 (δ 5.32 ppm). Peaks multiplicities in ^1H – NMR spectra were abbreviated as s (single), d (double), t (triplet), m (multiplet), br (broad).
- Molecular weights of pNB and poly(5-ethylidene-2-norbornene) (pENB) were determined using a size exclusion chromatography (SEC) instrument from a Varian apparatus equipped with TOSOHAAS TSK gel columns and a refractive index detector. The mobile phase was THF at a flow rate of $1 \text{ mL}\cdot\text{min}^{-1}$; the injected volume was $100 \mu\text{L}$. The MALS instrument was normalized using a THF solution of polystyrene standard.
- Thermogravimetric analysis (TGA) and differential scanning calorimetry (DSC) experiments were performed using, respectively, a TGA/DSC3+ (Mettler Toledo) and a DSC1 (Mettler Toledo) under nitrogen atmosphere. For TGA analysis, the samples (8 – 15 mg) were heated from $30 \text{ }^\circ\text{C}$ to $600 \text{ }^\circ\text{C}$ at a heating rate of $10 \text{ }^\circ\text{C}\cdot\text{min}^{-1}$. For DSC analysis, the samples (3 mg) were scanned from $-50 \text{ }^\circ\text{C}$ to $250 \text{ }^\circ\text{C}$ at a heating rate of $10 \text{ }^\circ\text{C}\cdot\text{min}^{-1}$.
- Atomic force microscopy (AFM) characterization was performed on a Bruker-MultiMode 8 controlled by NanoScope V. Information for the tip is NCLR-50, $k=48 \text{ N/m}$. The tip calibration was carried out prior to the analysis ($f_0 = 161.71 \text{ kHz}$, $\phi = 475$ and $k=22.2 \text{ N/m}$).
- Film morphology was observed by scanning electron microscopy (SEM), (SEM Fei Quanta 400, tungsten gun).
- To determine gel content, a polymer specimen ($\sim 50 \text{ mg}$) was placed into a 5 ml vial containing 4 mL of CH_2Cl_2 . After magnetic stirring for 24 h at room temperature, the solvent was removed and insoluble component was dried under vacuum at $40 \text{ }^\circ\text{C}$ until weight constant. The gel content was finally measured.
- ^1H - ^{13}C ramped CPMAS (Cross-Polarization Magic Angle Spinning) NMR spectra were recorded by using an Advance II Bruker Spectrometer (AscendTM magnet) ($B_0 = 9.4 \text{ T}$) operating at 400.18 MHz for the ^1H and 100.64 MHz for the ^{13}C and controlled by TOPSPIN 3.2 software. The solid films were grounded into fine powders prior to measurement. Experiments were performed at ambient temperature with a 4mm double resonance MAS Bruker probe at a speed of 12kHz, a ^1H $\pi/2$ pulse duration of $5.6 \mu\text{s}$, a contact time of 1 ms and a recycle delay of 2 s. Chemical shifts reported thereafter are relative to tetramethylsilane

and the de-convolution of the experimental spectra were carried out with the DMfit software. The fraction of pendant cyclopentene rings involved in olefin coupling reaction can be determined from the ^{13}C spectrum. DCPD contains initially 4 sp^2 and 6 sp^3 carbons. The ratio of $\text{sp}^2\text{-C}$ to $\text{sp}^3\text{-C}$ does not change when cyclopentene reacts by ROMP. Conversely, olefin coupling leads to the replacement of 2 $\text{sp}^2\text{-C}$ by 2 $\text{sp}^3\text{-C}$. This change can be used to estimate the fraction of cyclopentene reacting via olefin coupling (x) in pDCPD film (eq. 1)³⁵:

$$\frac{I_{\text{sp}^2\text{-C}}}{I_{\text{sp}^3\text{-C}}} = \frac{4-2x}{6+2x} = \frac{2-x}{3+x} \quad (1)$$

where $I(\text{sp}^2\text{-C})$ and $I(\text{sp}^3\text{-C})$ are the integrated areas of the signals associated to olefinic carbons ($\sim 125 - 130$ ppm) and aliphatic carbons ($30 - 60$ ppm), respectively. This equation was changed to adapt to our specific copolymer structure resulting from copolymerization of NB and DCPD (eq. 2):

$$\frac{I_{\text{sp}^2\text{-C}}}{I_{\text{sp}^3\text{-C}}} = 0.43 * x_{\text{NB}} + (1 - x_{\text{NB}}) \frac{2-x}{3+x} \quad (2)$$

where 0.43 is the value of the experimental ratio $I(\text{sp}^2\text{-C})/I(\text{sp}^3\text{-C})$ in pNB (calculated from sample NB-100), and x_{NB} is the molar fraction of NB in the NB/DCPD monomer mixture.

- FTIR spectra were recorded with a Nicolet 8700 Spectrophotometer (Thermo Scientific) using a mercury cadmium telluride detector. Two modes were used, transmission for the real-time kinetics of photoROMP in solution and ATR for characterization of polymer films. All the spectra were recorded in range of 4000 cm^{-1} – 600 cm^{-1} . The real-time measurements used a scanning velocity of $11.45 \text{ cm sec}^{-1}$ corresponding to a resolution of 0.964 cm^{-1} in the infrared spectra. Monomer conversion was determined from the temporal evolution of different stretching modes at 1566 cm^{-1} (NB, C=C stretch) and 3047 cm^{-1} (DCPD, $\text{sp}^2 =\text{CH}-$) (**Figure A.IV.6**). To ensure a good reproducibility of these data, each experiment was performed at least three times.

4.3. RESULTS AND DISCUSSION

4.3.1. Study and optimization of the tandem photocatalytic system

a. NHC photogeneration

There are two possible photochemical pathways to deprotonate the IMesH^+ imidazolium cation in **1**, and thereby generate the targeted NHC **IMes** (**Scheme 1**). Both approaches rely on the photochemistry of tetraphenylborate counter-anion: a *direct photolysis*

of BPh_4^- ,³⁶ or a *sensitized reaction* involving an additional electron acceptor species such as isopropylthioxanthone (ITX).^{28,29} Photolysis was carried out by exposure of **1** in THF-*d*₈ (0.03 M) to 254 nm, while the sensitized reaction was conducted in similar conditions with a mixture of **1** and **ITX** (1/1 equiv.) upon irradiating this time at 365 nm or 405 nm (thanks to the higher wavelength absorption of the sensitizer). The precise reaction mechanisms in both cases have been commented on elsewhere.^{28,29,37,38} And **Table 4.1** only compares the efficiency of the two methods in the light of the amount of NHC generated after 5 min irradiation.³⁹ Clearly, the combination of **1** and ITX at 365 nm (*entry a*) and 405 nm (*entry b*) shows improved activity in comparison with **1** irradiated alone at 254 nm (*entry c*). Only 11 % **IMes** was liberated in this latter case versus 29 % (405 nm) and 67 % (365 nm) in the sensitized reaction. This suggests that the photoinduced route using the 2-component system **1**/ITX is more efficient. However, since the two photochemical mechanisms are completely different, there is no obvious explanation. To account for the poor NHC yield after the direct photolysis, one possible reason is the fact that **IMes** has a non-negligible absorption band at 254 nm ($\epsilon_{254} = 9.1 \times 10^3 \text{ M}^{-1} \cdot \text{cm}^{-1}$), while it does not absorb in the UVA range. This could reduce the amount of photons absorbed by **1**, and undermine the yield of the photolysis reaction. Therefore, the mixture **1**/ITX was employed as NHC photogenerator in the rest of the study.

Table 4.1. Effect of excitation wavelength on the release of free NHC **IMes** in THF-*d*₈ ([**1**] = 0.03 M, [ITX] = 0.03 M) after 5 min of irradiation.

Entry	NHC photogenerator	Irradiation wavelength ^a nm	IMes yield ^b %
<i>a</i>	1 /ITX	365	67
<i>b</i>	1 /ITX	405	29
<i>c</i>	1	254	11

^a Irradiances values: 65 $\text{mW} \cdot \text{cm}^{-2}$ (365 nm), 100 $\text{mW} \cdot \text{cm}^{-2}$ (405 nm) and 75 $\text{mW} \cdot \text{cm}^{-2}$ (254 nm). ^b NHC yield was obtained indirectly after addition of 1,3-di-*p*-tolylcarbodiimide (CDI) ([CDI] = 0.03 M, 1 equiv). The stable IMes-CDI adduct is formed, which can be precisely quantified by ¹H NMR.²⁹

b. Nature of the (photo)generated active catalyst

Having proved the aptitude of **1** to act as NHC precursor under irradiation (in combination with a sensitizer), we studied the subsequent reaction of **IMes** with $[\text{RuCl}_2(\textit{p}\text{-cymene})]_2$ dimer **Ru-1** to form an active catalyst. Though the formation of $\text{RuCl}_2(\textit{arene})(\text{NHC})$ **Ru-1-IMes** is basically acceptable,^{28,29} experiments were conducted to probe the structure of the active metathesis catalyst. For this, we performed a control

experiment in which **Ru-1** was reacted with free **IMes** in THF- d_8 at room temperature. An orange solution formed spontaneously, and subsequent ^1H NMR analysis (performed without prior isolation) established that the expected catalyst structure (*p*-cymene) $\text{RuCl}_2(\text{IMes})$ was formed in high yield (**Figure 4.1**). The spectrum found was indeed in full agreement with previous literature data.³⁴ This suggests that (*p*-cymene) $\text{RuCl}_2(\text{IMes})$ could be actually the active catalytic species when the tandem system NHC photogenerator/Ru precatalyst is irradiated. However, all attempts to characterize by ^1H NMR the photogenerated active catalyst have failed, preventing to confirm our hypothesis. The spectra of the catalytic reaction mixture **1/Ru-1/ITX** show after irradiation too many signals, preventing the unequivocal identification of the chelated NHC-Ru complex (see **Figure A.IV.7**).

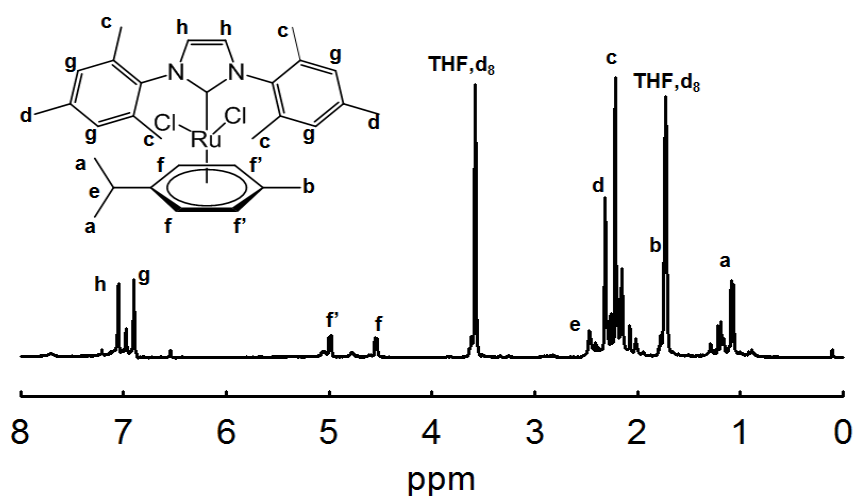


Figure 4.1. ^1H NMR spectrum of the reaction medium after reaction of $[(p\text{-cymene})\text{RuCl}_2]_2$ (**Ru-1**, 1 equiv.) with **IMes** (2.02 equiv.) in THF- d_8 ($[\text{Ru-1}] = 0.05$ M).

c. Catalyst photolateny

Photochemical latency is a very important characteristic for practical implementation of a photocatalytic system. For this, the catalytic activities of **Ru-1** (in presence of ITX) has been tested with exclusion of light by using standard ROMP substrates such as NB. Results are presented in **Table 4.2** using CD_2Cl_2 as a solvent. The photochemical latency of **Ru-1** was found to be poor since 18 % conversion (*entry a*) was obtained after 4 h at room temperature. Although the mechanism of this secondary reaction is still elusive, we propose that ROMP could proceed by a decooordination of the η^6 -arene ligand to afford a highly unsaturated ruthenium center that evolves into a propagating alkylidene after addition of a NB molecule.^{40,41} In agreement with this hypothesis, no premature reaction took place with ENB (*entry b*) due to its higher steric hindrance which limits the reaction with the ruthenium

center. In the search of other ruthenium pre-catalysts able to ensure a complete photolateny, **Ru-1** [RuCl₂(*p*-cymene)]₂ was substituted with [RuI₂(*p*-cymene)]₂ (**Ru-2**) and [RuCl₂(COD)]₂ (**Ru-3**, with COD = 1,5-cyclooctadiene) to probe separately the effect of the halogen and the ligand in the Ru dimer. Remarkably, **Ru-2** afforded less than 1 % conversion after 4 h (*entry c*) and only 1.4 % monomer consumption after 168 h (*entry d*). Addition of **1** did not increase the conversion, illustrating the minor role played by the NHC precursor in the instability issue. Conversely, the **Ru-3** complex exhibited nearly no latency since 90 % conversion was reported after 4 h (*entry e*). These results showed the size of the halogen as a crucial parameter affecting the equilibrium for olefin binding.^{42,43} As expected, a larger halogen than chloride such as iodide disfavors olefin binding due to steric hindrance, resulting in a better latency. In all instances, a low content of *cis* double bond ($\sigma_{cis} = 23\text{-}30\%$) was determined in the polymer structure, which is consistent with the literature data for ROMP relying on ruthenium dimers as catalyst.^{44,45} In conclusion, **Ru-2** seems the best precatalyst candidate, however it remains an open question whether it will form an active metathesis catalyst when coupled with **IMes**.

Table 4.2. Photolateny results of Ru dimer/ITX/monomer mixture in CD₂Cl₂ ([Monomer] = 1 M). All the samples were stored in the dark (Ru dimer/ITX/monomer = 1/2.5/510 equiv.).

Entry	Precatalyst	Monomer	Reaction time	Conv. ^a	σ_{cis}^a
			h	%	
<i>a</i>	Ru-1	NB	4	17.6	30
<i>b</i>	Ru-1	ENB	4	0	n.d
<i>c</i>	Ru-2	NB	4	<1	n.d
<i>d</i>	Ru-2	NB	168	1.4	23
<i>e</i>	Ru-3	NB	4	90	24

^a Determined by ¹H-NMR.

d. Photoactivated ROMP in solution

The catalytic activity of the three-component system Ru precatalyst/**1**/ITX (1/5/2.5 equiv.) was evaluated for the ROMP of NB (**Table 4.3**). The **1**/ITX acts as NHC photogenerator in this case, and the reaction was performed in CD₂Cl₂ inside a NMR tube. As expected, the irradiation (365 nm, 1 min) of a solution devoid of Ru dimer resulted in no reaction (*entry a*). By contrast, a small conversion was observed when the **Ru-1** precatalyst was irradiated alone (1 %, *entry b*) or in presence of ITX (7 %, *entry c*). This result can be reconciled with the poor latency of **Ru-1** noted earlier (see section c), and suggests that the η^6 -arene ligand displacement could be enhanced by a photochemical activation. The vacant

site created on the Ru can form subsequently an active Ru-NHC complex after the addition of a monomer molecule.^{31, 40}

Table 4.3. Photopolymerization results of NB using Ru dimer/**1**/ITX photoinitiating system in CD₂Cl₂ ([NB] = 1 M, 510 equiv.). Irradiation conditions: 365 nm, 6.5 mW·cm⁻², 1 min.

Entry	Precatalyst	Pre-catalyst/ 1 /ITX equiv.	Conv. ^a %	σ_{cis}^b	$M_{n\text{-th}}^c$ kg·mol ⁻¹	$M_{n\text{-SEC}}^d$ kg·mol ⁻¹	\bar{D}^d
<i>a</i>	Ru-1	0/5/2.5	0	n.d	n.d	n.d	n.d
<i>b</i>	Ru-1	1/0/0	1	9	0.36	n.d.	n.d.
<i>c</i>	Ru-1	1/0/2.5	7	23	1.60	n.d.	n.d.
<i>d</i>	Ru-1	1/5/2.5	78	52	18.69	146.8	3.02
<i>e</i>	Ru-1	1/5/5	94	52	22.57	108.4	1.96
<i>f</i> ^e	Ru-1	1/5/2.5	22	65	5.27	63.4	2.05
<i>g</i>	Ru-2	1/5/2.5	69	52	16.43	447.2	1.59
<i>h</i>	Ru-3	1/5/2.5	67	48	16.10	n.d.	n.d.

^a Determined by ¹H-NMR. ^b Calculated from ¹H-NMR spectrum, ^c Theoretical number average molar mass $M_{n\text{-th}} = \text{Conv.} \times \frac{[\text{NB}] \times M_{\text{NB}}}{2 \times [\text{Ru-1}]}$, ^d Experimental number average molar mass $M_{n\text{-th}}$ obtained by SEC, ^e Irradiation at 405 nm, 4.7 mW·cm⁻², 1 min. n.d. means not determined due to the absence of reaction or the formation of an insoluble polymer.

The question of the mechanism and the nature of the metathesis initiating species will be addressed in the next section. A much higher catalytic activity was achieved in presence of **1** (entry *d*), with 78 % conversion after 1 min, suggesting the successful formation of a highly active Ru-arene complex, which is likely to be **Ru-1-IMes**. The content of *cis* double bond ($\sigma_{\text{cis}} = 52$ %) was similar to that obtained with previous systems and supports this assumption.^{40,46} By comparison, much lower *cis* contents are generally reported with phosphine-coordinated ruthenium complex.⁴⁷ Upon increasing the proportion of ITX proportion from 2.5 equiv. to 5 equiv., a significant increase of conversion was noted (94 %, entry *e*). In contrast, irradiation at 405 nm instead of 365 nm led to drop the conversion (22 %, entry *f*). This can be rationalized on the basis of a lower **IMes** yield at higher excitation wavelength (see section a). For the polymer produced with the tandem approach precatalyst/NHC photogenerator (entries *d-f*), the molecular weight distributions were

monomodal (SEC data), suggesting that only one mechanism is involved in the catalysis. However, high molecular weights (M_{n-SEC}) and rather broad polydispersities (\mathcal{D}) were obtained, which reflect a poor control of the initiation step. The source of the problem is the ill-defined initiation mechanism and above all, the poor initiation efficiency resulting in only a small number of propagating centers produced in solution. This issue has been widely reported with such class of NHC-coordinated Ru complex.^{31, 32, 48}

The effect of the precatalyst structure was also examined. Upon replacing **Ru-1** by **Ru-2**, the rate of polymerization slightly decreased (69 %, *entry g*). By the same reasoning used above to explain latency, it was expected that catalyst activity would decrease from Cl to I. This result is also consistent with previous investigations about the lower catalytic activity of $RuI_2(\text{arene})(\text{phosphine})$ complexes.⁴⁹ In this case, there are consequently less backbiting reactions, resulting in polymer with higher molecular weight and a fairly narrow dispersity index. **Ru-3** precatalyst (*entry h*) led to similar conversions, but the polymer was not soluble in THF, indicative of an even lower initiation efficiency.

Our photocatalytic system was also active in the ROMP of ENB. The results are summarized in **Table 4.4**. The reaction process was performed under similar conditions to those described for NB, except for irradiation time that was extended to 10 min. Indeed, we expect that a functional NB derivative such as ENB would be less reactive due to a greater steric crowding. Accordingly, only 64 % conversion was achieved after 10 min irradiation at 365 nm and lower M_n values were obtained (*entry a*). The influence of sensitizer concentration (*entry b*), excitation wavelength (*entry c*) and precatalyst nature (*entries d-e*) are consistent with previous observations.

Table 4.4. Photopolymerization results of ENB using Ru dimer/ $IMesH^+BPh_4^-$ /ITX photoinitiating system in CD_2Cl_2 ($[ENB] = 1 \text{ M}$, 510 equiv.). Irradiation conditions: 365 nm, $6.5 \text{ mW}\cdot\text{cm}^{-2}$, 10 min.

Entry	Precatalyst	Precatalyst/1/ITX equiv.	Conv. ^a %	M_{n-th} ^c $\text{kg}\cdot\text{mol}^{-1}$	M_{n-GPC} ^d $\text{kg}\cdot\text{mol}^{-1}$	\mathcal{D}^d
<i>a</i>	Ru-1	1/5/2.5	64	20	37.9	5.6
<i>b</i>	Ru-1	1/5/5	84	26	40.7	6.0
<i>c^e</i>	Ru-1	1/5/2.5	11	3	28.1	4.6
<i>d</i>	Ru-2	1/5/2.5	71	22	55.6	2.7
<i>e</i>	Ru-3	1/5/2.5	78	24	31.6	4.7

Refer to **Table 4.3** for superscript information

e. Mechanism of catalyst activation

Our approach relies on the in situ formation of an active Ru-arene complex from reaction between $[\text{RuCl}_2(p\text{-cymene})]_2$ **Ru-1** and the photogenerated **IMes** ligand. However, the presumed NHC-coordinated catalyst **Ru-1-IMes** identified in this study (section b) as the active metathesis catalyst lacks a suitable metal–carbene fragment to initiate ROMP. The literature reports an ill-defined mechanism involving *p*-cymene decoordination and a subsequent reaction between the resultant highly unsaturated ruthenium and a cyclic olefin as being accountable to the formation of active species.^{31,50} This last section questions the role(s) played by irradiation (365 nm) in this mechanism. As established earlier, light has a clear role in the generation of NHC ligand (section a). Bench stability experiments (section b) also demonstrate a second role in the disengagement of the η^6 -arene ligand. To shed further light on the other possible effects of light on polymerization mechanism, NB conversion kinetics was measured in situ by real-time FTIR spectroscopy. For this, the reactive monomer mixture was introduced in a liquid IR cell. IR spectra were acquired continuously during UV exposure (LED spotlight 365 nm) in order to construct a conversion-time curve. **Figure 4.2** shows a typical conversion-time curve while alternating between periods of radiation exposure (white area) and dark (grey area). Surprisingly from the mechanistic hypothesis, a temporal control of polymer chain growth was demonstrated through intermittent exposure of the reaction to UV light since an almost stop of polymerization was observed when light was switched off. This result is in apparent contradiction with the hypothesis of a formation of an active Ru catalyst whose activity could be preserved without irradiation. While almost no conversion occurred in the dark (off periods), polymerization could be re-initiated by re-exposure to light. This has been attributed to the fact that radiation might promotes the multiple insertion of new NB units into the propagating center.^{33,40,51}

Further experiments, in particular to study the effect of irradiance and wavelength, are required to understand the complete role by irradiation. Nevertheless, one can propose a putative reaction mechanism (**Scheme 4.2**) for the ROMP photoinitiation. First, the active complex $\text{RuCl}_2(\text{arene})(\text{NHC})$ **Ru-1-IMes** is subjected to the rapid loss of *p*-cymene ring upon photochemical activation to form an unsaturated Ru species **A**.^{33,40,51} As a subsequent step, the insertion of NB into the metal center occurs to form the Ru complex $\text{RuCl}_2(\text{IMes})(\text{NB})$ **B**. Then a sigmatropic [1,2-*H*] rearrangement leads to the formation of a ruthenium-alkylidene complex **C** (initiating species).⁴⁷ The next steps follow the typical chain-growth polymerization mechanism involving the metallacyclization and cycloreversion steps, with

the particularity that the insertion of new cyclic olefin molecules could be facilitated by light. According to this proposed mechanism, unsuccess in the ROMP of cyclooctene probably relates to the restrictive [1,2-*H*] rearrangement of such monomer.⁴⁷ On the other hand, a local excess of **IMes** photogenerated is supposed to afford a bis(**IMes**)-Ru.⁵¹ Unfortunately, it is well-known that the bis-NHC ligated Ru analogue is inactive at ambient temperature owing to its difficulty in dissociating of one NHC ligand to form the active species **C**.^{23,52} Thus, total number of active ROMP **C** decreases and thus producing the polymer with M_n that is significantly higher than its theoretical value.

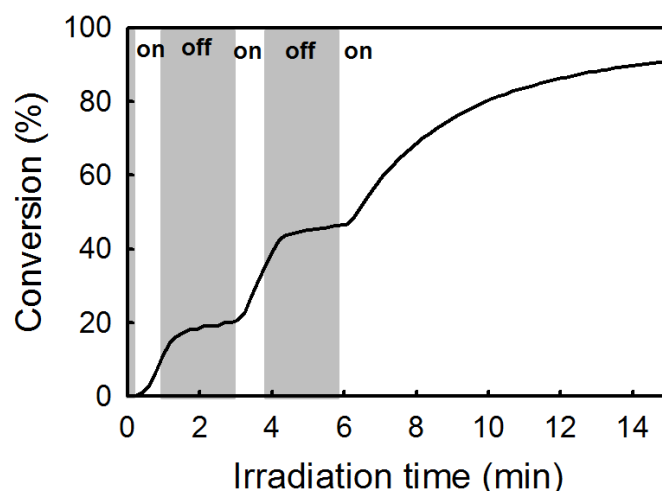
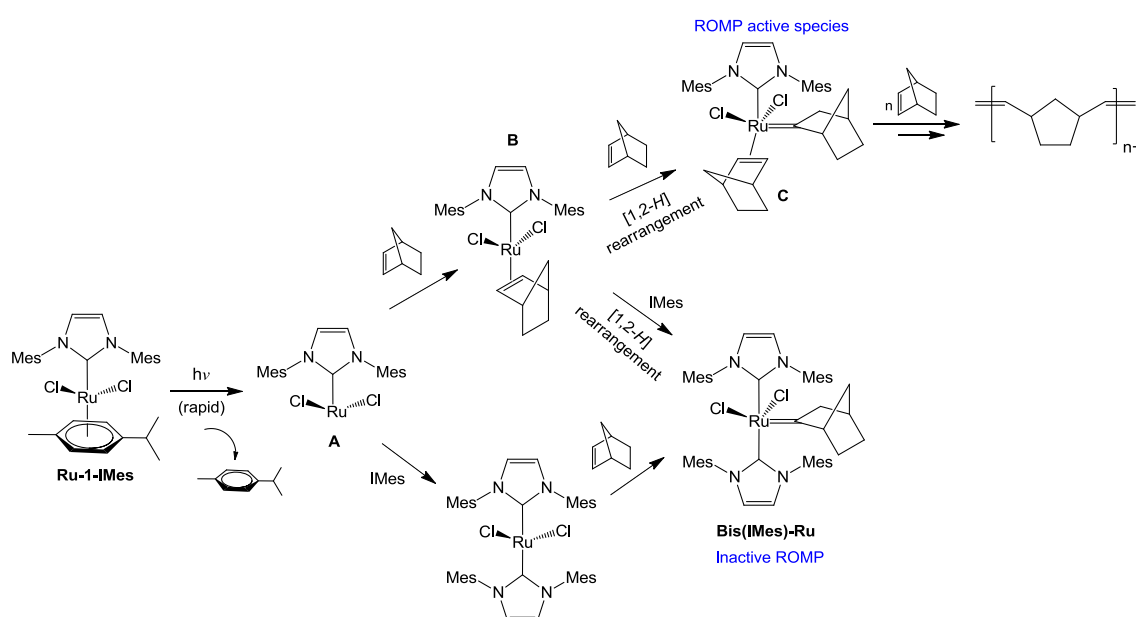


Figure 4.2. Conversion-time curve for the ROMP of NB in solution in CH_2Cl_2 : light off (grey area), light on (white area). NB/**Ru-1**/**ITX** = 510/1/5/0.5 equiv. Irradiation conditions: LED@365 nm, 65 $\text{mW}\cdot\text{cm}^{-2}$.



Scheme 4.2. Proposed photoactivation mechanism of Noels' catalyst.

4.3.2. Preparation of cross-linked ROMP polymer films

a. Scouting experiments

For the preparation of UV-cured films by photoactivated ROMP, emphasis has been made on DCPD because this monomer is able to form a cross-linked structure with high stiffness and impact resistance.⁵³ To assess to which extent DCPD could react with our photocatalytic system (**Ru-1/1/ITX**), preliminary tests were carried in CH₂Cl₂ by monitoring the photopolymerization kinetics using real-time FTIR. **Figure 4.3** shows a typical conversion kinetics of DCPD, together with that of NB. As expected, DCPD exhibited a much slower polymerization rate compared to NB.⁵⁴⁻⁵⁶ To increase reactivity and achieve a cross-linked structure unattainable with NB only, we proposed a copolymerization of DCPD with NB.^{13,55} As shown on the same plot, a mixture of DCPD/NB (50/50 mol%) resulted in intermediate polymerization rates and almost full conversion after 30 min irradiation.

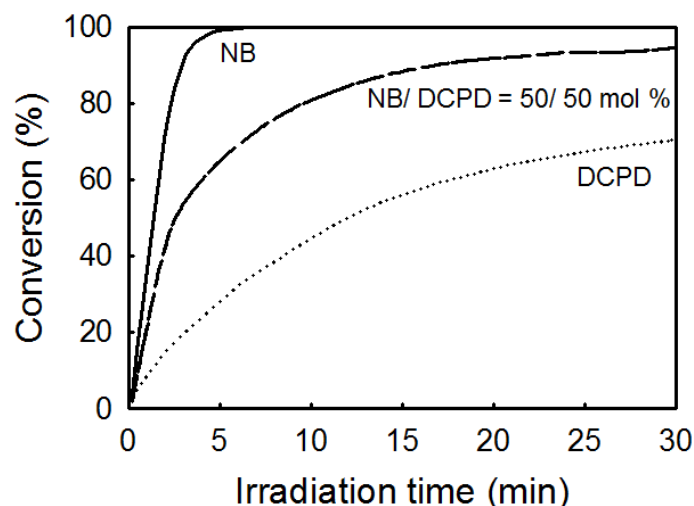


Figure 4.3. Photopolymerization kinetic of NB, DCPD and NB/DCPD (50/50 mol%) using photocatalyst system **Ru-1/1/ITX** in CH₂Cl₂ (Monomer/**Ru-1/1/ITX** = 510/1/5/2.5 equiv.). Conversions of NB, NB/DCPD (50/50 mol%) and DCPD were 100 %, 94 % and 70, respectively.

Given the potential of this approach, a range of different (co)polymer films were prepared from a mixture of NB and DCPD (NB-25: 25/75 mol%; NB-50: 50/50 mol% and NB-75: 75/25 mol%). For comparison, two control experiments using NB (NB-100) and DCPD (DCPD-100) alone were also performed under similar conditions. As can be seen in **Figure 4.4**, a mixture of monomer and photocatalyst dissolved in CH₂Cl₂ was placed in a Teflon mold, covered with a glass slide to avoid evaporation, and irradiated for 1 h through a LED panel (365 nm, 5.5 mW·cm⁻²) (see experimental section for details). The gels were then dried, and characterized using a range of spectroscopic techniques (FTIR-ATR, ¹³C CPMAS), gravimetry, gel content, TGA, DSC, AFM and SEM. All these techniques are intended to

give insight into the structure of the polymer, and in particular the possibility of cross-linking. With regard to this last point, **Scheme 4.3** shows the various possible structures arising from the copolymerization of DCPD with NB. We assume that the two norbornenyl-derived double bonds from DCPD and NB could copolymerize first, resulting in the formation a linear backbone. Much less reactive is the cyclopentene-derived double bond which can react subsequently to form a cross-linked network. It has been established that the pendant cyclopentene ring from DCPD monomer may react via two possible pathways: ROMP and olefin addition through radical coupling.^{35,57,58}

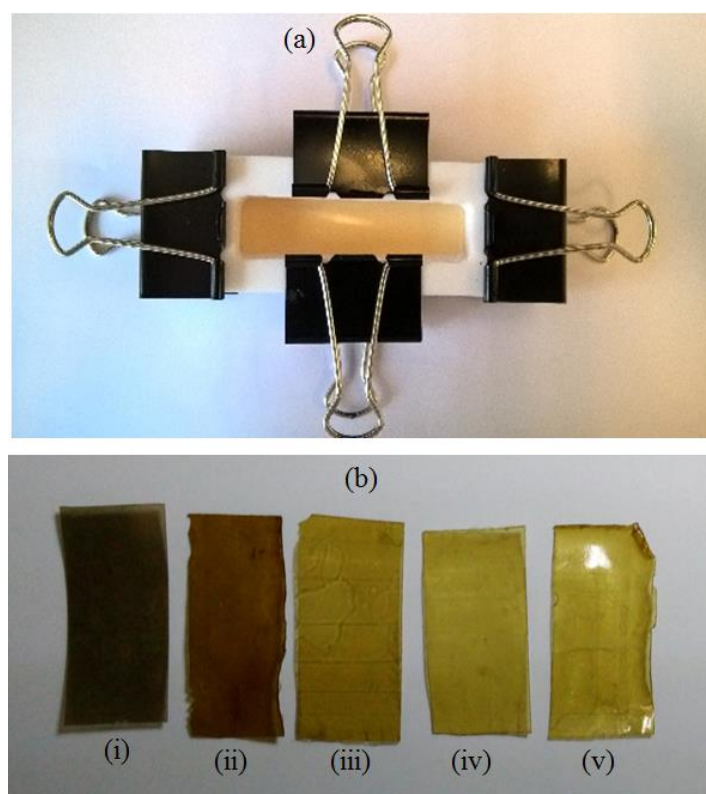
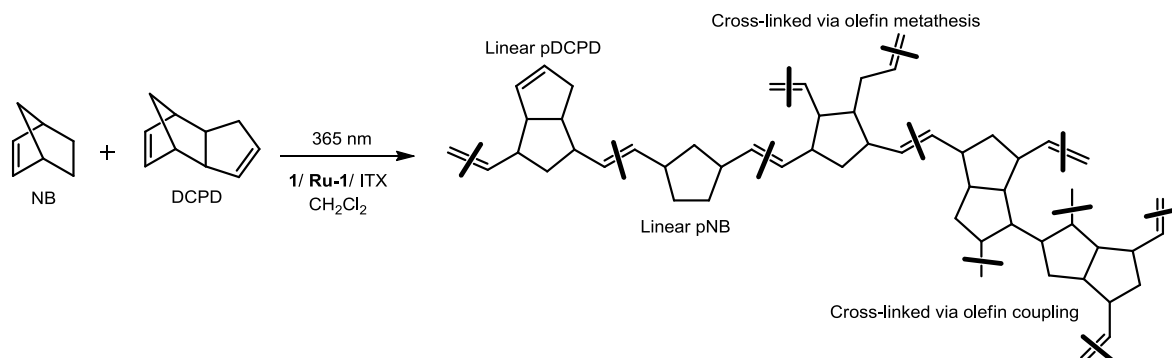


Figure 4.4. Photographs of: (a) General set up for the preparation of cross-linked films and (b) Images of polymeric films (i) NB-100, (ii) NB-75, (iii) NB-50, (iv) NB25 and (v) DCPD-100.



Scheme 4.3. Schematic preparation of a cross-linked film through ROMP of NB and DCPD.

b. Polymer yield and gel content

Polymer yield and gel contents were determined for the NB/DCPD-based films containing different NB loadings (**Figure 4.5**). As expected, owing to lower relative reactivity of DCPD compared to that of NB monomer, there is a gradual decrease of the polymer yield at higher concentrations in DCPD. Indeed, the reaction was almost quantitative for NB-100 (yield > 98 %) while the yield was minimal for DCPD-100 (50 %). Between these two homopolymers, the hybrid samples displayed a continuous range of intermediate values. To assess the possible formation of cross-linked network, the gel fraction of the cured specimens was also evaluated. NB-100 film devoid of DCPD showed consistently no gel content, and in agreement the formation of linear chains. The gel fraction of the films steadily increased with addition of more DCPD, but never reached 100 wt%. This result suggests that our photocatalytic system makes possible the cross-linking of a fraction of cyclopentene rings. This is in contrast with 1st generation Grubbs catalysts which are effective only at polymerizing the norbornene ring.^{53,59,60}

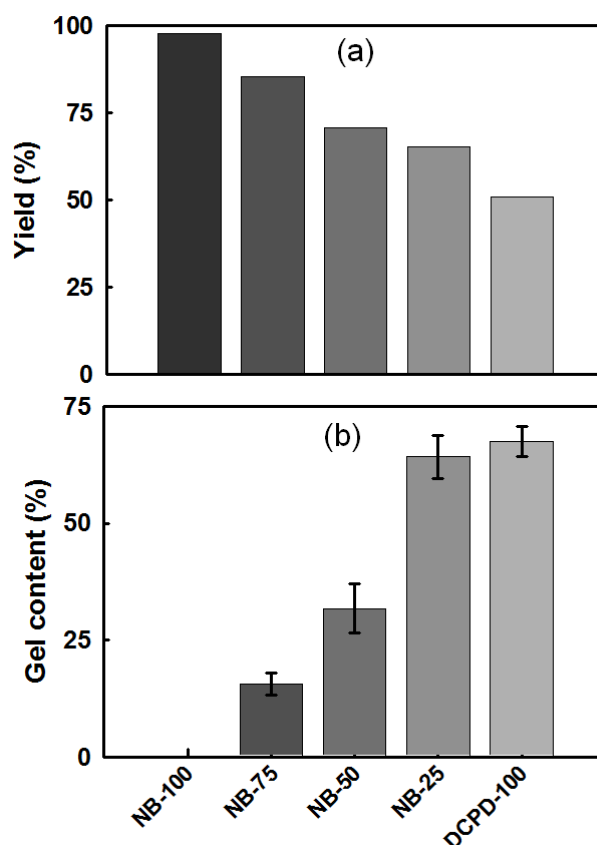


Figure 4.5. Characterizations of different polymeric specimens: (a) Polymer yield determined by gravimetry method and (b) Gel content determined by extracting with CH_2Cl_2 .

c. FTIR spectroscopy

Turning to chemical structure, the same series of five films was analyzed by ATR-FTIR spectroscopy. In **Figure 4.6A**, all spectra show the absence of signal at 1566 cm^{-1} ascribed to the alkene C=C stretching vibration of norbornenyl groups (present indistinctly in NB or DCPD).^{28,61} This suggests that norbornenyl rings were either completely reacted or removed upon drying. Because cyclopentene has a lower ring strain than NB, the frequency of the C=C stretching vibration is decreased and generally arises at $\sim 1610 - 1650\text{ cm}^{-1}$. The $\nu(\text{C}=\text{C})$ of the internal double bond of cyclopentene is not visible in our system regardless of DCPD content.

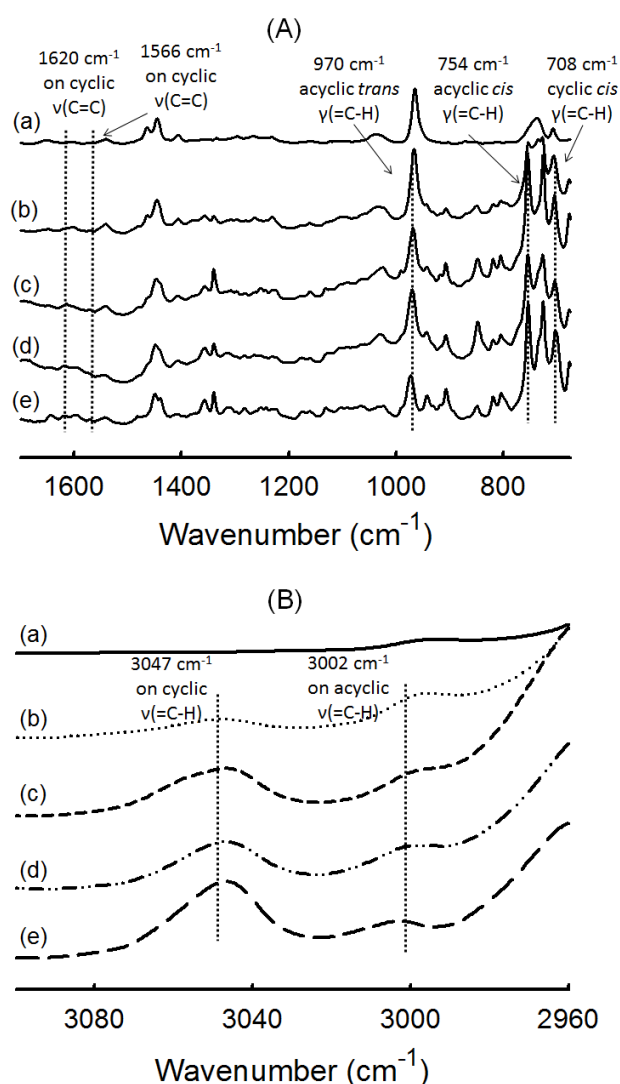


Figure 4.6. FTIR- ATR spectra of polymer films obtained by photoROMP at 365 nm: (a) NB-100, (b) NB-75, (c) NB-50, (d) NB-25 and (e) DCPD-100: **(A)** Expanded spectra in a range of $675 - 1700\text{ cm}^{-1}$ and **(B)** Expanded spectra in a range of $2960 - 3100\text{ cm}^{-1}$.

However, it is difficult to draw conclusions because this vibrational mode as it generally gives rise to a weakly intense band. To estimate the presence of cyclopentene rings, it is more reliable to look at the specific out-of-plane deformation vibration at $\sim 710\text{ cm}^{-1}$. Clearly visible at 708 cm^{-1} , its presence supports an incomplete cross-linking process.⁵⁸ The signals at 970 cm^{-1} and 754 cm^{-1} are attributed to the deformation vibrations of $=\text{C-H}$ bonds on *trans* and *cis* acyclic double bonds, respectively.^{58,62,62} They indicate that the chain backbone is made up of a mixture of both *trans*- and *cis*-disubstituted alkene $-(\text{CH}=\text{CH})-$ in accordance with a ROMP mechanism. The $=\text{C-H}$ stretching region at $3000 - 3100\text{ cm}^{-1}$ is also informative because it is not overlapped by alkane C-H stretching absorption occurring below 3000 cm^{-1} . As shown in **Figure 4.6B**, we found two broad signals at 3047 cm^{-1} and 3002 cm^{-1} in the spectra of polymer films containing DCPD, readily ascribed to the $=\text{C-H}$ stretching of $-\text{CH}=\text{CH}-$ vinylene groups. The higher frequency can be associated to cyclic olefins (residual cyclopentene) while the second signal at 3002 cm^{-1} reflects acyclic olefin (cyclopentene reacted by ROMP).^{35,61,63} In conclusion, the FTIR data of DCPD-based films show a partial cross-linking, which occurs through a metathesis mechanism. The possibility of cross-linking via olefin coupling was studied in the next section using solid state ^{13}C NMR.

d. CPMAS ^{13}C NMR

In **Figure 4.7**, the ^{13}C CPMAS spectra of the different NB/DCPD samples display strong similarities. The region at $\sim 130\text{ ppm}$ represents olefinic carbons ($\text{sp}^2\text{-C}$) while the signals at $30 - 60\text{ ppm}$ is reflective of aliphatic carbons ($\text{sp}^3\text{-C}$). As mentioned above, the $\text{C}=\text{C}$ double bonds of cyclopentene ring can undergo either metathesis or olefin coupling reactions. Of interest is that CPMAS ^{13}C -NMR can be used to estimate the contribution of olefin coupling. Occurrence of olefin coupling is manifested by the conversion of two sp^2 carbons (from cyclopentene) into two sp^3 carbons (**Scheme 4.3**). Consequently, the ratio of integrated area of $\text{sp}^2\text{-C}$ and $\text{sp}^3\text{-C}$ gives access to the fraction x of cyclopentene involved in olefin coupling (see experimental section for calculation details).^{35,64} Our calculations reveal a significant contribution from olefin coupling which ranges from 11 to 34 %. Olefin coupling of cyclopentene ring tends to increase with a higher concentration of NB: 11 % (DCPD-100) < 22 % (NB-25) < 26 % (NB-50) < 34 % (NB-75). This trend can be rationalized on the basis that ROMP of NB is known to be highly exothermic and that olefin coupling is activated by heat.⁵⁷

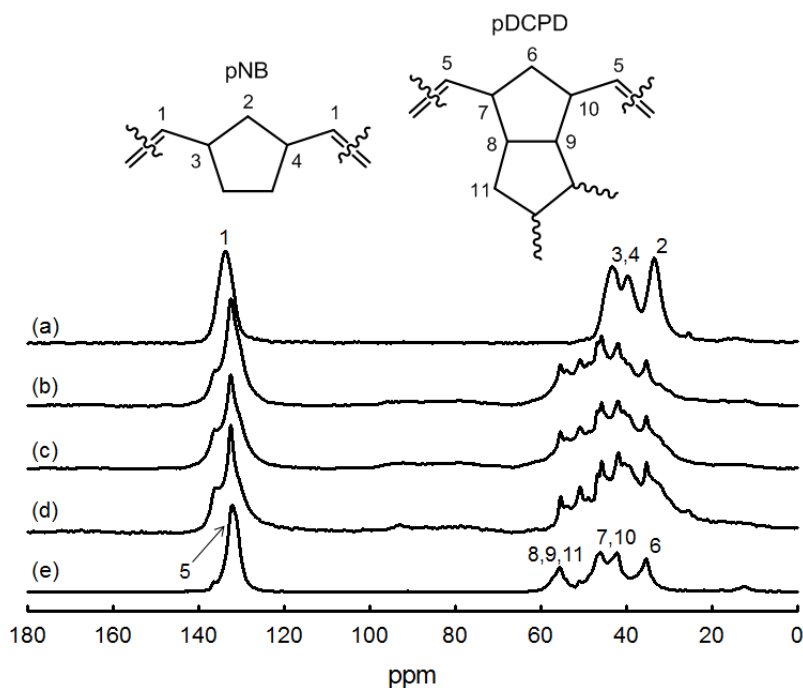


Figure 4.7. ^{13}C NMR CPMAS spectra of polymeric films: (a) NB-100, (b) NB-75, (c) NB-50, (d) NB-25 and (e) DCPD-100.

e. Thermal analysis

The same series of NB/DCPD-based specimens was analyzed by DSC and TGA under N_2 . As shown in **Figure 4.8A**, the DSC thermograms indicate a strong impact of DCPD content on the glass transition temperature (T_g). As expected, the lowest T_g value was found in **Table 4.5** for pure polynorbornene (pNB) (NB-100); the value of 27 °C is fully consistent with literature data.^{65,66} Upon increasing the content of DCPD, higher T_g values were gradually obtained, with a maximum of 114 °C found for DCPD-100. This tendency is likely to be caused by the increase of cross-linking density as more cyclopentene rings react. In the literature, the T_g of polydicyclopentadiene (pDCPD) generally ranges from 53–165 °C.^{53,54} Hence, our intermediate T_g value agrees with a significant fraction of non-reacted cyclopentene rings as evidenced by FTIR and solid-state NMR. The TGA traces in **Figure 4.8B** are much less dependent on the DCPD concentration and show systematically two distinct decomposition regions. The gradual weight loss during the first decomposition stage arising at 200 °C is suggestive of low-molecular weight chains decomposition. Because of its sluggish polymerization rates, pure pDCPD is likely to contain a higher fraction of short linear chains. This drives a weight loss at low temperature that is significantly more marked than for NB-samples. During second decomposition stage taking place at 400 – 500 °C, all curves exhibited a serious decline in the weight loss, illustrating prompt degradation of main

polymer chains.^{53,67} DCPD-100 showed the greatest thermal stability. A slight and progressive decrease was noted upon increasing NB loading. This is consistent with the drop of cross-linking density.⁶⁷ Also noteworthy is that a single main decomposition peak is observed regardless of NB content, suggesting a good homogeneity of the copolymer network. All samples left practically char coal residues with the highest amount of 23 % from DCPD-100 at high temperature.

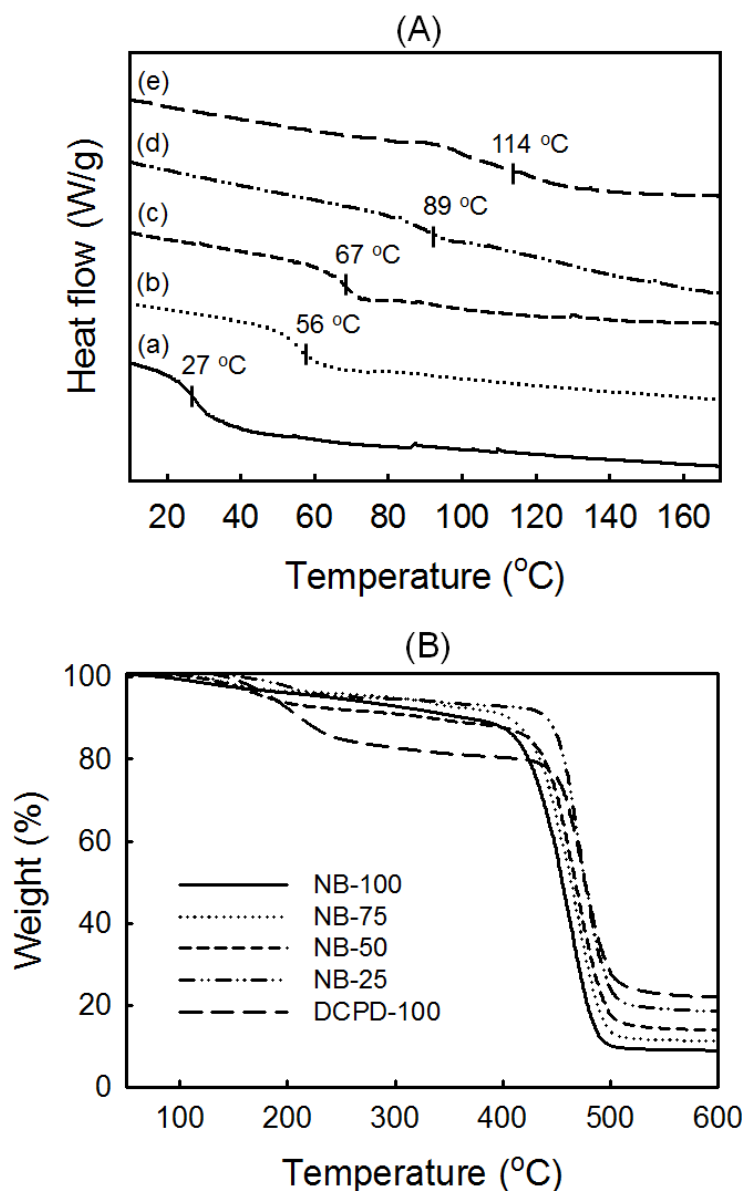


Figure 4.8. (A) Glass transition temperature as measured by DSC of different polymer films in nitrogen with (a) NB-100, (b) NB-75, (c) NB-50, (d) NB-25 and (e) DCPD-100 and (B) TGA thermograms of different polymer films obtained as heating under nitrogen environment.

Table 4.5. Thermo-mechanical results of curing NB/ DCPD films using **Ru-1/1/ITX** photoinitiating system in CH₂Cl₂. Irradiation conditions: 365 nm, 5.5 mW·cm⁻².

Sample	T_g^a (°C)	$T_{10\%}^b$ (°C)	T_{max}^c (°C)	E^d (GPa)
NB-100	27	345	454	1.82 ± 0.13
NB-75	56	397	460	1.51 ± 0.03
NB-50	67	302	464	1.43 ± 0.07
NB-25	89	437	472	1.36 ± 0.03
DCPD-100	114	207	474	1.23 ± 0.08

^a Glass transition temperature determined by DSC, ^bThe temperature at which 10 % weight loss occurring determined by TGA, ^cThe temperature at which maximum weight loss occurring determined by TGA and ^d Young's modulus determined by AFM.

f. AFM and microscopy study

The Young's modulus (E) which represents elasticity does not vary largely upon changing the incorporation ratio of NB in copolymers (**Table 4.5**). Generally, the configuration of polymeric structures can have a highly influence on the E value. Herein, the polymer films, consisting of a binary blend of the *trans* and *cis* configuration on the polymeric backbone, are more malleable than the ones initiated by Ru complex without NHC ligand.⁵⁵ Besides, a highly brittle structure of pure pNB, showing a higher E value, is likely responsible for a moderate increase of E with NB feeding. The microstructure of the ruptured solid films has been observed by scanning electron microscopy (SEM), as presented in **Figure 4.9**. Consistent with literature,⁶⁷ the higher DCPD loading is, the relative smoother the surface morphology is. This characteristic is in accordance with the increase in π -interaction of double bonds which exhibits better packing of the polymeric chains.^{67,68}

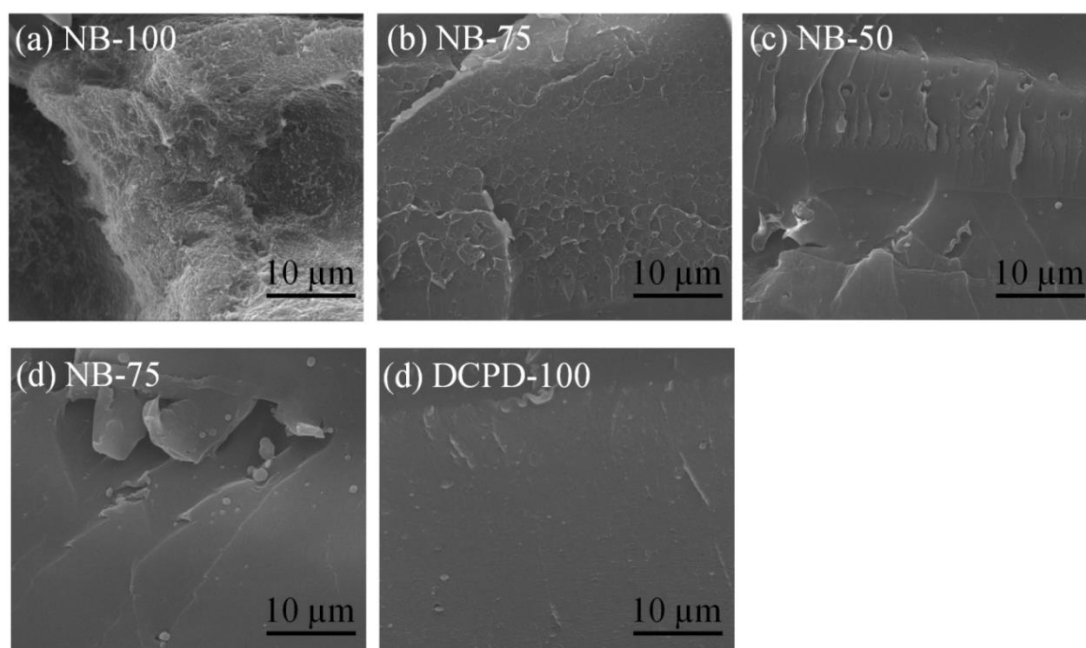


Figure 4.9. SEM images of the fracture surface of homo and copolymer specimens with 5000 \times magnification.

4.4. CONCLUSIONS

We have demonstrated that cross-linked polymer films could be produced under UV irradiation through the copolymerization of NB with DCPD. The approach for photoactivated olefin metathesis used a NHC photogenerator ($\text{IMesH}^+\text{BPh}_4^-$ and ITX) combined with an inactive Ru precatalyst (**Ru-1**, **Ru-2** and **Ru-3**). Though the detailed mechanism of photoactivation remains uncertain, an active NHC-coordinated Ru-arene complex is presumed to form by reaction between the ruthenium precatalyst and the photogenerated NHC **IMes**. Irradiation at 365 nm was also proved to have a critical role in the formation of the active metathesis species by promoting the decoordination of the *p*-cymene ligand and the multiple insertions of new NB units into the propagating center. The films are homogeneous, and the possibility of cross-linking was attested by the measurement of gel contents (10 – 70 %) and the rising T_g value when increasing DCPD loading. FTIR data show a complete conversion of norbornenyl group in both monomers, but an incomplete ring-opening of the cyclopentene pendant group from DCPD. This lower ring-strained cyclic olefin is subjected to metathesis but also olefin addition reactions as evidenced by ^{13}C solid-state NMR. We anticipate that photoROMP of NB and DCPD derivatives will enable the development of more UV-curable coatings with chemical, thermal and mechanical properties currently not attainable with a conventional radical photopolymerization.

4.5. REFERENCES

- 1 J. B. Matson and R. H. Grubbs, Synthesis of Fluorine-18 Functionalized Nanoparticles for use as in vivo Molecular Imaging Agents, *J. Am. Chem. Soc.*, 2008, **130**, 6731–6733.
- 2 X. Bantreil and S. P. Nolan, Synthesis of N-heterocyclic carbene ligands and derived ruthenium olefin metathesis catalysts, *Nat. Protoc.*, 2011, **6**, 69–77.
- 3 K. J. Arrington, J. B. Waugh, S. C. Radzinski and J. B. Matson, Photo- and Biodegradable Thermoplastic Elastomers: Combining Ketone-Containing Polybutadiene with Polylactide Using Ring-Opening Polymerization and Ring-Opening Metathesis Polymerization, *Macromolecules*, 2017, **50**, 4180–4187.
- 4 P. Schwab, M. B. France, J. W. Ziller and R. H. Grubbs, A Series of Well-Defined Metathesis Catalysts–Synthesis of $[\text{RuCl}_2(=\text{CHR})(\text{PR}_3)_2]$ and Its Reactions, *Angew. Chem. Int. Ed.*, 1995, **34**, 2039–2041.
- 5 R. R. Schrock, J. S. Murdzek, G. C. Bazan, J. Robbins, M. DiMare and M. O'Regan, Synthesis of molybdenum imido alkylidene complexes and some reactions involving acyclic olefins, *J. Am. Chem. Soc.*, 1990, **112**, 3875–3886.
- 6 M. Scholl, S. Ding, C. W. Lee and R. H. Grubbs, Synthesis and Activity of a New Generation of Ruthenium-Based Olefin Metathesis Catalysts Coordinated with 1,3-Dimesityl-4,5-dihydroimidazol-2-ylidene Ligands, *Org. Lett.*, 1999, **1**, 953–956.
- 7 J. Huang, E. D. Stevens, S. P. Nolan and J. L. Petersen, Olefin Metathesis-Active Ruthenium Complexes Bearing a Nucleophilic Carbene Ligand, *J. Am. Chem. Soc.*, 1999, **121**, 2674–2678.
- 8 S. B. Garber, J. S. Kingsbury, B. L. Gray and A. H. Hoveyda, Efficient and Recyclable Monomeric and Dendritic Ru-Based Metathesis Catalysts, *J. Am. Chem. Soc.*, 2000, **122**, 8168–8179.
- 9 C. W. Bielawski and R. H. Grubbs, Highly Efficient Ring-Opening Metathesis Polymerization (ROMP) Using New Ruthenium Catalysts Containing N-Heterocyclic Carbene Ligands, *Angew. Chem. Int. Ed.*, 2000, **39**, 2903–2906.
- 10 W. A. Green, Industrial Photoinitiators - A Technical Guide, *J. Mol. Catal. Chem.*, 2010, **213**, 39–45.
- 11 Z. Yao, L. Zhou, B. Dai and K. Cao, Ring-opening metathesis copolymerization of dicyclopentadiene and cyclopentene through reaction injection molding process, *J. Appl. Polym. Sci.*, 2012, **125**, 2489–2493.
- 12 J. Asrar, Reaction injection molding (RIM) system based on metathesis, *J. Appl. Polym. Sci.*, 1993, **47**, 289–293.
- 13 A. E. Goetz and A. J. Boydston, Metal-Free Preparation of Linear and Cross-Linked Polydicyclopentadiene, *J. Am. Chem. Soc.*, 2015, **137**, 7572–7575.
- 14 A. Ben-Asuly, E. Tzur, C. E. Diesendruck, M. Sigalov, I. Goldberg and N. G. Lemcoff, A Thermally Switchable Latent Ruthenium Olefin Metathesis Catalyst, *Organometallics*, 2008, **27**, 811–813.
- 15 C. Slugovc, D. Burtcher, F. Stelzer and K. Mereiter, Thermally Switchable Olefin Metathesis Initiators Bearing Chelating Carbenes: Influence of the Chelate's Ring Size, *Organometallics*, 2005, **24**, 2255–2258.
- 16 M. Barbasiewicz, A. Szadkowska, R. Bujok and K. Grela, Structure and Activity Peculiarities of Ruthenium Quinoline and Quinoxaline Complexes: Novel Metathesis Catalysts, *Organometallics*, 2006, **25**, 3599–3604.
- 17 A. Piermattei, S. Karthikeyan and R. P. Sijbesma, Activating catalysts with mechanical force, *Nat. Chem.*, 2009, **1**, 133–137.

-
- 18 A. Ben-Asuly, A. Aharoni, C. E. Diesendruck, Y. Vidavsky, I. Goldberg, B. F. Straub and N. G. Lemcoff, Photoactivation of Ruthenium Olefin Metathesis Initiators, *Organometallics*, 2009, **28**, 4652–4655.
 - 19 A. Aharoni, Y. Vidavsky, C. E. Diesendruck, A. Ben-Asuly, I. Goldberg and N. G. Lemcoff, Ligand Isomerization in Sulfur-Chelated Ruthenium Benzylidenes, *Organometallics*, 2011, **30**, 1607–1615.
 - 20 Y. Ginzburg, A. Anaby, Y. Vidavsky, C. E. Diesendruck, A. Ben-Asuly, I. Goldberg and N. G. Lemcoff, Widening the Latency Gap in Chelated Ruthenium Olefin Metathesis Catalysts, *Organometallics*, 2011, **30**, 3430–3437.
 - 21 B. K. Keitz and R. H. Grubbs, A Tandem Approach to Photoactivated Olefin Metathesis: Combining a Photoacid Generator with an Acid Activated Catalyst, *J. Am. Chem. Soc.*, 2009, **131**, 2038–2039.
 - 22 A. Y. Khalimon, E. M. Leitao and W. E. Piers, Photogeneration of a Phosphonium Alkylidene Olefin Metathesis Catalyst, *Organometallics*, 2012, **31**, 5634–5637.
 - 23 C. Theunissen, M. A. Ashley and T. Rovis, Visible-Light-Controlled Ruthenium-Catalyzed Olefin Metathesis, *J. Am. Chem. Soc.*, 2019, **141**, 6791–6796.
 - 24 O. Eivgi and N. Lemcoff, Turning the Light On: Recent Developments in Photoinduced Olefin Metathesis, *Synthesis*, 2018, **50**, 49–63.
 - 25 R. A. Weitekamp, H. A. Atwater and R. H. Grubbs, Photolithographic Olefin Metathesis Polymerization, *J. Am. Chem. Soc.*, 2013, **135**, 16817–16820.
 - 26 D. Wang, K. Wurst, W. Knolle, U. Decker, L. Prager, S. Naumov and M. R. Buchmeiser, Cationic RuII Complexes with N-Heterocyclic Carbene Ligands for UV-Induced Ring-Opening Metathesis Polymerization, *Angew. Chem. Int. Ed.*, 2008, **47**, 3267–3270.
 - 27 D. Wang, K. Wurst and M. R. Buchmeiser, Cationic versus Neutral RuII-N-Heterocyclic Carbene Complexes as Latent Precatalysts for the UV-Induced Ring-Opening Metathesis Polymerization, *Chem.: Eur. J.*, 2010, **16**, 12928–12934.
 - 28 J. Pinaud, T. K. H. Trinh, D. Sauvanier, E. Placet, S. Songsee, P. Lacroix-Desmazes, J.-M. Becht, B. Tarablsi, J. Lalevée, L. Pichavant, V. Héroguez and A. Chemtob, In Situ Generated Ruthenium-Arene Catalyst for Photoactivated Ring-Opening Metathesis Polymerization through Photolabile N-Heterocyclic Carbene Ligand, *Chem.: Eur. J.*, 2018, **24**, 337–341.
 - 29 T. Thi Kim Hoang, M. Jean-Pierre, M.-S. Fabrice, P. Julien, L.-D. Patrick, R. Corine, H. Valérie and C. Abraham, Mixture of azolium tetraphenylborate with isopropylthioxanthone: a new class of N-heterocyclic carbene (NHC) photogenerator for polyurethane, polyester and ROMP polymers synthesis, *Chem.: Eur. J.*, 2019, DOI: doi.org/10.1002/chem.201901000.
 - 30 W. A. Herrmann, M. Alison, J. Fischer, C. Köcher and G. R. J. Artus, N-Heterocyclic Carbenes: Generation under Mild Conditions and Formation of Group 8–10 Transition Metal Complexes Relevant to Catalysis, *Chem.: Eur. J.*, 1996, **2**, 772–780.
 - 31 A. Tudose, A. Demonceau and L. Delaude, Imidazol(in)ium-2-carboxylates as N-heterocyclic carbene precursors in ruthenium–arene catalysts for olefin metathesis and cyclopropanation, *J. Organomet. Chem.*, 2006, **691**, 5356–5365.
 - 32 L. Delaude, M. Szypa, A. Demonceau and A. F. Noels, New In situ Generated Ruthenium Catalysts Bearing N-Heterocyclic Carbene Ligands for the Ring-Opening Metathesis Polymerization of Cyclooctene, *Adv. Synth. Catal.*, 2002, **344**, 749.

-
- 33 L. Delaude, A. Demonceau and A. F. Noels, Visible light induced ring-opening metathesis polymerisation of cyclooctene, *Chem. Commun.*, 2001, 986–987.
- 34 L. Jafarpour, J. Huang, E. D. Stevens and S. P. Nolan, (p-cymene)RuLCl₂ (L = 1,3-Bis(2,4,6-trimethylphenyl)imidazol-2-ylidene and 1,3-Bis(2,6-diisopropylphenyl)imidazol-2-ylidene) and Related Complexes as Ring Closing Metathesis Catalysts, *Organometallics*, 1999, **18**, 3760–3763.
- 35 D. P. Mohite, S. Mahadik-Khanolkar, H. Luo, H. Lu, C. Sotiriou-Leventis and N. Leventis, Polydicyclopentadiene aerogels grafted with PMMA: I. Molecular and interparticle crosslinking, *Soft Matter*, 2013, **9**, 1516–1530.
- 36 J. D. Wilkey and G. B. Schuster, Irradiation of tetraphenylborate does not generate a borene anion, *J. Org. Chem.*, 1987, **52**, 2117–2122.
- 37 X. Sun, J. P. Gao and Z. Y. Wang, Bicyclic Guanidinium Tetraphenylborate: A Photobase Generator and A Photocatalyst for Living Anionic Ring-Opening Polymerization and Cross-Linking of Polymeric Materials Containing Ester and Hydroxy Groups, *J. Am. Chem. Soc.*, 2008, **130**, 8130–8131.
- 38 X. Sun, Development of tetraphenylborate-based photobase generators and sacrificial polycarbonates for radiation curing and photoresist applications. *PhD Thesis, Carleton University*, 2009.
- 39 A. V. Zhukhovitskiy, J. Geng and J. A. Johnson, Cycloelimination of Imidazolidin-2-ylidene N-Heterocyclic Carbenes: Mechanism and Insights into the Synthesis of Stable “NHC-CDI” Amidinates, *Chem.: Eur. J.*, 2015, **21**, 5685–5688.
- 40 Y. Zhang, D. Wang, P. Lönnecke, T. Scherzer and M. R. Buchmeiser, Novel Initiators for Thermally and UV-Triggered ROMP, *Macromol. Symp.*, 2006, **236**, 30–37.
- 41 A. Hafner, A. Mühlebach and P. A. van der Schaaf, One-Component Catalysts for Thermal and Photoinduced Ring Opening Metathesis Polymerization, *Angew. Chem. Int. Ed.*, 1997, **36**, 2121–2124.
- 42 E. L. Dias, S. T. Nguyen and R. H. Grubbs, Well-Defined Ruthenium Olefin Metathesis Catalysts: Mechanism and Activity, *J. Am. Chem. Soc.*, 1997, **119**, 3887–3897.
- 43 M. S. Sanford, J. A. Love and R. H. Grubbs, Mechanism and Activity of Ruthenium Olefin Metathesis Catalysts, *J. Am. Chem. Soc.*, 2001, **123**, 6543–6554.
- 44 L. Delaude, A. Demonceau and A. F. Noels, Probing the Stereoselectivity of the Ruthenium-Catalyzed Ring-Opening Metathesis Polymerization of Norbornene and Norbornadiene Diesters, *Macromolecules*, 2003, **36**, 1446–1456.
- 45 A. Demonceau, A. F. Noels, E. Saive and A. J. Hubert, Ruthenium-catalysed ring-opening metathesis polymerization of cycloolefins initiated by diazoesters, *J. Mol. Catal.*, 1992, **76**, 123–132.
- 46 L. Delaude, A. Demonceau and A. F. Noels, Synthesis and Application of New N-Heterocyclic Carbene Ruthenium Complexes in Catalysis: A Case Study, *Curr. Org. Chem.*, 2006, **10**, 203–215.
- 47 D. Wang, J. Unold, M. Bubrin, W. Frey, W. Kaim and M. R. Buchmeiser, Ruthenium(IV)-Bis(methallyl) Complexes as UV-Latent Initiators for Ring-Opening Metathesis Polymerization, *ChemCatChem*, 2012, **4**, 1808–1812.
- 48 M. Ahr, C. Thieuleux, C. Copéret, B. Fenet and J.-M. Basset, Noels’ vs. Grubbs’ Catalysts: Evidence for One Unique Active Species for Two Different Systems!, *Adv. Synth. Catal.*, 2007, **349**, 1587–1591.

-
- 49 A. Demonceau, A. W. Stumpf, E. Saive and A. F. Noels, Novel Ruthenium-Based Catalyst Systems for the Ring-Opening Metathesis Polymerization of Low-Strain Cyclic Olefins, *Macromolecules*, 1997, **30**, 3127–3136.
- 50 P. Alvarez, J. Gimeno and E. Lastra, Catalytic Synthesis of Polynorbornene and Polynorbornadiene of Low Polydispersity Index by $[\text{Ru}(\eta^5\text{-C}_9\text{H}_7)\text{Cl}(\text{COD})]$ (COD = 1,5-Cyclooctadiene), *Organometallics*, 2002, **21**, 5678–5680.
- 51 C. S. Day and D. E. Fogg, High-Yield Synthesis of a Long-Sought, Labile Ru-NHC Complex and Its Application to the Concise Synthesis of Second-Generation Olefin Metathesis Catalysts, *Organometallics*, 2018, **37**, 4551–4555.
- 52 T. M. Trnka, J. P. Morgan, M. S. Sanford, T. E. Wilhelm, M. Scholl, T.-L. Choi, S. Ding, M. W. Day and R. H. Grubbs, Synthesis and Activity of Ruthenium Alkylidene Complexes Coordinated with Phosphine and N-Heterocyclic Carbene Ligands, *J. Am. Chem. Soc.*, 2003, **125**, 2546–2558.
- 53 S. Saha, Y. Ginzburg, I. Rozenberg, O. Iliashevsky, A. Ben-Asuly and N. Gabriel Lemcoff, Cross-linked ROMP polymers based on odourless dicyclopentadiene derivatives, *Polym. Chem.*, 2016, **7**, 3071–3075.
- 54 J. Chen, F. P. Burns, M. G. Moffitt and J. E. Wulff, Thermally Crosslinked Functionalized Polydicyclopentadiene with a High Tg and Tunable Surface Energy, *ACS Omega*, 2016, **1**, 532–540.
- 55 G. Yang, T. C. Mauldin and J. K. Lee, Cure kinetics and physical properties of poly(dicyclopentadiene/5-ethylidene-2-norbornene) initiated by different Grubbs' catalysts, *RSC Adv.*, 2015, **5**, 59120–59130.
- 56 K. Nomura and X. Hou, Synthesis of vanadium–alkylidene complexes and their use as catalysts for ring opening metathesis polymerization, *Dalton Trans.*, 2016, **46**, 12–24.
- 57 T. A. Davidson, K. B. Wagener and D. B. Priddy, Polymerization of Dicyclopentadiene: A Tale of Two Mechanisms, *Macromolecules*, 1996, **29**, 786–788.
- 58 G. Raptopoulos, G. C. Anyfantis, D. Chriti and P. Paraskevopoulou, Synthesis and structural characterization of poly(dicyclopentadiene) gels obtained with a novel ditungsten versus conventional W and Ru mononuclear catalysts, *Inorganica Chim. Acta*, 2017, **460**, 69–76.
- 59 S. J. Cantrill, R. H. Grubbs, D. Lanari, K. C.-F. Leung, A. Nelson, K. G. Poulin-Kerstien, S. P. Smidt, J. F. Stoddart and D. A. Tirrell, Template-Directed Olefin Cross Metathesis, *Org. Lett.*, 2005, **7**, 4213–4216.
- 60 L. Gong, K. Liu, E. Ou, F. Xu, Y. Lu, Z. Wang, T. Gao, Z. Yang and W. Xu, ROMP of acetoxy-substituted dicyclopentadiene to a linear polymer with a high Tg, *RSC Adv.*, 2015, **5**, 26185–26188.
- 61 Q. Sun, S. Ma, Z. Ge and Y. Luo, Preparation and curing behavior of high-stress solid propellant binder based on polydicyclopentadiene, *High Perform. Polym.*, 2017, **29**, 931–936.
- 62 M. J. Abadie, M. Dimonie, C. Couve and V. Dragutan, New catalysts for linear polydicyclopentadiene synthesis, *Eur. Polym. J.*, 2000, **36**, 1213–1219.
- 63 S. Saha, Y. Ginzburg, I. Rozenberg, O. Iliashevsky, A. Ben-Asuly and N. Gabriel Lemcoff, Cross-linked ROMP polymers based on odourless dicyclopentadiene derivatives, *Polym. Chem.*, 2016, **7**, 3071–3075.
- 64 A. Bang, D. Mohite, A. M. Saeed, N. Leventis and C. Sotiriou-Leventis, Polydicyclopentadiene aerogels from first- versus second-generation Grubbs' catalysts: a molecular versus a nanoscopic perspective, *J. Sol-Gel Sci. Technol.*, 2015, **75**, 460–474.
- 65 R. F. Ohm and T. M. Vial, A New Synthetic Rubber Norsorex® Polynorbornene, *J. Elastomers Plast.*, 1978, **10**, 150–162.

-
- 66 A. M. Spring, D. Maeda, M. Ozawa, K. Odoi, F. Qiu, K. Yamamoto and S. Yokoyama, Glass transition temperature control by poly(norbornene-dicarboximide) copolymers, *Polym. Bull.*, 2015, **72**, 503–521.
- 67 M. R. Kessler and S. R. White, Cure kinetics of the ring-opening metathesis polymerization of dicyclopentadiene, *J. Polym. Sci. Part A: Polym. Chem.*, 2002, **40**, 2373–2383.
- 68 V. P. Carvalho, C. P. Ferraz and B. S. Lima-Neto, Tailored norbornene-based copolymer with systematic variation of norbornadiene as a crosslinker obtained via ROMP with alternative amine Ru catalysts, *Eur. Polym. J.*, 2012, **48**, 341–349.

GENERAL CONCLUSIONS

In the search of novel approaches to photolabile ROMP initiators, a NHC photogenerating system activable at 365 nm is reported, which is based on a mixture of azolium tetraphenylborate ($\text{NHCH}^+\text{BPh}_4^-$) and isopropylthioxanthone (ITX). Unlike conventional methods to generate in situ carbene that require strong bases, only mild and air-stable precursors are used and NHC ligand can be generated via a step-wise mechanism in which electron/proton transfer reactions occur sequentially. The photoinduced electron transfer (PET) reaction between BPh_4^- anion and $^3\text{ITX}^*$ is exergonic ($\Delta G_{\text{et}} = -0.07$ eV) and produces the ITX radical anion ($\text{ITX}^{\bullet-}$) and a boranyl radical (BPh_4^{\bullet}). According to the laser flash photolysis study, upon increasing the amount of BPh_4^- anion, $^3\text{ITX}^*$ was found to decay faster. The electron transfer rate k_q was evaluated from Stern-Volmer plot as $4.9 \times 10^7 \text{ M}^{-1}\cdot\text{s}^{-1}$, a value which is similar to the determined value of $\text{NaBPh}_4/\text{ITX}$ ($4.1 \times 10^7 \text{ M}^{-1}\cdot\text{s}^{-1}$). This highlights the role of BPh_4^- as electron donating species, and ITX as an electronically electron acceptor sensitizer, while excluding the role of azolium cation NHCH^+ in PET. The $\text{ITX}^{\bullet-}$ species is supposed to subsequently deprotonate the NHCH^+ cation to yield a ketyl radical (ITXH^{\bullet}) and the targeted NHC. Meanwhile, the BPh_4^{\bullet} radical undergoes further reactions: C–B bond cleavage and auto-oxidation give a biphenyl and diphenylborinic acid (Ph_2BOH), as proved by a combination of different characterization techniques including EPR, GC-MS and ^{11}B NMR spectroscopy.

The liberation of the desired NHC **IMes** is successfully identified via the transformation into **IMes**- CS_2 and **IMes**-radical adducts visible in ^{13}C NMR and EPR spectra, respectively. Unexpectedly, the carbene released can react with other species such as Ph_2BOH and $^3\text{ITX}^*$, thus affecting the overall yield of NHC. Evidence for the formation of **IMes**- Ph_2BOH complex was provided by the appearance of a new chemical resonance ($\delta = 1.1$ ppm) in ^{11}B NMR, while the interaction between NHC and $^3\text{ITX}^*$ was inferred from the observation of ITX bleaching during steady-state photolysis and high triplet quenching rate of ITX in the presence of the free NHC.

Amount of the NHC photoliberated in the mixture of $\text{NHCH}^+\text{BPh}_4^-/\text{ITX}$ was evaluated based on an acid/base titration, using phenol red as titrant or a quantitative reaction between NHC and 1,3-di-*p*-tolylcarbodiimide (CDI). Basically, the acid/base titration grounded on the deprotonation of phenol red by the carbene photogenerated owing to its high $\text{p}K_a$ and gave the basic form of phenol red. Thereby, based on absorbances of the phenol red

derivatives in UV-Vis spectroscopy, amount of NHC existing in the solution can be estimated. In the other hand, the generation of NHC–CDI adduct turns out to quantitative and easily monitored by ^1H NMR. The maximum yield of **IMes** was respectively of 70 % (formation of **IMes**–CDI adduct) after 5 min of irradiation at 365 nm. Depending on exposure wavelength, amount of **IMes** released decreased following the order: 70 % (365 nm) > 29 % (405 nm) > 11% (254 nm).

Combining the bi-component NHC photogenerator ($\text{NHCH}^+\text{BPh}_4^-/\text{ITX}$) and a metathesis inactive Ru dimer such as $[\text{RuCl}_2(p\text{-cymene})]_2$ afforded a highly active Noels' catalysts which readily initiated the ROMP of norbornene (NB), 5-ethylidene-2-norbornene (ENB) and dicyclopentadiene (DCPD) in the matter of minutes at room temperature. Both quantitative ^1H NMR and real-time FT-IR spectroscopy were used to determine the monomer conversions. The molecular weights (M_n) of the ROMP polymers are much higher than their theoretical values which suggests that the initiation efficiency is poor and that growth of polymer chains is faster than initiation process. Additionally, cross-linked pDCPD network films with various NB loadings were synthesized and characterized in terms of thermo-mechanical properties and microstructure. Success in the preparation of cross-linked films opens broad avenues for the replacement of UV coating based on radical pathway by the photoROMP curing process. Furthermore, the present findings in this PhD thesis enable to develop the one-pot fabrication of patterned materials with the low cost, ease in handling and safety manner.

Preliminary trials using the NHC photogenerator as photolatent organocatalyst were carried out for the synthesis of polyurethane and polyester. In both cases, high yields (> 95 %) and polymers with narrow polydispersities were obtained within 1 h. These promising results pave the way for future investigations on photoNHC-driven polymerizations. Additionally, in respect of faster and large-scale polymeric production, the next strategy will focus on broadening the structure of the photolatent NHCs relying on the versatile *N*-substituents.

APPENDIX

1. Additional figures in Chapter II

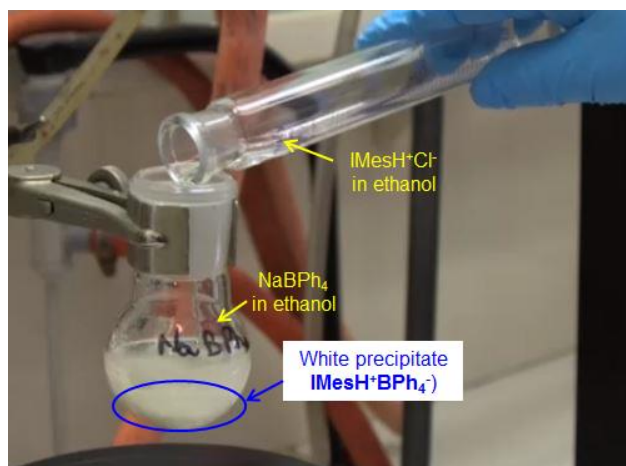


Figure A.II.1. Formation of $\text{IMesH}^+\text{BPh}_4^-$ as NaBPh_4 put in contact with $\text{IMesH}^+\text{Cl}^-$ in ethanol.

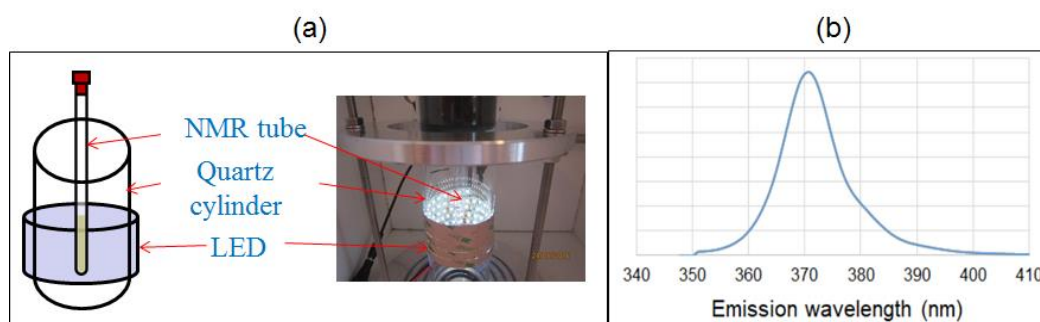


Figure A.II.2. (a) A set-up for photopolymerization with LED at 365 nm light stripe (SMD3528-60LED/Meter, Lightingwill, $6.5 \text{ mW}\cdot\text{cm}^{-2}$) and (b) Emission spectra of the Lightingwill LED.

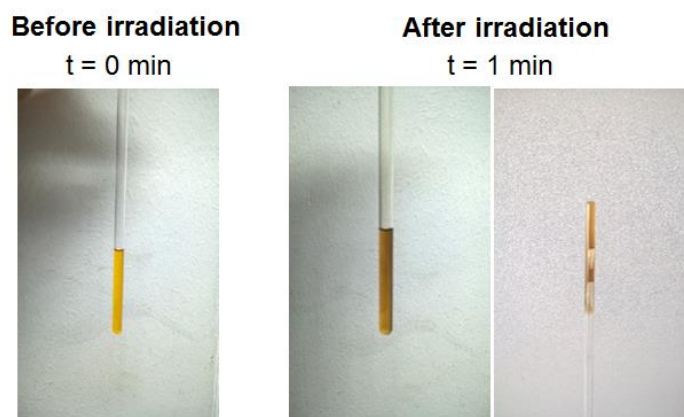


Figure A.II.3. Changes of a mixture containing NB/ **Ru-1**/ $\text{IMesH}^+\text{BPh}_4^-$ / ITX in CD_2Cl_2 as irradiated with LED at 365 nm light tripe ($6.5 \text{ mW}\cdot\text{cm}^{-2}$).

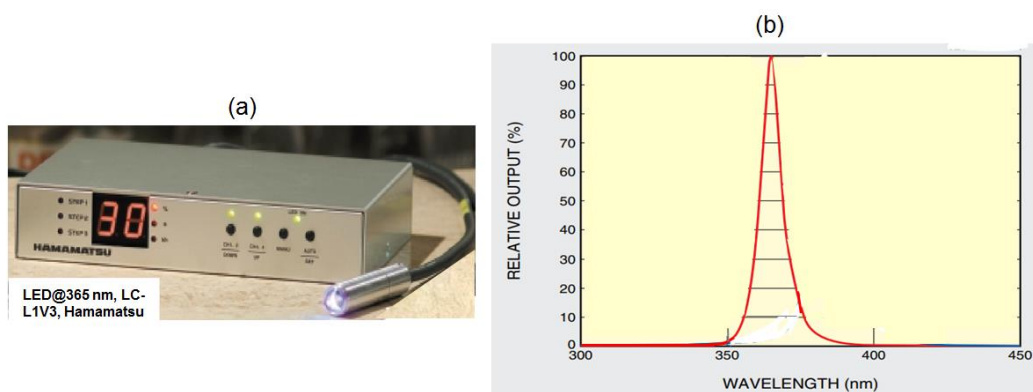


Figure A.II.4. A LED at 365 nm (LC-L1V3, Hamamatsu, $65 \text{ mW}\cdot\text{cm}^{-2}$): **a)** an image of the set-up and **(b)** its emission spectra.

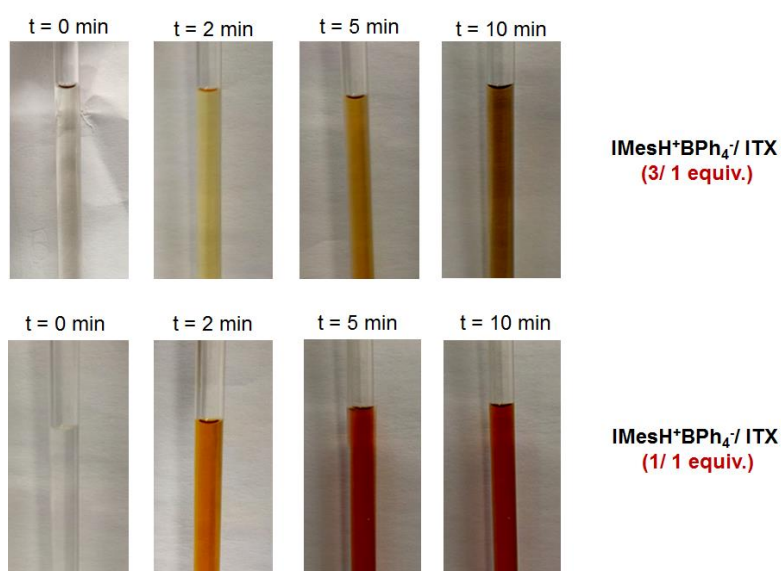


Figure A.II.5. Color changes of an as-irradiated **IMesH⁺BPh₄⁻/ITX** in THF-*d*₈ at different given times

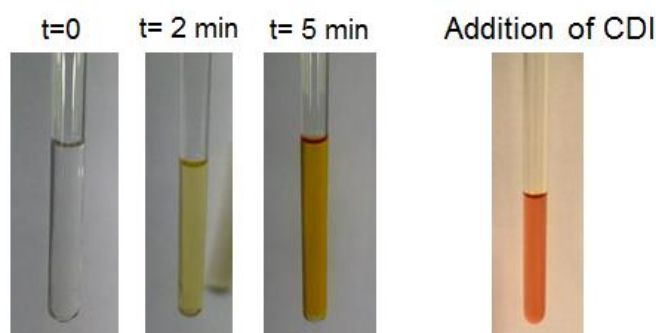


Figure A.II.6. Color changes of an as-irradiated **IMesH⁺BPh₄⁻/ITX** (3/ 1 equiv.) in THF-*d*₈ at different given times and after an addition of CDI (irradiation conditions: LED at 365 nm (LC-L1V3, Hamamatsu, $65 \text{ mW}\cdot\text{cm}^{-2}$)).

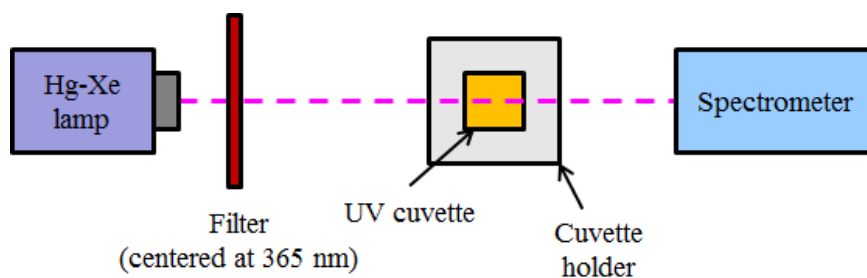


Figure A.II.7. A set-up for photo-bleaching experiment.

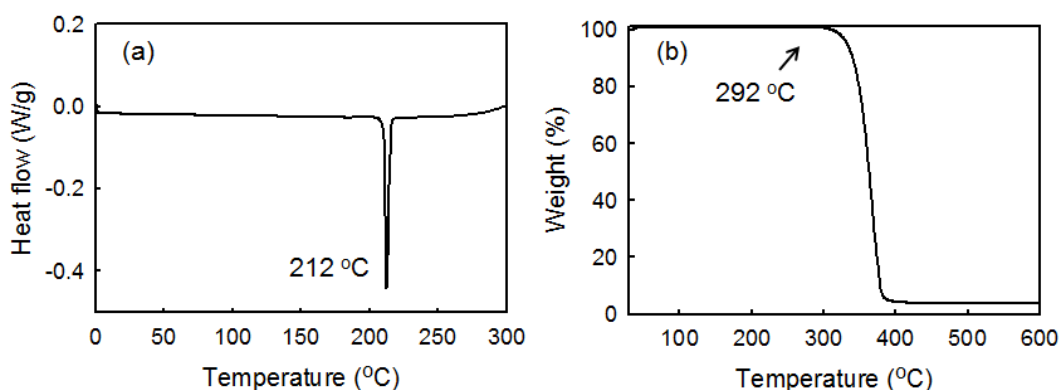


Figure A.II.8. Thermal analysis of tetraphenylborate imidazolium **IMesH⁺BP₄⁻**: (a) DSC thermogram, (b) TGA thermogram.

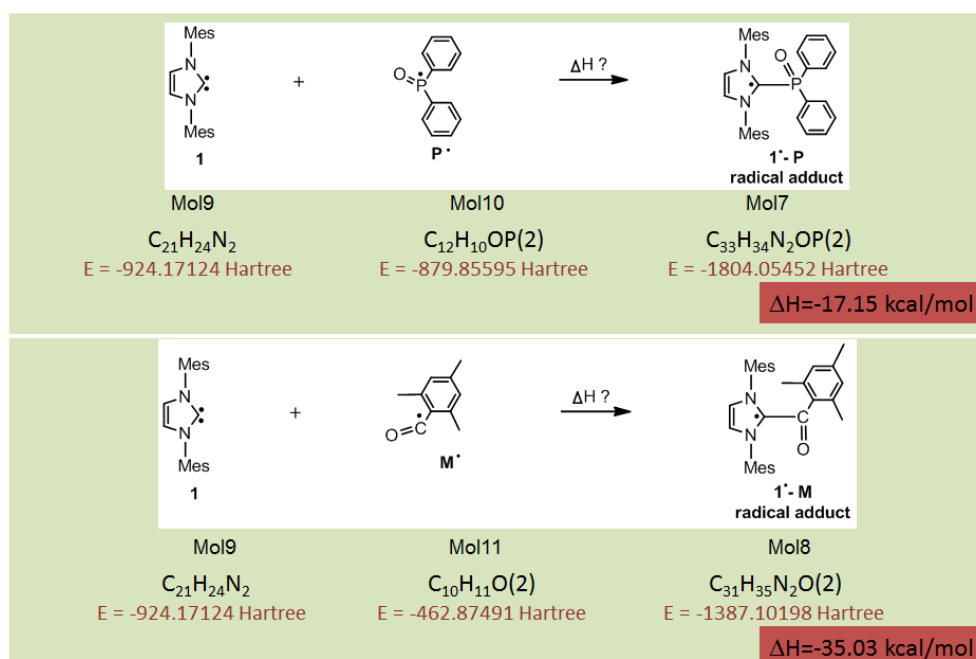


Figure A.II.9. Enthalpy calculation of reactions of **IMes** with phosphonyl (**P[•]**) and mesityl (**M[•]**) radicals by using uB3LYP/6-31G* level of theory.

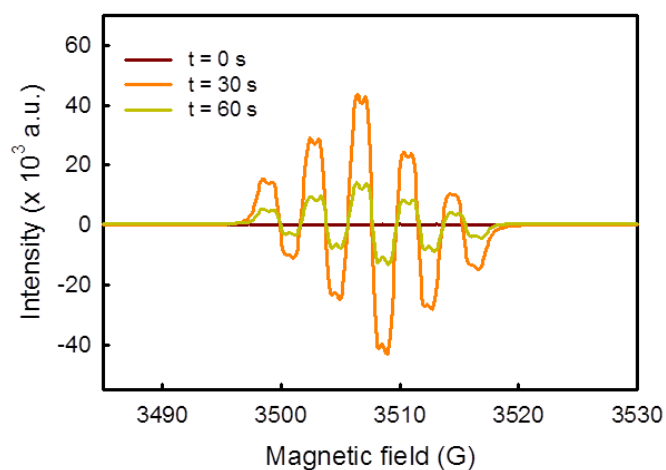


Figure A.II.10. EPR spectrum obtained at different given irradiation times of a solution of **IMes/TPO** in THF (5/1 equiv., [TPO] = 3×10^{-3} M).

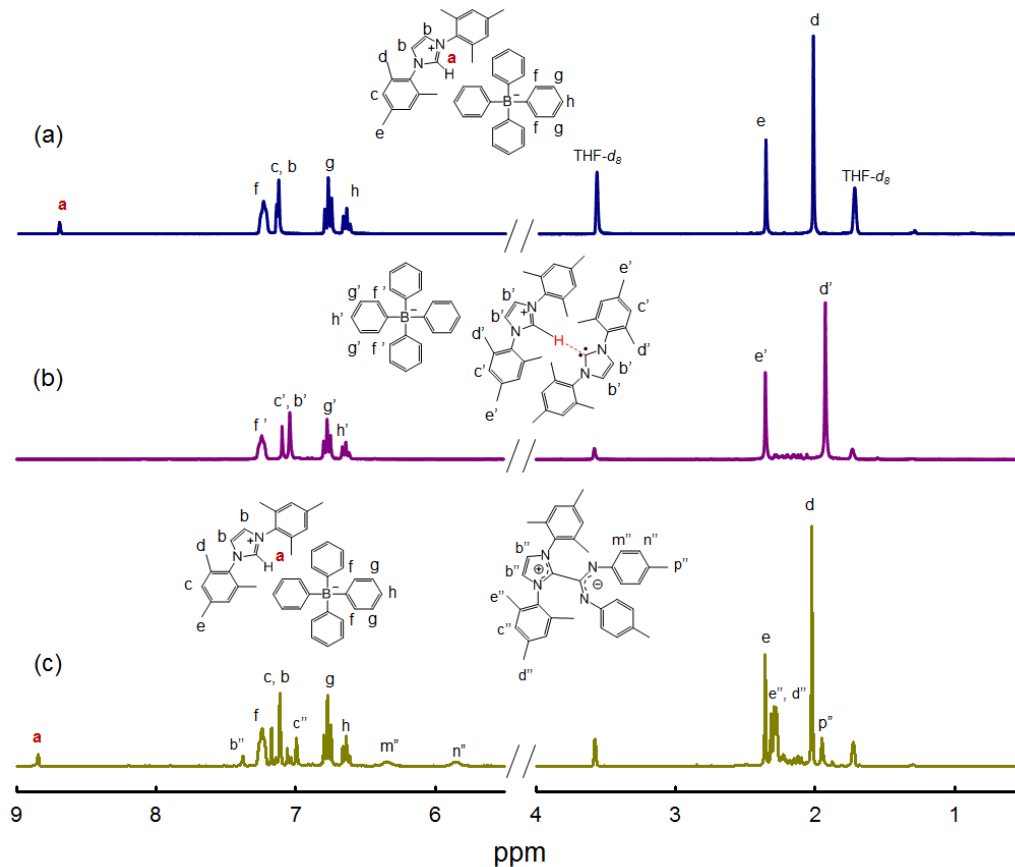
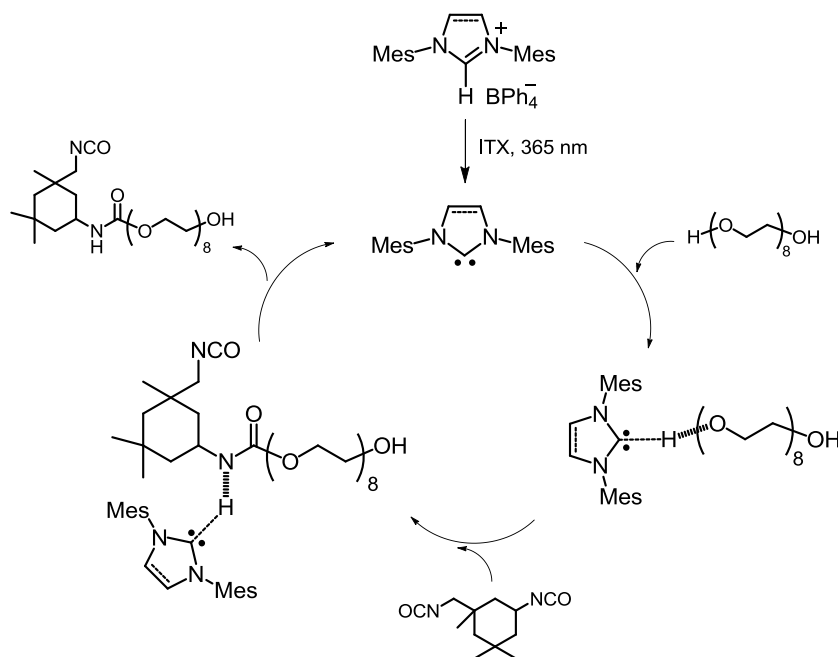


Figure A.II.11. ^1H NMR spectra in THF- d_8 of: (a) **IMesH⁺BPh₄⁻** (0.03 M), (b) **IMes/IMesH⁺BPh₄⁻** (1/3 equiv., [IMes] = 0.01 M), (c) The later mixture, then addition of 3 equiv. of CDI.



Scheme A.II.1. Proposed mechanism of urethane formation for reaction of PEG₄₀₀ and IPDI catalyzed by in situ generated **IMes** (or **SIMes**).

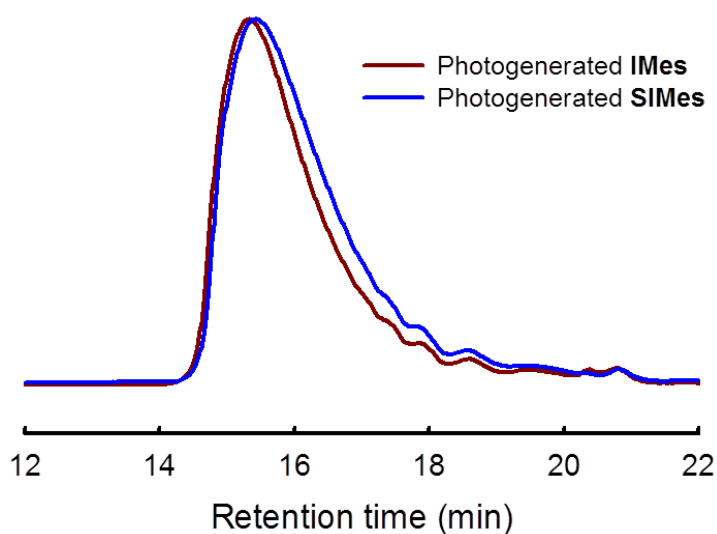


Figure A.II.12. SEC traces in THF of precipitated polyurethane samples prepared by step-growth polymerization of PEG₄₀₀/IPDI (342/342 equiv.). Reactions were conducted at 60°C for 4 h after the addition of as-irradiated solution: **IMesH⁺BPh₄⁻**/ITX (1/1 equiv., brown trace) and **SIMesH⁺BPh₄⁻**/ITX (1/1 equiv., blue trace).

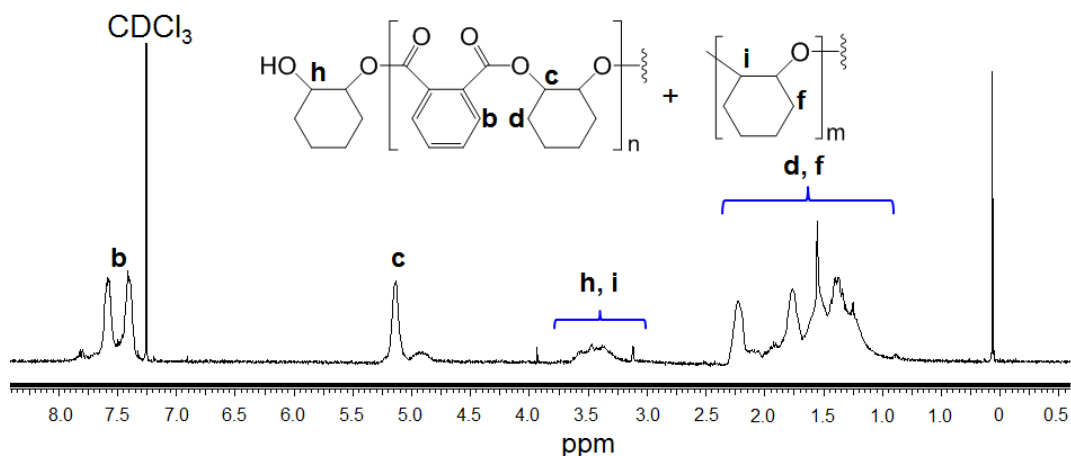


Figure A.II.13. ^1H NMR spectrum of refined (precipitated) polyester in CDCl_3 obtained by the ROCOP of CHO/PA (500/100 equiv.) at 110°C for 60 min using an as-irradiated $\text{IMesH}^+\text{BPh}_4^-/\text{ITX}$ solution (1/1 equiv.) (photogenerated IMes) as an initiator.

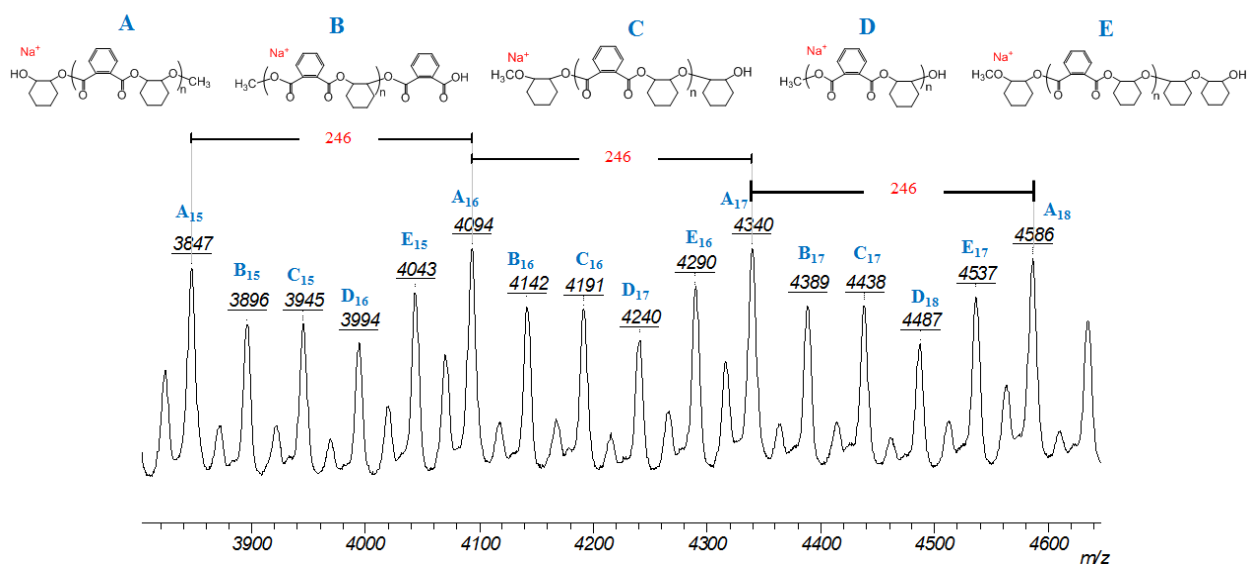
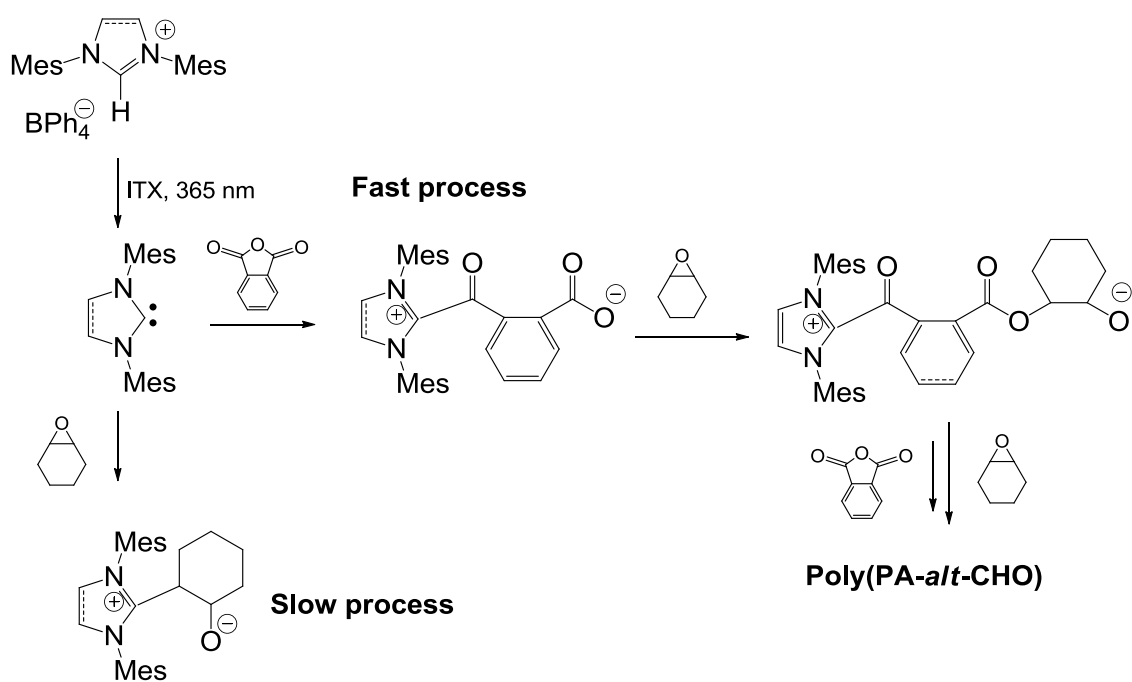


Figure A.II.14. Positive MALDI-ToF MS spectrum of isolated poly(PA-*alt*-CHO) obtained by the ROCOP of CHO/PA (500/100 equiv.) at 110°C for 60 min using an as-irradiated $\text{IMesH}^+\text{BPh}_4^-/\text{ITX}$ solution (1/1 equiv.) (photogenerated IMes) as an initiator (entry **a** in **Table 2.3**). Note: A_{15} is structure A with repeating unit $n = 15$.



Scheme A.II.2. Possible mechanism for ring-opening copolymerization of CHO and PA.

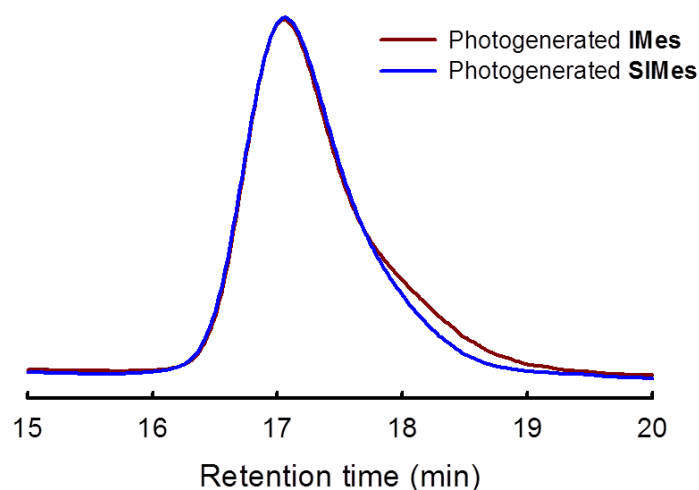


Figure A.II.15. SEC traces in THF of refined polyesters gained from entry **a** and **b** (Table 2.3) prepared by the ROCOP of CHO/PA (500/100 equiv.) at 110°C for 60 min using different initiators: as-irradiated **IMesH⁺BPh₄⁻**/ITX solution (1/1 equiv., brown trace) and as-irradiated **SIMesH⁺BPh₄⁻**/ITX solution (1/1 equiv., blue trace).

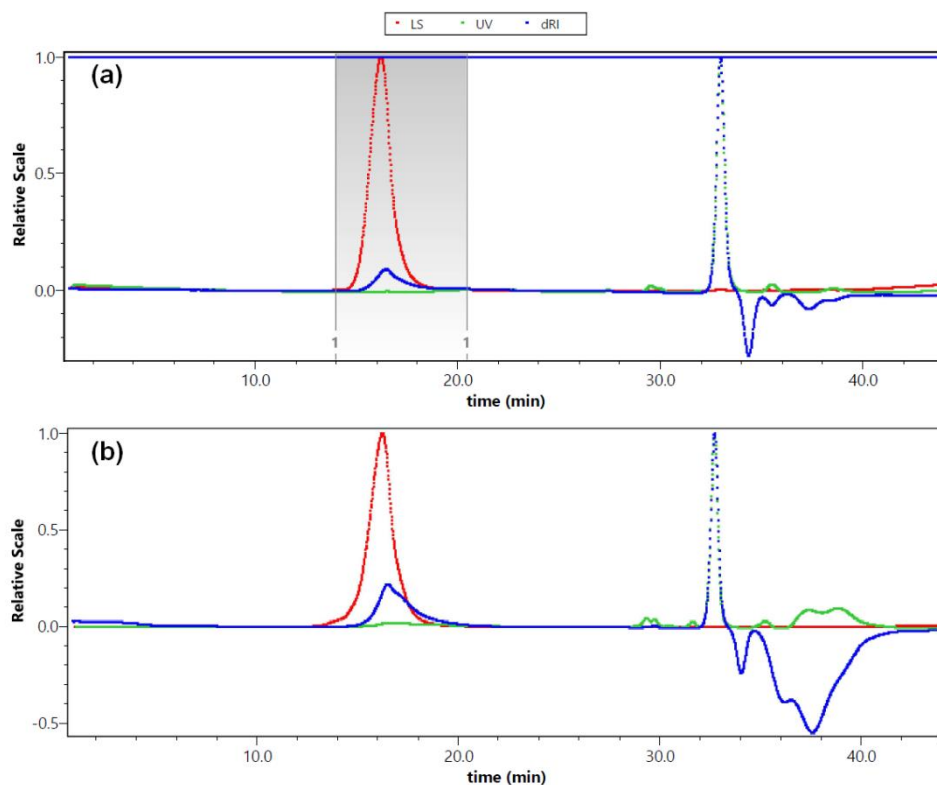


Figure A.II.16. SEC traces of precipitated polynorbornene prepared by the ROMP of NB (510 equiv.) irradiated for 60 s with LED 365 nm (6.5 mW cm^{-1}) using different catalysts: **(a)** $\text{IMesH}^+\text{BPh}_4^-/\text{ITX}/[\text{RuCl}_2(p\text{-cymene})]_2$ solution (5/2.5/1 equiv.) and **(b)** $\text{SIMesH}^+\text{BPh}_4^-/\text{ITX}/[\text{RuCl}_2(p\text{-cymene})]_2$ solution (5/2.5/1 equiv.). Three detectors were used: 1/. LS: light scattering detector, 2/. UV, and 3/. dRI: refractive index detector.

2. Additional figures in Chapter III

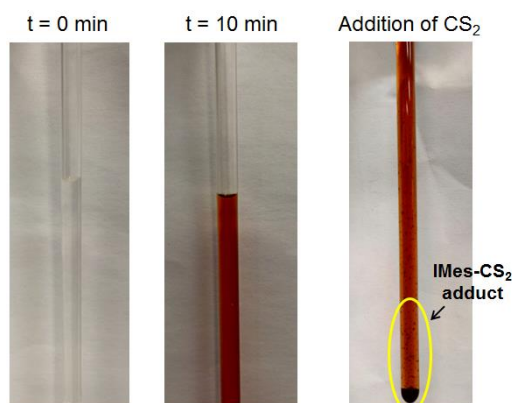


Figure A.III.1. Color changes of an as-irradiated $\text{IMesH}^+\text{BPh}_4^-/\text{ITX}$ (3/ 3 equiv.) in $\text{ACN-}d_3$ at different given time and formation of IMes-CS_2 adduct after CS_2 added.

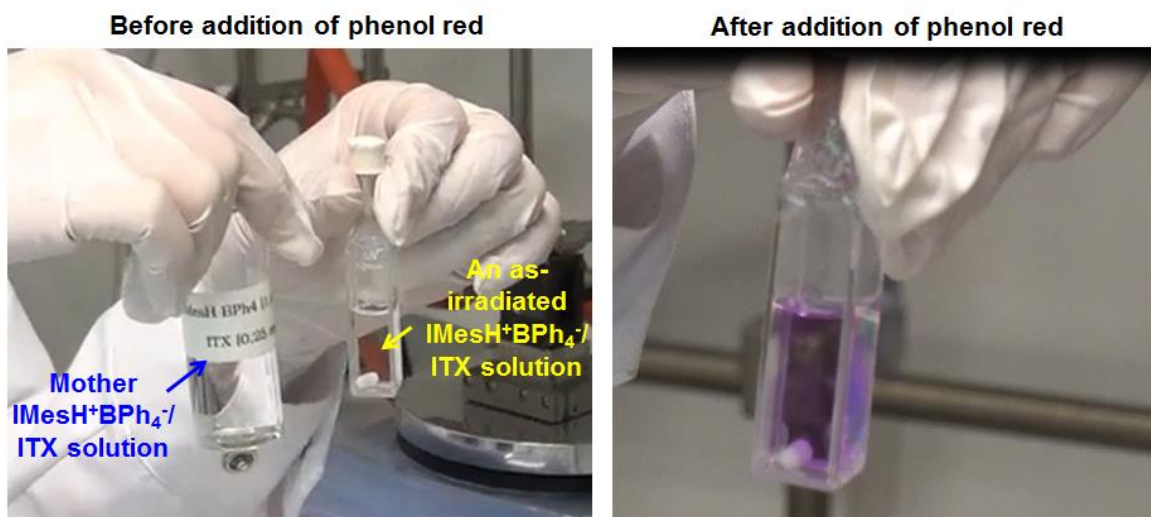


Figure A.III.2. Color changes of an as-irradiated $\text{IMesH}^+\text{BPh}_4^-/\text{ITX}$ (3/ 1 equiv.) in ACN before and after addition of phenol red.

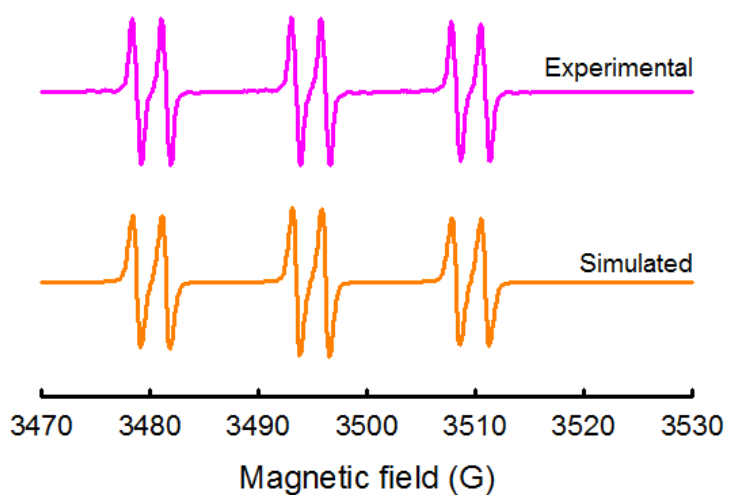


Figure A.III.3. EPR spectra of Ph-PBN radical from a solution $\text{ITX} - \text{IMesH}^+\text{BPh}_4^- - \text{PBN}$ in acetonitrile after exposing under LED 365 nm for 60 s (concentration: $[\text{ITX}] = 5 \times 10^{-3} \text{ M}$, $[\text{IMesH}^+\text{BPh}_4^-] = 1.5 \times 10^{-2} \text{ M}$ and $[\text{PBN}] = 3 \times 10^{-3} \text{ M}$, respectively).

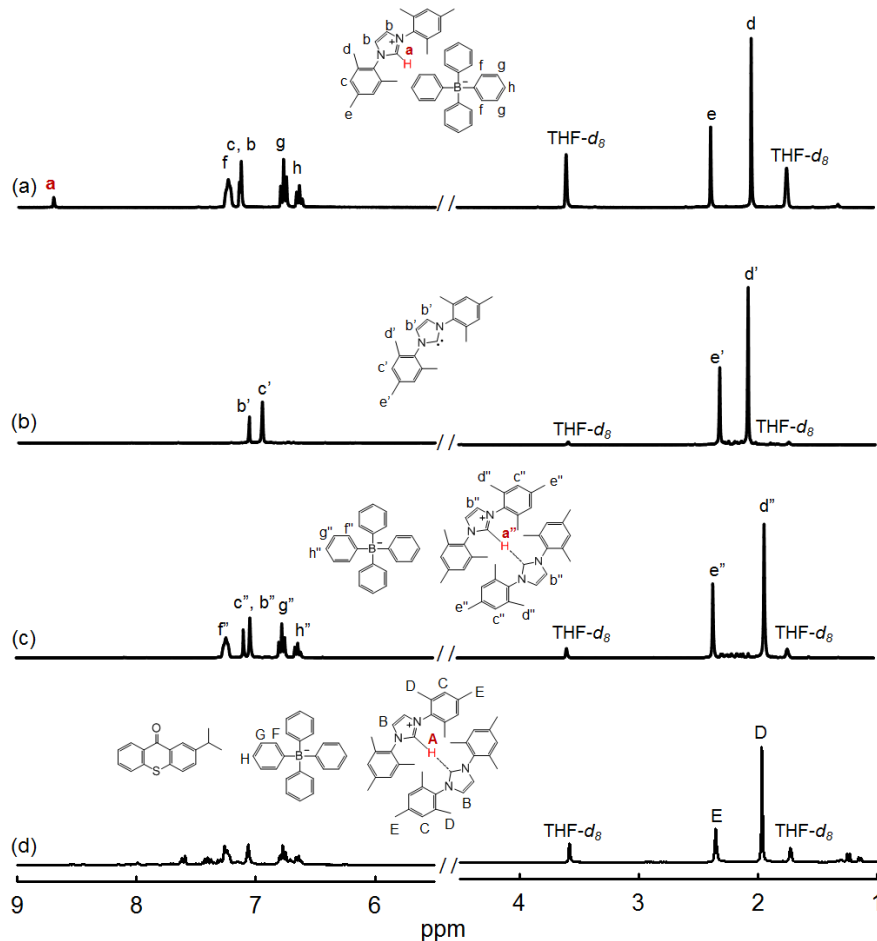


Figure A.III.4. ^1H NMR spectra in $\text{THF-}d_8$ of: (a) $\text{IMesH}^+\text{BPh}_4^-$, (b) IMes , (c) the mixture of $\text{IMesH}^+\text{BPh}_4^-$ and IMes (9/1 equiv.) and (d) irradiated $\text{ITX-IMesH}^+\text{BPh}_4^-$ (1/1 equiv.).

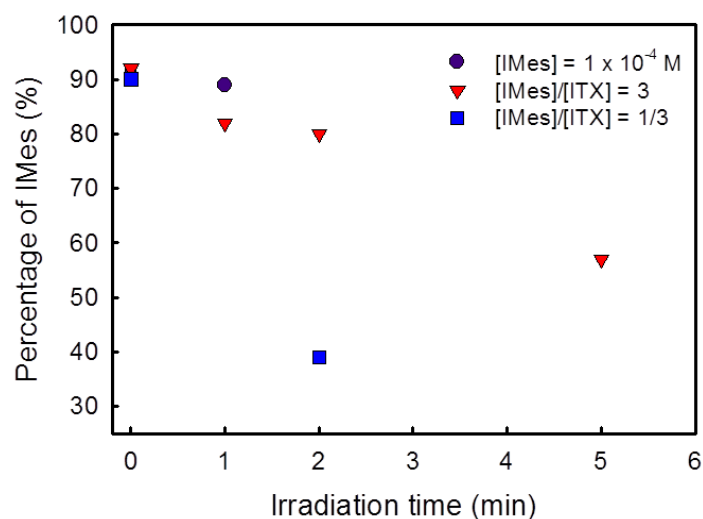
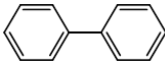
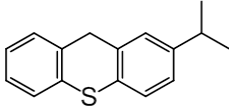
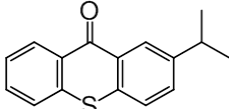
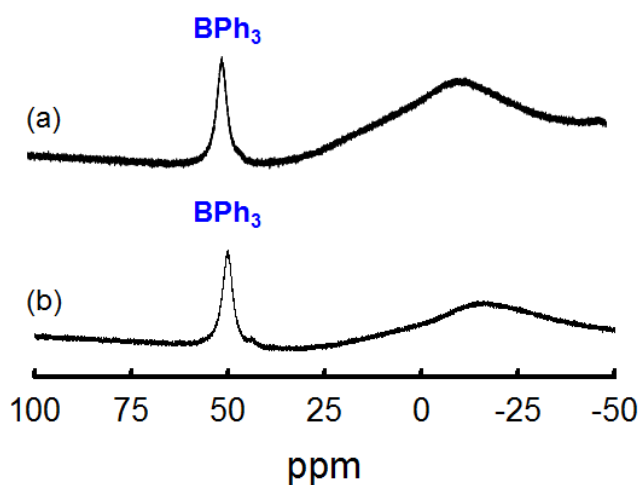


Figure A.III.5. Amount of IMes existing in acetonitrile against exposure time determined by an acid/base titration with phenol red.

Table A.III.1. Identification of photoproducts by GC-MS after the photolysis course of ITX- $\text{IMesH}^+\text{BPh}_4^-$

Compound	Retention time (min)	EI-MS: m/z (relative abundance)	Molar mass (g/mol)	Chemical structure
Biphenyl	22.065	63 (7), 76 (15), 89 (2), 102 (4), 115 (5), 128 (6), 153 (40), 154 (100)	154	
Isopropylthioxanthone	39.186	65 (4), 75 (5), 91 (14), 105 (15), 135 (11), 147 (16), 165 (25), 178 (6), 191 (12), 197 (40), 223 (38), 225 (85), 240 (100)	240	
ITX	42.790	50 (3), 69 (4), 77 (5), 89 (3), 105 (6), 139 (9), 152 (6), 165 (5), 178 (6), 196 (11), 210 (7), 224 (7), 239 (100), 254 (54)	254	

**Figure A.III.6.** ^{11}B -NMR spectra of photolysis of $[\text{ITX}] = 0.03 \text{ M}$ - $[\text{BPh}_3] = 0.03 \text{ M}$ in $\text{THF-}d_8$: (a) prior to exposure, (b) after exposure for 10 min ($\text{LED } 365 \text{ nm}$, $65 \text{ mW} \cdot \text{cm}^{-2}$).

3. Additional figures in Chapter IV

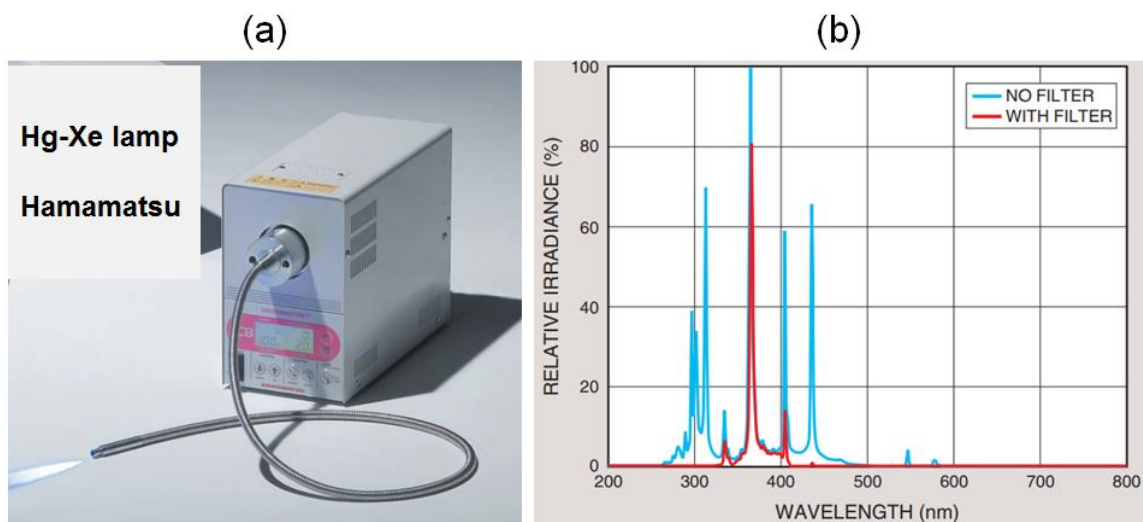


Figure A.IV.1. A Hg-Xe lamp at 254 nm (LC-9588/01A, Hamamatsu, $75 \text{ mW}\cdot\text{cm}^{-2}$): (a) an image and (b) its emission spectra with (red color) and without a filter at 365 nm (blue color).

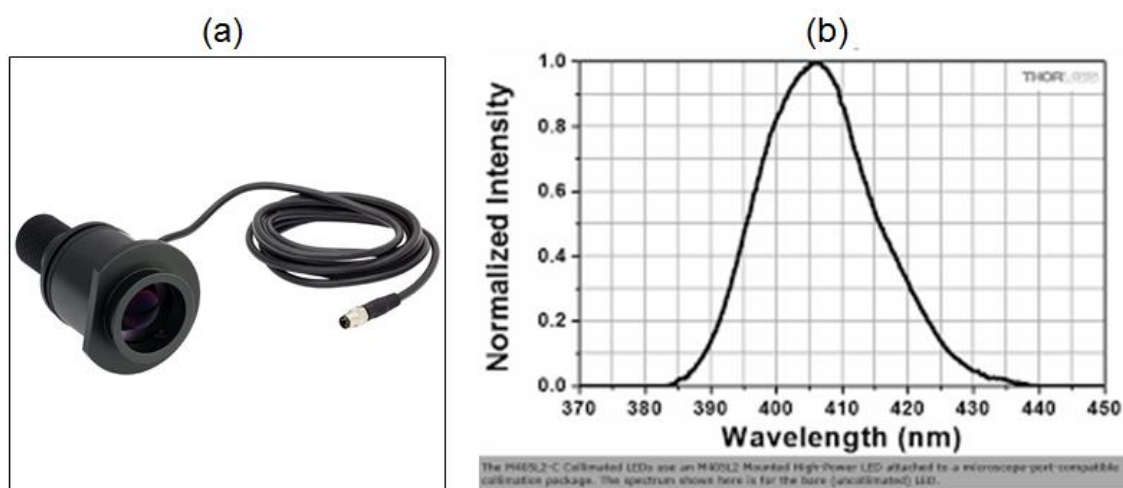


Figure A.IV.2. A LED at 405 nm (M405L2, ThorLabs, $100 \text{ mW}\cdot\text{cm}^{-2}$): (a) an image and (b) its emission spectra.

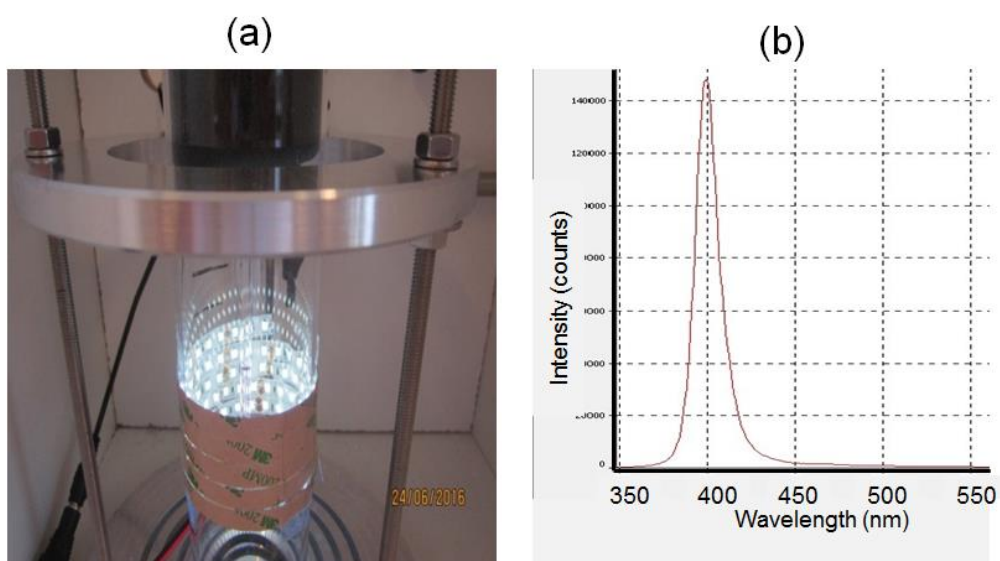


Figure A.IV.3. (a) A set-up for photopolymerization with LED at 405 nm (SMD2835-60LED/Meter, Banggood, $4.7 \text{ mW}\cdot\text{cm}^{-2}$) and (b) Emission spectra of the Banggood LED.

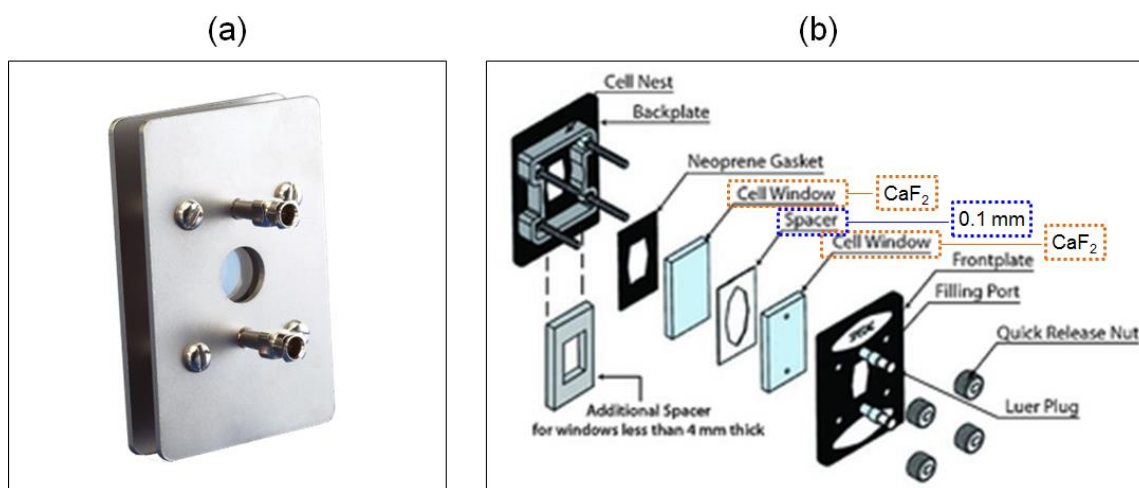


Figure A.IV.4. (a) An image of Specac® sealed flow cell for IR spectroscopy and (b) Insight component parts of the Specac® sealed flow cell (the cell windows are CaF_2 pellets, Teflon space has a thickness of 0.1 mm).

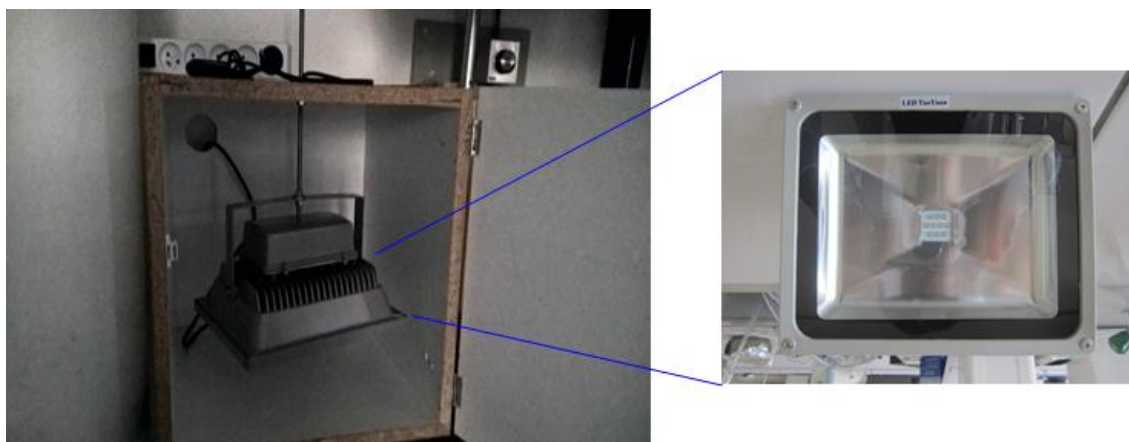


Figure A.IV.5. A set-up of top UV curing LED at 365 nm (Tao Yuan , $5.5 \text{ mW}\cdot\text{cm}^{-2}$).

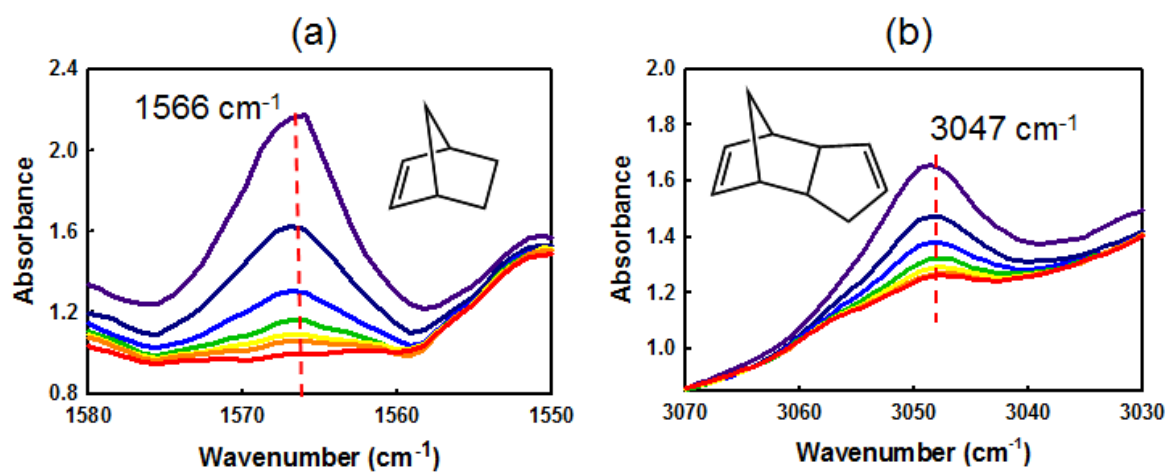


Figure A.IV.6. Changes in FT-IR profiles during photopolymerization in solution CH_2Cl_2 using the catalytic system **Ru-1**/**IMesH⁺BPh₄⁻**/**ITX** of various monomers: (a) NB and (b) DCPD.

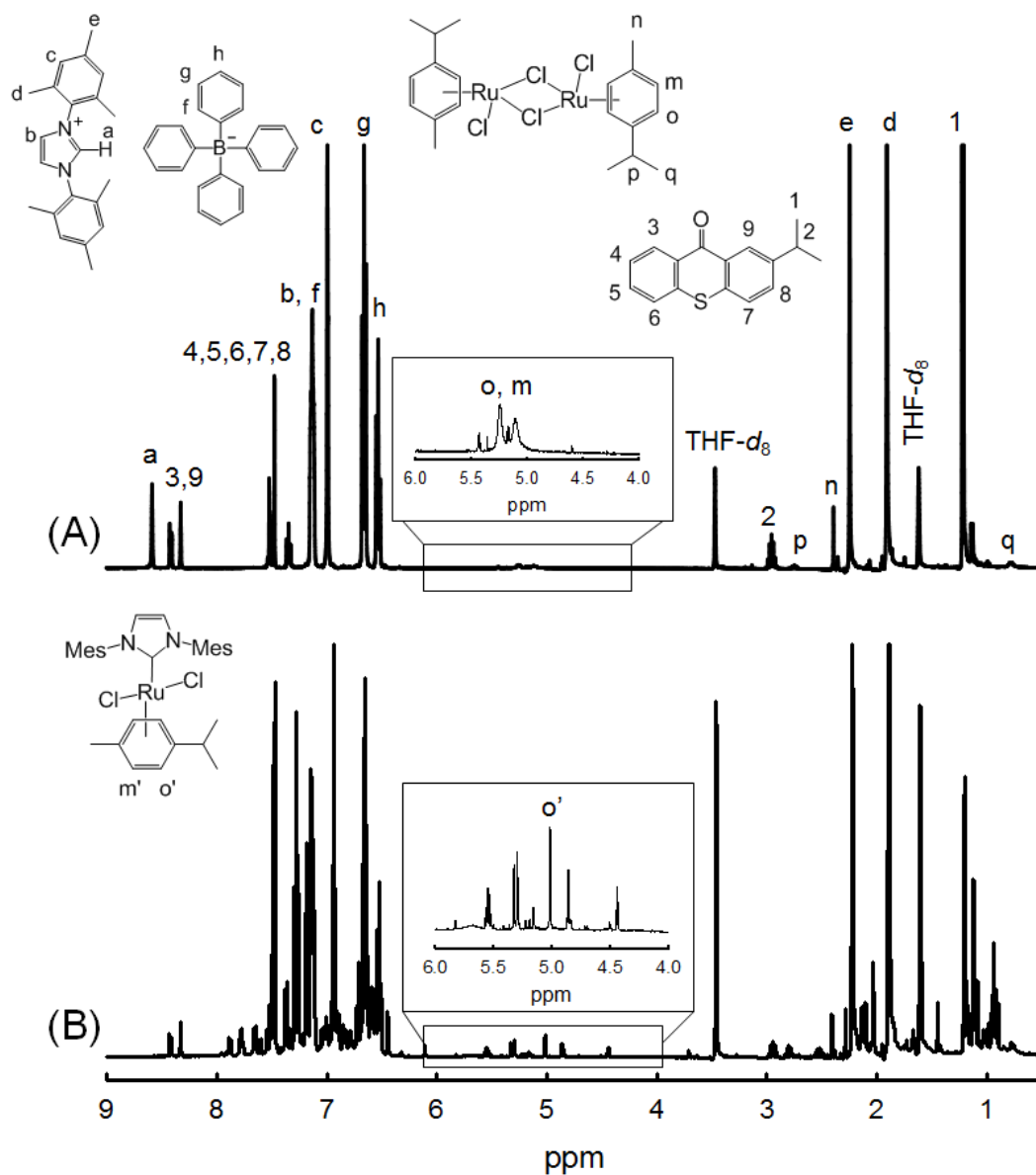


Figure A.IV.7. ^1H NMR of $1/\text{Ru-1}/\text{ITX}$ in $\text{THF-}d_8$: (a) Prior to exposure to light and (b) After 30 min of irradiation (Conditions: $1/\text{Ru-1}/\text{ITX} = 5/1/2.5$ equiv., $[\text{Ru-1}] = 0.002\text{M}$, Xe-Hg lamp@ 254 nm with intensity of $20\text{ mW}\cdot\text{cm}^{-2}$).

SUMMARY IN FRENCH OF CHAPTER II, III AND IV

Chapitre II. Mélange d'azolium tétraphénylborate avec l'isopropylthioxanthone: une nouvelle classe de photogénérateur de NHC pour la synthèse de polyuréthane, polyester et polymère de ROMP

Les carbènes N-hétérocycliques (NHC) sont à l'avant-garde en chimie organométallique,^{1,2} catalyse,³ et plus récemment en polymérisation.⁴ À ce jour, le 1,3-bis(mésityle)imidazol-2-ylidène (**IMes**, **1**) et son congénère saturé le 1,3-bis (mésityle)imidazolidine-2-ylidène (**SIMes**, **2**) sont les NHCs les plus fréquemment rencontrés (**Figure R.II.1**). Les ligands NHCs ont progressivement remplacé les phosphines, qui ne sont pas inoffensifs pour l'environnement.^[6-8] Après réaction avec des métaux de transition, ils peuvent former des complexes métalliques bien définis présentant une activité catalytique exceptionnelle. Les exemples les plus importants sont les complexes alkyldène de ruthénium avec un ligand coordonné NHC utilisé dans la métathèse d'oléfine.⁸ De plus, leur nucléophilie forte et leur basicité au sens de Brønsted ont contribué à leur utilisation comme organocatalyseurs. Dans la polymérisation, ils peuvent remplacer les composés organométalliques avec pour avantages une réduction des coûts et de la toxicité. La gamme des polymérisations induites par des NHC^{4,9,10} couvre déjà la polymérisation par ouverture de cycle (lactone,¹¹ lactame,¹² époxyde¹³), ainsi que des polymérisations par étapes pour la synthèse de polybenzoïne¹⁴ ou de polyuréthane.¹⁵

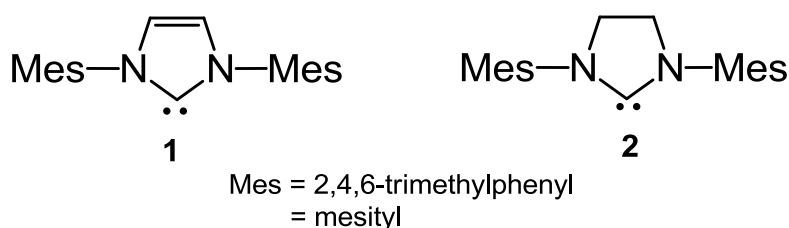


Figure R.II.1. **1** et **2** sont parmi les NHCs les plus fréquemment employés

En dépit de la richesse des recherches menées à ce jour, l'utilisation pratique de NHCs présente un certain nombre de défis: les NHCs sont très sensibles à l'humidité et doivent être manipulés sous atmosphère sèche. De plus, ils réagissent avec des acides en raison de leur pK_a élevé, et sont également sujets à une dimérisation.^{16,17} En raison de ces contraintes, les NHCs sont généralement mis en contact avec des substrats ou des monomères au dernier moment. Considérant le rôle central de la chimie des NHCs, il est essentiel de contrôler et

d'optimiser leurs conditions de formation. Les enjeux sont de faciliter le stockage, la manipulation, le traitement, et de façon plus générale, promouvoir le passage du laboratoire à la production industrielle. À l'heure actuelle, la déprotonation in situ d'un sel d'azolium est de loin la méthode la plus couramment utilisée pour accéder à un NHC libre.¹⁹⁻²¹ Cependant, cette méthode nécessite une base forte, qui limite le champ d'application de substrats et cette base peut aussi intervenir dans le procédé de polymérisation en tant qu'amorceur.²¹ Dans la recherche de routes plus intelligentes pour libérer le NHC, des NHCs « masqués » ou « protégés » ont été étudiés récemment.^{21,22} D'un grand intérêt sont les précurseurs de NHC thermiquement labiles sur la base de produits d'addition NHC-CO₂ stables à l'air,²³ des NHC-isothiocyanate²⁴ ou des complexes NHC-métal.²⁵ En dépit des résultats prometteurs, cette approche a des limites importantes liées au clivage réversible, la faible solubilité de nombreux adduits NHC et la latence incomplète.²¹

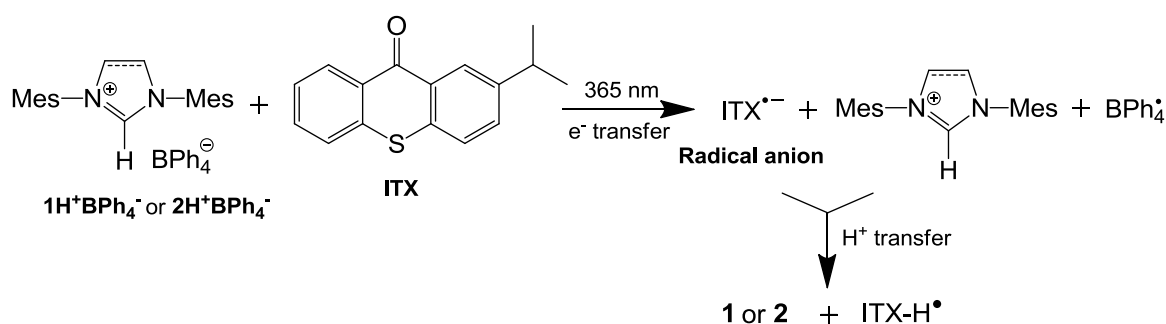


Schéma R.II.1. Mécanisme de photolyse pour la photogénération de **1** (ou **2**) à partir du système bicomposant ITX / **1H⁺BPh₄⁻**.

Malgré les nombreux développements dans le domaine de photoamorceurs,^{26,27} très peu d'attention a été accordée aux précurseurs de NHC photolatents. En 2015, Denning *et al.*²⁸ a étudié la réduction photochimique d'un imidazolium-2-carboxylate d'éthyle (NHC-CO₂) en utilisant un donneur d'électrons à l'état excité, la N,N,N',N'-tétraméthylbenzidine. L'effort de recherche limité sur les photogénérateurs de NHC contraste avec le vif intérêt pour d'autres Générateurs de PhotoBase (PBG), capables de libérer des organosuperbases de type amidine ou guanidine.²⁹ La plupart des PBGs passent par une réaction de transfert de proton photoinduite en utilisant un sel contenant la superbase sous forme protonée et un chromophore anionique de type kétoprofène,³⁰ thioxanthone,³¹ ou tétraphénylborate.^[33-35]

Aujourd'hui, il existe de fortes motivations pour le développement de réactions induites par des photoNHCs: un contrôle temporel et spatial de la réaction, l'utilisation d'une

stimulation sans contact, et la libération NHC dans des conditions ambiantes grâce un dosage énergétique et spatial précis du rayonnement. Notre objectif est de concevoir un nouveau photogénérateur de NHC, à la fois stable en l'absence de lumière et capable de libérer in situ un NHC libre sous exposition au rayonnement UV, de préférence UVA (320-400 nm) pour éviter l'excitation du substrat ou du solvant. A cet effet, des sels d'imidazolium ou d'imidazolium semblent les structures les plus appropriées en tant que précurseurs NHC photolatents. Comme beaucoup de liquides ioniques, ils sont stables à l'air et humidité, thermiquement et chimiquement inertes. Le défi est donc de promouvoir une réaction de transfert de protons induite par photochimie qui convertirait le sel d'azolium inactif en un NHC actif. La solution proposée est de produire un anion radical approprié par une réaction de transfert d'électrons photoinduit (TEP), qui sera ensuite capable de déprotoner le cation azolium (**Schéma R.II.1**). À cette fin, nous proposons un mélange d'isopropylthioxanthone (ITX) avec un azolium stable à l'air à base de tétraphénylborate, tels que le 1,3-bis(mésityle)imidazolium tétraphénylborate $\mathbf{1H^+BPh_4^-}$, ou 1,3-bis(mésityle)imidazolium tétraphénylborate $\mathbf{2H^+BPh_4^-}$.³⁵ Tout d'abord, l'ITX est bon marché, disponible commercialement, et connu pour son aptitude à servir de médiateur de transfert d'électrons après excitation photochimique.³⁶ D'autre part, l'anion tétraphénylborate peut agir en tant que donneur d'électrons approprié pour rendre le transfert d'électron thermodynamiquement possible.^{37,38}

Encouragé par les résultats préliminaires prouvant la libération de NHC lors de l'irradiation,³⁵ ce travail se veut une étude approfondie de cette nouvelle classe de photogénérateur de NHC bicomposant avec quatre parties distinctes. Tout d'abord, nous proposons deux nouvelles méthodes d'analyse pour caractériser les NHCs libérés photochimiquement grâce à leur conversion en produits d'addition. D'autre part, pour soutenir la voie photochimique en deux étapes sur la base de réactions de transfert d'électrons/protons, des expériences de « photobleaching » en temps réel sont effectuées ainsi que le calcul de la variation d'énergie libre de transfert d'électrons avec l'équation de Rehm-Weller. En troisième lieu, le rendement en NHC est optimisé en étudiant notamment l'effet du temps d'irradiation, de la concentration du sensibilisateur. Dans une dernière partie, le photogénérateur de NHC est mis à profit pour préparer une variété de structures polymères grâce à son double rôle. En tant qu'organocatalyseur, des polyuréthane et polyester ont été préparés par polymérisation par étapes et copolymérisation par ouverture de cycle, respectivement. En tant que ligand, du

polynorbornène a été synthétisé par polymérisation par métathèse par ouverture de cycle (ROMP) en utilisant un catalyseur du type Ru-NHC.

Références

- 1 B. Hogan and M. Albrecht, in *Reference Module in Chemistry, Molecular Sciences and Chemical Engineering*, Elsevier, 2016.
- 2 E. Peris, Smart N-Heterocyclic Carbene Ligands in Catalysis, *Chem. Rev.*, 2018, **118**, 9988–10031.
- 3 D. M. Flanigan, F. Romanov-Michailidis, N. A. White and T. Rovis, Organocatalytic Reactions Enabled by N-Heterocyclic Carbenes, *Chem. Rev.*, 2015, **115**, 9307–9387.
- 4 S. Naumann and A. P. Dove, N-Heterocyclic carbenes for metal-free polymerization catalysis: an update, *Polym. Int.*, 2016, **65**, 16–27.
- 5 N. D. Clement, L. Routaboul, A. Grotevendt, R. Jackstell and M. Beller, Development of Palladium-Carbene Catalysts for Telomerization and Dimerization of 1,3-Dienes: From Basic Research to Industrial Applications, *Chem. - Eur. J.*, 2008, **14**, 7408–7420.
- 6 F. E. Hahn and M. C. Jahnke, Heterocyclic Carbenes: Synthesis and Coordination Chemistry, *Angew. Chem. Int. Ed.*, 2008, **47**, 3122–3172.
- 7 S. Díez-González, N. Marion and S. P. Nolan, N-Heterocyclic Carbenes in Late Transition Metal Catalysis, *Chem. Rev.*, 2009, **109**, 3612–3676.
- 8 M. Scholl, S. Ding, C. W. Lee and R. H. Grubbs, Synthesis and Activity of a New Generation of Ruthenium-Based Olefin Metathesis Catalysts Coordinated with 1,3-Dimesityl-4,5-dihydroimidazol-2-ylidene Ligands, *Org. Lett.*, 1999, **1**, 953–956.
- 9 M. Fèvre, J. Pinaud, Y. Gnanou, J. Vignolle and D. Taton, N-Heterocyclic carbenes (NHCs) as organocatalysts and structural components in metal-free polymer synthesis, *Chem. Soc. Rev.*, 2013, **42**, 2142–2172.
- 10 S. Naumann and A. P. Dove, N-Heterocyclic carbenes as organocatalysts for polymerizations: trends and frontiers, *Polym. Chem.*, 2015, **6**, 3185–3200.
- 11 N. E. Kamber, W. Jeong, S. Gonzalez, J. L. Hedrick and R. M. Waymouth, N-Heterocyclic Carbenes for the Organocatalytic Ring-Opening Polymerization of ϵ -Caprolactone, *Macromolecules*, 2009, **42**, 1634–1639.
- 12 S. Naumann, S. Epple, C. Bonten and M. R. Buchmeiser, Polymerization of ϵ -Caprolactam by Latent Precatalysts Based on Protected N-Heterocyclic Carbenes, *ACS Macro Lett.*, 2013, **2**, 609–612.
- 13 J. Raynaud, W. N. Ottou, Y. Gnanou and D. Taton, Metal-free and solvent-free access to α,ω -heterodifunctionalized poly(propylene oxide)s by N-heterocyclic carbene-induced ring opening polymerization, *Chem. Commun.*, 2010, **46**, 3203.
- 14 J. Pinaud, K. Vijayakrishna, D. Taton and Y. Gnanou, Step-Growth Polymerization of Terephthaldehyde Catalyzed by N-Heterocyclic Carbenes, *Macromolecules*, 2009, **42**, 4932–4936.
- 15 O. Coutelier, M. El Ezzi, M. Destarac, F. Bonnette, T. Kato, A. Baceiredo, G. Sivasankarapillai, Y. Gnanou and D. Taton, N-Heterocyclic carbene-catalysed synthesis of polyurethanes, *Polym. Chem.*, 2012, **3**, 605.
- 16 D. C. Graham, K. J. Cavell and B. F. Yates, Dimerization mechanisms of heterocyclic carbenes, *J. Phys. Org. Chem.*, 2005, **18**, 298–309.

-
- 17 A. Poater, F. Ragone, S. Giudice, C. Costabile, R. Dorta, S. P. Nolan and L. Cavallo, Thermodynamics of N-Heterocyclic Carbene Dimerization: The Balance of Sterics and Electronics, *Organometallics*, 2008, **27**, 2679–2681.
 - 18 P. de Frémont, N. Marion and S. P. Nolan, Carbenes: Synthesis, properties, and organometallic chemistry, *Coord. Chem. Rev.*, 2009, **253**, 862–892.
 - 19 H.-J. Schönherr and H.-W. Wanzlick, Chemie nucleophiler Carbene, XVIII(1) 1.3.4.5-Tetraphenylimidazoliumperchlorat, *Justus Liebigs Ann. Chem.*, 1970, **731**, 176–179.
 - 20 W. A. Herrmann, M. Elison, J. Fischer, C. Köcher and G. R. J. Artus, N-Heterocyclic Carbenes: Generation under Mild Conditions and Formation of Group 8–10 Transition Metal Complexes Relevant to Catalysis, *Chem. - Eur. J.*, 1996, **2**, 772–780.
 - 21 S. Naumann and M. R. Buchmeiser, Liberation of N-heterocyclic carbenes (NHCs) from thermally labile progenitors: protected NHCs as versatile tools in organo- and polymerization catalysis, *Catal Sci Technol*, 2014, **4**, 2466–2479.
 - 22 F. Bonnette, T. Kato, M. Destarac, G. Mignani, F. P. Cossío and A. Baceiredo, Encapsulated N-Heterocyclic Carbenes in Silicones without Reactivity Modification, *Angew. Chem. Int. Ed.*, 2007, **46**, 8632–8635.
 - 23 B. Bantu, G. M. Pawar, U. Decker, K. Wurst, A. M. Schmidt and M. R. Buchmeiser, CO₂ and Sn^{II} Adducts of N-Heterocyclic Carbenes as Delayed-Action Catalysts for Polyurethane Synthesis, *Chem. - Eur. J.*, 2009, **15**, 3103–3109.
 - 24 B. C. Norris, D. G. Sheppard, G. Henkelman and C. W. Bielawski, Kinetic and Thermodynamic Evaluation of the Reversible N-Heterocyclic Carbene–Isothiocyanate Coupling Reaction: Applications in Latent Catalysis, *J. Org. Chem.*, 2011, **76**, 301–304.
 - 25 S. Naumann, F. G. Schmidt, W. Frey and M. R. Buchmeiser, Protected N-heterocyclic carbenes as latent pre-catalysts for the polymerization of ϵ -caprolactone, *Polym. Chem.*, 2013, **4**, 4172.
 - 26 N. Corrigan, J. Yeow, P. Judzewitsch, J. Xu and C. Boyer, Seeing the Light: Advancing Materials Chemistry through Photopolymerization, *Angew. Chem. Int. Ed.*, 2019, **58**, 5170–5189.
 - 27 C. Fu, J. Xu and C. Boyer, Photoacid-mediated ring opening polymerization driven by visible light, *Chem. Commun.*, 2016, **52**, 7126–7129.
 - 28 D. M. Denning, M. D. Thum and D. E. Falvey, Photochemical Reduction of CO₂ Using 1,3-Dimethylimidazolyliidene, *Org. Lett.*, 2015, **17**, 4152–4155.
 - 29 K. Suyama and M. Shirai, Photobase generators: Recent progress and application trend in polymer systems, *Prog. Polym. Sci.*, 2009, **34**, 194–209.
 - 30 E. Placet, J. Pinaud, O. Gimello and P. Lacroix-Desmazes, UV-Initiated Ring Opening Polymerization of L-Lactide Using a Photobase Generator, *ACS Macro Lett.*, 2018, **7**, 688–692.
 - 31 X. Dong, P. Hu, G. Zhu, Z. Li, R. Liu and X. Liu, Thioxanthone acetic acid ammonium salts: highly efficient photobase generators based on photodecarboxylation, *RSC Adv.*, 2015, **5**, 53342–53348.
 - 32 X. Sun, J. P. Gao and Z. Y. Wang, Bicyclic Guanidinium Tetraphenylborate: A Photobase Generator and A Photocatalyst for Living Anionic Ring-Opening Polymerization and Cross-Linking of Polymeric Materials Containing Ester and Hydroxy Groups, *J. Am. Chem. Soc.*, 2008, **130**, 8130–8131.

-
- 33 S. Chatani, T. Gong, B. A. Earle, M. Podgórski and C. N. Bowman, Visible-Light Initiated Thiol-Michael Addition Photopolymerization Reactions, *ACS Macro Lett.*, 2014, **3**, 315–318.
- 34 J. Shin, H. Matsushima, C. M. Comer, C. N. Bowman and C. E. Hoyle, Thiol–Isocyanate–Ene Ternary Networks by Sequential and Simultaneous Thiol Click Reactions, *Chem. Mater.*, 2010, **22**, 2616–2625.
- 35 J. Pinaud, T. K. H. Trinh, D. Sauvanier, E. Placet, S. Songsee, P. Lacroix-Desmazes, J.-M. Becht, B. Tarablsi, J. Lalevée, L. Pichavant, V. Héroguez and A. Chemtob, In Situ Generated Ruthenium-Arene Catalyst for Photoactivated Ring-Opening Metathesis Polymerization through Photolabile N-Heterocyclic Carbene Ligand, *Chem.: Eur. J.*, 2018, **24**, 337–341.
- 36 S. Dadashi-Silab, C. Aydogan and Y. Yagci, Shining a light on an adaptable photoinitiator: advances in photopolymerizations initiated by thioxanthenes, *Polym. Chem.*, 2015, **6**, 6595–6615.
- 37 A. M. Sarker, A. Lungu, A. Mejiritski, Y. Kaneko and D. C. Neckers, Tetraorganylborate salts as convenient precursors for photogeneration of tertiary amines, *J. Chem. Soc. Perkin Trans. 2*, 1998, 2315–2322.
- 38 S. Chatterjee, P. D. Davis, P. Gottschalk, M. E. Kurz, B. Sauerwein, X. Yang and G. B. Schuster, Photochemistry of carbocyanine alkyltriphenylborate salts: intra-ion-pair electron transfer and the chemistry of boranyl radicals, *J. Am. Chem. Soc.*, 1990, **112**, 6329–6338.

Chapitre III. Photoréduction d'un dérivé du thioxanthone par un sel d'azolium tétraphénylborate: Un moyen de photogénérer des N-carbènes hétérocycliques

Les dérivés arylborates sont très importants en photochimie. Ce sont des dérivés tétravalents du bore, de géométrie tétraédrique, contenant une charge négative formelle et au moins un substituant aryle. Bien que leur réactivité photochimique soit étudiée depuis la fin des années 1970,^{1,2} les progrès dans ce domaine ont été réalisés au prix d'intenses débats,³ et beaucoup d'inconnues demeurent.⁴ La photoréactivité de arylborates est organisée autour de deux grands types de réactions (**Schéma R.III.1**): 1/ photolyse directe et 2/ transfert d'électrons photoinduit (PET). Récemment, d'autres réactions telles que l'isomérisation ou photoélimination photochromique ont été décrites.⁵

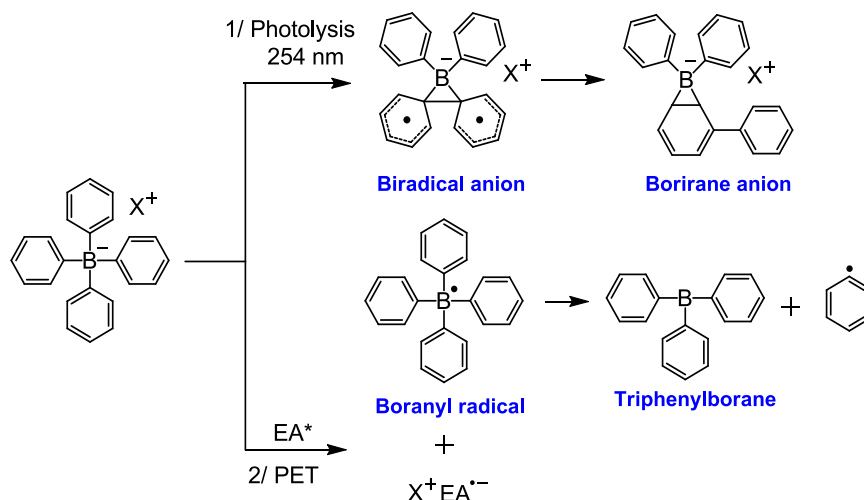


Schéma R.III.1. Réactivité photochimique des espèces arylborate. La voie 1 est basée sur la photolyse directe alors que la voie 2 est un transfert d'électron photoinduit (TEP) avec un sensibilisateur accepteur d'électron (EA). L'astérisque désigne un état excité.

- *Photolyse.* Lors d'une exposition à 254 nm (voie 1), le mécanisme le plus accepté implique un réarrangement di- π -borate conduisant à un anion biradical, évoluant vers un isomère anion borirane plus stable. La plupart des études sur l'irradiation directe ont tenté d'identifier les photoproduits (biphényle, 1-phénylcyclohexadiène la plupart du temps) et d'élucider le mécanisme photochimique.^{1,6,7} Son utilité en photochimie préparatoire a été démontrée récemment. Constatant que les

espèces anioniques intermédiaires pouvaient arracher les protons acides de d'eau et d'alcools,^{7,8} Sun *et al.* ont proposé en 2008 un sel de tétraphénylborate contenant comme cation l'acide conjugué d'une base azotée (BH⁺).⁶ La base a été photogénérée par l'arrachement de protons photoinduit au cours de la photolyse à 254 nm. Par exemple, TBDH⁺BPh₄⁻ a été utilisé comme générateur de photobase (PBG) pour la polymérisation par ouverture de cycle d'esters cycliques⁶ ou la polymérisation thiol-époxy.⁹

- En raison de leur potentiel d'oxydation relativement faible,¹⁰ les aryle borates tels que Ph₄B⁻ ou triarylalkylborate (Ph₃BR⁻) ont également été utilisés en tant que donneur d'électrons dans des réactions inter et intra-TEP (voie **2**) avec des sensibilisateurs accepteurs d'électrons cationique ou neutre (EA) tels que lez carbocyanine,¹¹ fullerène,¹² coumarine,¹³ fluorone,¹⁴ les dérivés de benzophénone.¹⁵ Un radical boranyl est formé, qui à son tour subit un clivage rapide donnant un triphénylborane et un groupe phényle (ou un groupe alkyle) radical.

Récemment, nous avons proposé une autre application pour l'oxydation photoamorcée de arylborates, la photogénération de carbènes N-hétérocyclique (NHC) à partir d'un sel d'azolium arylborate (NHCH⁺BPh₄⁻) (**Schéma R.III.2**).¹⁶ Lorsqu'il est associé à un sensibilisateur tel que l'isopropylthioxanthone (ITX), un transfert d'électrons à partir du borate (Ph₄B⁻) vers l'état excité triplet de l'ITX (³ITX*) peut se produire comme décrit ci-dessus. Contrairement au cas précédent, le cation azolium (NHCH⁺) permet à une étape ultérieure d'arrachement de protons avec l'anion radical ITX⁻ (**1**) d'avoir lieu, ce qui donne le NHC libre attendu (**2**).¹⁶ Nos récentes recherches ont prouvé qu'il était possible de former **IMes** et son analogue saturé **SIMes**, les deux NHCs les plus employés.¹⁶ L'utilité de ce photogénérateur de NHC deux composants NHCH⁺BPh₄⁻/ITX a également été démontrée dans des réactions de photopolymérisation pour former le polyuréthane, le polyester et le polynorbornène.¹⁷ En effet, bien que les NHCs aient apporté des changements profonds dans la synthèse organique catalytique,²³⁻²⁵ ils nécessitent généralement une atmosphère inerte et des conditions difficiles pour leur génération. En conséquence, un photogénérateur stable capables de créer des NHC sous exposition aux UV est très recherché. Il est vrai que les précurseurs NHC thermiquement latents existent également.^{21,22}

Bien que l'hypothèse mécanistique de photoréduction du thioxantone par l'arylborate soit acceptable, des preuves concluantes sont nécessaires. À l'exception de

la molécule de NHC photogénérée (**2**), on sait très peu de choses sur les espèces transitoires — $^3\text{ITX}^*$, $\text{ITX}^{\bullet-}$ (**1**), ITXH^\bullet (**3**), $\text{Ph}_4\text{B}^\bullet$ (**4**), Ph^\bullet (**5**) — qui sont censées se former. Pour fournir des preuves concluantes à l'appui de notre mécanisme, il est important d'établir clairement l'identité des espèces transitoires et des photoproduits. La structure des dérivés organiques du bore formés est particulièrement importante étant donné que BPh_3 est susceptible de former des complexes avec le NHC, avec des conséquences importantes pour la réactivité du carbène.²³ En effet, les espèces trivalentes du bore ont généralement des caractéristiques de type acide de Lewis, alors que les NHCs se comportent comme des bases de Lewis. Motivé par cette situation, la présente étude examine l'identité des espèces transitoires et les photoproduits générées par l'irradiation de 1,3-bis (mésityle) imidazolium tétraphénylborate ($\text{IMesH}^+\text{BPh}_4^-$, **Schéma R.III.2**) avec ITX pour former le NHC **IMes**.

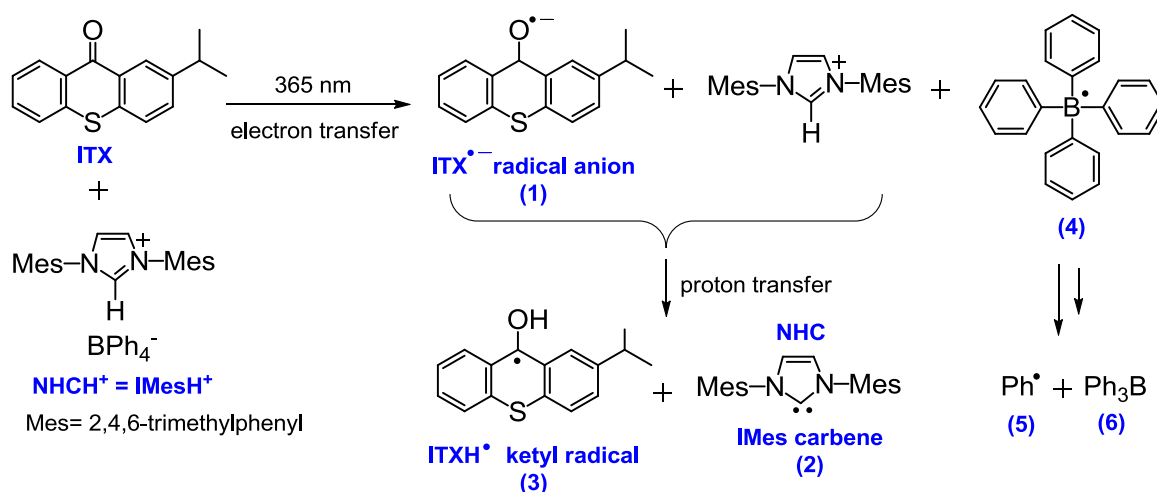


Schéma R.III.2. Mécanisme photochimique pour la production de NHC

Références

- 1 J. L. R. Williams, J. C. Doty, P. J. Grisdale, Roger. Searle, T. H. Regan, G. P. Happ and D. P. Maier, Boron photochemistry. I. Irradiation of sodium tetraarylborates in aqueous solution, *J. Am. Chem. Soc.*, 1967, **89**, 5153–5157.
- 2 A. Pelter, R. T. Pardasani and P. Pardasani, The Photochemistry of Boron Compounds, *Tetrahedron*, 2000, **56**, 7339–7369.
- 3 J. Radtke, S. K. Mellerup, M. Bolte, H.-W. Lerner, S. Wang and M. Wagner, Aryl Insertion vs Aryl–Aryl Coupling in C,C-Chelated Organoborates: The “Missing Link” of Tetraarylborate Photochemistry, *Org. Lett.*, 2018, **20**, 3966–3970.

-
- 4 W. G. Santos, J. Pina, D. H. Burrows, M. D. E. Forbes and D. R. Cardoso, New insight into the photophysics and reactivity of trigonal and tetrahedral arylboron compounds, *Photochem. Photobiol. Sci.*, 2016, **15**, 1124–1137.
 - 5 T. Baumgartner and F. Jaekle, *Main Group Strategies Towards Functional Hybrid Materials*, John Wiley & Sons, 2018.
 - 6 X. Sun, J. P. Gao and Z. Y. Wang, Bicyclic Guanidinium Tetraphenylborate: A Photobase Generator and A Photocatalyst for Living Anionic Ring-Opening Polymerization and Cross-Linking of Polymeric Materials Containing Ester and Hydroxy Groups, *J. Am. Chem. Soc.*, 2008, **130**, 8130–8131.
 - 7 J. D. Wilkey and G. B. Schuster, Irradiation of tetraphenylborate does not generate a borene anion, *J. Org. Chem.*, 1987, **52**, 2117–2122.
 - 8 J. L. R. Williams, J. C. Doty, P. J. Grisdale, T. H. Regan, G. P. Happ and D. P. Maier, Boron photochemistry. II. Irradiation of sodium tetraarylborates in alcohol solutions, *J. Am. Chem. Soc.*, 1968, **90**, 53–55.
 - 9 Y. H. Zhao, D. Vuluga, L. Lecamp and F. Burel, Photoinitiated thiol–epoxy addition for the preparation of photoinduced self-healing fatty coatings, *RSC Adv.*, 2016, **6**, 32098–32105.
 - 10 S. Murphy and G. B. Schuster, A Kinetic Method for Determination of Redox Potentials: Oxidation of Tetraarylborates, *J. Phys. Chem.*, 1995, **99**, 511–515.
 - 11 S. Chatterjee, P. D. Davis, P. Gottschalk, M. E. Kurz, B. Sauerwein, X. Yang and G. B. Schuster, Photochemistry of carbocyanine alkyltriphenylborate salts: intra-ion-pair electron transfer and the chemistry of boranyl radicals, *J. Am. Chem. Soc.*, 1990, **112**, 6329–6338.
 - 12 T. Konishi, Y. Sasaki, M. Fujitsuka, Y. Toba, H. Moriyama and O. Ito, Persistent C60 anion-radical formation via photoinduced electron transfer from tetraphenylborate and triphenylbutylborate, *J. Chem. Soc. Perkin Trans. 2*, 1999, 551–556.
 - 13 R. Popielarz, A. M. Sarker and D. C. Neckers, Applicability of Tetraphenylborate Salts as Free Radical Initiators, *Macromolecules*, 1998, **31**, 951–954.
 - 14 A. Y. Polykarpov, S. Hassoon and D. C. Neckers, Tetramethylammonium Tetraorganylborates as Coinitiators with 5,7-Diiodo-3-butoxy-6-fluorone in Visible Light Polymerization of Acrylates, *Macromolecules*, 1996, **29**, 8274–8276.
 - 15 S. Hassoon, A. Sarker, A. Y. Polykarpov, M. A. J. Rodgers and D. C. Neckers, Photoinduced Inter- and Intra-Ion-Pair Electron Transfer Reactions in N-(p-Benzoylbenzyl)-N,N,N-tri-n-butylammonium Triphenyl-n-butylborate and -Gallate Salts, *J. Phys. Chem.*, 1996, **100**, 12386–12393.
 - 16 J. Pinaud, T. K. H. Trinh, D. Sauvanier, E. Placet, S. Songsee, P. Lacroix-Desmazes, J.-M. Becht, B. Tarablsi, J. Lalevée, L. Pichavant, V. Héroguez and A. Chemtob, In Situ Generated Ruthenium-Arene Catalyst for Photoactivated Ring-Opening Metathesis Polymerization through Photolabile N-Heterocyclic Carbene Ligand, *Chem.: Eur. J.*, 2018, **24**, 337–341.
 - 17 T. Thi Kim Hoang, M. Jean-Pierre, M.-S. Fabrice, P. Julien, L.-D. Patrick, R. Corine, H. Valérie and C. Abraham, Mixture of azolium tetraphenylborate with isopropylthioxanthone: a new class of N-heterocyclic carbene (NHC) photogenerator for polyurethane, polyester and ROMP polymers synthesis, *Chem.:Eur.J.*, 2019, DOI: doi.org/10.1002/chem.201901000.

-
- 18 M. Scholl, S. Ding, C. W. Lee and R. H. Grubbs, Synthesis and Activity of a New Generation of Ruthenium-Based Olefin Metathesis Catalysts Coordinated with 1,3-Dimesityl-4,5-dihydroimidazol-2-ylidene Ligands, *Org. Lett.*, 1999, **1**, 953–956.
 - 19 N. E. Kamber, W. Jeong, S. Gonzalez, J. L. Hedrick and R. M. Waymouth, N-Heterocyclic Carbenes for the Organocatalytic Ring-Opening Polymerization of ϵ -Caprolactone, *Macromolecules*, 2009, **42**, 1634–1639.
 - 20 J. Raynaud, W. N. Ottou, Y. Gnanou and D. Taton, Metal-free and solvent-free access to α,ω -heterodifunctionalized poly(propylene oxide)s by N-heterocyclic carbene-induced ring opening polymerization, *Chem. Commun.*, 2010, **46**, 3203.
 - 21 B. Bantu, G. M. Pawar, U. Decker, K. Wurst, A. M. Schmidt and M. R. Buchmeiser, CO₂ and Sn^{II} Adducts of N-Heterocyclic Carbenes as Delayed-Action Catalysts for Polyurethane Synthesis, *Chem. - Eur. J.*, 2009, **15**, 3103–3109.
 - 22 S. Naumann, F. G. Schmidt, W. Frey and M. R. Buchmeiser, Protected N-heterocyclic carbenes as latent pre-catalysts for the polymerization of ϵ -caprolactone, *Polym. Chem.*, 2013, **4**, 4172.
 - 23 J. Zhang, N. Pidlynyi, M. Nieger, J. C. Namyslo and A. Schmidt, Zwitterionic borane adducts of N-heterocyclic carbenes from mesomeric betaines of uracil, *Org. Biomol. Chem.*, 2014, **12**, 2737–2744.

Chapitre IV. La combinaison d'un photogénérateur de ligand et d'un précatalyseur de ruthénium: une approche photoinduite pour la synthèse de film polymère réticulé par ROMP

Outil précieux pour la génération de doubles liaisons C=C, la métathèse des oléfines a été exploitée dans de nombreuses applications, telles que la synthèse d'architectures complexes,¹ de produits pharmaceutiques,² ou de copolymères biodégradables.³ Dans tous ces cas, les progrès ont été principalement obtenus grâce au développement de complexes alkylidène métalliques avancés et bien définis, comme les catalyseurs de Grubbs et Schrock.^{4,5} A cet égard, un progrès important a été en 1999 l'introduction de ligand à base de carbène N-hétérocyclique (NHC) à la place des composés de type phosphine.⁶ Cependant, les principaux développements dans la catalyse de métathèse des oléfines ont répondu davantage aux besoins de la chimie de synthèse (comme le montrent les exemples mentionnés ci-dessus), mais ont été moins utiles pour la préparation de matériaux polymères. La polymérisation par métathèse par ouverture de cycle (ROMP) des oléfines cycliques est actuellement le principal type de polymérisations par métathèse.^{6,7} À ce jour, l'utilisation de polymères ROMP a été limitée à la fabrication de matériaux massifs. Cela malgré le large spectre de propriétés des principaux polymères de ROMP, dérivés du norbornène (NB), cyclopentène, cyclooctène ou dicyclopentadiène (DCPD). Par exemple, les élastomères polycyclooctène (Vestamer®) et polyNB (Norsorex®) sont utilisés après vulcanisation comme amortisseurs et matériaux anti-adhérence. Le polyNB hydrogéné (Zeonex®) est un thermoplastique à haute performance optique, tandis que polyDCPD (Metton® ou Telene®) est connu comme un thermodurcissable ayant des propriétés mécaniques semblables aux thermoplastiques d'ingénierie. La plupart de ces polymères de ROMP ont été utilisés en tant que matériaux de structure, parce que leurs méthodes de fabrication sont restrictives.

Pour déverrouiller le potentiel de matériaux polymères de ROMP, des catalyseurs « intelligents » sont indispensables. Pour faire face à ce défi, des catalyseurs de métathèse latents complexes sont apparus, en mesure de libérer des espèces actives in situ et « à la demande » par une stimulation externe. Chaleur,⁸⁻¹⁰ force mécanique,¹¹ et rayonnement¹²⁻¹⁴ sont les stimuli les plus courants. Une catégorie distincte concerne des catalyseurs activés après l'addition d'un agent chimique externe.¹⁵⁻¹⁷ Parmi ces différentes options, l'activation provoquée par l'irradiation visible ou ultraviolette est particulièrement attrayante.¹⁸ Les catalyseurs de ROMP photolatente peuvent être activés à la température ambiante, et rendent

possible l'utilisation de formulations stables au stockage et prêtes à l'utilisation. Comme produit standard d'une polymérisation photoactivée, des films minces sont également attendus avec la possibilité de développer de nouveaux revêtements photoréticulables. Enfin, à la différence des autres déclencheurs, la réaction peut être contrôlée spatialement.^{17,19}

Dans le domaine de la métathèse des oléfines activées par photochimie, trois approches ont été proposées, dans lequel l'activation se fait généralement par une réaction photochimique impliquant le ligand d'un complexe de métal de transition. Les deux voies les plus courantes reposent sur une photodissociation de ligand^{20,21} et une photoisomérisation de ligand.^{12,14} La troisième voie, qui est la moins étudiée, est l'objet de la présente étude. Dans cette dernière, un catalyseur de métathèse d'oléfine actif est généré à partir d'un précatalyseur inactif et non-absorbant après réaction avec un ligand libéré par un second composé photosensible (un photogénérateur de ligand). Cette méthodologie a été introduite par Grubbs *et al.* en 2009 en utilisant un complexe de Ru-alkylidène ligaturé par l'acétylacétonate (acac) comme précatalyseur et un générateur de photoacide (PAG) à base de chlorure de triphénylsulfonium.¹⁵ Lors d'une irradiation à 254 nm, HCl a été libéré, et le déplacement ultérieur de acac par Cl⁻ a donné lieu à un catalyseur actif en métathèse. Une méthode similaire a également été employée par Pier *et al.* en utilisant un carbure de ruthénium et Ph₃S triflate (OTf).¹⁶ Récemment, nous avons remplacé le PAG avec un photogénérateur NHC utilisé et un complexe stable, dimérique Ru (II) disponible dans le commerce en tant que catalyseur de métathèse inactif. Notre système en tandem composé du précurseur de NHC 1,3-bis (mésityle) imidazolium tétraphénylborate **IMesH⁺BPh₄⁻** (**1**) et du précatalyseur [RuCl₂(*p*-cymène)]₂ (**Ru-1**) s'est révélé être très efficace pour la ROMP du NB.^{22,23} En comparaison avec les exemples décrits ci-dessus, un rayonnement UVA (320 - 400 nm) a été utilisé, et il n'y a pas de déplacement de ligand. Comme le montre le **Schéma R.IV.1**, le clivage des ponts Ru-chlorido de **Ru-1** est induit enthalpiquement par l'addition de 2 équivalents du NHC **IMes**, photogénéré à partir du composé **1**. En conséquence, le catalyseur actif présumé (**Ru-1-IMes**) dispose d'un cycle *p*-cymène, de deux ligands chlorido et d'un ligand **IMes**. D'abord présenté par Herman *et al.*²⁴ cette classe de catalyseur RuCl₂(*p*-cymène)NHC a été ensuite largement étudié par Noels *et al.* pour la ROMP du NB et du cyclooctène.²⁵⁻²⁷

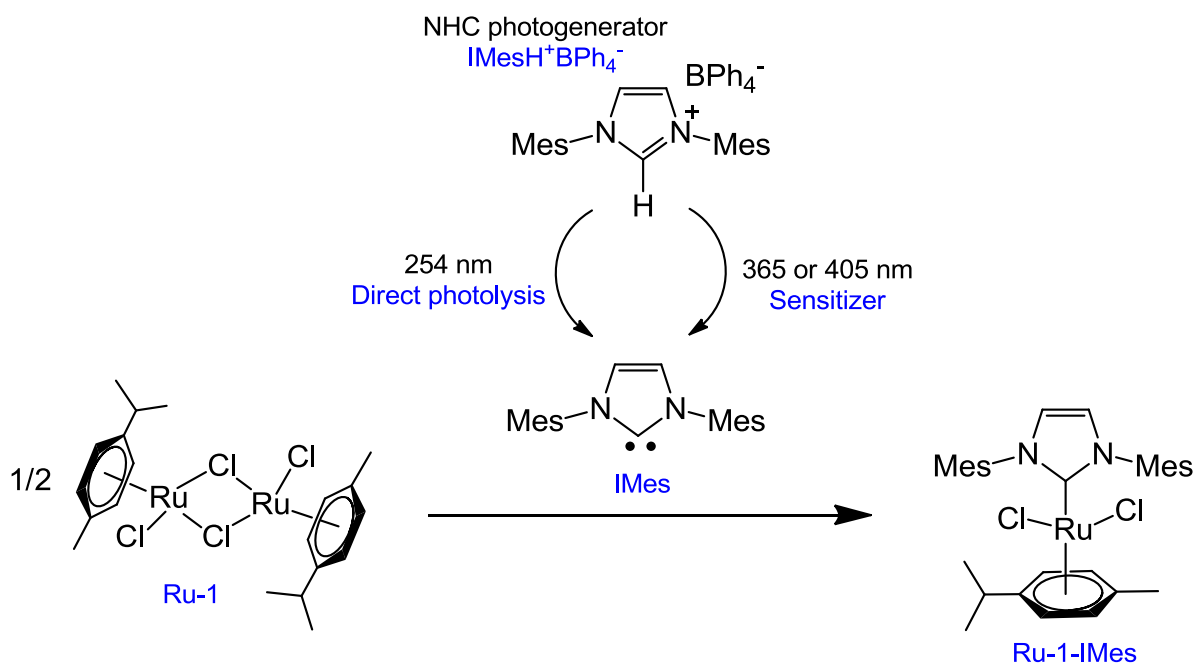


Schéma R.IV.1. L'irradiation d'un mélange d'un photogénérateur NHC (**1**) et d'un catalyseur inactif (**Ru-1**) conduit à un catalyseur de métathèse actif (**Ru-1-IMes**).

Dans cette contribution, le principal objectif est de démontrer l'utilité de cette approche en tandem pour la préparation photoinduite de films réticulés. A cet effet, nous présentons nos efforts pour améliorer le système photocatalytique en abordant un certain nombre de problèmes : optimiser le rendement des NHC photogénérés (**IMes**), assurer une photolabilité, identifier le catalyseur de métathèse actif et l'espèce amorçante (complexe ruthénium-carbène), et enfin, collecter des résultats préliminaires sur la photoROMP en solution de monomères communs tels que NB. Dans une seconde partie, une série de films de copolymère a été préparée par ROMP photoinduite entre NB et DCPD en utilisant le mélange photocatalytique **1/Ru-1**.

Références

- 1 J. B. Matson and R. H. Grubbs, Synthesis of Fluorine-18 Functionalized Nanoparticles for use as in vivo Molecular Imaging Agents, *J. Am. Chem. Soc.*, 2008, **130**, 6731–6733.
- 2 X. Bantreil and S. P. Nolan, Synthesis of N-heterocyclic carbene ligands and derived ruthenium olefin metathesis catalysts, *Nat. Protoc.*, 2011, **6**, 69–77.
- 3 K. J. Arrington, J. B. Waugh, S. C. Radzinski and J. B. Matson, Photo- and Biodegradable Thermoplastic Elastomers: Combining Ketone-Containing Polybutadiene with Polylactide Using Ring-Opening Polymerization and Ring-Opening Metathesis Polymerization, *Macromolecules*, 2017, **50**, 4180–4187.

-
- 4 P. Schwab, M. B. France, J. W. Ziller and R. H. Grubbs, A Series of Well-Defined Metathesis Catalysts– Synthesis of $[\text{RuCl}_2(=\text{CHR}')(\text{PR}_3)_2]$ and Its Reactions, *Angew. Chem. Int. Ed.*, 1995, **34**, 2039–2041.
 - 5 R. R. Schrock, J. S. Murdzek, G. C. Bazan, J. Robbins, M. DiMare and M. O'Regan, Synthesis of molybdenum imido alkylidene complexes and some reactions involving acyclic olefins, *J. Am. Chem. Soc.*, 1990, **112**, 3875–3886.
 - 6 M. Scholl, S. Ding, C. W. Lee and R. H. Grubbs, Synthesis and Activity of a New Generation of Ruthenium-Based Olefin Metathesis Catalysts Coordinated with 1,3-Dimesityl-4,5-dihydroimidazol-2-ylidene Ligands, *Org. Lett.*, 1999, **1**, 953–956.
 - 7 C. W. Bielawski and R. H. Grubbs, Highly Efficient Ring-Opening Metathesis Polymerization (ROMP) Using New Ruthenium Catalysts Containing N-Heterocyclic Carbene Ligands, *Angew. Chem. Int. Ed.*, 2000, **39**, 2903–2906.
 - 8 A. Ben-Asuly, E. Tzur, C. E. Diesendruck, M. Sigalov, I. Goldberg and N. G. Lemcoff, A Thermally Switchable Latent Ruthenium Olefin Metathesis Catalyst, *Organometallics*, 2008, **27**, 811–813.
 - 9 C. Slugovc, D. Burtscher, F. Stelzer and K. Mereiter, Thermally Switchable Olefin Metathesis Initiators Bearing Chelating Carbenes: Influence of the Chelate's Ring Size, *Organometallics*, 2005, **24**, 2255–2258.
 - 10 M. Barbasiewicz, A. Szadkowska, R. Bujok and K. Grela, Structure and Activity Peculiarities of Ruthenium Quinoline and Quinoxaline Complexes: Novel Metathesis Catalysts, *Organometallics*, 2006, **25**, 3599–3604.
 - 11 A. Piermattei, S. Karthikeyan and R. P. Sijbesma, Activating catalysts with mechanical force, *Nat. Chem.*, 2009, **1**, 133–137.
 - 12 A. Ben-Asuly, A. Aharoni, C. E. Diesendruck, Y. Vidavsky, I. Goldberg, B. F. Straub and N. G. Lemcoff, Photoactivation of Ruthenium Olefin Metathesis Initiators, *Organometallics*, 2009, **28**, 4652–4655.
 - 13 A. Aharoni, Y. Vidavsky, C. E. Diesendruck, A. Ben-Asuly, I. Goldberg and N. G. Lemcoff, Ligand Isomerization in Sulfur-Chelated Ruthenium Benzylidenes, *Organometallics*, 2011, **30**, 1607–1615.
 - 14 Y. Ginzburg, A. Anaby, Y. Vidavsky, C. E. Diesendruck, A. Ben-Asuly, I. Goldberg and N. G. Lemcoff, Widening the Latency Gap in Chelated Ruthenium Olefin Metathesis Catalysts, *Organometallics*, 2011, **30**, 3430–3437.
 - 15 B. K. Keitz and R. H. Grubbs, A Tandem Approach to Photoactivated Olefin Metathesis: Combining a Photoacid Generator with an Acid Activated Catalyst, *J. Am. Chem. Soc.*, 2009, **131**, 2038–2039.
 - 16 A. Y. Khalimon, E. M. Leitao and W. E. Piers, Photogeneration of a Phosphonium Alkylidene Olefin Metathesis Catalyst, *Organometallics*, 2012, **31**, 5634–5637.
 - 17 C. Theunissen, M. A. Ashley and T. Rovis, Visible-Light-Controlled Ruthenium-Catalyzed Olefin Metathesis, *J. Am. Chem. Soc.*, 2019, **141**, 6791–6796.
 - 18 O. Eivgi and N. Lemcoff, Turning the Light On: Recent Developments in Photoinduced Olefin Metathesis, *Synthesis*, 2018, **50**, 49–63.
 - 19 R. A. Weitekamp, H. A. Atwater and R. H. Grubbs, Photolithographic Olefin Metathesis Polymerization, *J. Am. Chem. Soc.*, 2013, **135**, 16817–16820.
 - 20 D. Wang, K. Wurst, W. Knolle, U. Decker, L. Prager, S. Naumov and M. R. Buchmeiser, Cationic RuII Complexes with N-Heterocyclic Carbene Ligands for UV-Induced Ring-Opening Metathesis Polymerization, *Angew. Chem. Int. Ed.*, 2008, **47**, 3267–3270.

-
- 21 D. Wang, K. Wurst and M. R. Buchmeiser, Cationic versus Neutral RuII–N-Heterocyclic Carbene Complexes as Latent Precatalysts for the UV-Induced Ring-Opening Metathesis Polymerization, *Chem.: Eur. J.*, 2010, **16**, 12928–12934.
 - 22 J. Pinaud, T. K. H. Trinh, D. Sauvanier, E. Placet, S. Songsee, P. Lacroix-Desmazes, J.-M. Becht, B. Tarablsi, J. Lalevée, L. Pichavant, V. Héroguez and A. Chemtob, In Situ Generated Ruthenium-Arene Catalyst for Photoactivated Ring-Opening Metathesis Polymerization through Photolabile N-Heterocyclic Carbene Ligand, *Chem.: Eur. J.*, 2018, **24**, 337–341.
 - 23 T. Thi Kim Hoang, M. Jean-Pierre, M.-S. Fabrice, P. Julien, L.-D. Patrick, R. Corine, H. Valérie and C. Abraham, Mixture of azolium tetraphenylborate with isopropylthioxanthone: a new class of N-heterocyclic carbene (NHC) photogenerator for polyurethane, polyester and ROMP polymers synthesis, *Chem.: Eur. J.*, 2019, DOI: doi.org/10.1002/chem.201901000.
 - 24 A. Hafner, A. Mühlebach and P. A. van der Schaaf, One-Component Catalysts for Thermal and Photoinduced Ring Opening Metathesis Polymerization, *Angew. Chem. Int. Ed. Engl.*, 1997, **36**, 2121–2124.
 - 25 A. Tudose, A. Demonceau and L. Delaude, Imidazol(in)ium-2-carboxylates as N-heterocyclic carbene precursors in ruthenium–arene catalysts for olefin metathesis and cyclopropanation, *J. Organomet. Chem.*, 2006, **691**, 5356–5365.
 - 26 L. Delaude, M. Szypa, A. Demonceau and A. F. Noels, New In situ Generated Ruthenium Catalysts Bearing N-Heterocyclic Carbene Ligands for the Ring-Opening Metathesis Polymerization of Cyclooctene, *Adv. Synth. Catal.*, 2002, **344**, 749.
 - 27 L. Delaude, A. Demonceau and A. F. Noels, Visible light induced ring-opening metathesis polymerisation of cyclooctene, *Chem. Commun.*, 2001, 986–987.

List of Publications

1. T. K. H. Trinh, J. P. Malval, F. Morlet-Savary, J. Pinaud, P. Lacroix-Desmazes, C. Reibel, V. Héroguez and A. Chemtob, Mixture of azolium tetraphenylborate with isopropylthioxanthone: a new class of N-heterocyclic carbene (NHC) photogenerator for polyurethane, polyester and ROMP polymers synthesis, *Chem.: Eur. J.*, 2019, DOI: doi.org/10.1002/chem.201901000.
2. E. Cao, L. Pichavant, T. K. H. Trinh, A. Chemtob, D. Quémener, J. Pinaud, V. Héroguez, “Emerging trends in ring opening metathesis polymerization”, *Macromolecular Engineering: From Precise Synthesis to Macroscopic Materials and Applications*, 2019 (Book chapter, accepted).
3. J. Pinaud, E. Placet, P. Lacroix-Desmazes, T. K. H. Trinh, J. P. Malval, A. Chemtob, and V. Héroguez, “Photogeneration of N-Heterocyclic Carbenes: Application in Photoinduced Ring-Opening Metathesis Polymerization”. *J.Vis.Exp.*, 2018, 141.
4. J. Pinaud, T. K. H. Trinh, D. Sauvanier, E. Placet, S. Songsee, P. Lacroix-Desmazes, J.-M. Becht, B. Tarablsi, J. Lalevée, L. Pichavant, V. Héroguez and A. Chemtob, In Situ Generated Ruthenium-Arene Catalyst for Photoactivated Ring-Opening Metathesis Polymerization through Photolabile N-Heterocyclic Carbene Ligand, *Chem.: Eur. J.*, 2018, **24**, 337–341.